# MODIS Cloud Optical Properties: User Guide for the Collection 6 Level-2 MOD06/MYD06 Product and Associated Level-3 Datasets

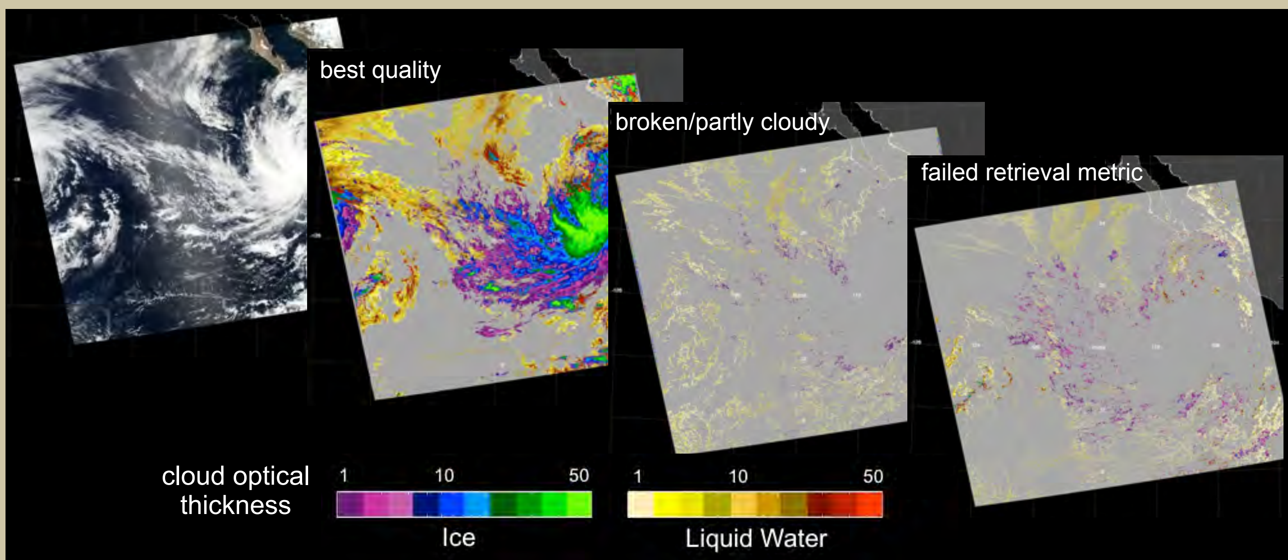


**Version 1.0**

***October 2015***

Steven Platnick[1], Michael D. King[2], Kerry G. Meyer[3,1], Gala Wind[4,1], Nandana Amarasinghe[4,1], Benjamin Marchant[3,1], G. Thomas Arnold[4,1], Zhibo Zhang[5], Paul A. Hubanks[6,1], Bill Ridgway[4,1], Jérôme Riedi[7]

[1] Earth Sciences Division, NASA Goddard Space Flight Center, Greenbelt, MD
[2] Laboratory for Atmospheric and Space Physics, University of Colorado, Boulder, CO
[3] Universities Space Research Association (USRA), Columbia, MD
[4] Science Systems and Applications, Inc., Lanham, MD
[5] University of Maryland Baltimore County, Baltimore, MD
[6] ADNET Systems, Inc., Lanham, MD
[7] Laboratoire d'Optique Atmosphérique, Université des Sciences et Technologies de Lille/CNRS, Villeneuve d'Ascq, France

## 1. Introduction

One of the primary atmospheric products produced from the MODIS sensor on the Terra and Aqua satellites is the cloud product. This product (Earth Science Data Set names **MOD06** and **MYD06** for Terra and Aqua MODIS, respectively) contains pixel-level retrievals of cloud-top properties (pressure, temperature, and height–both day and night), and cloud optical properties (optical thickness, effective particle radius, and water path for both liquid water and ice cloud thermodynamic phases–daytime only). For conciseness, we will typically abbreviate cloud optical thickness, effective radius, and water path as **COT**, **CER**, and **CWP**, respectively. Unless otherwise noted, further mention of MOD06 also includes the Aqua MODIS products as the algorithms are mostly identical.

The original pre-launch cloud optical retrieval algorithm was described in an Algorithm Theoretical Basis Document (**ATBD**), cf. modis-atmos.gsfc.nasa.gov/reference_atbd.html. While this was useful for communicating algorithm details to the retrieval community and providing a mechanism for community review, the ATBD has been superseded by NASA ROSES solicitation reviews, publications, and our focus on web-delivered "user guides."

This document describes the physical basis and algorithm updates for the optical property datasets, focusing on changes in the Collection 6 (**C6**) version vs. Collection 5 (**C5**), the structure and content of the MODIS cloud product (including the science data sets, metadata, and quality assurance), and frequently asked questions. The document is intended as an essential resource for all users of the C6 MODIS cloud optical properties products. While the emphasis is on the cloud optical properties component, overall MOD06 cloud product information will be provided when relevant.

The "Level" terminology is used to denote broad categories of NASA data products: Level 0 (**L0**) denotes raw spectral channel counts, Level 1B (**L1B**) denotes calibrated and geolocated reflectances and/or radiances, Level 2 (**L2**) denotes orbital-swath science (geophysical) products, and finally Level 3 (**L3**) denotes gridded spatial/temporal aggregations of the L2 products.

The MODIS cloud product is a L2 product, and is archived in version 4 of a self-described Hierarchical Data Format (**HDF4**) file based upon the platform (Terra or Aqua) and temporal period of collection (every 5 minutes along the orbit track). One 5 min file, or **data granule**, contains data from roughly 2330 km across-track (1354 1 km pixels) to 2000 km along-track of Earth located data. Thus, a data granule is comprised of approximately 2.7 M 1 km pixels. The Terra overpass time at the equator is around 1030 local solar time in its descending (daytime) mode and 2230 local solar time in its ascending (nighttime) mode. The Aqua overpass time is around 1330 local solar time in ascending (daytime) mode and 0130 local solar time in descending (nighttime) mode.

Each L2 cloud parameter is retrieved at a spatial resolution determined by the sensitivity of the retrieval, not necessarily on a native single field of view (**FOV**) basis for the MODIS spectral band used in the retrieval. Resolutions of L2 cloud products are at 1×1 km (nadir) for all cloud optical properties, and either 5×5 km or 1×1 km (new in C6) for cloud-top properties.

MODIS Level-2 HDF product files have standardized filenames, described below.

*Terra MODIS*: **MOD06_L2.AYYYYDDD.HHMM.VVV.YYYYDDDHHMMSS.hdf**

*Aqua MODIS*: **MYD06_L2.AYYYYDDD.HHMM.VVV.YYYYDDDHHMMSS.hdf**

The definition of the highlighted text is as follows:

**MOD06** = Earth Science Data Type name

**L2** = Denotes a Level-2 product

**A** = indicates following date/time information is for the acquisition (observation)
**YYYYDDD** = acquisition year and day-of-year
**HHMM** = acquisition hour and minute start time
**VVV** = collection (e.g., '006' for Collection 6)
**YYYYDDDHHMMSS** = production data and time
**hdf** = denotes HDF file format

Note that all times are UTC times, not local, and the MOD prefix represents a Terra platform file (data granule); Aqua platform files have the prefix MYD.

MODIS (re)processing streams are referred to as data "collections." An increment in the collection number (or version) denotes comprehensive changes (additions and/or updates) to the science algorithms. Collection 5 (C5) was completed in calendar year 2006, and a reprocessing to C5.1 was completed in calendar year 2010. Atmosphere Team C6 Aqua L2 reprocessing began in December 2013 and was completed in early May 2014 (data acquisition dates 4 July 2002 through 31 December 2013); Aqua forward processing began on 1 January 2014. Atmosphere Team C6 Terra L2 reprocessing began in November 2014 and was completed in March 2015 (data acquisition dates 24 January 2000 through 31 December 2014); Terra forward processing began on 1 January 2015. Atmosphere Team L3 and Terra (re)processing began in October 2014 and was completed in March 2015.

Details on the changes implemented in each collection are available in the "products" section of the MODIS Atmosphere Team web site (modis-atmos.gsfc.nasa.gov). Occasionally significant updates are implemented in the middle of a collection. This is only done when an operational algorithm software bug is discovered that seriously impacts one or more of the **Scientific Data Sets (SDSs)** contained within a L2 (or L3) file. Scientists working with MODIS data should always be aware of updates applied to the operational software, especially those applied in the middle of a collection, by visiting the 'Known Problems' page (modis-atmos.gsfc.nasa.gov/MOD06_L2/qa.html) in the "cloud" section of the MODIS-Atmosphere web site, or by checking the Data Processing Calendar (modis-atmos.gsfc.nasa.gov/products_calendar.html).

In addition to the separate suite of MODIS Atmosphere Team data product files (cloud, aerosol, clear sky profiles, and precipitable water products), the team also provides a L2 Joint Atmosphere Team Product (**MODATML2**/**MYDATML2**) for users interested in selected atmosphere parameters, e.g., for climate studies, trend analysis, aggregation sensitivity studies, or correlative studies requiring more than one atmosphere L2 file. MODATML2 is generated by subsetting key science parameters from each atmosphere product and combining them into a single L2 file with a resolution of 10 km (aerosol) or 5 km (profiles, cloud-top properties, subsampled native 1 km cloud optical properties datasets). The sampling of 1 km fields is consistent with the Atmosphere Team L3 sampling approach (filename **MOD08/MYD08**), ensuring that MODATML2 can serve as a basis for research-level aggregation efforts in a manner that is fully consistent with the pixels used in the existing MOD08 product. The relatively small ATML2 file size (depending on cloud fraction) is more practical for downloading large time periods and has a significant number of users. Format and content information for the C6 ATML2 product are at modis-atmos.gsfc.nasa.gov/_docs/ATML2_C6_SDS.pdf.

All team products are distributed by the NASA GSFC Land and Atmospheres Archive and Distribution System (**LAADS**, ladsweb.nascom.nasa.gov/data/) and are available via search interface or direct ftp download. Production is done by the MODIS Adaptive Processing System (**MODAPS**), also located at GSFC.

## 1.1. The MODIS Cloud Product

MODIS on Terra and Aqua provides unique spectral and spatial capability for retrieving cloud optical properties. Relative to previous generation global imagers (e.g., AVHRR), MODIS has a number of additional spectral channels, including 1.6 and 2.1 µm window channels that, in addition to an AVHRR heritage 3.7 µm channel, provide cloud microphysical information. $CO_2$-slicing bands (13 µm spectral region) and the related cloud-top algorithm have heritage with the HIRS instrument [e.g., *Wylie and Menzel*, 1999]. Native spatial resolution is at 250 m (0.66 and 0.87 µm channels), 500 m (five channels including 3 shortwave-infrared), and 1 km (all others).

### *1.1.1. Cloud-top properties overview*

The cloud top properties (cloud top pressure, temperature, and effective cloud amount) are produced for the cloudy portion of the 5×5 pixel arrays wherein the cloud pixels identified by the probably cloudy and cloudy bits of the cloud mask are averaged to reduce noise. The MODIS science team utilizes an extended suite of channels, in particular in the $CO_2$ absorption region from 13.3 to 14.2 µm. These so-called $CO_2$-slicing channels have a long history of use in identifying cloud top pressure for high clouds due to the opacity of $CO_2$, a uniformly mixed, but temporally changing, gas in the Earth's atmosphere [*Chahine*, 1974; *King et al.*, 1992]. They are, however, less capable of determining cloud top pressure (or altitude) for low boundary-layer clouds. In MODIS, the $CO_2$-slicing channels are supplemented with an infrared window channel at 11 μm for optically thicker and lower-level clouds.

C6 improvements in the cloud top properties algorithm and changes in the product datasets have been described in the updated ATBD (modis-atmos.gsfc.nasa.gov/_docs/MOD06_ATBD_2013_03_06.pdf) and in *Baum et al*. [2012], and include: (i) improved knowledge of the spectral response functions of the thermal infrared channels, based largely on comparison with corresponding hyperspectral measurements from collocated AIRS (Atmosphere Infrared Sounder) observations on Aqua, (ii) restrictions to the $CO_2$-slicing method based on the infrared phase retrieval information, (iii) introduction of surface emissivity maps, (iv) introducing a latitude dependent 11 μm brightness temperature lapse rate over the ocean, (v) improvements to the thermal infrared-derived thermodynamic phase, and (vi) introduction of cloud top properties using 1 km spatial resolution.

### *1.1.2. Cloud optical and microphysical properties overview*

Multispectral reflectances are used to simultaneously retrieve cloud optical thickness (**COT**), effective radius (**CER**), and derived cloud water path (**CWP**) globally during the daytime for liquid and ice phases. The optical/microphysical algorithm makes primary use of six visible (**VIS**), near-infrared (**NIR**), shortwave-infrared (**SWIR**) and midwave-infrared (**MWIR**) MODIS channels, as well as several thermal channels. In addition to the 1 km MODIS Level-1B data, the optical property algorithm requires as input the MODIS cloud mask (**MOD35**), the cloud-top pressure portion of MOD06 [*Ackerman et al.*, 2008; *Holz et al.*, 2008], and a variety of ancillary datasets including gap-filled MODIS land and snow/ice surface spectral albedos, snow/ice data (Near-real-time Ice and Snow Extent, NISE), and forecast analysis fields (NCEP GDAS).

Cloud optical and microphysical properties (COT, CER, and integrated CWP of both liquid water and ice clouds) are produced for pixels identified as probably cloudy or cloudy by the cloud mask during the daytime portions of each orbit; daytime for MOD06 is defined by a threshold applied to the solar zenith angle $\theta_0$, i.e., $\theta_0 < 81.36°$. The basic physical principle behind the simultaneous retrieval of COT and CER is the bi-spectral solar reflectance method first described by *Nakajima and King* [1990] and applied to airborne data. MOD06-specific heritage work also includes *Platnick and Twomey* [1994], *Platnick and Valero* [1995] (microphysical retrievals using the AVHHR 3.7 μm channel), *Platnick et al.* [2001] (1.6-2.1 μm retrievals over snow/ice surfaces), and thermodynamic phase retrievals [*King et al.*, 2004]. Basic algorithm details are described in the C5 Algorithm Theoretical Basis Document (ATBD) addendum (link) and original ATBD [*King et al.*, 1997]. An overview of the MODIS cloud product algorithms (at the time of Collection 4) along with example results is provided in *Platnick et al.* [2003] and *King et al.* [2003]. Collection 5 algorithm-related publications include ice models [*Baum et al.*, 2005; *Yang et al.*, 2007], multilayer detection [*Wind et al.*, 2010; *Joiner et al.*, 2010], Clear Sky Restoral filtering [*Zhang and Platnick*, 2011; *Pincus et al.*, 2012], pixel-level uncertainties [*Platnick et al.*, 2004], and L3 statistics [*King et al.*, 2013]. Evaluation-specific publications include cloud phase [*King et al.*, 2010; *Riedi et al.*, 2010], view angle biases [*Liang et al.*, 2009; *Maddux et al.*, 2010], and the impacts of non-plane-parallel clouds [*Zhang et al.*, 2010; *Zhang and Platnick*, 2011; *Zhang et al.*, 2012].

The more significant updates for the C5 processing stream [Platnick *et al*., 2003: King *et al*., 2003] included: (i) new ice crystal size/habit distribution models and the corresponding ice reflectance library calculations [Baum *et al*., 2005], (ii) a clear sky restoral algorithm that attempts to identify pixels that are poor retrieval candidates due to sunglint, edges of clouds, heavy dust or smoke contamination, or spatially variable (partly cloudy) pixels, in which case these 'cloudy' pixels are *restored* to clear sky and no cloud optical property retrievals are attempted, (iii) improved snow-free surface albedo maps [*Moody et al*., 2005, 2008], and (iv) spectral sea ice and snow-covered land surface albedo characteristics by ecosystem [*Moody et al*., 2007].

Major C6 improvements in the cloud optical properties algorithm include (i) improving the ice cloud optical properties, based in part on comparison with CALIOP and thermal IR retrievals of COT [*Holz et al.*, 2015], (ii) improved surface albedo maps [*Schaaf et al.,* 2011], (iii) enhancements of the shortwave-derived cloud thermodynamic phase, (iv) incorporation of wind-speed interpolated bidirectional reflectance properties over the ocean, especially important for optically thin clouds, (v) separate CER retrievals at 1.6, 2.1, and 3.7 µm, (vi) improvements to pixel-level retrieval uncertainty calculations, and (vii) new cloud radiative transfer code and lookup table (**LUT**) approaches including the use of a full range of cloud optical thickness instead of asymptotic theory.

C6 cloud optical property algorithm changes have been extensive. The code is numerically intensive, depending on explicit forward radiative calculations for cloud, gases and surface interactions. The Collection 6 L2 MODIS Cloud Product contains 128 SDSs, which are listed in Appendix A. Uncertainties for each retrieved L2 pixel are provided for many non-3-D error sources and include error correlations across the retrieval spectral channels. Estimates of uncertainty in aggregated means are also provided in the joint atmosphere team L3 product. **Quality Assessment (QA)** information now includes separate retrievals of pixels unlikely to meet plane-parallel model assumptions, including multiple CER derived from various spectral channel combinations whose differences may be symptomatic of forward model failures, subpixel spatial heterogeneity, and additional phase detection tests. New ancillary datasets have been incorporated. Recent ice particle radiative transfer calculations [*Yang et al.*, 2013] enabled studies of habit and surface roughness sensitivity across the MODIS spectral and particle size domain, leading to new ice models that provide closure with infrared (**IR**) and next-version Cloud-Aerosol Lidar with Orthogonal Polarization (**CALIOP**) retrievals. The lines of core science code have doubled since C5. Processing requirements are viable only because MODAPS technical capabilities have increased in tandem.

C6 updates are representative of evolving passive imager cloud retrieval science as spectral information from MODIS and other capable sensors continues to be explored. For example, synergistic A-Train studies have provided important constraints on ice particle radiative models [*Holz et al.*, 2015]. The climate modeling community continues to improve its ability to exploit the product, e.g., the MODIS CFMIP COSP simulator [*Pincus et al.*, 2012] and NASA Working Group for Observations for Modeling Intercomparison Studies (obs4MIPs). Cloud assessment reports (e.g., GEWEX, *Stubenrauch et al.* [2013]; VIIRS/MODIS, *Platnick et al.* [2013]) acknowledge the challenges in establishing cloud climate data records.

## 1.2. Theoretical Basis of Cloud Optical Retrievals

### *1.2.1. Theoretical basis of primary cloud optical properties algorithm*

The simultaneous retrieval of cloud optical thickness and effective radius is best achieved by simultaneously measuring the reflection function in a non-absorbing and absorbing spectral channel (e.g., VIS/NIR and SWIR, respectively), and comparing the resulting measurements with theoretical forward model calculations, as demonstrated with airborne data by *Nakajima and King* [1990] (also see historical papers on airborne/spaceborne observations and retrievals by *Twomey and Cocks* [1982, 1987], *Curran and Wu* [1982], *Rawlins and Foot* [1990], *Nakajima et al.* [1991], *Han et al.* [1994], *Platnick and Twomey* [1994], *Platnick and Valero* [1995], *Minnis et al.* [1997]). The technique is especially accurate over dark ocean surfaces because the reflection function of the earth–atmosphere system arises primarily from light scattering by the cloud layer, with little influence from the underlying surface. In comparing measurements with theory, however, it is essential that the light-scattering properties of the cloud are modeled realistically, and that the cloud is properly ascribed to either a liquid water or ice cloud with corresponding optical properties. For applications of this technique to global observations, involving clouds over snow and sea ice surfaces, or various land surfaces, it is further necessary to estimate realistic values of the underlying surface reflectance in the appropriate channels.

**Figure 1.2-1** illustrates the underlying principle behind the simultaneous retrieval of COT and CER from reflected solar radiation measurements for (a) liquid water clouds and (b) ice clouds, shown here for clouds over snow and sea ice surfaces. The minimum values of the reflection function at 1.24 and 2.13 μm correspond to the reflection functions of the underlying surface at those wavelengths in the absence of an atmosphere. The dashed curves represent reflection function contours for fixed COT, and the solid curved contours are for fixed CER. Over snow and sea ice surfaces, as shown here, the reflection function of liquid water clouds at 1.24 μm decreases as COT increases from 0 to about 2, where it begins to increase; over land (ocean) surfaces where 0.66 μm (0.87 μm) is used instead, the reflection function of the surface is small and this would not be the case. The data points superimposed on the theoretical curves of Fig. 1.2-1 correspond to Aqua MODIS observations over Greenland, ac-

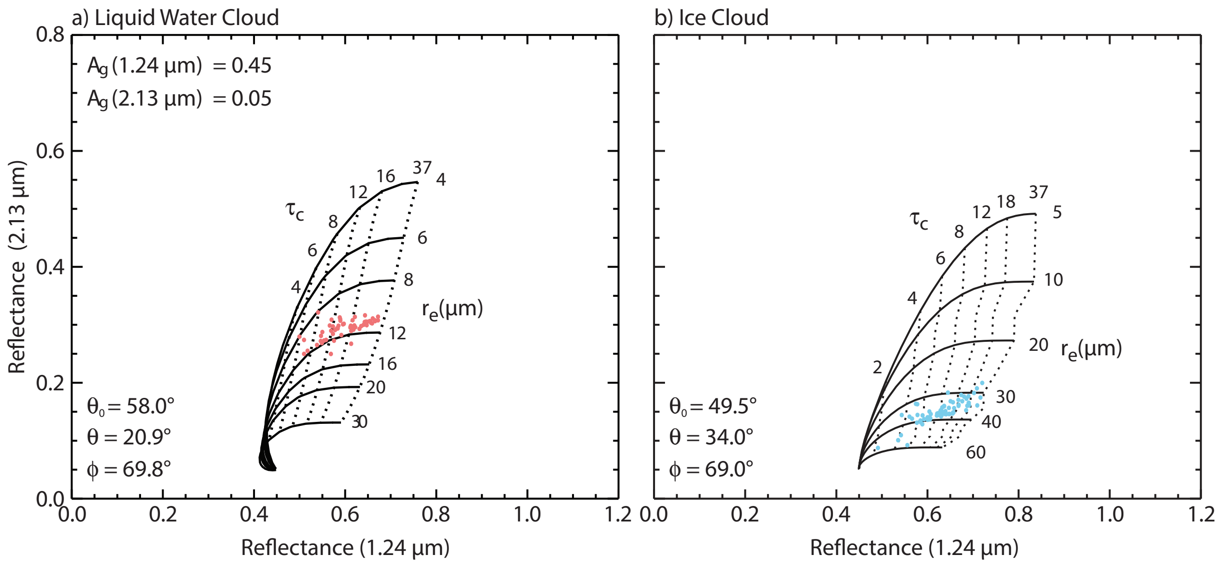


Figure 1.2-1. Theoretical relationship between the reflection function at 1.24 µm and 2.13 µm for (a) liquid water and (b) ice clouds for various values of COT (dashed lines) and CER (solid lines) for specified values of surface albedo and solar/view geometry. Data from measurements above arctic liquid water and ice clouds are superimposed on the figure.

quired at the observational solar and viewing directions specified in the figures on July 28 (1345 UTC) and 29 (1250 UTC) 2008 for ice and liquid water clouds, respectively.

Other channel pairs can be used to retrieve COT and CER. While the primary or standard channel pair uses the 2.13 µm channel for microphysical information, the 1.63 µm and 3.79 µm MODIS channels can also be used as described in Sect. 2. The next subsection describes an alternate retrieval using two SWIR channels to minimize errors over snow and ice surfaces that was first implemented in C5 processing.

### *1.2.2. Theoretical basis of 1.6 and 2.1 µm cloud optical properties algorithm*

Due to the relatively high surface albedo at 0.87 µm or 1.24 µm (used in standard retrievals) over snow and sea ice surfaces, *Platnick et al*. [2001] proposed an alternative method for simultaneously retrieving COT and CER from reflectance measurements. This method takes advantage of the fact that the surface albedo of snow and sea ice is quite low at 1.63 µm (cf. *Moody et al*. [2007]). **Figure 1.2-2** illustrates the theoretical relationship and corresponding data points of the simultaneous retrieval of COT and CER using measurements at 1.63 and 2.13 µm, where it is assumed that the surface albedo of sea ice is 0.03 at both wavelengths. Although the solution space loses the near-orthogonality of the COT and CER retrievals using standard channel pairs, and therefore is more sensitive to calibration uncertainties in the measurements, the sensitivity to COT is generally better than the standard method because of decreased uncertainty in the value of the surface albedo. This technique is notice-

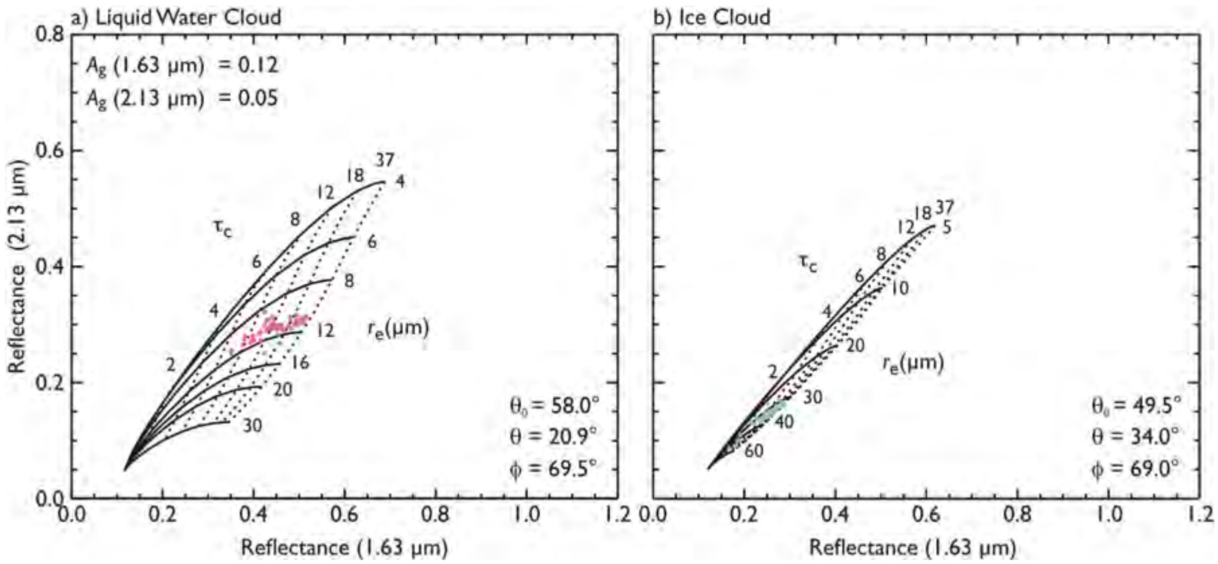


Figure 1.2-2. Theoretical relationship between the reflection function at 1.63 µm and 2.13 µm for (a) liquid water and (b) ice clouds for various values of COT ($\tau_C$, dashed lines) and CER ($r_e$, solid lines) for specified values of surface albedo and solar/view geometry. Data from measurements above arctic liquid water and ice clouds are superimposed on the figure.

ably more robust for liquid water clouds (Fig. 1.2-2a) than for ice clouds, however, where the more appreciable lack of orthogonality is apparent (Fig. 1.2-2b).

MODIS applies this supplemental cloud optical properties retrieval for COT and CER over the ocean as well as snow and sea ice surfaces, in addition to the standard algorithm, a feature that was first implemented in C5.

## 2. Level-2 Collection 6 Changes

Recent Collection Overview

The C6 algorithm development and testing efforts have been extensive. The major algorithm efforts are also summarized in the **Appendix G** table. Highlights include:

- **Radiative transfer/Look-up Tables** (**LUT**s): Eliminated the use of asymptotic parameter radiative transfer code (reduces code complexity/maintenance); generated precomputed LUTs with separate single and multiple scattering components to reduce the number of angular grid points and linear interpolation errors (median errors are typically $\ll 1\%$ across the solution domain).
- **Thermodynamic retrieval phase**: Improved algorithm using a variety of separate tests with assigned weights (MOD06 IR phase product [*Baum et al.*, 2012], microphysical retrievals for each phase, cloud-top temperature, and 1.38 µm channel reflectance). Comparisons against CALIOP and POLDER phase products show a substantial improvement in the overall global skill.
- **Ice radiative models**: Severely roughened aggregated columns [Y*ang et al.*, 2013] provide closure with global cirrus COT from IR methods and new CALIOP lidar ratios [*Holz et al.*, 2012].
- **Spectral retrievals**: In C5, the 1.6 and 3.7 µm CER retrievals were provided as differences with respect to the 2.1 µm CER retrieval. In C6, all spectral retrievals are now reported in separate SDSs (i.e., separate absolute COT, CER, and WP retrievals for channel combinations that include the 1.6, 2.1, and 3.7 µm channels). The 1.6 and 3.7 µm retrievals are found in SDS names <*parameter name*>_16 and <*parameter name*>_37, respectively; the legacy 2.1 µm C5 retrieval SDSs are not appended with a channel designation qualifier.
- **Retrieval failure metrics**: Provided for those pixels where the observations fall outside the LUT solution space (Retrieval_Failure_Metric SDS).
- **Quality Assessment (QA)**: Now includes separate SDSs for lower quality scenes identified by C5-like Clear Sky Restoral algorithms [e.g., *Zhang and Platnick*, 2011] that flag pixels not expected to be overcast (referred to as 'Partly Cloudy' retrievals and found in SDSs <*parameter name*>_PCL), a 1 km sub-pixel 250 m reflectance heterogeneity index SDS (Cloud_Mask_SPI), and an updated multilayer detection scheme [*Pavolonis and Heidinger*, 2004; *Wind et al.*, 2010; *Joiner et al.*, 2010].
- **Quantitative pixel-level uncertainty**: Provided for all spectral optical/microphysical retrievals [*Platnick et al.*, 2004] and updated to include scene-dependent L1B uncertainties [*Sun et al.*, 2012], cloud model and surface albedo error sources (cloud effective variance, ocean surface wind speed and direction), and 3.7 µm emission error sources. Does not include estimates of 3D radiative transfer biases or ice habit model error sources. Provided in SDS names <*parameter name*>_Uncertainty_<*channel/pair designation* (if appropriate)>.
- **Water surfaces**: Wind speed interpolated bidirectional reflectance properties (Cox-Munk model) of water surfaces.

- **Surface ancillary datasets**: New dynamic 8-day sampling surface spectral albedo dataset derived from gap-filled C5 Aqua+Terra MODIS data (MCD43B3, *Schaaf et al.* [2011]), and adoption of land spectral emissivities consistent with cloud-top property code [*Seemann et al.*, 2008].

Details on individual C6 science tests and accompanying browse imagery are available at modis-atmos.gsfc.nasa.gov/team/pge06_test_details.html; algorithm enhancement details are at modis-atmos.gsfc.nasa.gov/products_C006update.html.

## 2.1. New Ice Cloud Models

Comparisons of forward RT calculations, using new ice crystal light scattering models, with satellite remote sensing using polarization of reflected sunlight from Polarization and Directionality of the Earth's Reflectances (POLDER) suggest that severely-roughened ice crystals significantly outperform their counterparts assuming smooth ice crystals [*Cole et al*., 2013]. Moreover, reflectance-based cloud optical property retrievals using a single habit, namely severely-roughened compact aggregates composed of eight solid columns (hereafter referred to as simply *aggregated columns*), were found to provide closure with thermal IR-based retrievals and are in better agreement with CALIOP [*Holz et al*., 2015]. Consequently, the smooth ice crystal size/habit distribution cloud models used in C5 [*Baum et al*., 2005] have been replaced with a gamma particle size distribution consisting of severely-roughened aggregated columns.

**Figure 2.1-1** shows the effect of using severely roughened ice crystals on calculations of the asymmetry factor ($g$). In all cases considered (solid bullet rosettes, solid aggregate plates, and aggregated columns), the roughened particles yield substantially smaller asymmetry factors than the C5 models. Since cloud reflectance at a non-absorbing wavelength is largely a function of scaled optical thickness $(1–g)\tau$, where $\tau$ denotes COT, it follows that differences between C5 COT retrievals and those using roughened particles (C6) can be approximated by

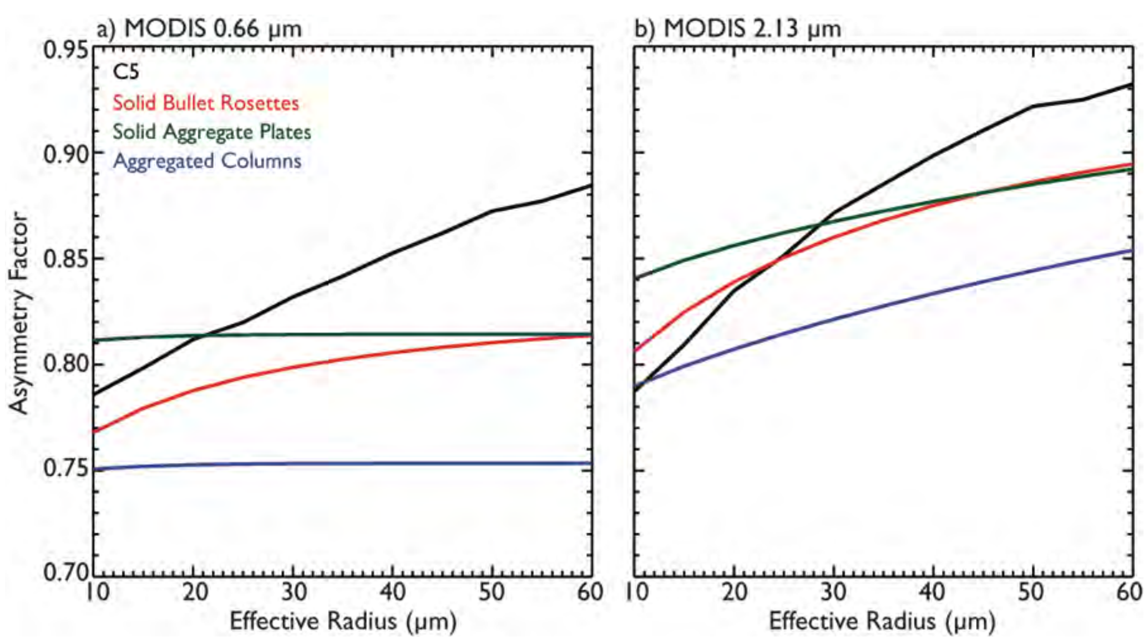


Figure 2.1-1. Asymmetry factor as a function of effective radius for ice crystals having the size/habit distribution used in C5 (black line), and gamma distribution of roughened solid bullet rosettes (red), solid aggregate plates (green), and aggregated columns used in C6 (blue) for the (a) 0.66 µm (b) 2.13 µm wavelength channels. Note that ice crystals having severely roughened surfaces have significantly lower asymmetry factors than those assumed in C5.

$$\frac{\tau^{C6}}{\tau^{C5}} \cong \frac{1-g^{C5}(r_e)}{1-g^{C6}(r_e)} \qquad (2.1\text{-}1)$$

Thus using roughened ice crystals will yield smaller COT retrievals than those of C5. This result provides better closure with CALIOP and thermal IR retrievals of COT than does C5

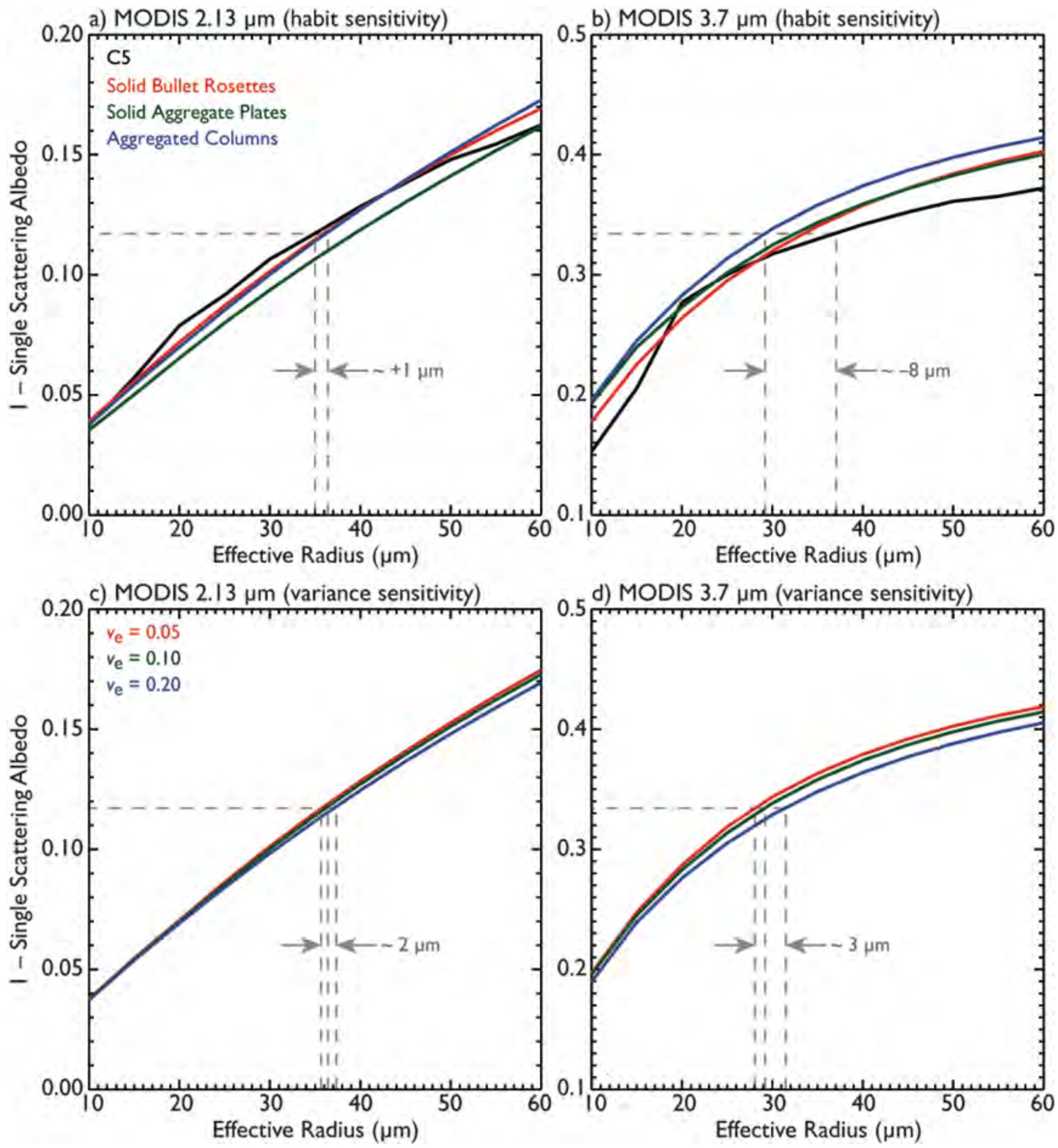


Figure 2.1-2. Simulations of co-albedo as a function of CER for crystals having the size/habit distribution used in C5 (black line), and gamma distribution of roughened solid bullet rosettes (red), solid aggregate plates (green), and the aggregated columns used in C6 (blue) for the (a) 2.13 μm and (b) 3.7 μm wavelength channels. Ice crystals having severely roughened surfaces have smaller (larger) absorption than those assumed in Collection 5 at 2.13 μm (3.7 μm), which can potentially lead to larger (smaller) values of CER in C6. Calculations of co-albedo for aggregate columns at various values of effective variance are shown in (c) and (d) for 2.13 and 3.7 μm, respectively.

[*Holz et al.*, 2015], which has been shown to be biased large in the case of COT retrievals of optically thin clouds (i.e., those that can be retrieved by CALIOP).

In addition to cloud asymmetry factor, the cloud single scattering albedo ($\omega_0$) derived from the new roughened ice crystal models is also generally larger at the absorbing SWIR wavelengths, as shown in **Figure 2.1-2** by the smaller values of co-albedo $1-\omega_0$ for the 2.13 µm MODIS channel. In the MWIR, namely 3.7 µm, $1-\omega_0$ is larger than that found in C5. Because the SWIR and MWIR wavelength channels are primarily used to infer particle size, assuming roughened ice crystals will often lead to larger values of CER at 2.13 µm than the smooth ice crystal models of C5, and smaller values of CER at 3.7 µm.

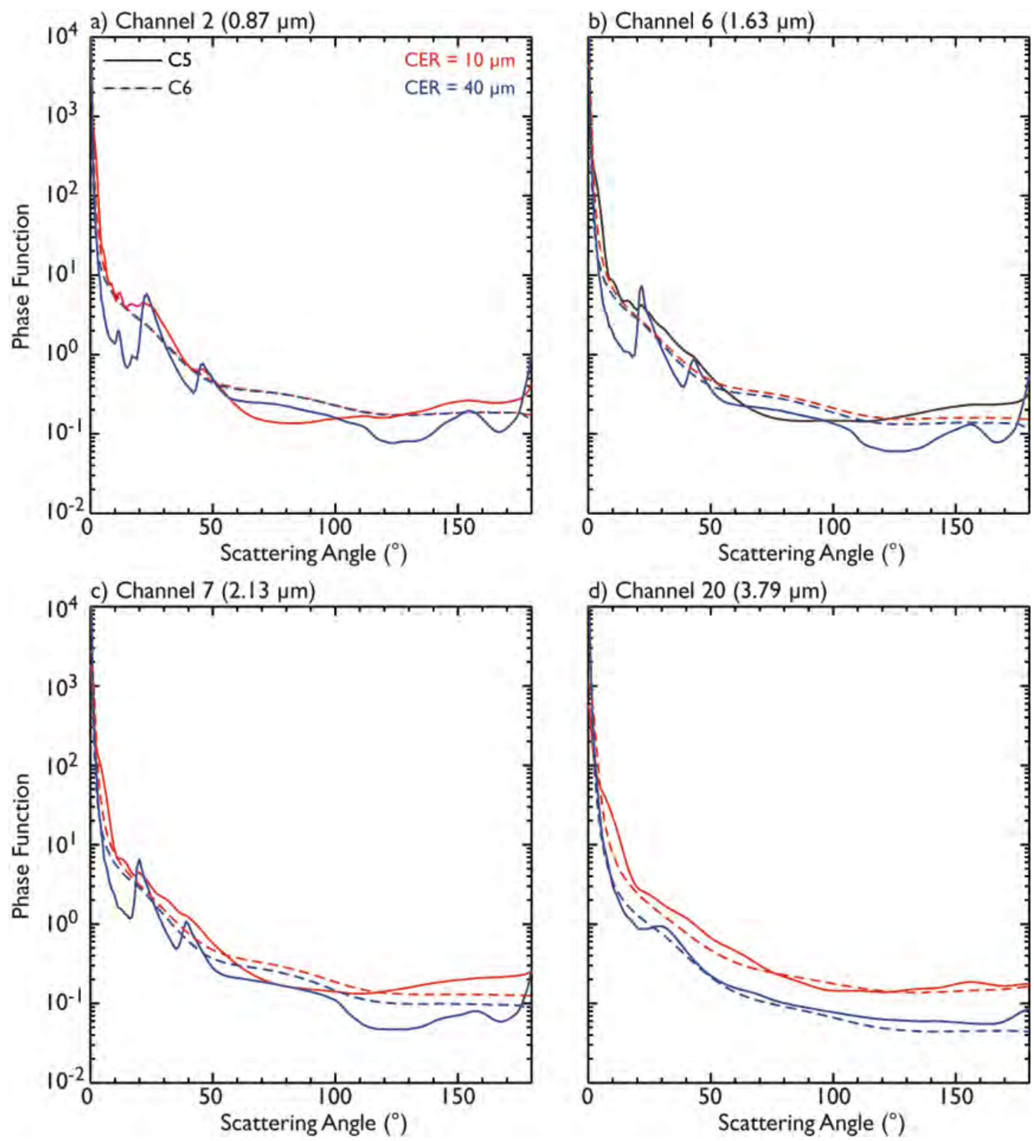


Figure 2.1-3. C5 (solid line) vs. C6 (dotted line) ice model phase functions for two effective radii (red: 10 µm; blue: 40 µm).

We have also examined the impact of effective variance ($v_e$) of the gamma size distribution on the single scattering albedo of roughened aggregate columns (cf. Figure 2.1-2c and 2.1-2d for 2.13 and 3.7 µm, respectively). Although the true effective variance of ice clouds is not known, we have chosen to use an effective variance of 0.1 in the C6 models, consistent with the liquid water gamma distribution models. Note the sensitivity to this assumption is considered in calculating retrieval uncertainty estimates (Sect. 2.7).

The ice and liquid water scattering properties (asymmetry parameter, single scattering albedo, and extinction efficiency) used in the C6 LUTs are provided in the MOD06 L2 data file and in **Appendix D**. They are provided for seven MODIS spectral channels and 18 and 12 CERs for liquid and ice phase, respectively. The 2-D parameter SDSs for ice phase are named *Asymmetry_Parameter_Ice*, *Single_Scatter_Albedo_Ice*, and *Extinction_Efficiency_Ice*. An example of the C6 ice model phase functions for four MODIS channels are shown in **Fig. 2.1-3** along with the corresponding C5 phase functions. With these parameters, a user can scale MODIS ice retrievals to other model scattering property assumptions using scaling formulae similar to Eq. 2.1-1 (see Sect. 5 FAQ).

## 2.2. Wind-speed Interpolated Ocean Bidirectional Reflectance Properties

Look-up-tables (**LUTs**) for the reflection function of clouds overlying an ocean surface subject to non-isotropic reflection are now used. The ocean bidirectional reflectance model uses the wind speed and direction-dependent Cox-Munk wave-slope distribution [*Cox and Munk*, 1954]. Separate LUTs were calculated for three different wind speeds (3, 7, and 15 m s$^{-1}$), each one averaged over four vector wind directions (0, 90, 180, and 270° relative azimuth). Pigment concentration and salinity are set to 0.15 mg m$^{-3}$ and 34 parts-per-thousand, respectively. A parameterization for white cap (foam) reflectance is taken from *Koepke* [1984]. Consequently, the LUTs now more accurately model the reflectance of optically thin clouds over the ocean that are sensitive to the non-isotropic sunglint distribution. In C5 and earlier collections, all reflectance of the underlying surface, both land and ocean, were modeled as Lambertian (isotropic), with an ocean surface albedo $A_g = 0.05$ that is characteristic of diffuse illumination. While the Lambertian ocean surface assumption is appropriate for sufficiently optically thick clouds, it is especially prone to errors for thin clouds near and away from sunglint. Our analysis shows that once COT becomes less than about 3, large differences are observed in cloud top reflectance between a Cox-Munk surface and a Lambertian surface with $A_g = 0.05$. Consequently, the 10 m altitude wind speed over the ocean is now a required ancillary field and is obtained from the NCEP GDAS model.

**Figure 2.2-1** shows calculations of the cloud top bidirectional reflectance distribution function for both (a) liquid water and (b) ice clouds overlying an ocean surface. The left-hand column applies to the Cox-Munk wave-slope distribution model and the right-hand column applies to a Lambertian ocean surface. The calculations are for a solar zenith angle $\theta_0 = 18.2°$ and COT = 1, with a wind speed of 1 m s$^{-1}$ for the Cox-Munk model. With the Lambertian model, the cloud top reflectance is more isotropic, and generally brighter away from sunglint, whereas for a more realistic Cox-Munk distribution the ocean reflectance is darker away from the sunglint angles. For optically thin clouds where sunglint and the ocean reflectance is more apparent, this modification to the surface scattering model leads to more accurate COT and CER retrievals, and generally fewer failed retrievals. **Fig. 2.2-2** shows the same cloud-top reflectance distribution function but for COT = 4. At this optical thickness, there is little distinction between the two surface models.

However, the accuracy of the Cox-Munk reflectance distribution for this application is not obvious given the practical need for ancillary ocean surface wind speed data (coarse resolution) over large geographic regions. An empirical evaluation of the model is shown in **Figure 2.2-3**. Here MODIS 0.86 µm clear sky reflectances are calculated for two MODIS Terra sunglint scenes. To understand the sensitivity to the clear sky atmospheric constituents, calculations are made with no Rayleigh scattering (green line) and Rayleigh scattering plus a coarse-mode sea-salt boundary layer aerosol model of optical thickness 0.1 (blue line). The average of five individual pixel scan lines (taken every 10th line) are used to compute the mean reflectance and azimuth and zenith angles. Ocean surface wind speeds are temporally interpolated from the 1° NCEP GDAS 10 m wind data for that day and location. Calculated

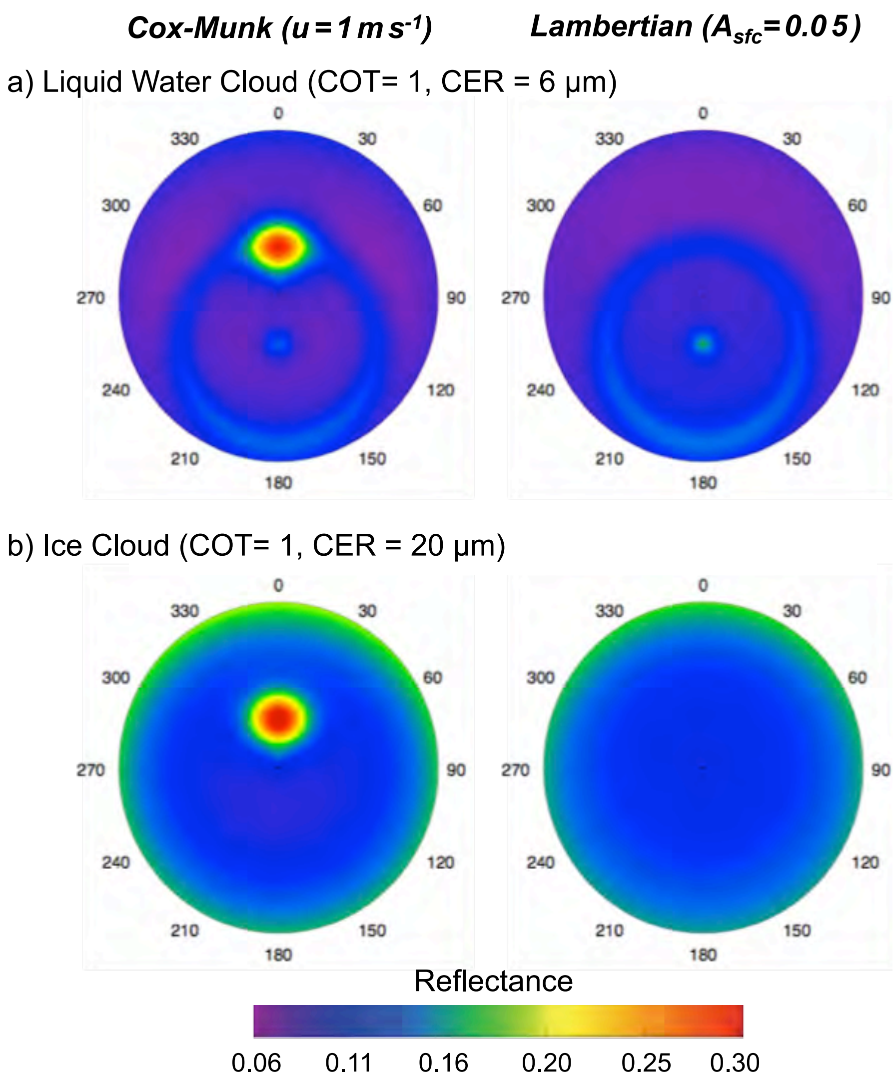


Figure 2.2-1. The angular cloud top distribution of reflectance in MODIS channel 1 (0.66 μm) for COT = 1 overlying the ocean surface for (a) liquid water clouds (CER = 10 μm) and (b) C6 ice cloud model (CER = 20 μm). The left-hand column applies to a Cox-Munk surface reflectance model with a wind speed of 1 ms$^{-1}$; the right-hand column applies to a Lambertian surface reflectance model with a surface albedo of 0.05 (used in C5). The glory and rainbow scattering pattern for water clouds is evident.

reflectance compares well with the observations away from the glint, but there is a significant difference near the glint peak, especially for the October scene. Note a default pristine aerosol optical depth (AOD) of 0.1 is used in calculating the ocean LUTs; it was found that the MOD04 AOD was nominally around 0.1 in the non-glint regions of these granules and therefore would not explain the differences. However, a reasonable match was obtained in both the glint peak and tail regions if the wind speed was increased by about 4 m s$^{-1}$ and 1 m s$^{-1}$ for the May and October granules, respectively (not plotted). This suggests caution in using thin cirrus and other small COT retrievals in sunglint, though surface sensitivity may be accounted

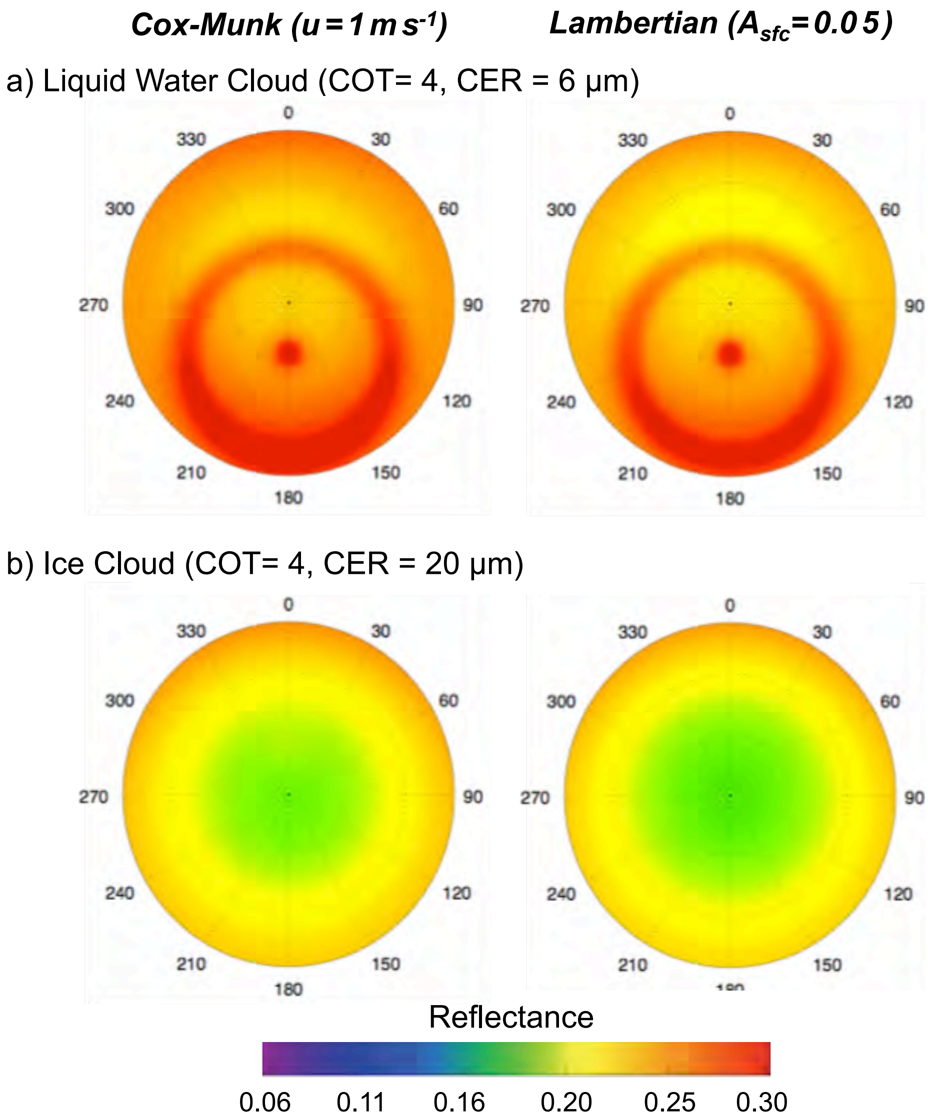


Figure 2.2-2. Same as Fig. 2.2-1 except COT=4.0.

for to some extent in the retrieval uncertainties that include a wind speed/direction error source (Sect. 2.7).

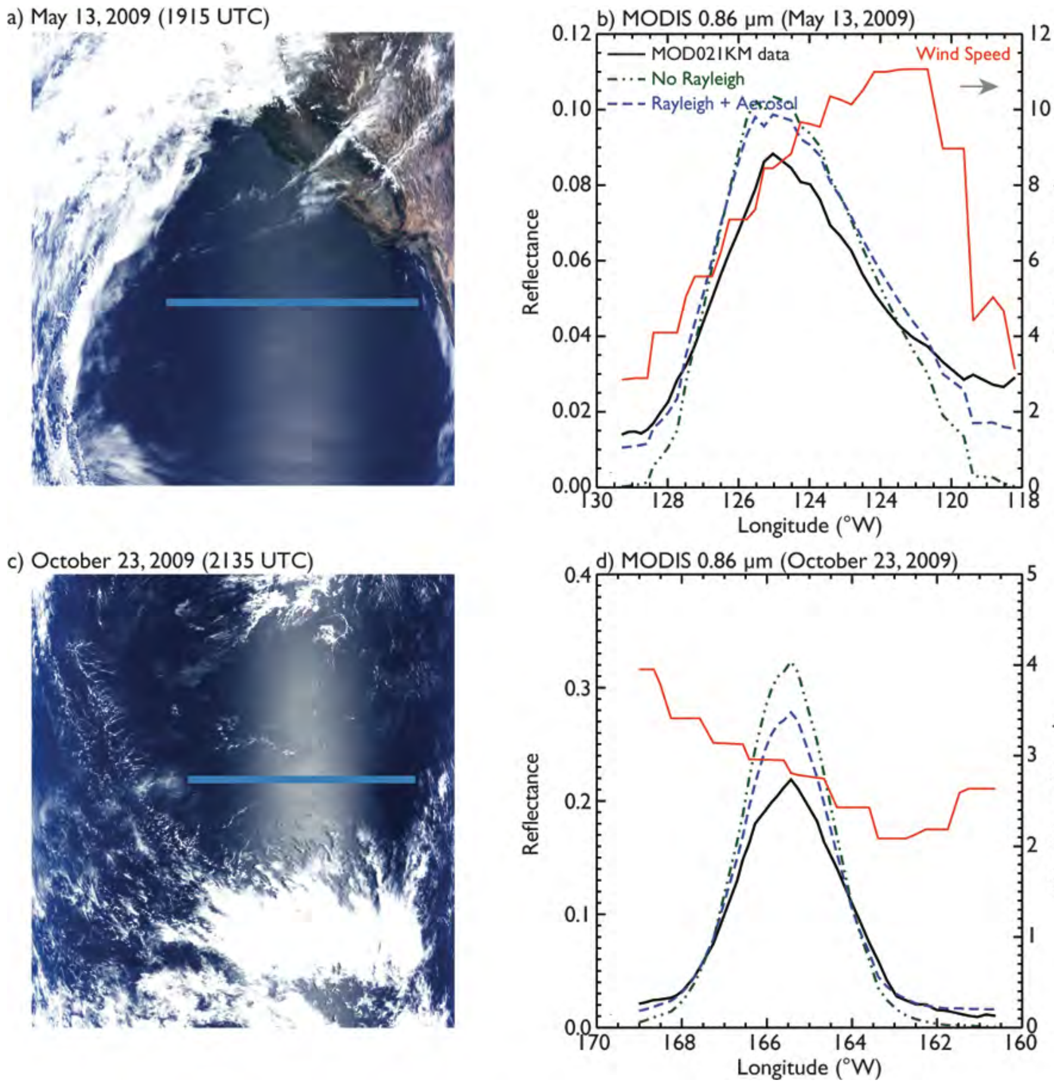


Figure 2.2-3. Cross section (blue rectangle) of the observed and calculated clear sky reflectances with the Cox-Munk surface bidirectional reflectance model in channel 2 for two MODIS Terra sunglint scenes. Ocean surface wind speeds are take from NCEP analysis.

### 2.3. New Gap-filled Spectral Surface Albedo Dataset

A recently developed high-resolution spatially complete snow-free surface albedo dataset was implemented that builds on the pioneering work of *Moody et al*. [2005, 2008] that was, in turn, based on a 5 year climatology of Terra Collection 4 land surface albedo data (MOD43B3 product). The new dataset (i) utilizes a combination of both Terra and Aqua MODIS data (Collection 5) that increases the number of angular samples needed to characterize the surface bidirectional reflectance distribution function (BRDF), (ii) has enhanced spatial resolution of 30 arc sec (~1 km), (iii) increases the time sampling to an 8-day periodicity (based on 16 days of observation), (iv) uses 20 months of data to establish seasonal phenology, (v) does gap-filling based on the RossThickLiSparse reciprocal BRDF model, rather than on the white-sky albedo, and (vi) has data available for each calendar year from 2000 to 2013.

**Figure 2.3-1** shows a comparison between the new high-resolution MODIS-derived gap-filled surface albedo at 0.66 µm (the primary channel used for COT retrievals over land) on (a) January 1-8, 2006 and (c) May 27-June 3, 2007, with (b) and (d) showing the difference between these new surface albedos and those used previously in C5 (based on *Moody et al*. [2008]). Similar to Collection 5, the surface albedo of snow-covered regions is overlain on these figures using the ecosystem-dependent spectral albedo of snow derived from 5 years of

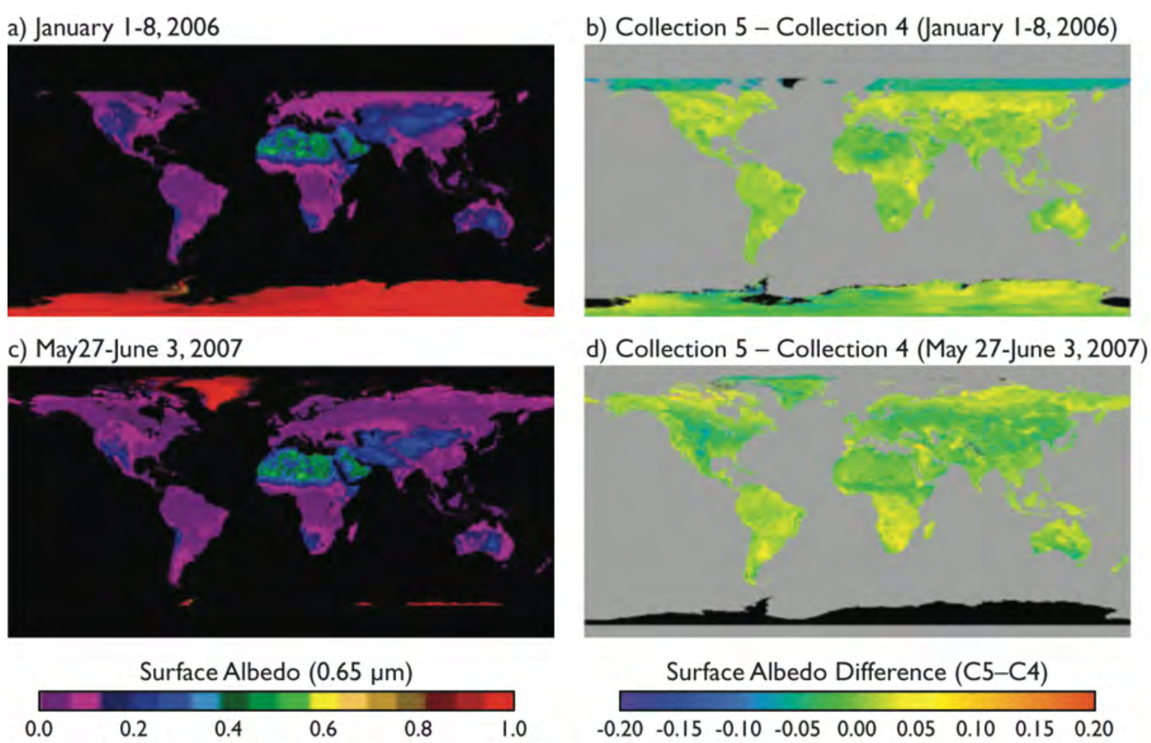


Figure 2.3-1. Spatially complete white-sky albedo at 0.66 µm after the temporal interpolation technique was applied to the 8-day periods of (a) January 1-8, 2006 and (c) May 27-June 3, 2007, with (b) and (d) showing the difference between these new surface albedos (based on C5 land processing) and the corresponding values from *Moody et al*. [2008] that were based on C4 land processing.

Terra data [Moody *et al.*, 2007], except for permanent snow regions where the new C5-derived surface albedo data set (e.g., Figures 2.3-1a and 2.3-1c) is used.

**Figure 2.3-2** shows a comparison of (a) COT and (b) CER retrievals using the new (C5 land processing) and old (C4) surface albedos, where the left hand column applies to liquid water clouds and the right hand column to ice clouds. This test run was performed for January 2006. Aside from differences in the polar region, the effects of the ancillary surface albedo change are overall quite small. Note, however, while the old albedo dataset was a 5-year climatology, the new dataset is dynamic through 2013 (the 2014+ forward processing stream uses equivalent time periods from 2013). Thus any significant changes to the land cover status in any particular year will likely affect the cloud retrievals over those areas, particularly for optically thinner clouds.

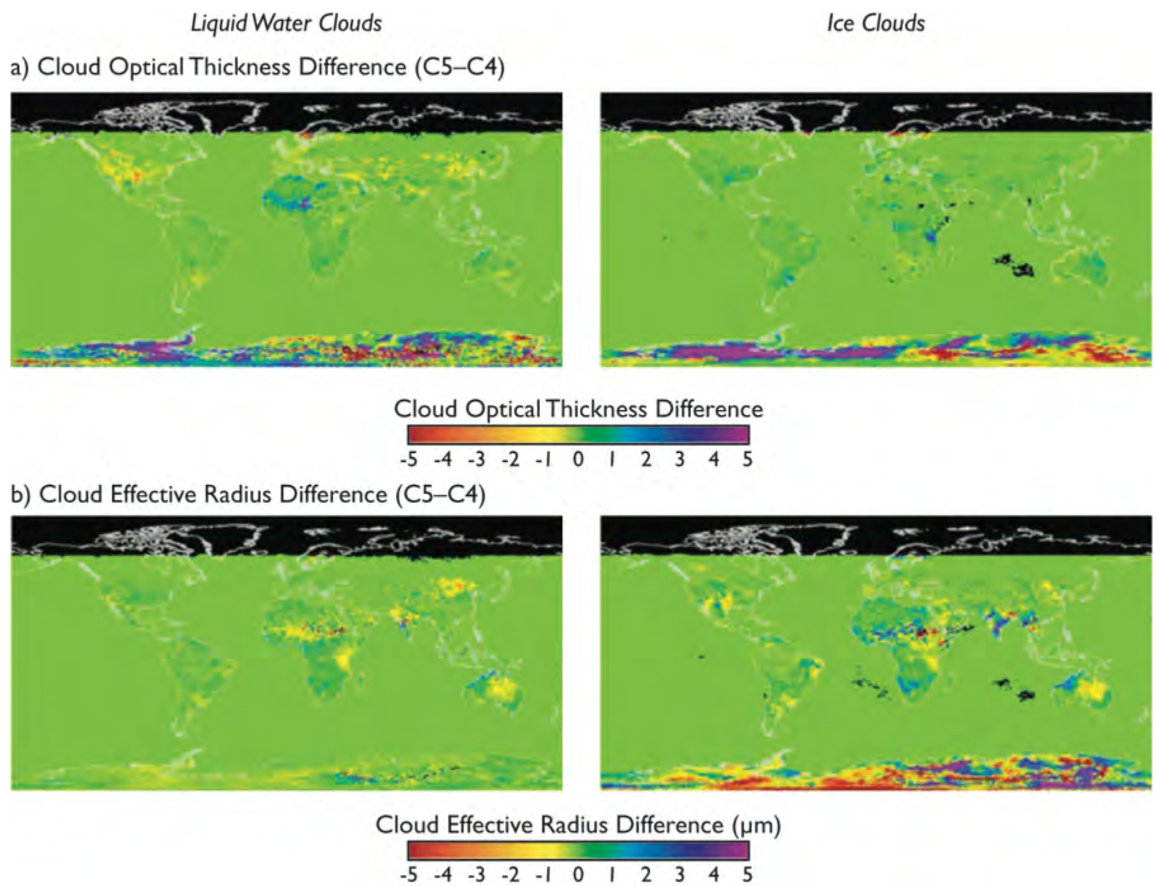


Figure 2.3-2. Differences in (a) cloud optical thickness and (b) cloud effective radius for liquid water (left column) and ice (right column) clouds for Aqua MODIS in January 2006, where an identical algorithm was run using either the new (C5) or previous (C4) spectral white-sky surface albedos. Large differences are most noticeable in polar regions.

## 2.4. Improved Shortwave-Derived Cloud Thermodynamic Phase

Cloud thermodynamic phase classification is a critical initial step in the MOD06 retrieval process. Because ice and liquid phase clouds have very different scattering and absorbing properties, an incorrect cloud phase decision can lead to substantial errors in COT, CER, and CWP. For C6, the cloud thermodynamic phase algorithm has been completely redesigned. Changes include: (i) a new cloud phase discrimination logic, (ii) removal of the use of cloud mask tests (see MODIS C5 Cloud Phase flowchart), and (iii) replacement of the C5 SWIR/NIR reflectance ratio tests with logic utilizing separate ice and liquid phase spectral CER retrievals (though the ratio tests are retained for thin clouds over snow and ice surfaces).

The new phase algorithm [*Marchant et al.*, 2015] was optimized via extensive global and regional comparisons between Aqua MODIS and the A-Train CALIPSO lidar (CALIOP), yielding improved skill over C5, particularly for broken clouds as well as optically thin ice cloud edges previously misidentified as liquid cloud phase; similar improvement is observed with respect to collocated polarimetric observations from the POLDER instrument (on the PARASOL mission, also in the A-Train). As in C5, cloud phase results are reported in an independent SDS (**Table 2.4-1**) and in heritage QA bits in the *Quality_Assurance_1km* SDS.

Table 2.4-1: SDS name for the cloud thermodynamic phase algorithm used to determine the phase reported by the optical retrieval algorithm.

| Dataset | SDS Name |
|---|---|
| Cloud Thermodynamic Phase used in Optical Retrievals | Cloud_Phase_Optical_Properties |

### 2.4.1. *Phase retrieval algorithm overview*

All MOD/MYD35 cloudy or probably cloudy pixels, excluding those identified as not cloudy by the Clear Sky Restoral (CSR) algorithm (see **Section 2.8**), pass through the cloud thermodynamic phase classification logic shown in **Appendix E**. The C6 logic includes the tri-spectral IR phase result [*Baum et al.*, 2012] that is separately reported in the SDSs *Cloud_Phase_Infrared_1km* and *Cloud_Phase_Infrared* (5km dataset), cloud top temperature (**CTT**) tests, and ice and liquid spectral CER retrieval tests; all tests provide a signed integer result (positive for liquid, negative for ice, 0 for undetermined) with the total sum determining the phase. Final phase results are reported in the *Cloud_Phase_Optical_Properties* SDS as integer values as described in **Table 2.4-2**.

It is important to understand that, similar to C5, pixels having undetermined phase are processed as liquid phase, though they are excluded from the liquid retrieval population in L3 aggregations, and are in fact aggregated separately. Note also that cloud phase is reported for all cloudy pixels regardless of the success of the optical/microphysical retrievals, including

Table 2.4-2: Summary of reported values in the Cloud_Phase_Optical_Properties SDS and C5-heritage QA bits.

| SDS (or QA Bit) Value | Phase Result |
|---|---|
| 0 | Cloud Mask unavailable, missing data, etc.: *No Phase Result* |
| 1 | Cloud Mask Clear or Probably Clear, or Pixel Restored to Clear Sky: *No Phase Result* |
| 2 | *Liquid Water* |
| 3 | *Ice* |
| 4 | *Undetermined* |

those pixels identified as partly cloudy by the CSR algorithm (see **Section 2.8**) or those lying outside the retrieval solution space (see **Section 2.6**).

*2.4.2. C6 changes*

For C6, the NIR-SWIR cloud thermodynamic phase algorithm has been completely re-written in an effort to improve the phase discrimination skill for a variety of cloudy scenes (e.g., thin/thick clouds, over ocean/land/desert/snow/ice surface, etc.). While the C5 phase algorithm used a linear sequential logic structure, which makes it difficult to improve and adapt to a large variety of cloud scenes, the new C6 phase algorithm uses a voting discrimination logic that includes several tests providing signed integer votes of different weights. The voting weights have been optimized through extensive comparisons between Aqua MODIS and the collocated CALIOP cloud layer products, with further evaluation using POLDER.

Four main categories of cloud phase tests comprise the C6 phase algorithm (see the flowchart in **Appendix E** for details):

1. *Tri-Spectral IR Tests*: These tests (actually including a 4th IR water vapor channel) use the results of the 1 km IR cloud thermodynamic phase algorithm [*Baum et al.,* 2012] that is run as part of the MOD06 Cloud Top Properties algorithm.

2. *Cloud Top Temperature Tests*: These tests use the MOD06 1 km CTT retrievals. Note the C5 warm cloud sanity check, in which the phase is forced to liquid when CTT > 270 K, was retained in modified form for C6 (mainly as a larger liquid phase vote), though only when retrieved liquid phase COT > 2.

3. *1.38 μm Channel Test*: This test uses the 1.38 μm high cloud flag from the MOD35 cloud mask product. The capacity of this test to discriminate high-altitude ice clouds from low-altitude liquid clouds is based on the strong water vapor absorption at 1.38 μm [*Gao*

*et al.*, 1993]. Note that this test is applied only when sufficient water vapor is present (roughly 1 cm perceptible water) and ice phase COT < 2 to avoid spurious ice votes in the case of optically thick liquid clouds. In C5 this test was used only when the bi-spectral IR cloud phase decision was undetermined.

4. *Spectral Cloud Effective Radii Tests*: These tests replace the C5 SWIR/NIR reflectance ratio tests. While it is difficult to define linear reflectance ratio thresholds to discriminate ice and liquid phase pixels, since reflectance ratios might depend on COT, viewing geometries, etc, CER retrievals implicitly account for such dependencies. **Figure 2.4-1** shows an example of the retrieval solution space for COT and CER over a dark surface for the geometry specified in the figure. The red and blue curves are computations for liquid and ice phase clouds, respectively. Some of the solution space is unambiguously liquid water and some unambiguously ice, but there are overlapping regions in which either thermodynamic phase leads to a viable physical solution. Comparison of retrievals using all three SWIR wavelengths can reduce this ambiguity in the choice of thermodynamic phase. The approach to using this information is described in the flow chart in Appendix E (see panel AE-2). To implement these tests, the C6 optical retrieval algorithm needs to attempt CER retrievals twice, once for each phase, thereby doubling the processing time devoted to the retrieval solution logic.

Evaluation over a wide variety of granules shows an overall improvement of the thermodynamic phase determination as compared with C5, especially for optically thin clouds on the

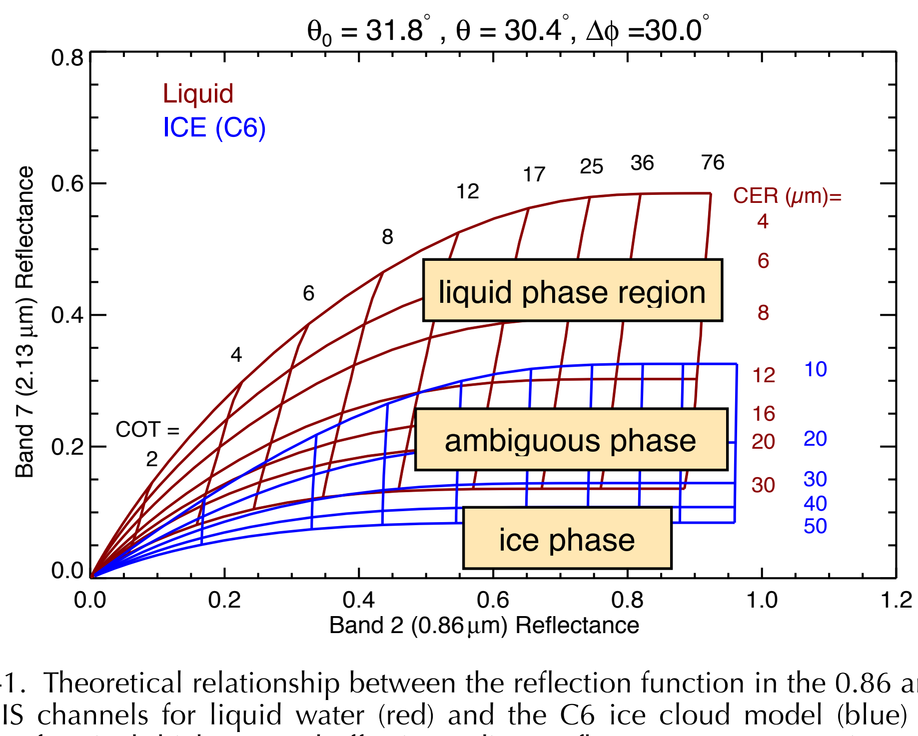


Figure 2.4-1. Theoretical relationship between the reflection function in the 0.86 and 2.13 μm MODIS channels for liquid water (red) and the C6 ice cloud model (blue) for various values of optical thickness and effective radius. Reflectances can occur in regions of the solution space that are unambiguously liquid or ice, but may also lie in regions that are ambiguous regarding phase.

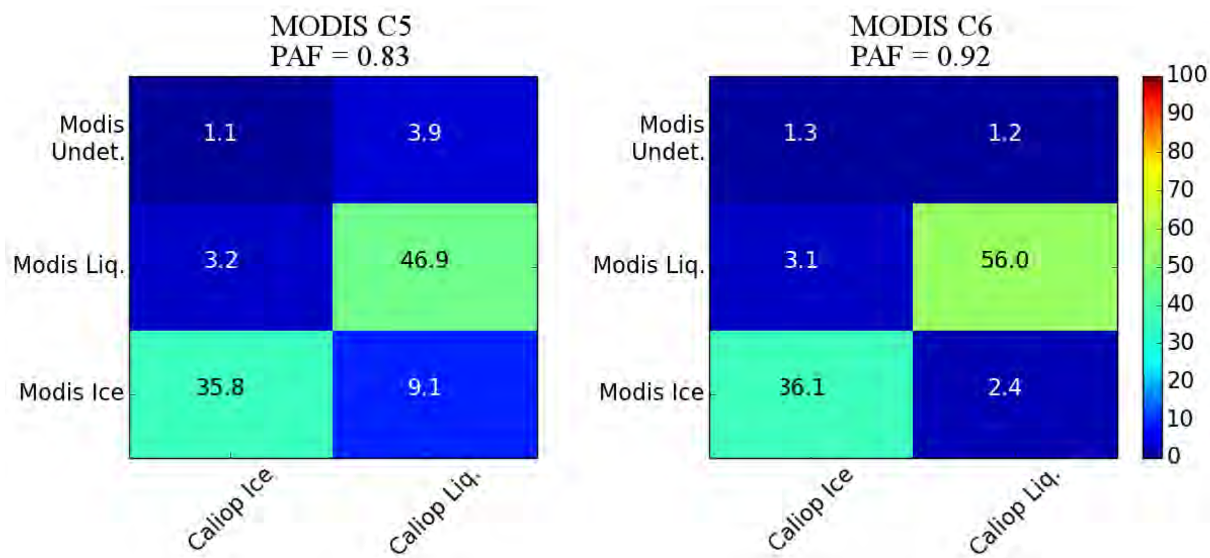


Figure 2.4-2. Global evaluation of the Aqua MODIS C5 and C6 NIR-SWIR thermodynamic phase algorithms vs. CALIOP over all surface types during January 2008. The population is from all collocations where CALIOP observed a single phase in the column. The overall Phase Agreement Fraction (PAF) skill score increases by ~10% for C6.

edge of cloud fields that were previously misidentified as liquid water clouds. The evaluation methodology and results are described in the following section (2.4.3).

### *2.4.3. Phase algorithm evaluation*

To evaluate the performance of the C6 cloud thermodynamic phase algorithm, extensive granule-level and global comparisons have been conducted against the heritage C5 algorithm, CALIOP, and POLDER. A wholesale improvement is seen for C6 compared to C5.

**Figure 2.4-2** shows a summary skill table comparing Aqua MODIS C6 phase results to the collocated CALIOP v3 Cloud Layer product for global scenes (all surface types) where CALIOP identified a single phase in the column during January 2008. Both 1 km and 5 km CALIOP cloud layer products are used, with the 5 km product (more sensitive to thin cirrus) sampled to 1 km resolution and merged with the 1 km product. When a cloud layer is present in only one of the products, or when a cloud layer is present in both products and the phase is in agreement, that profile is used in the skill assessment; when a cloud layer is present in both products but the phase is inconsistent, that profile is not used. Assuming CALIOP as "truth," the skill of the C6 NIR-SWIR phase algorithm can be defined as the number of collocated cloudy pixels for which MODIS and CALIOP cloud phase are in agreement divided by the total number of collocated cloudy pixels (including undetermined MODIS phase retrievals). This skill definition is referred to as the **Phase Agreemen**t **Fraction** (**PAF**). The C6 PAF is 0.92 for all global collocations, indicating that the MODIS C6 NIR-SWIR phase agrees with CALIOP for 92% of all collocated CALIOP profiles that meet the above criteria. This is a marked improvement over the C5 PAF of 0.83. The global PAF for single-phase cloud layers over different surface types and for optically thin (non-opaque for CALIOP) and opaque

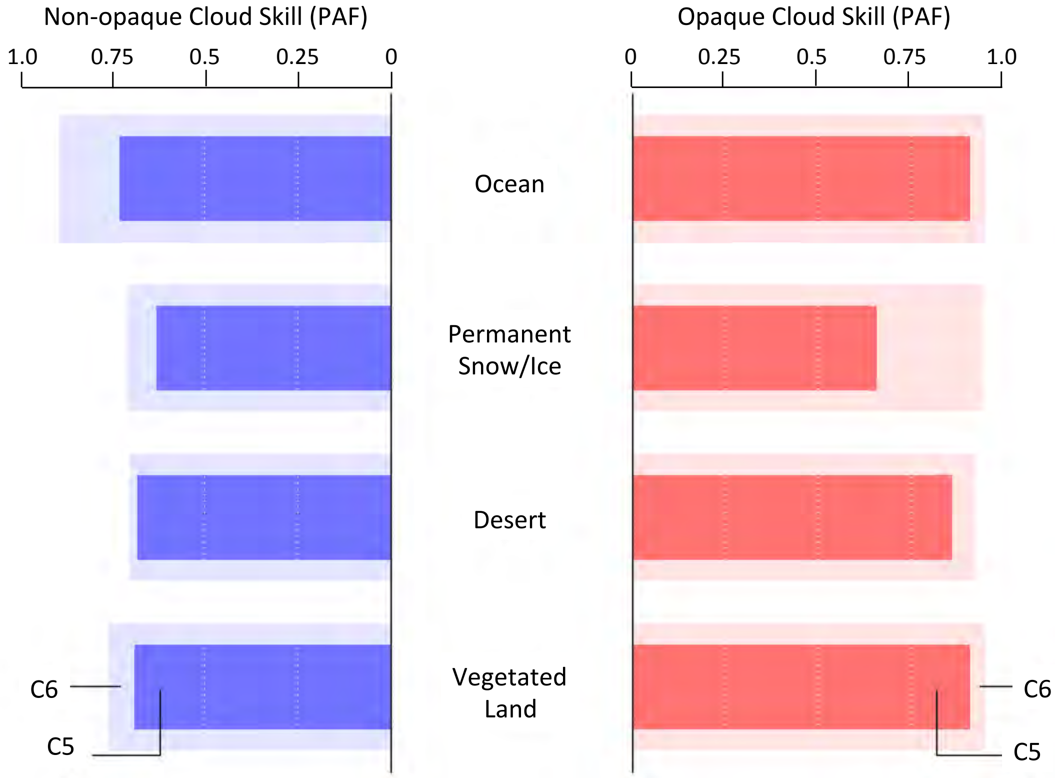


Figure 2.4-3. Global evaluation of the Aqua MODIS C5 and C6 thermodynamic phase algorithms vs. CALIOP, categorized by surface type, during January 2008. The population is from all collocations where CALIOP observed a single cloud phase throughout the column. The bar plots to the left are for scenes where the lidar was not completely attenuated by the cloud layers (COT less than about 3); bars to the right are for scenes where the lidar was completed attenuated (no ground return).

cloudy columns is shown in **Figure 2.4-3** where dark and light shading corresponds to the C5 and C6 phase algorithms, respectively. Over all surface types for this month, the C6 algorithm has a higher PAF score than C5. The greatest improvements are seen for opaque clouds over permanent snow/ice (e.g., Greenland, Antarctica) and thin clouds over the ocean; more minor differences are found for thin clouds over non-polar desert regions and opaque clouds over vegetation. Global gridded PAF for January 2008 is shown in **Figure 2.4-4** for the (a) C5 and (b) C6 phase algorithms. Again, C6 improvement over C5 is evident in nearly all regions of the globe for this month and year.

**Figure 2.4-5** shows global gridded maps of C5 and C6 phase fractions for January 2008. For C5, fractions only include those pixels for which successful retrievals were obtained and the CSR algorithm indicated that the pixel was "overcast" (see Sect. 2.8). For C6, however, the pixel population includes successful "partly cloudy" PCL pixels as well as failed retrievals; no retrievals were attempted on PCL pixels in C5. Therefore the figure shows C6 results with a C5-equivalent filtering (CSR=0, middle panels) along with the full population (lower panels). Several differences are worth noting. Most obvious is that the C6 algorithm yields an increase in liquid phase over the southern oceans, along with a corresponding de-

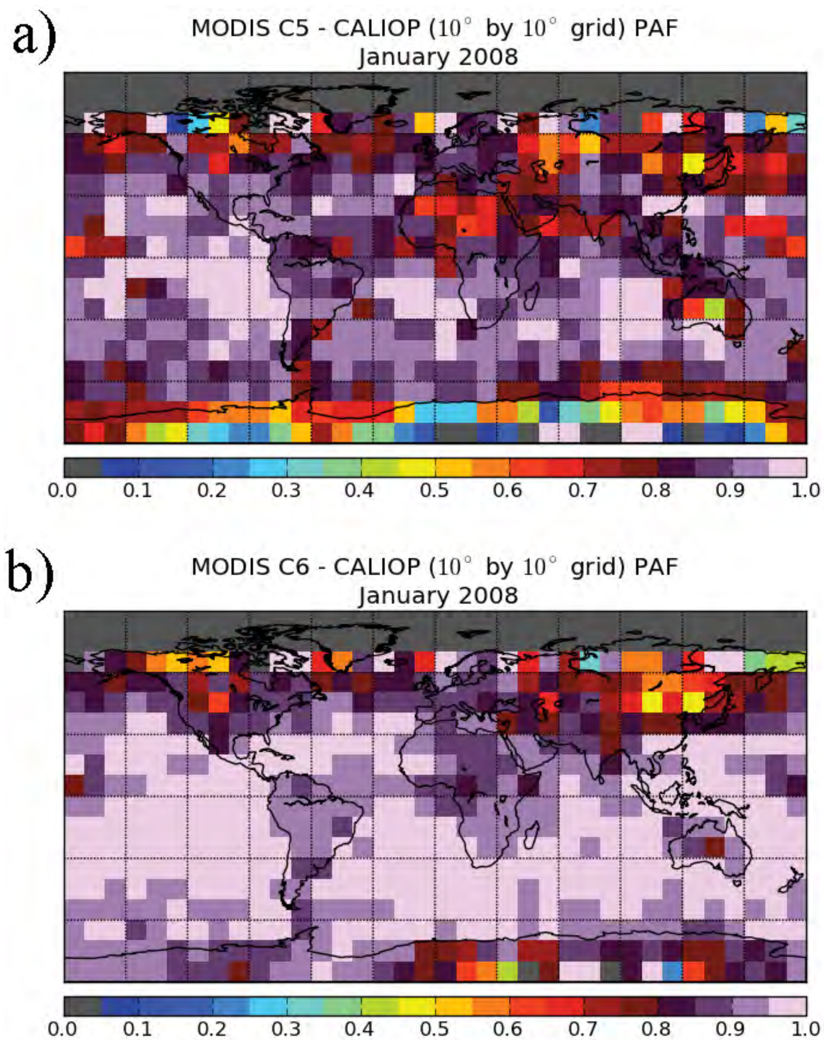


Figure 2.4-4. Global gridded PAF for the (a) C5 and (b) C6 NIR-SWIR thermodynamic phase algorithm during January 2008. The population is from all collocations where CALIOP observed a single cloud phase throughout the column.

crease in ice phase. There is also an increase in liquid phase over many non-polar vegetated land areas, though there is a notable decrease in south America.

**Figure 2.4-6** shows an example thermodynamic phase comparison between C5 and C6 for a selected Aqua MODIS granule. Panel (a) is a true color image showing optically thin cirrus clouds and low marine boundary layer clouds off the west coast of northern Africa. Panel (b) shows the 1 km cloud top temperature retrievals, and panels (c) and (d) show the retrieved phase of this granule using the C5 and C6 algorithms, respectively. Note the improved identification of ice phase clouds on the edge of optically thin cirrus clouds (especially over the desert) and liquid water clouds in the low boundary layer.

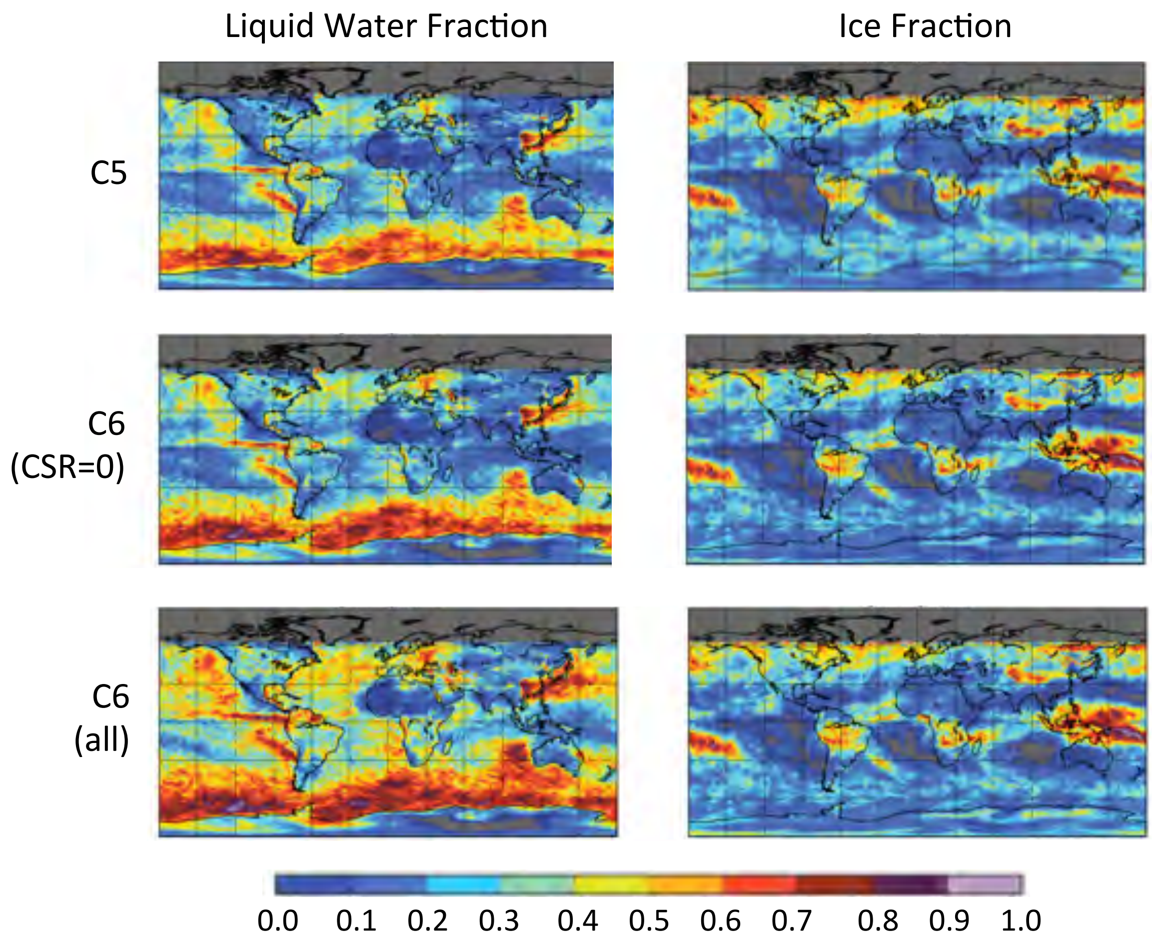


Figure 2.4-5. Global cloud thermodynamic phase comparisons between C5 and C6 for January 2008 (Aqua). Note that cloud phase in C6 is reported for all cloudy pixels having successful or partially successful optical/microphysical retrievals, including those identified as partly cloudy (see Sect. 2.8) as well as those lying outside the retrieval solution space (Sect. 2.6).

### *2.4.4. Known issues*

Although the C6 cloud phase discrimination algorithm is significantly improved over C5, some situations continue to be problematic. Examples include:

- *Optically thin cirrus over warm surfaces*: A particularly acute problem in C5, some thin cirrus may continue to be incorrectly identified as liquid phase over warm surfaces, though C6 provides better skill in such circumstances.

- *Broken liquid phase clouds*: False ice phase discrimination is greatly improved in low maritime broken cloudy scenes, though still evident. However, these pixels are often associated with partly cloudy scenes as identified by the CSR algorithm and are thereby provided in separate *_PCL SDSs (see Sect. 2.8). An example is shown in **Fig. 2.4-7**. Note the better identification of liquid phase clouds in the low boundary layer (verified by CALIOP and cloud top temperatures) with fewer occurrences of ice phase in the center of small cells in the eastern part of the granule (see zoomed panels). In addition to having fewer spurious ice results, many of the broken cloud edges are identified in C6 as “undetermined,” which is often a safer choice in these problematic clouds.

- *Oblique sun angles*: In some particular viewing geometries with large solar zenith angles, the CER tests may yield incorrect phase results.

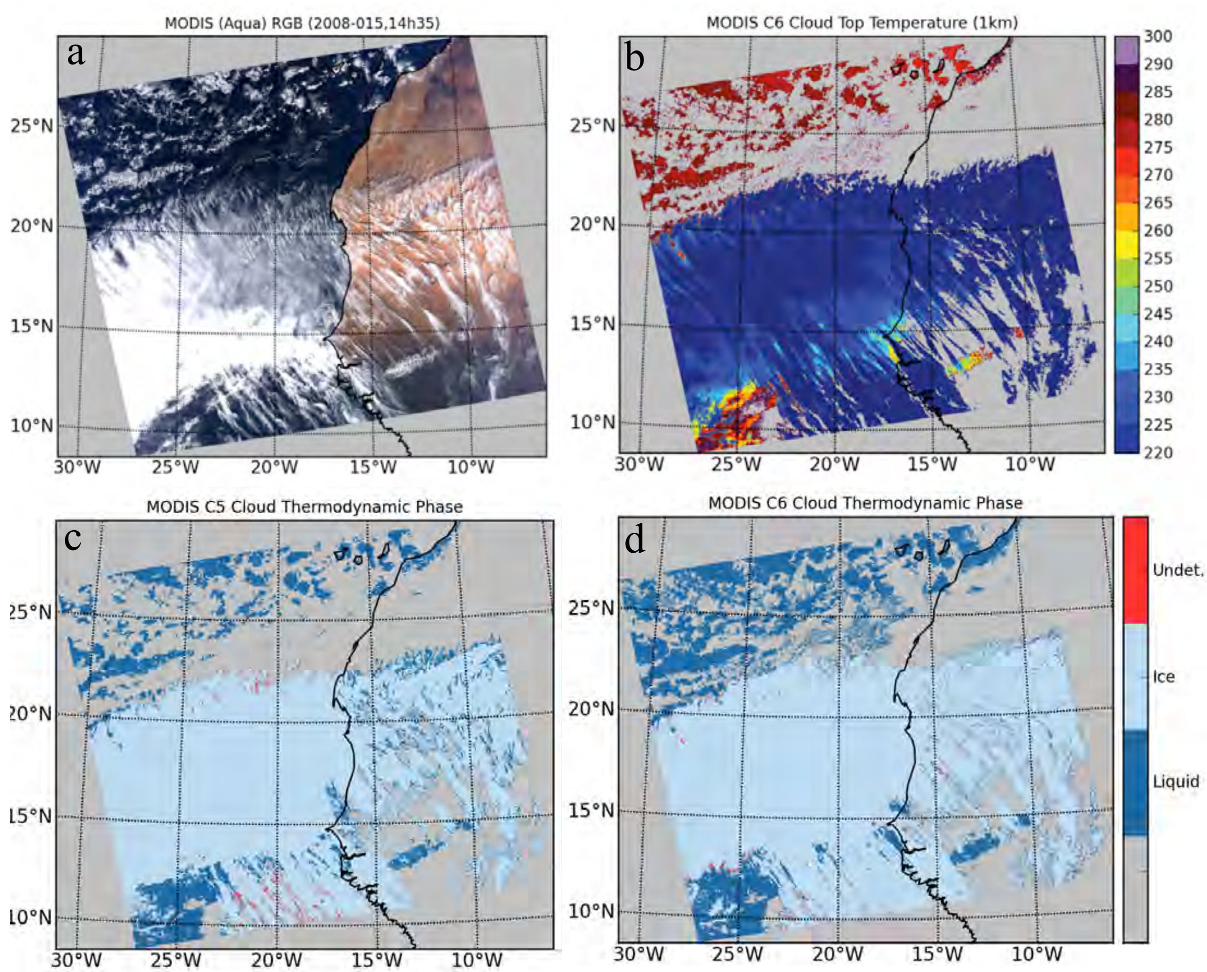


Figure 2.4-6. Example C5 and C6 phase retrievals for an Aqua MODIS granule centered off the coast of north Africa containing a combination of high clouds and marine boundary layer clouds (RGB composite in (a)). 1 km cloud top temperatures from MYD06 are shown in (b), while C5 and C6 phase results are in (c) and (d), respectively.

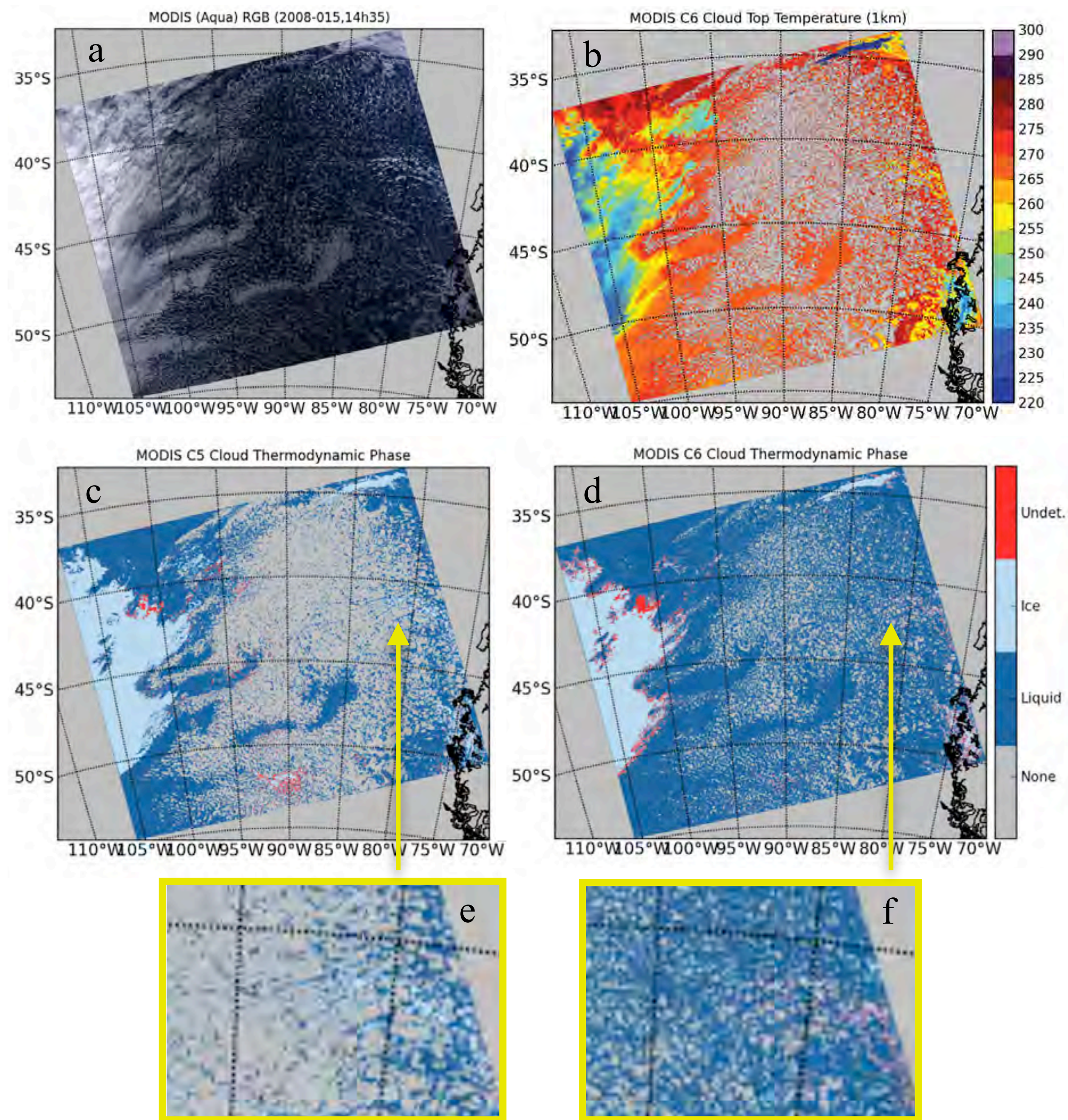


Figure 2.4-7. Example C5 and C6 phase retrievals for an Aqua data granule showing low marine clouds through much of the central/eastern portion of the image (RGB composite in panel a). Cloud-top temperatures from MYD06 are shown in panel b, while C5 and C6 phase are in panel c and d, respectively. An area with substantial broken clouds is shown in the bottom two panels (e and f) indicating less ice cloud retrievals for the C6 phase algorithm.

### 2.5. Separate Cloud Effective Radius Retrievals from 1.6, 2.1, and 3.7 μm

Cloud effective radius, optical thickness, and water path retrievals are now performed and reported separately for VNSWIR-SWIR channel pairs that include the 1.6 and 3.7 μm channels, to complement the heritage retrievals using the 2.1 μm channel. These spectral retrievals were also performed in C5 (and C5.1), though only the size results were reported, and then only as CER differences with respect to 2.1 μm (i.e., CER(1.6 μm)-CER(2.1 μm), CER(3.7 μm)-CER(2.1 μm)), with the "primary" suite of retrievals being reported only for the 2.1 μm channel. By reporting the retrievals as separate SDSs for channel pairs using 1.6, 2.1, and 3.7 μm, it is now possible to do analyses and L3 aggregations that enable improved spectral retrieval intercomparisons. **Table 2.5-1** gives the new C6 SDSs along with those from C5.

In addition to the desired result of enabling easy intercomparisons of the three retrieval outcomes, it is important to appreciate that the three different spectral cloud retrievals have sometimes dramatically different failure patterns [*Cho et al.*, 2015]. For example, retrievals sometimes fail (i.e., the observed reflectances lie outside the COT-CER LUT solution space) using the VNSWIR and 2.1 μm channel pair but may yield a successful retrieval using the VNSWIR and 3.7 μm channels (see Sect. 2.6 for retrieval failure details). Therefore, the pixel population comprising one retrieval pair may be significantly different than another; this can be particularly true for broken liquid water cloud scenes where cloud heterogeneity scales are on the order of, or less than, the 1 km nadir pixel scale and/or for cases where a significant drizzle mode is found in the column [*Lebsock et al.*, 2011; *Zhang et al.*, 2012]. Thus the C5

Table 2.5-1. Cloud property retrieval SDS listing.

| Spectral Retrieval | C5 SDS Name | C6 SDS Name |
|---|---|---|
| Optical Thickness 1.6μm | **N/A** | **Cloud_Optical_Thickness_16** |
| Effective Radius 1.6μm | **Effective_Radius_Difference (plane 1)** | **Cloud_Effective_Radius_16** |
| Water Path 1.6μm | **N/A** | **Cloud_Water_Path_16** |
| Optical Thickness 2.1μm | **Cloud_Optical_Thickness** | **Cloud_Optical_Thickness** |
| Effective Radius 2.1μm | **Cloud_Effective_Radius** | **Cloud_Effective_Radius** |
| Water Path 2.1 μm | **Cloud_Water_Path** | **Cloud_Water_Path** |
| Optical Thickness 3.7μm | **N/A** | **Cloud_Optical_Thickness_37** |
| Effective Radius 3.7μm | **Effective_Radius_Difference (plane 2)** | **Cloud_Effective_Radius_37** |
| Water Path 3.7μm | **N/A** | **Cloud_Water_Path_37** |

sampling of spectral CER differences, for instance between 3.7 and 2.1 µm, was dependent not only on the 3.7 µm retrieval success rate, but on the 2.1 µm retrieval success rate as well.

**Figure 2.5-1** illustrates the COT and CER retrievals available in C5. **Figure 2.5-2** illustrates data sets available for C6. Notice that the 3.7 µm retrieval in C6 has significantly more successful retrievals than 2.1 µm. When the 3.7 µm retrieval is stored as a difference from 2.1 µm in this particular case, as was done in C5, almost 140,000 additional successful retrievals are lost, a situation that is common. The C5 removal of successful 3.7 µm retrievals

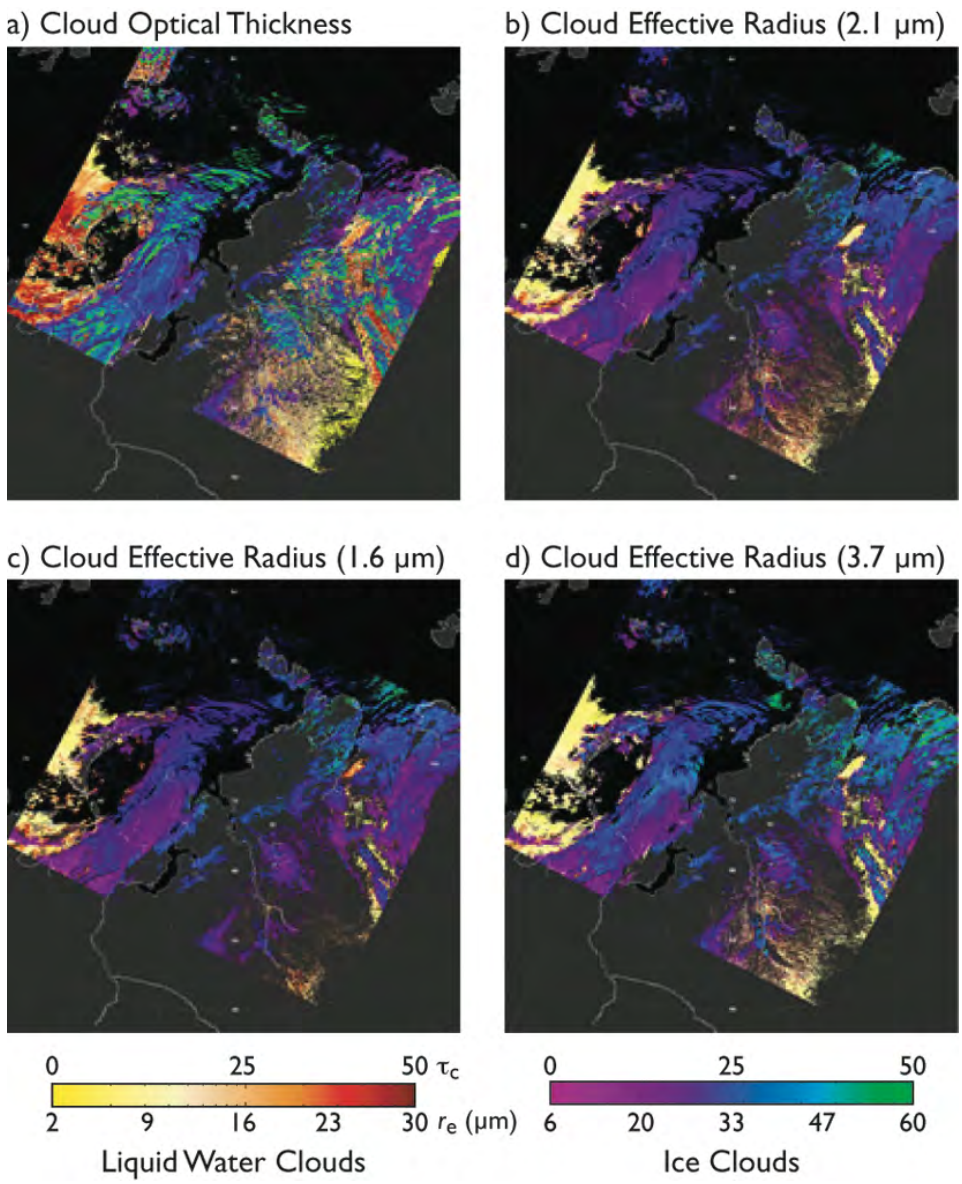


Figure 2.5-1. Terra MODIS (2005, day 091, 0635 UTC) C5 spectral CER retrievals from three channel pairs. Size retrievals from channel pairs using a VNSWIR plus the 1.6 or 3.7 µm channels were only available in C5 as differences relative to the VNSWIR and 2.1 µm channel pair, and thus were only available for successful 2.1 µm channel retrievals.

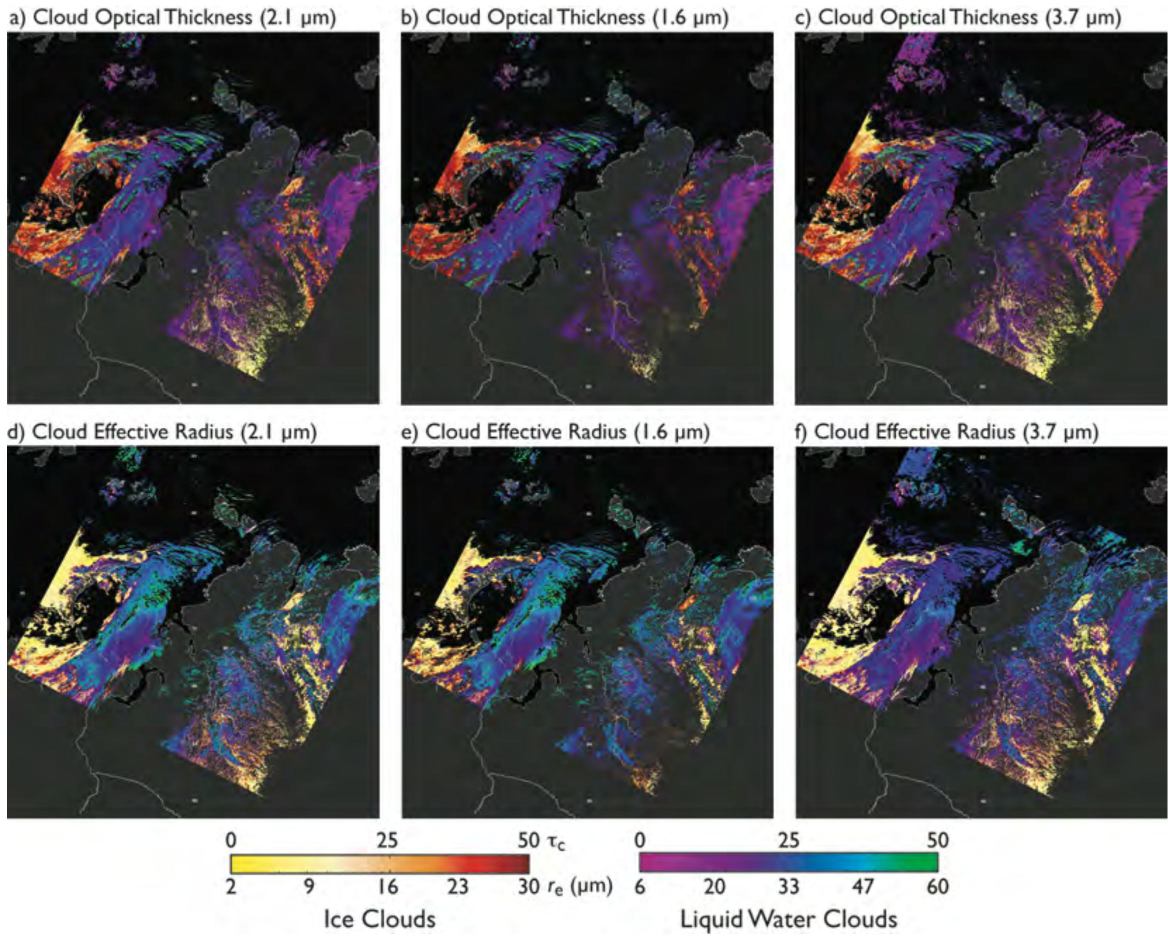


Figure 2.5-2. Same as Fig. 2.5-1 but using the new spectral CER SDSs from the C6 product. Successful retrieval fractions for retrieval pairs using the 1.6, 2.1, and 3.7µm channels are summarized in Table 2.5-2.

due to filtering by successful 2.1 µm retrievals also leads to a systematic shift in the CER retrieval statistics, as illustrated in **Figure 2.5-3** by the 3.7 µm CER histograms derived from the

Table 2.5-2. Successful cloud retrieval statistics for the data granule of Figs. 2.5-1 and 2.5-2 for pixels identified as CSR=0 .

| Retrieval Channel Pair | C5 successful retrievals (%) | C6 successful retrievals (%) |
|---|---|---|
| **VNIR + 1.6µm** | 74.2 | 64.9 |
| **VNIR + 2.1µm** | 81.7 | 76.6 |
| **VNIR + 3.7µm** | 79.3 | 86.7 |
| **Cloud Fraction** | 51.6 | 48.2 |

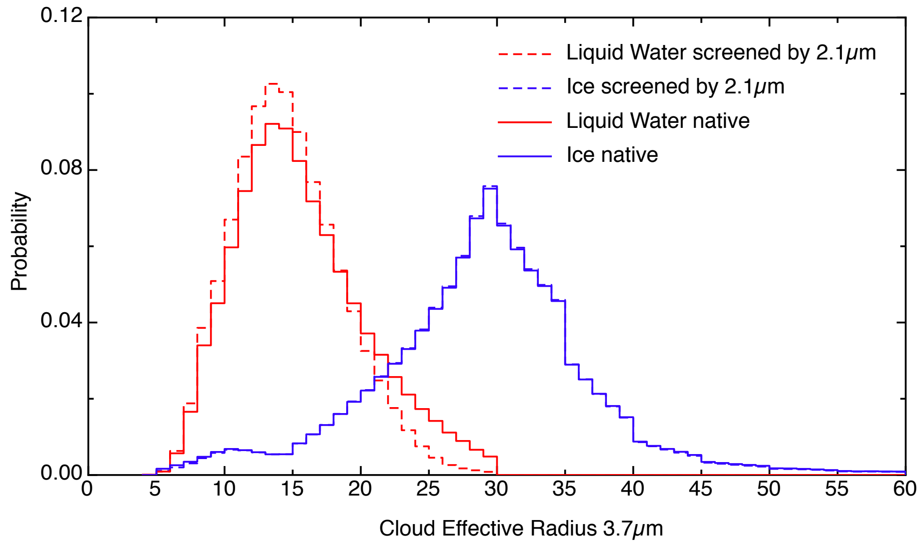


Figure 2.5-3. Set of 3.7 μm derived CER histograms based on the C6 retrievals from Fig. 2.5-2, showing sensitivity of liquid water cloud statistics to filtering by 2.1 μm successful retrievals.

granule in Figs. 2.5-1 and 2.5-2. The effect on liquid water retrievals is greater because liquid water 2.1 μm CER retrievals tend to fail more often than those at 3.7 μm, effectively removing the latter retrievals from the C5 dataset. Spectral retrieval successful fraction statistics are shown in **Table 2.5-2** for both the C5 and C6 algorithms. Note that the phase populations are

Table 2.5-3. Missing Aqua MODIS Band 6 (1.6 μm) 1 km aggregated measurement data by pixel row (with beginning of data granule as row number 1).

| Pixel Row | Status |
|---|---|
| 1 | Available |
| 2 | Available |
| 3 | Missing |
| 4 | Available |
| 5 | Available |
| 6 | Available |
| 7 | Missing |
| 8 | Missing |
| 9 | Available |
| 10 | Missing |

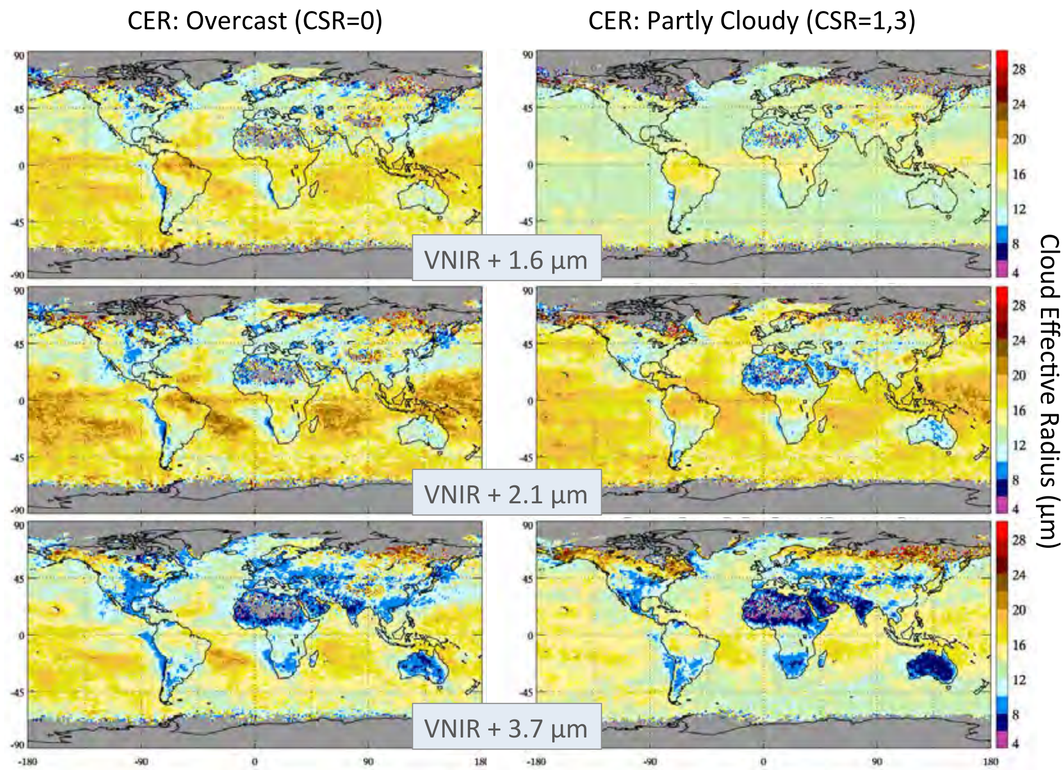


Figure 2.5-4. Aqua MODIS monthly (April 2005) mean 1° gridded effective radius for three separate SWIR/MWIR spectral channel combinations, filtered for liquid water pixels with cloud-top temperatures greater than 270K. Panels on the left are aggregated from pixels that the clear sky rostral (CSR) algorithm identifies as "overcast"; panels to the right are identified as "partly cloudy".

somewhat different between C5 and C6 (not shown), thus successful retrieval fraction results are not directly comparable.

**Figure 2.5-4** shows monthly mean gridded CER maps (Aqua MODIS, April 2005, 1° grid) for the main three spectral channel combinations. For this month, the successful VNIR + 2.1 µm effective radius retrievals (**CER_2.1**) generally exceed those of the other channel combinations in most grid boxes, regardless of whether the pixels were identified by the CSR algorithm as overcast or partly cloudy (i.e., CER_2.1 > CER_1.6 > CER_3.7), a result consistent with the findings of *Nakajima et al.* [2010]. Further, partly cloudy pixels have significantly smaller CER than the overcast pixels; this is surprising given the expectation of a general overestimate of CER in marine boundary layer broken cloud scenes due to the use of plane-parallel forward models (e.g., *Zhang and Platnick* [2011]; *Zhang et al.* [2012]). However, analysis of Terra means (not shown) are more consistent with those studies in that CER_1.6 increases such that CER_1.6 ~ CER_2.1 > CER_3.7. We note that the Aqua 1.6 µm channel, with native 500 m resolution, has 13 inoperable detectors. While the quality of the remaining detectors and their aggregation to the 1 km L1B file used by MYD06 is not suspect at this time, further study of individual detector results is warranted. For users interested in looking at individual L2 CER_1.6 retrievals, **Table 2.5-3** indicates which aggregated 1.6 µm 1 km pix-

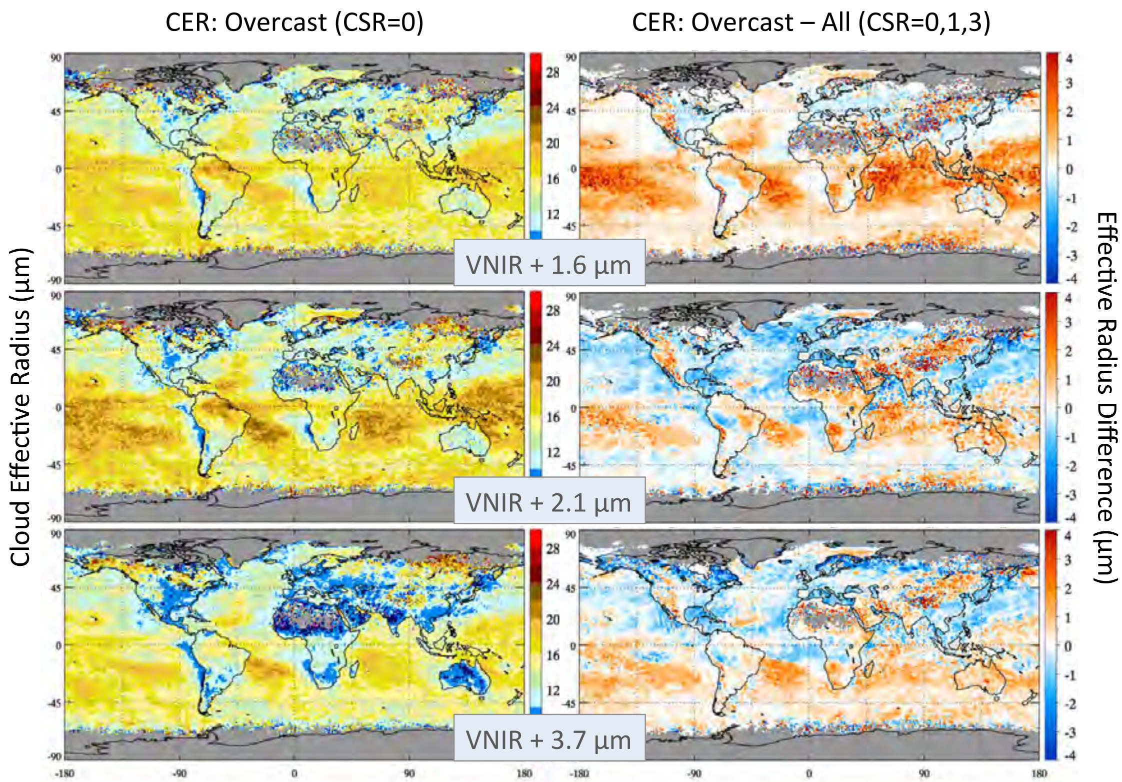


Figure 2.5-5. Same as Fig. 2.5-4 but for the right panels showing the difference CER calculated as the mean for overcast pixel population minus the mean for the total (overcast + partly cloudy) population.

el rows correspond to missing measurements in the MYD021KM (Aqua) L1B file. The pattern repeats with each 10 km along-track MODIS scan.

CER differences for April 2005, calculated as the monthly mean value of the overcast population minus the total population (overcast plus partly cloudy pixel population), is shown in **Fig. 2.5-5**. The overcast population's gridded CER can be larger or smaller than the total population, depending on the location. A positive (red) difference indicates that the partly cloudy pixels have reduced the grid mean CER while negative (blue) differences indicate an increase in the partly cloudy mean CER. An interesting region is the tropical Atlantic, where overcast pixel retrievals are larger than the total population in the west (near Brazil) but smaller in the central/eastern portion; this is especially pronounced for the CER_2.1 and CER_3.7 retrievals. While the reason for this gradient in sign is not obvious, the cloud retrieval fraction (not shown) has a gradient across that region with lower fraction (<0.1) corresponding to the positive difference and higher fraction (~0.4 and larger) corresponding to negative differences. This suggests that the differences in the tropical Atlantic may be related to cloud morphology. Significant gradients in sign are also seen over continents (e.g., North America).

## 2.6. Retrieval Failure Metrics (RFM)

In many cases, observed reflectances for the relatively non-absorbing VIS and NIR (VNIR) channels most sensitive to COT and the significantly absorbing SWIR or MWIR channels sensitive to CER will lie outside the pre-computed look-up table (LUT) solution space. Less frequently, observed reflectances may lie inside the solution space but yield multiple CER retrieval solutions, though these cases are typically only associated with optically thinner liquid water phase clouds. In these situations, the previously described standard solution logic (**SSL**) (Sect. 1.2) that is used to infer retrievals from the LUTs will fail to produce a successful COT/CER retrieval pair. In C5, pixels outside the solution space resulted in either partial COT retrievals (i.e., COT retrieved assuming a CER of 10 or 30 µm for liquid or ice phase clouds, respectively), with CER assigned fill values, or completely failed retrievals, with both COT and CER assigned fill values; pixels inside the solution space with multiple possible CER solutions were assigned the largest valid CER solution. In C6, an **alternate solution logic** (**ASL**) algorithm is now implemented that provides the COT and/or CER of the LUT grid point closest to the observation, as well as a *cost metric* indicating the relative distance of the observation from the LUT solution space. **Table 2.6-1** gives the new C6 **Retrieval_Failure_Metric** (**RFM**) SDS for pixels retrieved using the new alternate solution logic routine.

Table 2.6-1. The 3-element vector SDS used to provide information for pixels retrieved using the alternate solution logic.

| Dataset | SDS |
|---|---|
| COT | **Retrieval_Failure_Metric<_Wavelength*> (1)** |
| CER | **Retrieval_Failure_Metric<_Wavelength*> (2)** |
| Cost Metric | **Retrieval_Failure_Metric<_Wavelength*> (3)** |

* ***Wavelength*** is **16** or **37** for VNSWIR-1.6,-3.7 retrievals, **1621** for 1.6-2.1 retrievals, or omitted for VNSWIR-2.1 retrievals

### *2.6.1. Algorithm Overview*

For C6, all pixels that lie outside the LUT solution space, or those that lie within yet have multiple possible retrieval solutions for CER, will be passed to the ASL routine, which then selects the LUT grid point closest to the observation point as the final COT/CER solution. This is shown schematically by the 0.86 and 2.1 µm channel liquid water phase LUT in **Figure 2.6-1**, where the observation, denoted by the green diamond, is located well below the edge of the solution space. The vector **B** points from the observation to the closest LUT point which, for this pixel, would yield a retrieved COT of 26 and a 30 µm CER. The selection of the closest LUT point is made through the use of a cost metric (CM), defined here as

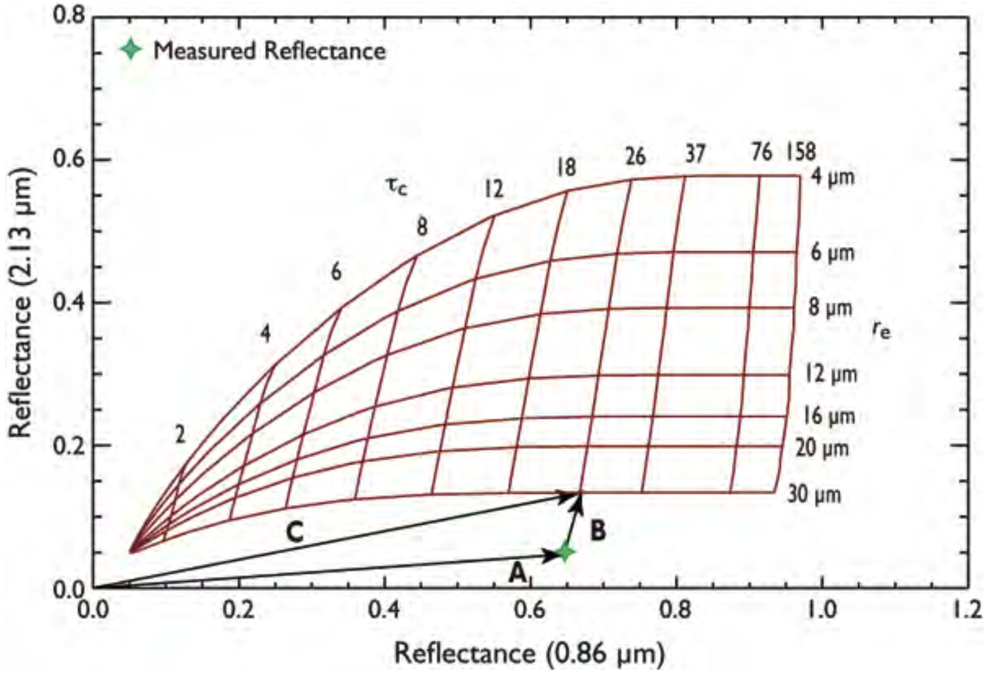


Figure 2.6-1. Bi-spectral solar reflectance look-up table (LUT) for a liquid water phase cloud over a land surface, with observed reflectance (green marker) outside the pre-computed solution space. Here, $\theta_0$=26.75°, θ=61.8°, and Δϕ=176.78°, with a 5% surface albedo. Also shown are the vectors **A**, **B**, and **C**, used for computing the cost metric (Eq. 2.6.1).

$$\text{cost metric (CM)} = 100\left|\frac{\mathbf{B}}{\mathbf{A}}\right| = 100\left|\frac{\mathbf{C}-\mathbf{A}}{\mathbf{A}}\right| \qquad (2.6\text{-}1)$$

where the vectors **A** and **C** are distances from the origin to the observation point and LUT grid point, respectively, as shown in Fig. 2.6-1. Thus the cost metric is essentially a measure of the percent relative distance between the observation and the closest LUT COT and CER grid point.

The ASL is applied to standard solution logic failure pixels in all cloud optical property retrieval channel combinations (i.e., combination of channel pairs with 1.6, 2.1, or 3.7 µm channel, as well as the 1.6 and 2.1 µm combination), with the resulting COT, CER, and cost metric assigned to the new RFM SDS. In order to make RFM assignments, the exterior of the LUT solution space is divided into four regions as shown by the shaded areas surrounding the liquid water phase LUT in **Figure 2.6-2**. Also shown are example pixel locations illustrating a successful full retrieval in the LUT interior (i.e., SSL solution, red diamond), a retrieval within the LUT interior having multiple CER solutions (ASL solution, blue diamond), and a retrieval in the LUT exterior (ASL, green diamond).

**Table 2.6-2** provides an overview of the RFM SDS assignments for each region of the solution space in Fig. 2.6-2. These SDSs will be assigned fill values for pixels having successful COT/CER retrieval pairs present in either the standard overcast SDSs or the partly cloud (PCL) SDSs (see Sect. 2.8). For all retrieval channel pairs except 1.6/2.1 µm, pixels with an x-

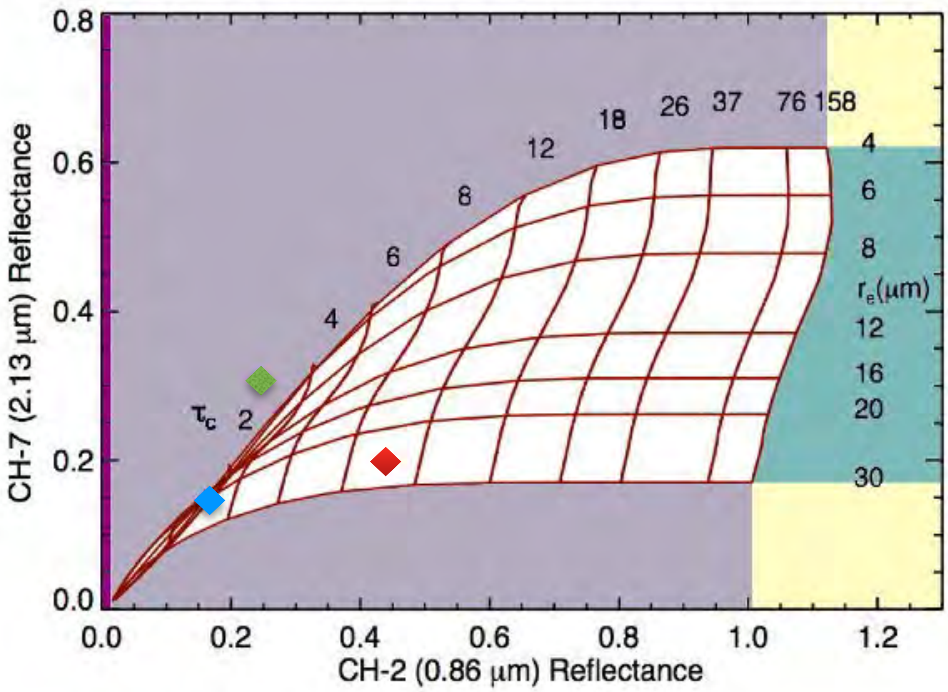


Figure 2.6-2. Retrieval space for a liquid phase cloud over an ocean surface, highlighting successful retrievals (solutions within the LUT space) and Retrieval Failure Metric (RFM) categories and cost metric assignments (see Table 2.6-2). Also shown are example pixels illustrating a successful retrieval (red marker), a retrieval outside the solution space (green), and a multiple CER solution retrieval (blue). The space is computed for $\theta_0$=19.89°, θ=22.39°, ϕ=174.4° and a 7 m-sec$^{-1}$ wind speed.

Table 2.6-2. Mapping of retrieved solutions and cost metric from the solution space regions in Figure 2.6-2 to the Retrieval Failure Metric (RFM) SDS.

| Region | Band Pairs | Retrieval Failure Metric SDS | | |
|---|---|---|---|---|
| | | COT | CER | Cost Metric (CM) |
| **Solution Space Interior** | | | | |
| Successful Solution | All | Fill | Fill | Fill |
| Multiple CER Solutions | All | Valid | Valid | ≥ 0 |
| **Solution Space Exterior** | | | | |
| | All | Fill | Fill | Max |
| | All | Fill | Fill | Fill |
| | All | Nearest LUT COT | Nearest LUT CER | ≥ 0 |
| | 1.6-2.1μm | Fill | Valid | ≥ 0 |
| | All Others | Fill | Fill | Fill |

axis reflectance larger than the maximum LUT reflectance (i.e, the green region to the right of the LUT in Fig. 2.6-2) are considered successful retrievals, with COT set to the maximum allowed value (note that the LUT COT maximum is 158 but the maximum reported value is limited to 150); thus, the RFM SDS for these pixels will contain fill values even though the solutions originate from the ASL routine. For the 1.6/2.1 µm channel pair, because of substantial cloud particle absorption for the x-axis reflectance (1.6 µm channel, see solution space plot in Fig. 1.2-2, Sect. 1.2.2, as an example), only the ASL CER retrieval is considered useful when the reflectance pair is in the green region of the solution space. Because there is no accompanying COT for this case, the CER solution is not considered a successful retrieval and therefore is not placed into the standard retrieval SDS; users interested in using the CER from this channel pair will find the value in the second element of the RFM vector as indicated in the above Table 2.6-1.

Note also that, due to differences in the absorbing CER wavelengths (e.g., penetration depths, sensitivities to cloud inhomogeneity or 3D radiative effects, atmospheric transmittance corrections, etc.), each spectral channel pairing has a different rate of retrieval failure [*Cho et al.*, 2015], thus the various spectral RFM SDSs should not be expected to contain identical populations of pixels. For instance, a pixel lying outside the VNSWIR-2.1 µm retrieval space, and thus requiring the alternate solution logic, may in fact lie inside the VNSWIR-1.6 µm or VNSWIR-3.7 µm retrieval spaces and yield successful COT/CER retrieval pairs. Spectral CER retrieval differences were discussed in Sect. 2.5 and in the recent literature [*Nakajima et al.*, 2010; *Zhang and Platnick*, 2011; *Zhang et al.*, 2012].

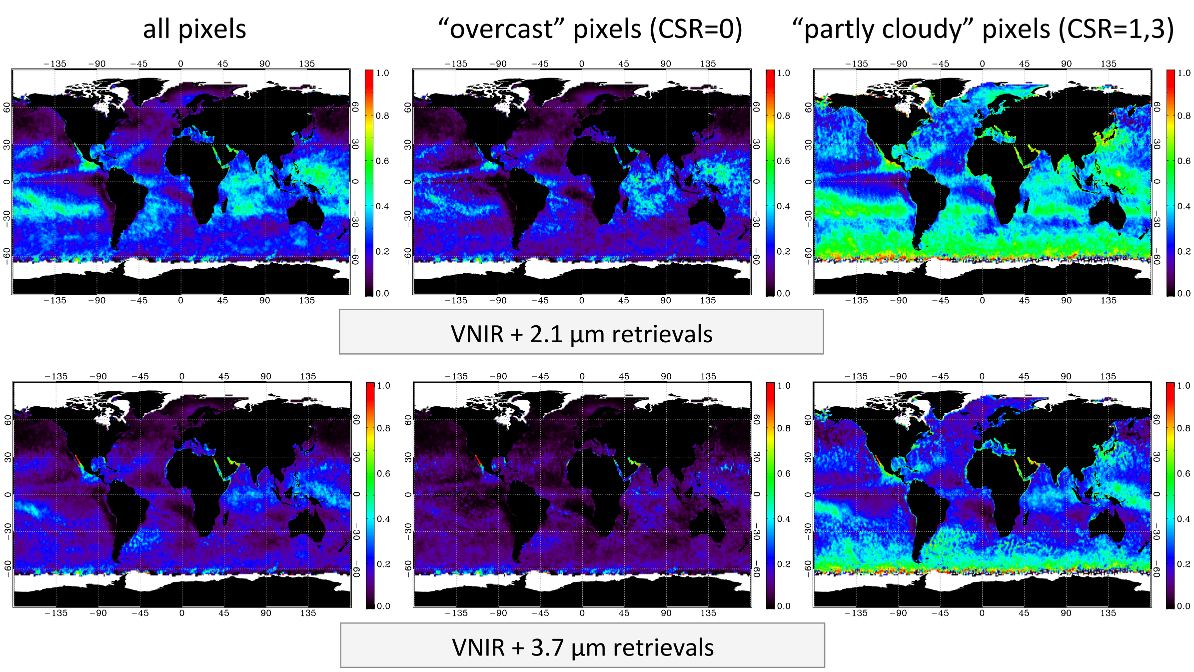


Figure 2.6-3. Gridded Aqua MODIS C6 cloud optical retrieval failure fractions for two band-pair retrievals for May 2007. The pixel population is for liquid water clouds over open ocean (no sea ice). [adapted *from Cho et al., 2015*]

**Figure 2.6-3** shows gridded liquid water retrieval failure statistics for Aqua MODIS in May 2007 over the open ocean for the C6 VNSWIR-2.1 and -3.7 µm retrievals. Pixels identified by the CSR algorithm as partly cloudy (CSR integer values of 1 or 3, see Sect. 2.8) have the highest failure rates, failing about 50% of the time in many remote ocean regions, whereas pixels that are likely overcast (CSR=0) have significantly smaller failure rates. It is also evident that the VNSWIR-2.1 µm retrievals have larger failure rates than the 3.7 µm retrievals, especially in the broken cloud marine BL regions. Thus, even if the C5 algorithm had attempted retrievals on this "partly cloudy" pixel population, a large fraction of these pixels would not have been retrievable (i.e., non-physical). Furthermore, the large failure rates–likely indicative of a failure in the homogeneous plane-parallel cloud radiative model–strongly suggests caution in using the successful retrievals that do manage to occur in this pixel population. The RFM SDS is available to provide diagnosis of the retrieval failure mechanism (e.g., SWIR observations result in CERs that are smaller/larger than the LUT min/max values).

## 2.7. Improved Pixel-level Uncertainties

Estimates of the pixel-level uncertainty (RMS relative uncertainty normalized to percent) in COT, CER, and CWP were added in C5 as first described by *Platnick et al.* [2004]. The uncertainty estimates are derived by propagating uncertainties applied to component error sources that are inherent to the retrieval. This is done by calculating partial derivative sensitivities (Jacobians)–for example, of cloud-top reflectance with respect to COT at the two channels used in the retrieval, while holding the other parameters (CER, surface spectral reflectance, etc.) constant–coupled with estimates of cloud top reflectance uncertainties associated with each error source. In this way, each error source uncertainty is mapped into cloud top reflectance uncertainty that is then mapped into retrieval uncertainty. The partial derivatives are calculated from the radiative transfer LUTs. For C6, error sources include the following four categories: (i) instrument calibration, (ii) atmospheric corrections, (iii) surface spectral reflectance, and (iv) other forward model error sources. While not currently part of the reported uncertainty budget, work on flagging, understanding, and perhaps improving 3-D error sources is ongoing.

The mapping of measured and model uncertainty components into retrieval uncertainty is represented by the covariance matrix $\mathbf{S}_{\mathrm{Ret}}$

$$\mathbf{S}_{\mathrm{Ret}} = \left(\mathbf{K}^T \mathbf{S}_y^{-1} \mathbf{K}\right)^{-1} + \sum_i \left(\mathbf{K}^{-1} \mathbf{K}_{b_i}\right) \mathbf{S}_{b_i} \left(\mathbf{K}^{-1} \mathbf{K}_{b_i}\right)^T \quad , \qquad (2.7\text{-}1)$$

where $\mathbf{S}_y$ and $\mathbf{S}_b$ are the measurement and model covariance matrices, respectively. Partial derivatives in $\mathbf{K}$ map cloud top reflectance error into retrieval error (e.g., matrix elements $\partial R_\lambda / \partial \tau$ and $\partial R_\lambda / \partial r_e$). For our two channel retrieval problem the matrices are of size $2 \times 2$. The elements of $\mathbf{K}_b$ contain partial derivatives of reflectance with respect to some channel-dependent model parameter (e.g., spectral surface albedo, spectral above-cloud atmospheric transmittance, etc.); the *i*-index summation is over each independent model error source. The $\mathbf{K}_b$ matrices are diagonal with the exception of atmospheric transmittance errors due to water vapor uncertainties that affect each channel in a correlated manner.

The matrix formulation of **Eq. 2.7-1** can be derived from standard variance algebra, only keeping first order (linear) terms, and is equivalent to the retrieval error covariance matrix formulation used in optimal estimation retrievals [*Rodgers*, 2000] when the *a priori* information is removed (i.e., given large error covariance values). Note the only difference in our retrieval solution and an optimal estimation solution is that we search through the entire solution space instead of iterating through the solution space starting with the *a priori* vector constrained by its covariances. If the *a priori* error covariance is large enough to effectively remove its constraint, the two solutions are equivalent as long as the cloud optical retrieval space is unique, i.e., the optimal estimation iteration does not get trapped in a cost function local minimum; similarly, the resulting retrieval uncertainties would be equivalent as well.

Table 2.7-1. C6 pixel-level error sources and associated uncertainty bounds.

| Category | Error Source | Specification |
|---|---|---|
| Ancillary Data Related to Surface Reflectance | MODIS-derived $A_{sfc}(\lambda)$ from MCD43B3 for land/snow surfaces, surface wind speed in Cox-Munk calculation | ±15% of $A_{sfc}(\lambda)$ from MCD43, ±20% of surface wind speed for water surfaces |
| Above-Cloud Atmospheric Corrections (water vapor, all bands) | Above-cloud ancillary Precipitable Water (PW) vapor | ±20% |
| | Above-Cloud Atmospheric Transmittance LUT | Provided in spectral transmittance LUT, derived from profile variances |
| Above-Cloud Atmospheric Corrections ($O_3$, MODIS Band 1) | Analytic transmittance formula | ±20% |
| Observations | Measurement Relative Error | Max. of value associated with L1B Uncertainty Index or 2% (bands 1-4) and 3% (bands 5-7) |
| Model | Cloud model error from size distribution effective variance ($v_e$) | Standard deviation from $v_e$ = 0.05 to 0.2 (0.1 nominal) for liquid water and ice clouds, provided in cloud LUTs, derived from analytic gamma distributions |
| | Water surface reflectance model error from using Cox-Munk reflectances averaged over wind direction | Standard deviation of 4 vector wind directions provided in cloud LUTs |
| 3.7 µm-specific cloud reflectance and cloud/surface emission | $\Delta T_c \Rightarrow$ cloud emission | |
| | $\Delta P_c$ ($CO_2$ slicing retrieval) | ±50 mb |
| | $\Delta PW$ (IR window retrieval) | ±20% |
| | $\Delta T_{sfc} \Rightarrow$ surface emission | ±1K |
| | $\Delta F_0/F_0$, $\Delta F_0 \Rightarrow$ reflectance calculation | ~4%, 0.42 W-m$^{-1}$-sr$^{-1}$-µm$^{-1}$ |

C5 processing assumed the instrument radiometric calibration relative uncertainty was fixed at 5% in all VNIR/SWIR spectral channels (this value was also intended to include nominal forward model error), the relative uncertainty in water vapor (from NCEP GDAS) used in above-cloud atmospheric corrections was set to 20%, and the spectral surface albedo

Table 2.7-2. Attributes for converting uncertainty index (UI) to relative uncertainty (%).

| **Band** | **CWL (μm)** | ***specified_uncertainty*** | ***scale_factor*** |
|---|---|---|---|
| 1 | 0.66 | 1.5 | 7 |
| 2 | 0.86 | 1.5 | 7 |
| 5 | 1.24 | 1.5 | 5 |
| 6 | 1.63 | 1.5 | 5 |
| 7 | 2.13 | 1.5 | 5 |

uncertainty associated with the MOD43B product was 15% in all spectral channels and in all land locations.

In C6 processing, error sources were modified/expanded to include: (i) scene-dependent calibration uncertainty that depends on the channel and detector-specific uncertainty index provided in the L1B file, (ii) new model error sources derived from the look-up tables, which include sensitivities associated with wind direction and speed over the ocean and uncertainties in liquid and ice size distribution effective variance, (iii) thermal emission uncertainties in the 3.7 μm channel associated with cloud and surface temperatures that are needed to extract reflected solar radiation from the total radiance signal, (iv) uncertainty in the solar spectral irradiance at 3.7 μm, and (v) addition of stratospheric ozone uncertainty in the visible (0.66 μm) atmospheric correction. These source uncertainty assignments used in C6 pixel-level retrieval uncertainty calculations are summarized in **Table 2.7-1**. Note retrieval uncertainties also depend on the solar and view zenith geometry in addition to the table items.

With respect to item (i) above, in C6 we now use the L1B pixel-level uncertainty index (**UI**) that ranges from 0-15 as an indication of relative measurement uncertainty instead of the constant uncertainty of 5% that was used for all channels in C5. To cover a broad range of relative uncertainty for all MODIS channels, the uncertainty is calculated from the UI as follows:

$$\text{uncertainty (\%)} = \textit{specified\_uncertainty} \times \exp\left(\frac{UI}{scale\_factor}\right) \qquad (2.7\text{-}2)$$

where the values of *specified_uncertainty* and *scale_factor* depend on the spectral channel (see **Table 2.7-2**) and are provided in the L1B files as SDS attributes. With this definition, relative uncertainties range between 1.5% (UI = 0) and 12.8% (UI = 15) for bands 1 and 2, between 1.5% (UI = 0) and 30% (UI = 15) for bands 5-7, and between 0.56% (UI=0) and 24% (UI=15) for band 20. These relative radiometric uncertainties, assumed to be uncorrelated spectrally, are used in the computation of optical property retrieval uncertainty. While useful for capturing scene-dependent calibration sensitivities, we nevertheless set a minimum allowable relative radiometric uncertainty of 2% for bands 1 and 2 and 3% for bands 5, 6, 7 and 20.

As was the case in C5, the uncertainty in cloud optical thickness over the ocean is typically smallest when the COT lies between 3 and 20, increasing with optical thickness due to satura-

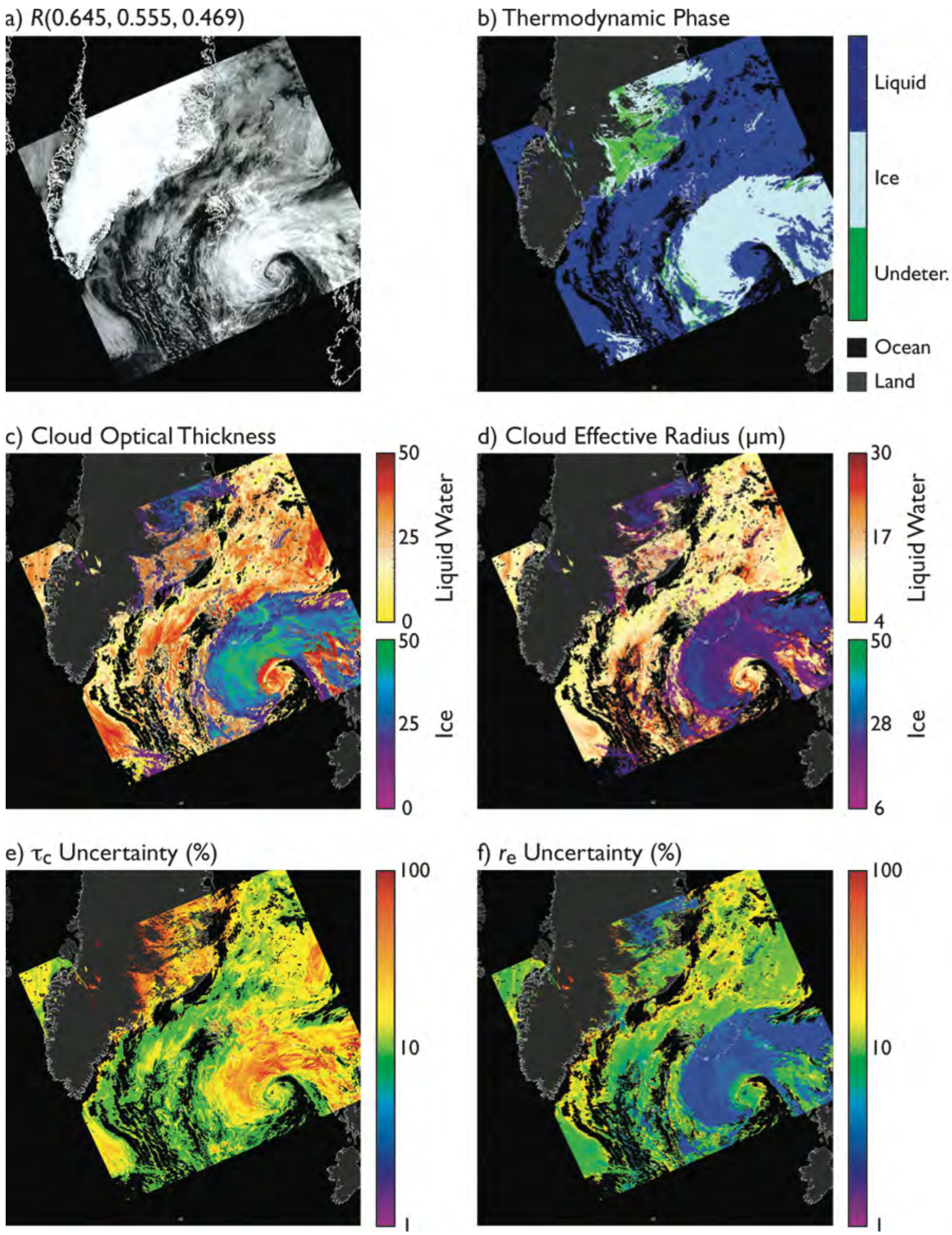


Figure 2.7-1. C5 COT and CER retrievals, from an Aqua MODIS data granule over Greenland (1 July 2008, 1400 UTC), using the 2.1 μm channel and their respective uncertainties.

tion in VNIR reflectance and thereby increased sensitivity to error source uncertainties affecting the knowledge of cloud top reflectance. Uncertainty is also large for small COT due to uncertainty in surface reflectance and atmospheric corrections. In all cases, the radiometric uncertainty component to the overall pixel-level uncertainty is much smaller in C6 than what

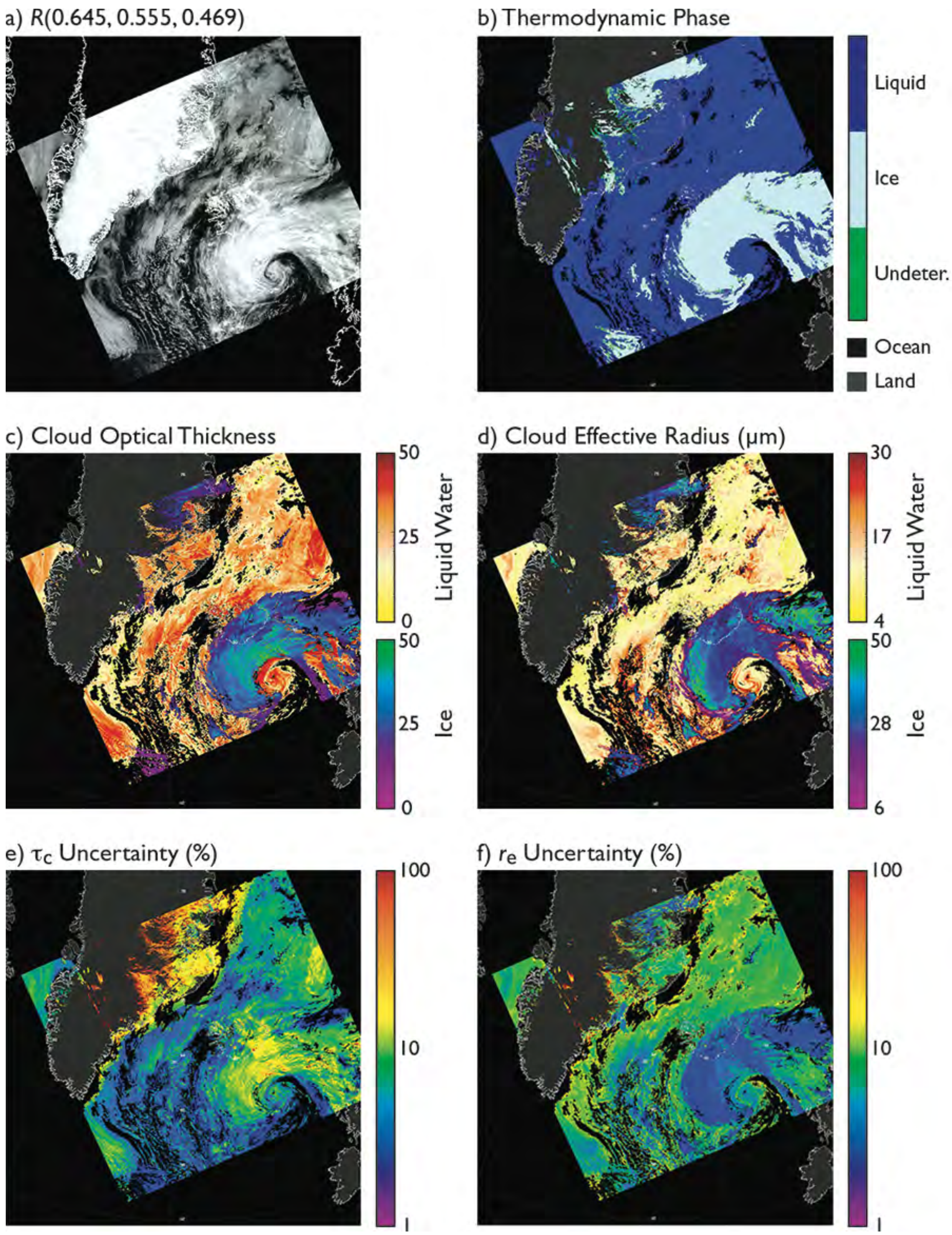


Figure 2.7-2. Same as Fig. 2.7-1 but for C6 retrievals. Uncertainties are generally reduced in C6 calculations due to the smaller instrument calibration uncertainty assignment, especially for high optically thick clouds where other error sources are more minor.

was assumed (5%) in C5. In contrast, the uncertainty in CER over the ocean is largest for small effective radius (due to atmospheric correction and calibration uncertainty) and at large effective radius (due to Cox-Munk surface reflectance uncertainty).

MODIS Aqua, 2 July 2008, 2105 UTC

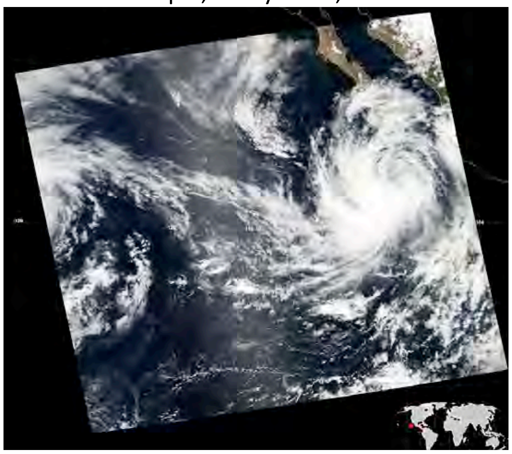

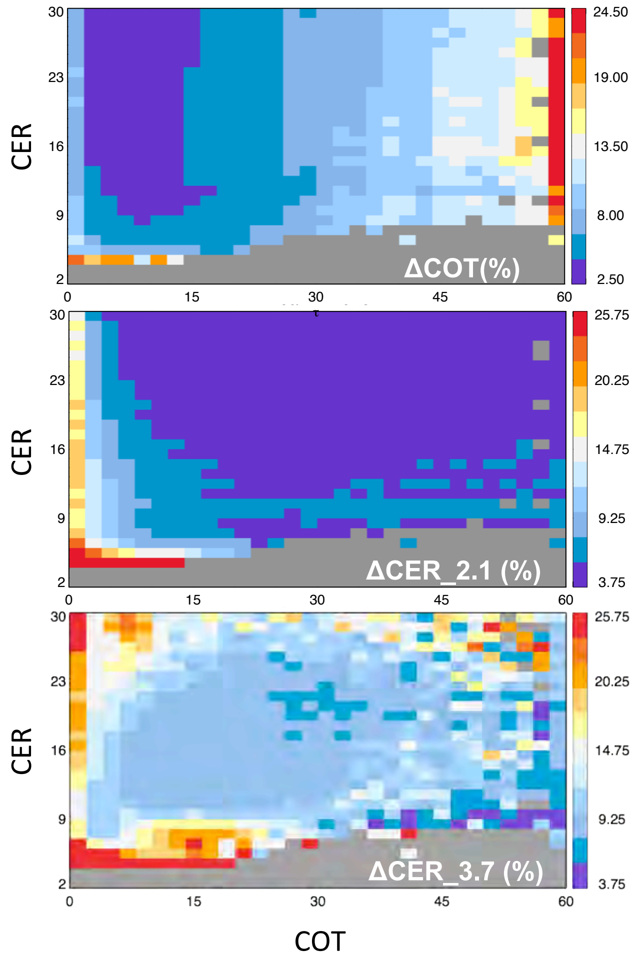


Figure 2.7-3. Mean liquid water cloud uncertainties binned as a function of COT and CER for all successful retrievals from the data granule shown above (note that COT and CER color bars are not equivalent). COT uncertainties (top right) are higher at the small and large COTs with little CER sensitivity. CER uncertainties are higher at the smallest CERs with little COT sensitivity after the SWIR/MWIR reflectances asymptote.

**Figures 2.7-1** and **2.7-2** show C5 and C6 retrievals, respectively, of COT and CER, and their uncertainties, for an Aqua MODIS data granule over Greenland and nearby ocean where clouds overly sea ice (1 July 2008, 1400 UTC). These examples highlight the pixel-level uncertainties over land, ocean, and ice surfaces, and for a wide variety of optical properties and cloud thermodynamic phase.

2-D and 1-D uncertainty distributions are shown in **Figs. 2.7-3** and **2.7-4**, respectively, for COT, CER_21 and CER_37 liquid water retrievals for a data granule off Baja California (2 July 2008, 2105 UTC). All successful retrievals from the 'overcast' pixel population are included in the distribution, and therefore a variety of view angles are also included. As expected, based on the solution space figures previously discussed (e.g., Fig. 2.6-1), the largest COT uncertainties in Fig. 2.7-3 occur at small and large COT where the solution space contours are most closely spaced, while the largest uncertainties for CER occur at the smaller COTs before the SWIR/MWIR reflectances asymptote (i.e., non-orthogonal solution space); however, CER_37 uncertainties also peak at the larger COT due to emission components (dashed green line in the right hand panel of Fig. 2.7-4).

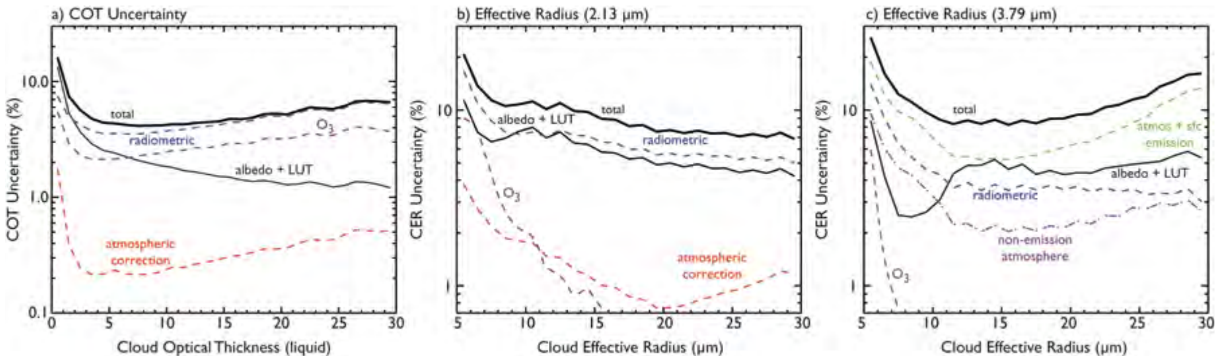


Figure 2.7-4. For the data granule of Fig. 2.7-3, mean liquid water retrieval uncertainties as a function of a single parameter (COT or CER) broken down into error source components: total (thick black line), instrument radiometric uncertainty (dashed blue), combined surface reflectance and LUT, i.e., size distribution effective variance (thin black), atmospheric correction (dashed red), $O_3$ transmittance correction for the 0.66 μm channel (dashed purple), 3.7 μm non-emitting atmospheric transmittance correction (purple dash-dot), and 3.7 μm combined atmospheric and surface emission error sources (dashed green).

The overall take-away message from **Figs. 2.7-1–2.7-4** is that asking for a single metric for the optical retrieval uncertainty is an ill-posed question. The answer rightly depends on surface type, solar/view geometry, atmospheric state, surface and cloud temperature (3.7 μm), and most importantly where the solution lies in the COT-CER space.

## 2.8 Clear Sky Restoral and Processing of Pixels Flagged as Partly Cloudy

Correctly identifying cloudy pixels appropriate for the MOD06 cloud optical and microphysical property retrievals is accomplished in large part using results from the MOD35 1 km cloud mask tests (note there are also two 250 m sub-pixel cloud mask tests that can independently report the 1 km cloudy designations as clear sky with a separate set of bits). However, because MOD35 is designed to be clear sky conservative (i.e., it seeks to identify "not clear" pixels), certain situations exist in which pixels identified by MOD35 as "cloudy" are nevertheless likely to be poor retrieval candidates. For instance, near the edge of clouds or within broken cloud fields, a given 1 km MODIS field of view (FOV) may in fact only be partially cloudy. This can be problematic for the MOD06 retrievals because in these cases the assumptions of a completely overcast homogenous cloudy FOV and 1-dimensional plane-parallel radiative transfer no longer hold, and subsequent retrievals will be of low confidence. Furthermore, some pixels may be identified by MOD35 as "cloudy" for reasons other than the presence of clouds, such as scenes with thick smoke or lofted dust, and should therefore not be retrieved as clouds. With such situations in mind, a Clear Sky Restoral (**CSR**) algorithm was introduced in C5 that attempts to identify pixels expected to be poor retrieval candidates. **Table 2.8-1** provides SDS locations for CSR and partly cloudy pixels.

Table 2.8-1. SDS locations for the CSR flag and partly cloudy pixels.

| Dataset | SDS Location |
|---|---|
| CSR Flag | **Quality_Assurance_1km** |
| Partly Cloudy Pixels | ***<Parameter_Name>*_PCL** |

### *2.8.1. Algorithm Overview*

All MOD35 "cloudy" pixels pass through the CSR logic shown in **Fig. 2.8-1** with the resulting CSR designations stored as bit values within the **Quality_Assurance_1km** SDS (see the Quality Assurance [QA] Table in **Appendix B** for specific bit locations). There are four possible outcomes of the CSR algorithm:

- *Overcast Cloudy (CSR = 0)*: Pixels that are not identified as clear or partly cloudy by the CSR tests. Note: MOD35 clear pixels will also have CSR=0.
- *Not Cloudy (CSR = 2)*: Pixels identified by spatial reflectance variability and spectral curvature tests as likely dust, smoke, or sunglint pixels, and are restored to clear sky.
- *Partly Cloudy (CSR = 3)*: Pixels over water surfaces that are identified by sub-pixel 250 m MOD35 cloud mask variability as partly cloudy.
- *Cloud Edge (CSR = 1)*: Overcast cloudy pixels (CSR = 0) with "clear" adjacent neighbors (i.e, adjacent pixels with MOD35 clear or CSR = 2)

Figure 2.8-1*a*

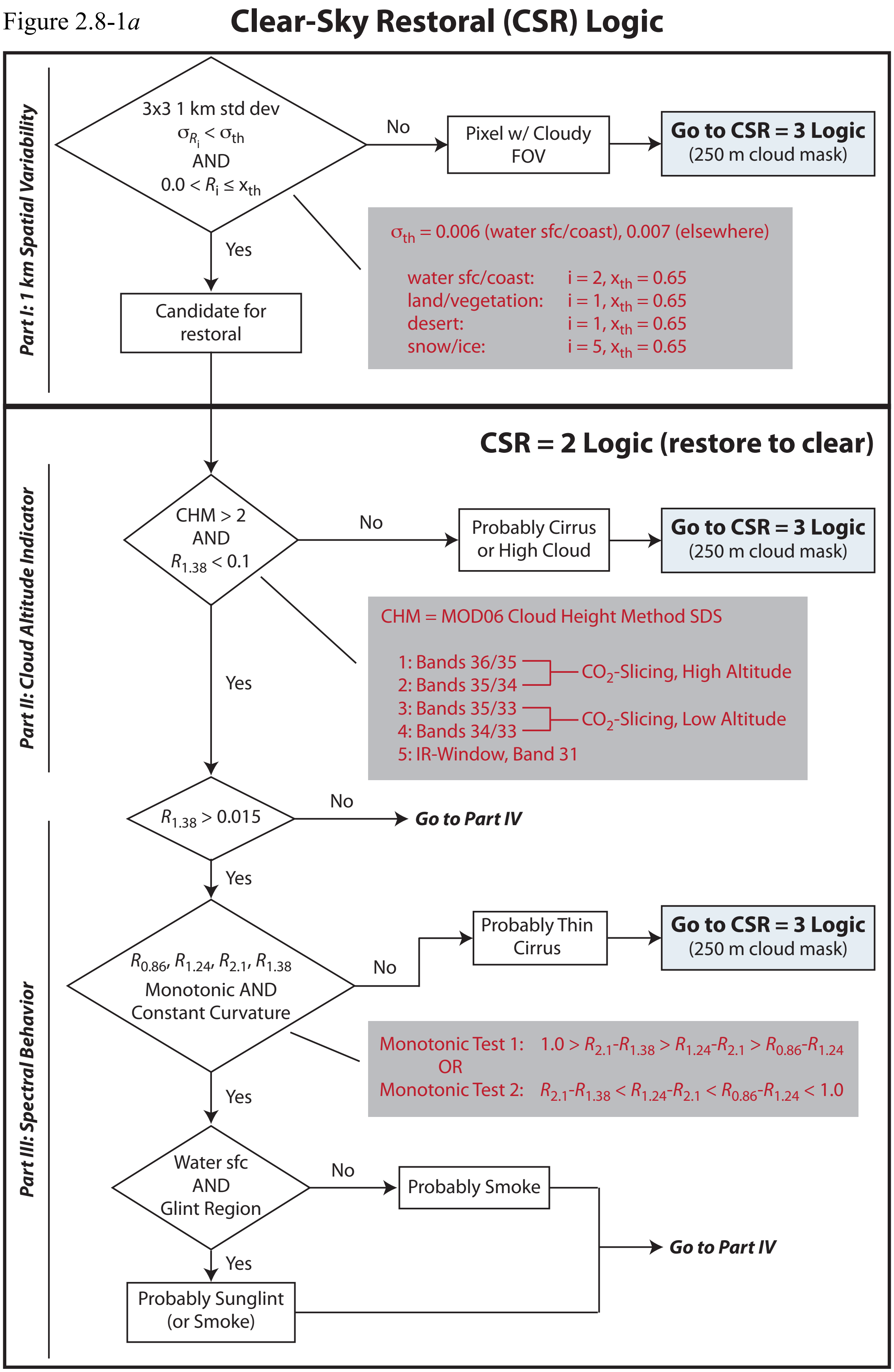

Clear-Sky Restoral (CSR) Logic
Part I: 1 km Spatial Variability
3x3 1 km std dev
$\sigma_{R_i} < \sigma_{th}$
AND
$0.0 < R_i \leq x_{th}$
No
Pixel w/ Cloudy FOV
Go to CSR = 3 Logic
(250 m cloud mask)
Yes
Candidate for restoral
$\sigma_{th}$ = 0.006 (water sfc/coast), 0.007 (elsewhere)
water sfc/coast: i = 2, $x_{th}$ = 0.65
land/vegetation: i = 1, $x_{th}$ = 0.65
desert: i = 1, $x_{th}$ = 0.65
snow/ice: i = 5, $x_{th}$ = 0.65
CSR = 2 Logic (restore to clear)
Part II: Cloud Altitude Indicator
CHM > 2
AND
$R_{1.38} < 0.1$
No
Probably Cirrus or High Cloud
Go to CSR = 3 Logic
(250 m cloud mask)
Yes
CHM = MOD06 Cloud Height Method SDS
1: Bands 36/35
2: Bands 35/34
$CO_2$-Slicing, High Altitude
3: Bands 35/33
4: Bands 34/33
$CO_2$-Slicing, Low Altitude
5: IR-Window, Band 31
Part III: Spectral Behavior
$R_{1.38} > 0.015$
No
Go to Part IV
Yes
$R_{0.86}$, $R_{1.24}$, $R_{2.1}$, $R_{1.38}$
Monotonic AND
Constant Curvature
No
Probably Thin Cirrus
Go to CSR = 3 Logic
(250 m cloud mask)
Monotonic Test 1: $1.0 > R_{2.1}-R_{1.38} > R_{1.24}-R_{2.1} > R_{0.86}-R_{1.24}$
OR
Monotonic Test 2: $R_{2.1}-R_{1.38} < R_{1.24}-R_{2.1} < R_{0.86}-R_{1.24} < 1.0$
Yes
Water sfc
AND
Glint Region
No
Probably Smoke
Go to Part IV
Yes
Probably Sunglint (or Smoke)

Figure 2.8-1*b* **Clear-Sky Restoral (CSR) Logic (*Cont.*)**

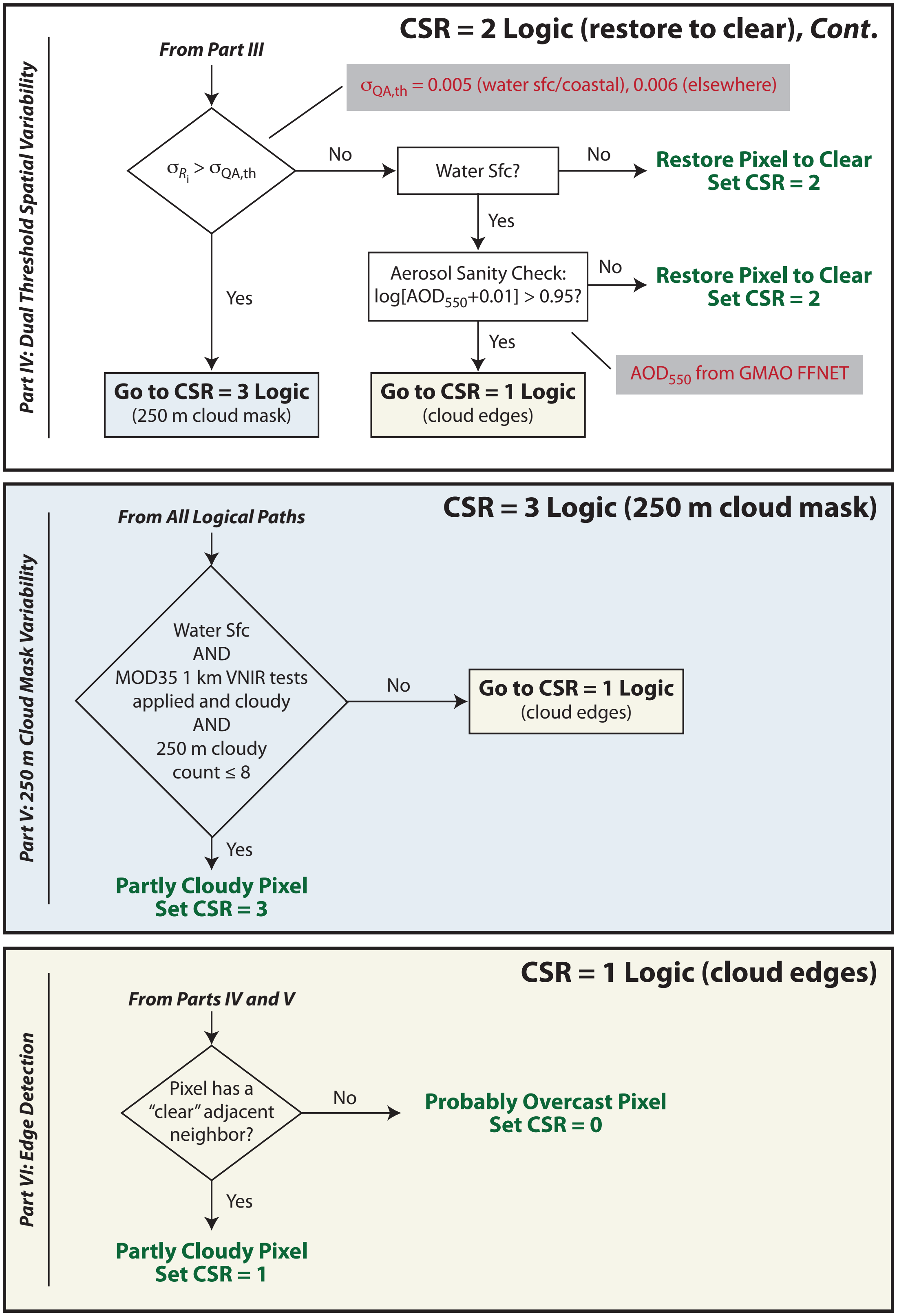

Note that for C6, optical and microphysical property retrievals are attempted on pixels designated as CSR = 1, 3 as well as CSR = 0 (overcast), as described below. Further, by default, all cross track pixels of along-track columns 2 and 1353 are set to PCL (CSR=1) because there is no available cloud mask for pixels 1 and 1354.

### *2.8.2. Changes for Collection 6*

The C6 CSR algorithm is nearly identical to its C5 counterpart, with only minor modifications and enhancements. C6 updates related to CSR include:

- *New SDSs for partly cloudy retrievals.* Previously in C5, all pixels identified by CSR as partly cloudy (CSR = 1, 3) or not clear (CSR = 2) were restored to clear sky, and the corresponding cloud retrieval SDSs were assigned fill values. For C6, only pixels having CSR = 2 are restored to clear sky and assigned fill values. Pixels identified by the CSR = 1 or 3 tests that also have successful cloud optical and microphysical property retrievals now populate the partly cloudy *PCL* SDSs. All pixels with unsuccessful or partially successful retrievals populate the Retrieval Failure Metric *RFM* SDSs (**Section 2.6**). Mapping of pixel retrieval outcome status to SDS assignments and *RFM* assignment details may be found in **Appendix B**.

- *Enhanced thin cirrus handling.* The CSR logic has been modified in an attempt to minimize cases of thin cirrus clouds being restored to clear sky via CSR = 2 tests. Previously, the altitude indicator test (see *Part II*, Figure 2.8-1a) relied on the inferred cloud thermodynamic phase, which may erroneously identify the optically thin edges of cirrus clouds as liquid water phase. For C6, cloud thermodynamic phase is replaced by the cloud height method (CHM) used for cloud top (CT) altitude determination. CT altitude is determined using one of five "methods," namely the infrared (IR) window technique or one of four $CO_2$ slicing band combinations. For high altitude clouds such as thin cirrus, the two longer-wavelength $CO_2$ slicing bands, which are more sensitive to the upper troposphere, are typically the bands that converge to a CT solution; their use by the cloud top algorithm for a given pixel is thus considered a high-confidence indicator of high altitude clouds.

- *New sanity check for low altitude stratocumulus clouds.* For C6, the CSR logic now includes a sanity check to minimize cases of low altitude, homogeneous stratocumulus clouds over water surfaces being inadvertently restored to clear sky via the CSR = 2 dual threshold spatial variability test (*Part IV*). The spatial reflectance variability of such clouds can be relatively small, and may result in positive CSR = 2 outcomes. This sanity check applies a threshold to 550 nm aerosol optical depth (AOD) inferred from a multispectral feed-forward neural network algorithm developed by NASA's Global Modeling and Assimilation Office (GMAO) (Arlindo da Silva, personal communication). CSR = 2 pixels in which the GMAO retrieval yields large AOD are assumed to be unphysical for typical aerosols, and are instead likely indicative of clouds; such pixels are thus reassigned to overcast, i.e., CSR = 0.

*2.8.3. Examples*

**Figure 2.8-2** shows an example granule from Aqua MODIS, observed on 9 April 2005 (1050 UTC) over the Black Sea, Turkey, and eastern Mediterranean Sea. What appears to be lofted dust is apparent over the Mediterranean at the bottom of the true color RGB (0.66-0.55-0.47 µm) in (a), and is identified as "cloudy", or not clear, by the MOD35 cloud mask (b). This feature, however, is correctly identified by the CSR algorithm (c), and is restored to clear sky by the CSR = 2 tests. Note also the CSR = 1 cloud edge pixels, visible as the regions of dark blue outlining the cloud features in the CSR image.

Also of interest is the fraction of restored pixels, that is, the number of 1 km pixels identified as CSR = 2, divided by the number of MYD35 "not clear" pixels. A global map of the mean restored pixel fraction in a 1° grid is shown in **Fig. 2.8-3 a** for MODIS Aqua, April 2005. For context, the MYD35 cloud fraction is shown in **Fig. 2.8-3 b**. April is an active time of year for Atlantic Saharan dust outbreaks (e.g., *Kaufman et al.* [2005]), a region of high restoral fraction in the figure. Likewise, a high fraction region to the southeast of Argentina may be associated with Patagonia dust transport [*Gassó et al.*, 2010; *Johnson et al.*, 2011] though such events typically occur further south. Also of note is the high restoral fractions in the Arabian Sea, Persian Gulf, and Red Sea. This could result from the CSR algorithm detecting a combination of both dust and sunglint signals. It is very likely that the elevated fraction

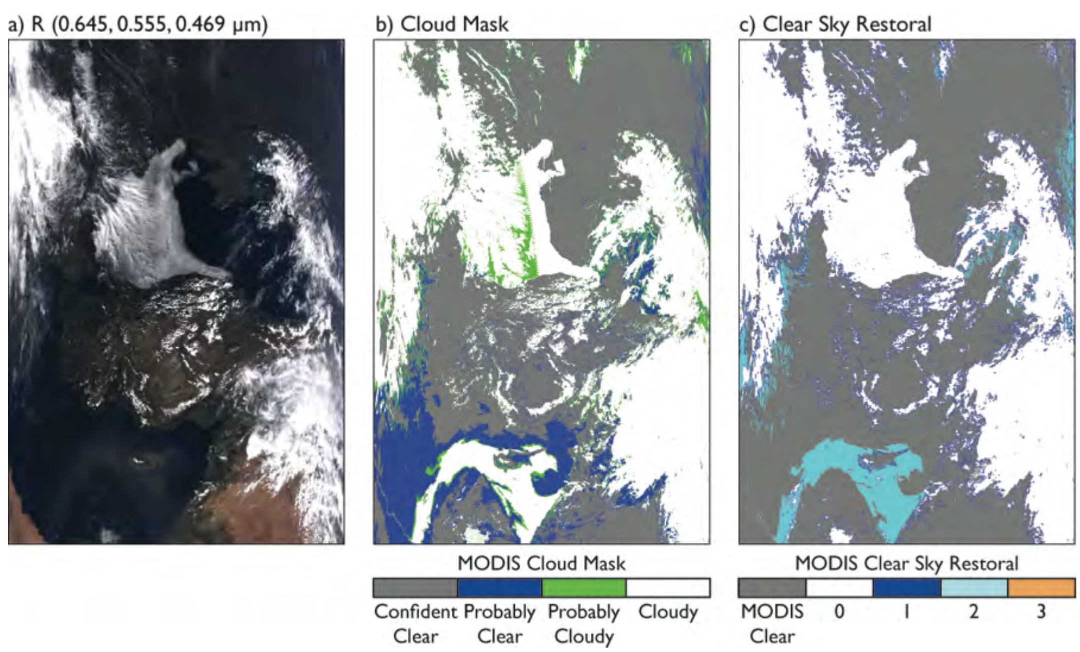


Figure 2.8-2. Left: True color RGB (0.66-0.55-0.47 µm) from an Aqua MODIS granule on 9 April 2005 (1050 UTC). Center: MOD35 cloud mask results. Right: MOD06 C6 CSR algorithm results (0: overcast; 1: cloud edge; 2: restored to clear sky; 3: partly cloudy).

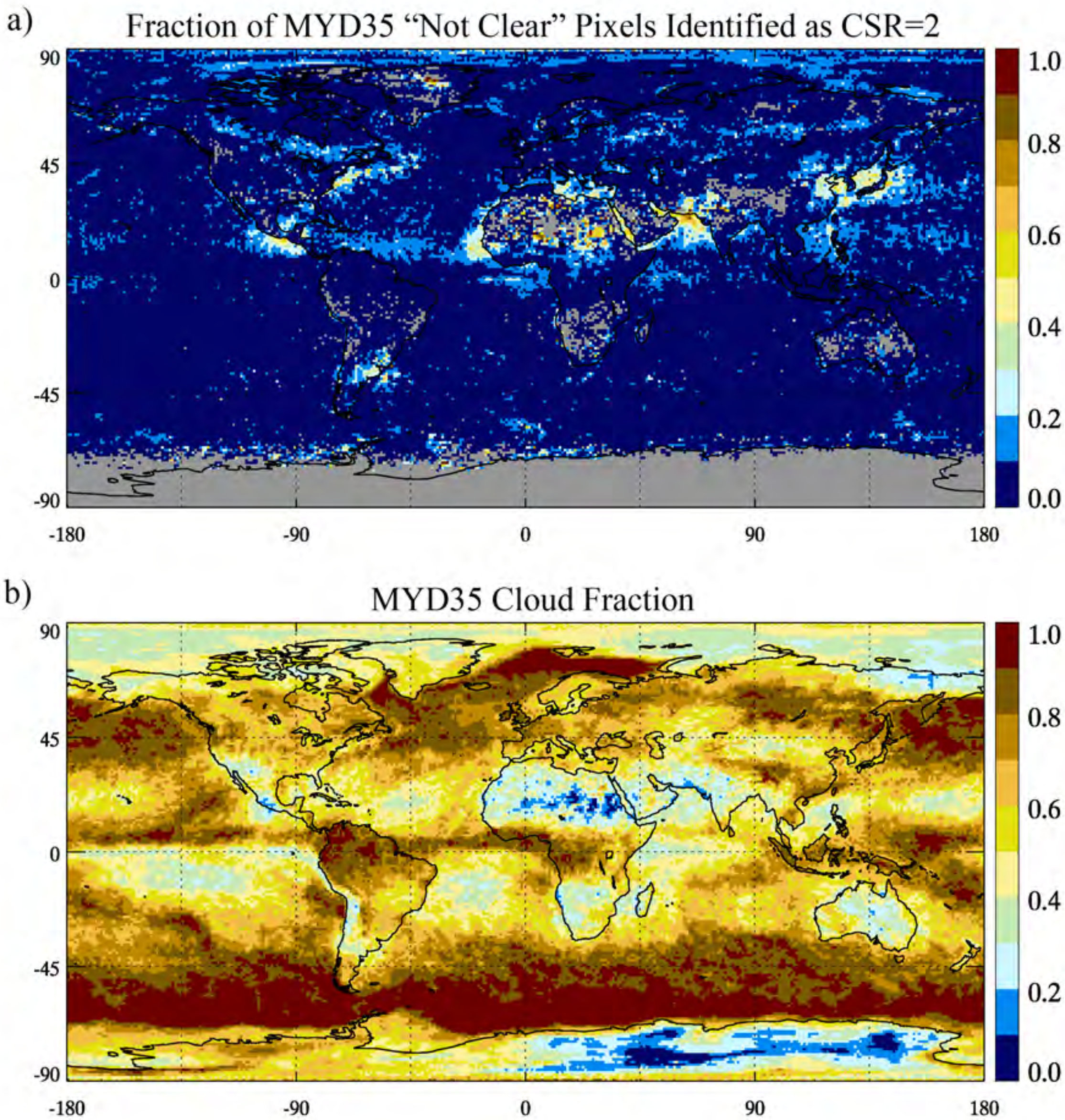


Figure 2.8-3. Monthly fraction of MYD35 “not clear” pixels identified as CSR = 2 (a) and MYD35 cloud fraction (b) for April 2005 Aqua MODIS.

off Baja California is due almost exclusively to sunglint detection by the CSR algorithm. Finally, the high fraction off the East China Sea and Sea of Japan may be dust and/or aerosol associated with pollution. While we have not quantified the incidence of clear sky false positives by the CSR algorithm, high restoral fractions appear to be occurring in sensible locations.

*2.8.4. Known Issues*

Thin Cirrus

Despite modifying the altitude test (see Fig. 2.8-1 a, Part II) to minimize cases of thin cirrus clouds being restored to clear sky, thin cirrus continue to be problematic for the CSR algorithm. In **Fig. 2.8-4** for example, on 6 April 2005 (1830 UTC) Aqua MODIS observed a layer of very thin cirrus clouds off the coast of the southeastern United States, as shown within the red outlined region of the true color RGB (0.66-0.55-0.47 µm). The 1.38 µm reflectance image in **Fig. 2.8-5 a** indicates the extent of this cirrus, as well as the optical thinness of the layer (note the reflectance is logarithmically scaled from 0.001 to 0.1). Much of this region is identified as "cloudy" by the C6 cloud mask in **Fig. 2.8-5 b**, even though MOD35 has some difficulty identifying the entire cirrus layer. Moreover, portions of what is identified as cloudy by MOD35 are subsequently restored to clear sky by the CSR = 2 tests, as indicated by the light blue regions.

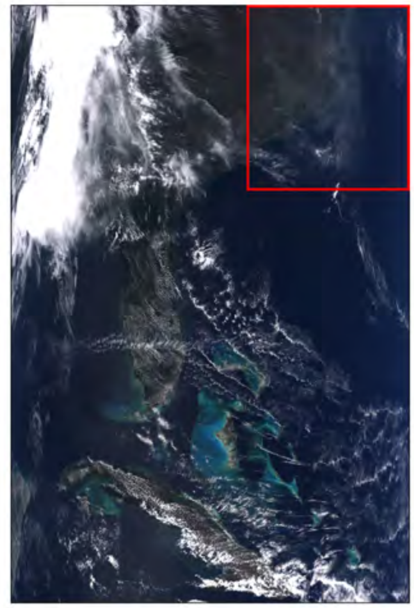

Figure 2.8-4. *Thin cirrus clouds*. On April 6, 2005 (1830 UTC), thin cirrus clouds were observed by Aqua MODIS off the SE coast of the Florida, as shown within the red outlined region in the true color RGB image.

Comparing to C5, shown in **Figs. 2.8-5 c**, the C6 CSR algorithm offers little improvement for this scene. The cirrus is sufficiently optically thin that the $CO_2$-slicing cloud height methods evidently do not converge on a so-

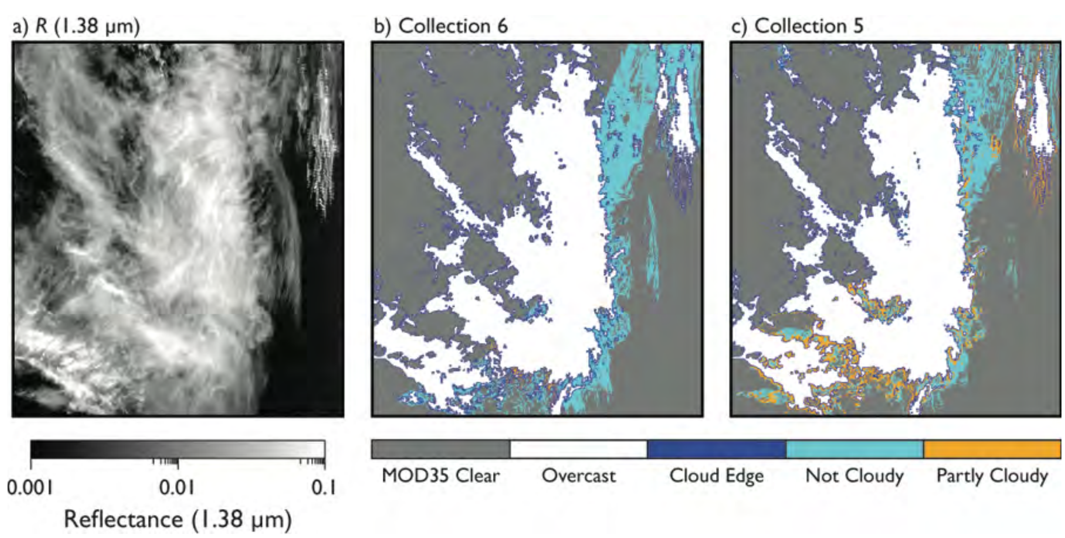


Figure 2.8-5. Reflectance at 1.38 µm (a), corresponding to the red outlined region in Figure 2.8-4, showing both the full spatial extent of the cirrus as well as the optically thin nature of the layer. The MOD35 cloud mask with MOD06 CSR results are shown for both C6 and C5 in (b) and (c), respectively. Colors other than gray denote MOD35 "not clear" pixels.

lution, thus the cloud altitude test (Part II) does not indicate the presence of high-altitude clouds, and the cirrus is restored to clear sky via the spectral behavior (Part III) or dual-threshold spatial variability (Part IV) tests. It is worth noting, however, that many of these thin cirrus pixels are likely to yield unsuccessful cloud optical and microphysical property retrievals, as the small reflectances associated with such clouds often lie outside the standard MOD06 retrieval space. Thus very thin cirrus clouds often will not be aggregated to level-3 global statistics regardless of the CSR results.

<u>Heavy Dust</u>

Dust, particularly when transported over water surfaces, is often identified as "not clear" by the MOD35 cloud mask, and may also remain identified as overcast after passing through the CSR tests. A remarkable example of this occurred on 1 July 2008, over the Persian Gulf. Here, a particularly strong dust event was observed by Terra MODIS (0720 UTC), as shown within the red outlined region in the true color RGB (0.66-0.55-0.47 µm) in **Fig. 2.8-6**. The C6 MOD35 cloud mask in **Fig. 2.8-7 a** clearly identifies much of this dust over the Gulf as "cloudy." The C6 CSR algorithm does correctly restore much of this dust to clear sky (i.e., CSR = 2), as indicated by the light blue regions. However, large portions remain overcast (i.e., CSR = 0), in part via the dual-threshold spatial variability test (Part IV), and MOD06 cloud optical and microphysical property retrievals are subsequently attempted on these pixels.

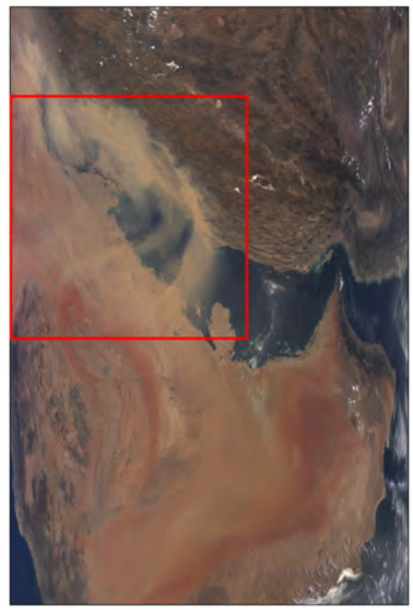

Figure 2.8-6. *Heavy dust*. On 1 July 2008 (0720 UTC), a strong dust storm was observed by Terra MODIS over the Persian Gulf, shown above by the true color RGB image.

Furthermore, disregarding cloud mask differences, the C6 CSR algorithm in fact restores less dust to clear sky than does C5, the MOD35 and CSR results of which are shown in **Fig. 2.8-7 b**. The apparently worsened performance of C6 is primarily a result of the new GMAO AOD sanity check, which is applied to all pixels over water surfaces having CSR = 2. Dust pixels previously restored to clear sky in C5 are now returned to "overcast" in C6 because the inferred AOD exceeds the sanity check threshold. This dust event was also observed three hours later by Aqua MODIS, albeit obliquely, with similar cloud mask and CSR results (not shown). It persisted over this region for several consecutive days, and is clearly evident in the Terra and Aqua MODIS visible imagery throughout that time.

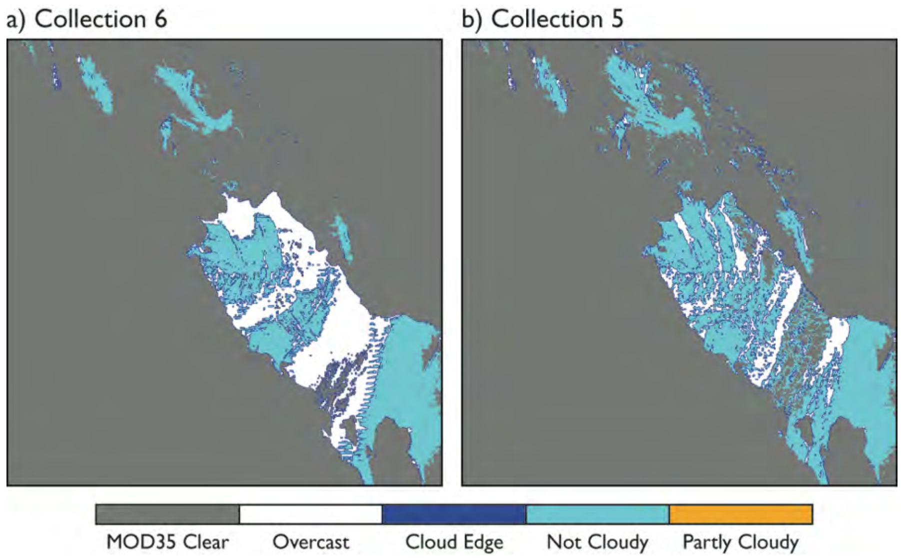


Figure 2.8-7. *Heavy dust identified as "overcast" cloud*. The C6 MOD35 cloud mask with MOD06 CSR results, corresponding to the red outlined region in Figure 2.8-6, are shown in (a). For comparison, the respective C5 results are shown in (b). Colors other than gray denote MOD35 "not clear" pixels.

<ins>Sunglint</ins>

While the MOD35 cloud mask attempts to account for sunglint using elevated thresholds for the visible/near-infrared (VIS/NIR) reflectance and reflectance ratio tests in regions where sunglint is expected, and the CSR algorithm is designed to identify glint using spatial variability and altitude indicator tests, occasionally glint regions are bright enough to not only be identified as "not clear" by the cloud mask but also to emerge from the CSR algorithm as overcast. In **Fig. 2.8-8**, for example, Aqua MODIS observed an exceptionally strong sunglint case on 10 April 2005 (0630 UTC) over the Gulf of Thailand, outlined by the red box in the true color RGB (0.66-0.55-0.47 μm) image. This "mega-glint" region, with 0.66 μm reflectances around or greater than 1.0 (0.86 μm is largely saturated), is bright enough to be identified as "cloudy" by the VIS/NIR reflectance test, despite taking the sunglint processing path in MOD35 (which uses the elevated reflectance thresholds); interestingly, the VIS/NIR reflectance ratio test also identifies much of this glint region as cloudy, notwithstanding saturation at 0.86 μm.

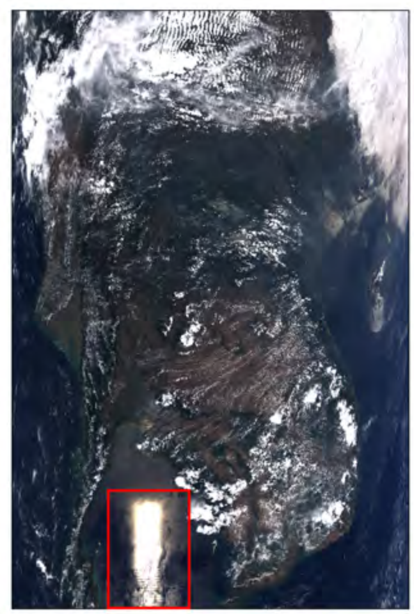

Figure 2.8-8. *Sunglint*. On 10 April 2005 (0630 UTC), an exceptional sunglint scene was observed by Aqua MODIS over the Gulf of Thailand, shown above by the true color RGB.

The reflectances in this sunglint region are so large, in fact, that these pixels do not even meet the criteria to be candidates for restoral to clear sky, as they clearly exceed the reflectance threshold applied in Part I and are thus not processed through the CSR = 2 logic. Similarly, the MOD35 250 m VIS/NIR tests also indicate clouds, negating the CSR = 3 logic, and the pixels either remain "overcast" or are identified as "cloud edge" (i.e., CSR = 1), as shown in **Fig. 2.8-9 a**. Comparing to its C5 counterpart, shown in **Fig. 2.8-9 b**, any differences in C6 are largely a result of improved performance by the cloud mask.

It is worth noting, however, that many of the pixels associated with this "mega-glint" region ultimately yield unsuccessful cloud optical and microphysical property retrievals and are therefore not aggregated in the L3 dataset regardless of the CSR results. Moreover, sunglint of this magnitude is fortunately not a common occurrence. Nevertheless, caution should be taken when using MOD06 retrievals in locations where sunglint is expected.

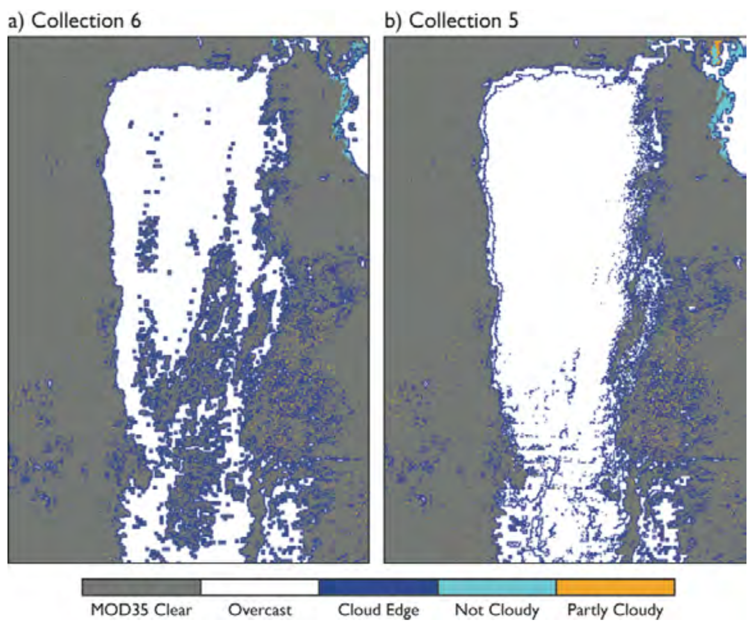


Figure 2.8-9. *Sunglint identified as overcast clouds*. The C6 MOD35 cloud mask with MOD06 CSR results, corresponding to the red outlined region in Fig. 2.8-8, are shown in (a). For comparison, the respective C5 results are shown in (b). Colors other than gray denote MOD35 "not clear" pixels.

## 2.9. New Cloud Radiative Transfer Look-up Tables (LUTs)

The use of asymptotic theory for optically thick atmospheres in C5 and earlier versions has been replaced with a straightforward use of cloud reflectance and emissivity look-up tables (LUTs) containing a complete range of optical thickness values. For optically thick atmospheres, the resulting reflectance computations are the same as those obtained from asymptotic theory, but this change simplifies the maintenance of the MOD06 code such that multiple paths (i.e., optically thin and optically thick atmospheres, followed by interpolation between them) are no longer required. In addition, more optically thin COTs are included in the LUTs.

In order to minimize angular interpolation errors during the retrieval process, only the multiple scattering (**MS**) component to the cloud top bidirectional reflectance function (***R***) is stored in the LUTs. During the retrieval process, the single scattering (**SS**) component is constructed dynamically ("on the fly") from the phase function that is also stored in the LUT, and added to the MS component. The SS calculation uses the exact pixel-level angular information. The LUTs contain the MS component for six MODIS channels centered at 0.66, 0.87, 1.24, 1.63, 2.13, and 3.79 μm, as a function of COT, CER, cosines of the solar zenith ($\mu_0$) and satellite viewing ($\mu$) angles, and relative azimuth angle between the sun and the satellite ($\Delta\phi$); separate LUTs are created for ocean/water surfaces with several wind speeds ($u$) and for land surfaces with a zero surface albedo. **Table 2.9-1** summarizes the number of grid points and the range of parameter values of the LUTs. Note while the liquid and ice phase LUT CERs range from 2 to 30 μm and 5 to 90 μm, respectively, the allowable retrieval solution space for liquid and ice clouds are limited to 4 to 30 μm and 5 to 60 μm, respectively, for C6.

In addition, reflected flux, transmitted flux, and spherical albedo for the above six channels, as well as the IR channel centered at 11 μm, are also computed and included in the land LUT for use with a Lambertian surface whose albedo is included separately (Section 2.9.1). Ocean LUTs also contain effective surface and cloud emissivities for the channels centered at

Table 2.9-1. Range of Values of Look up table (LUT) parameters.

| Variable | # of grid points and Range |
|---|---|
| COT | 34 (0, 159) |
| CER (μm) | 18 [2, 30] liquid water phase<br>15 [5, 90] ice phase |
| $\mu_0$ | 33 [0.15,1.0] |
| $\mu$ | 28 [0.4,1.0] |
| $\Delta\phi$ (deg) | 37 [0, 180] |
| $u$ ($ms^{-1}$) | 3 [3, 7, 15] |

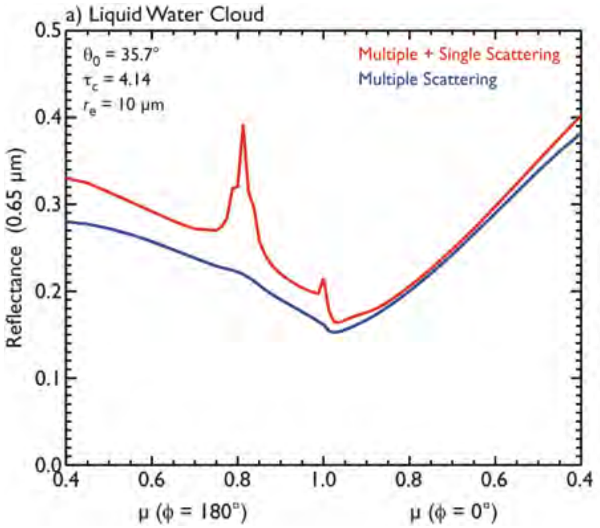


Figure 2.9-1. Total (red line) and MS (blue line) cloud top reflectance for MODIS band 1 (0.66 µm) for (a) liquid water clouds with CER = 10 µm, and (b) ice clouds (severely roughened aggregated columns) with CER = 60 µm; all calculations assume COT = 4.14 and $\mu_0$ = 0.813. The MS part of the reflectance is much smoother than the total reflectance that includes single plus multiple scattering. Note that the MS part of the reflectance function exhibits more linearity in µ space than θ space (used in C5, not shown).

3.7 and 11 µm; for the land LUTs, these effective emissivities are calculated from the flux and spherical albedo data.

Addition of ocean/water LUTs and separation of *R* into SS and MS components is a significant difference between the C6 LUTs and those used in previous collections. As previously stated, the SS component for a particular sun-satellite geometry is added dynamically to the interpolated MS component during the retrieval process. **Figure 2.9-1** illustrates the MS component and the total cloud top bidirectional reflectance (MS + SS) as a function of the cosine of the viewing zenith angle µ in the forward and backscattered directions for the 0.66 µm channel (MODIS band 1). It is evident that the MS component is a smoother function compared to the total reflectance, and thus minimizes the interpolation errors. The details of the radiative transfer calculations, discretization of the LUT variables, and the individual SDSs included in the LUTs are summarized in the sections below. Further details about the wind speed interpolated ocean reflectances can be found in Sect. 2.2.

### *2.9.1 Radiative Transfer Calculations*

Forward radiative transfer calculations for the LUTs were performed with the discrete ordinates radiative transfer (DISORT) model developed by *Stamnes et al*. [1988, 2000], using 64 streams to characterize the upwelling and downwelling radiance (32 up and 32 down). To account for the wind speed/direction dependence of ocean surface bidirectional reflectance, we have incorporated into DISORT the Cox-Munk ocean bidirectional reflectance model implemented in libRadTran 1.4 [*Mayer and Kylling*, 2005]. Subsequently, we have conducted a thorough investigation of the accuracy and efficiency of DISORT (including the Cox-Munk ocean BRDF), and have modified its routines to achieve significant improvement in computational efficiency for simulations over ocean surfaces (see Sect. 2.2).

For simulations over ocean surfaces, we assume an atmosphere-surface system consisting of three adjacent plane parallel homogeneous layers, and explicitly account for below-cloud Rayleigh scattering assuming a nominal profile of atmospheric pressure/altitude. The cloud is placed in the top layer, at an altitude of 8 km above the surface. All below-cloud Rayleigh scattering, except for the contribution from the lowest atmospheric profile layer, are combined to form the second layer. The bottom layer consists of the Rayleigh scattering contribution from the lowest atmospheric profile layer combined with a boundary-layer, coarse mode aerosol with an optical thickness of 0.1. The boundary layer aerosol radiative model (i.e., single scattering albedo, asymmetry parameter) is a coarse mode model used in the MOD04 Dark Target aerosol retrievals (see Table 2, aerosol mode 7, MOD04 ATBD [*Levy et al.*, 2009]); a Henyey-Greenstein model is assumed for the aerosol phase function. For simulations over land surfaces, the atmosphere-surface system consists of a single cloud layer overlying a black surface, i.e., zero surface albedo and no Rayleigh or aerosol layers. The land LUTs contain fluxes and spherical albedos that allow the incorporation of ancillary surface spectral albedo datasets (see Sect. 2.3). Note above cloud atmospheric gaseous absorption is ignored in both the land and ocean LUT simulations, and is dynamically accounted for during the retrieval process using the retrieved cloud top pressure, ancillary atmospheric profiles, and a pre-computed two-way spectral transmittance LUT; likewise, above cloud Rayleigh scattering at 0.66 µm is dynamically accounted for on a pixel-level basis using the iterative approach of *Wang and King* [1997].

The single scattering properties of liquid water clouds are calculated from Mie theory, and are integrated over a Modified Gamma droplet size distribution,

$$n(r) = N_0 r^{(1-3v_e)/v_e} exp\left(\frac{-r}{r_e v_e}\right) \tag{2.9.1}$$

assuming effective variance $v_e = 0.10$. Complex refractive indices for liquid water are obtained from *Hale and Querry* [1973] for wavelengths in the range $0.25 \leq \lambda \leq 0.69$ µm, *Palmer and Williams* [1974] for $0.69 < \lambda \leq 2.0$ µm, and *Downing and Williams* [1975] for $\lambda > 2.0$ µm. As detailed in Sect. 2.1, the single scattering properties of ice clouds are obtained from *Yang et al.* [2013] using the severely roughened aggregated column ice crystal habit, and are likewise integrated over a Modified Gamma size distribution (**Eq. 2.9.1**) with $v_e = 0.10$. Computed single scattering properties (single scattering albedo, asymmetry parameter, extinction efficiency, phase function) for both ice and liquid water clouds are stored in the LUT. To approximate the forward peak of the liquid and ice phase functions for the radiative transfer calculations, the δ-fit method of *Hu et al.* [2000] is implemented to truncate the phase functions, which are then approximated by a 64-term Legendre polynomial expansion. DISORT input parameters COT and single scattering albedo ($\omega_0$) are then adjusted with the truncation factor $f$ (i.e., the fraction of photons in the phase function forward peak due to diffraction), such that

$$\omega' = \frac{(1-f)\omega}{1-f\omega} \qquad \tau' = (1-f\omega)\tau, \tag{2.9.2}$$

where $\tau$, denoting COT in some band $\lambda_i$, has been scaled to MODIS band 1 ($\lambda_1$) by

$$\tau_{\lambda_i} = \frac{Q_e(r_e,\lambda_i)}{Q_e(r_e,\lambda_1)}\tau_{\lambda_1} . \tag{2.9.3}$$

The MS reflectance component is extracted from DISORT after the SS part is subtracted from the total reflectance calculation. For a particular sun-satellite geometry, the SS component ($R_{ss}$) is calculated by interpolating the phase function (*PF*) in scattering angle space ($\Theta$) and using the formula,

$$R_{SS}(\tau, r_e, \mu, \mu_0, \Delta\phi) = \frac{1}{4(\mu+\mu_0)} * \frac{\omega}{(1.0-f\omega)} * PF(\Theta, r_e)\ (1-exp[-\tau'(1/\mu+1/\mu_0)]), \tag{2.9.4}$$

where $r_e$ denotes CER. During the retrieval process the SS component is then added back dynamically to the interpolated MS component to obtain the total LUT reflectance.

Over land surfaces, a pixel-level Lambertian surface albedo is added to the LUT total cloud top reflectance $R_0$ following *King* [1987], such that

$$R_{A_g}(\tau, r_e, \mu, \mu_0, \Delta\phi) = R_0(\tau, r_e, \mu, \mu_0, \Delta\phi) + \frac{A_g\, t(\tau, r_e, \mu)\, t(\tau, r_e, \mu_0)}{1 - A_g \overline{r}(\tau, r_e)}, \tag{2.9.5}$$

where $t$ is the transmitted flux, $\overline{r}$ is the spherical albedo, and $A_g$ is the surface albedo. Over ocean/water surfaces, the MS reflectance component and effective cloud and surface emissivities are averaged over four vector wind directions (0°, 90°, 180°, 270°) to generate separate ocean LUTs for the three wind speeds (see Table 2.9-1).

### *2.9.2 Discretization of LUT parameters and interpolation error*

As shown in Fig. 2.9-1, the MS reflection function is much smoother than the total reflection function, implying that the SS component accounts for the angular structure of the total reflectance. Thus interpolation errors are greatly reduced when the SS component is calculated independently at pixel-level. To further reduce interpolation errors, we conducted an exhaustive interpolation error analysis to determine the best LUT discretization scheme. For COT, we followed the scheme suggested by *A. K. Heidinger* [2013, personal communication] in which COT values greater than 2 are discretized in equal intervals in log space. For solar and view angle space, multiple schemes were investigated. **Fig. 2.9-2** shows the median inter-

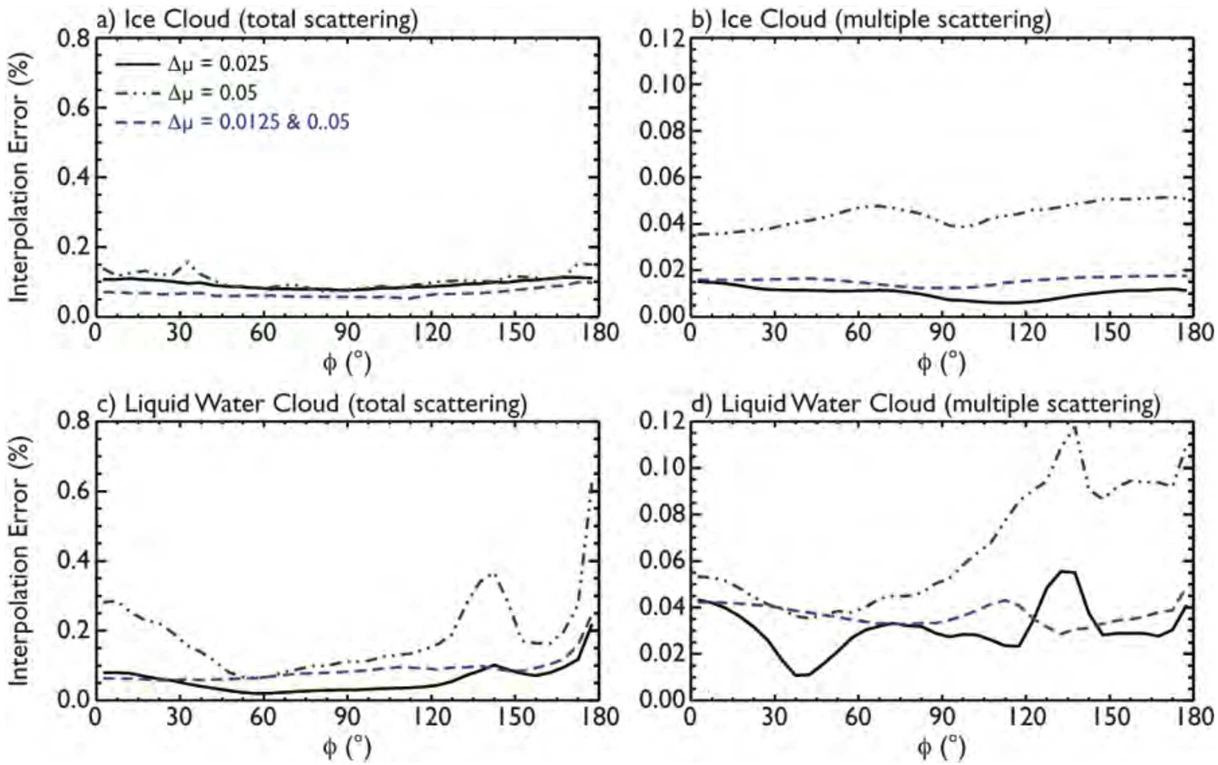


Figure 2.9-2. Median 0.66 μm LUT interpolation errors (averaged over all COT, CER, μ, and $\mu_0$ entries) as a function of relative azimuth $\Delta\varphi$ for three solar/view angle discretization schemes (see text). Shown are total reflectance (left column) and the MS component (right column) for ice clouds (severely roughened aggregated columns) with CER = 60 μm (top row) and liquid water clouds with CER = 10 μm (bottom row). Note the order of magnitude error reduction in the MS plots.

polation error for full reflectance LUTs and MS reflectance LUTs with three different μ and $\mu_0$ discretization schemes: (i) equally spaced with $\Delta\mu = 0.025$, (ii) equally spaced with $\Delta\mu = 0.05$, and (iii) a hybrid scheme with intervals of 0.0125 and 0.05 at larger and smaller μ, respectively (see **Table 2.9-2**). A decrease in interpolation error by an order of magnitude can be noted with the MS reflectance LUTs. The hybrid discretization scheme (broken blue lines in Fig. 2.9-2) produced the lowest maximum error for the MS LUTs and minimized the interpolation error near $\mu = 1.0$, as shown by the polar plots in **Figure 2.9-3**. As such, we implemented the hybrid discretization scheme for both solar and satellite zenith angles, while the relative azimuth angle is discretized in degree space. **Table 2.9-2** summarizes the grid points for COT, CER, μ, $\mu_0$ and $\Delta\phi$ used in constructing the C6 LUTs.

### *2.9.3 Effective variance and wind direction uncertainties*

To incorporate an effective variance model error in the retrieval uncertainty calculations, the total reflectances for clouds having droplet size distributions with effective variances of 0.05 and 0.2 are also computed for both ice and liquid water. The effective variance error is then the standard deviation of the total reflectances corresponding to the three effective variances (including the default 0.1 value); these errors are included in the MS reflectance land

Table 2.9-2. Grid point values of the lookup table (LUT) parameters.

| Quantity | # of points | Grid point values |
|---|---|---|
| COT | 34 | 0.05, 0.10, 0.25, 0.5, 0.75, 1.0, 1.25, 1.5, 1.75, 2.0, 2.39, 2.87, 3.45, 4.14, 4.97, 6.0, 7.15, 8.58, 10.30, 12.36, 14.83, 17.80, 21.36, 25.63, 30.76, 36.91, 44.30, 53.16, 63.80, 76.56, 91.88, 110.26,132.31,158.78 |
| CER (μm) | 18<br>12 | 2, 4, 5, 6, 7, 8, 9, 10, 12, 14, 16, 18, 20, 22, 24, 26, 28, 30 (liquid water cloud)<br>5, 10, 15, 20, 25, 30, 35, 40, 45, 50, 55, 60 (ice cloud) |
| $\mu$ | 28 | 0.40, 0.45, 0.50, 0.55, 0.60, 0.65, 0.70, 0.75, 0.7625, 0.7750, 0.7875, 0.8000, 0.8125, 0.8250, 0.8375, 0.8500, 0.8625, 0.8750, 0.8875, 0.900, 0.9125, 0.9250, 0.9375, 0.9500, 0.9625, 0.9750, 0.9875, 1.0 |
| $\mu_0$ | 33 | 0.15, 0.20, 0.25, 0.30, 0.35, 0.40, 0.45, 0.50, 0.55, 0.60, 0.65, 0.70, 0.75, 0.7625, 0.7750, 0.7875, 0.8000, 0.8125, 0.8250, 0.8375, 0.8500, 0.8625, 0.8750, 0.8875, 0.900, 0.9125, 0.9250, 0.9375, 0.9500, 0.9625, 0.9750, 0.9875, 1.0 |
| $\Delta\phi$ (°) | 37 | [0, 180] equally spaced with increments of 5° |
| $u$ (ms$^{-1}$) | 3 | 3, 7, 15 |

LUTs. For ocean/water surfaces, the effective variance error is combined with a wind vector model uncertainty for each of the three LUT wind speeds, calculated as the standard deviation of the total reflectances corresponding to the 0°, 90°, 180° and 270° vector wind directions. The wind direction and effective variance errors are assumed to be independent, such that they are combined via a root-sum-square (RSS) calculation. **Figure 2.9-4** shows the histograms of the land (effective variance) and ocean (effective variance + wind direction) LUT model errors (i.e., reflectance standard deviations) for the MODIS 0.87 and 3.7 μm channels; note the ocean errors are from the $u = 3$ m s$^{-1}$ LUT. There is no significant difference between the two histograms and therefore, to save computational time, we decided to use the effective variance standard deviations from the land LUTs for the ocean LUTs instead of calculating them separately. The net ocean LUT model uncertainty values are provided as separate LUTs due to file size constraints.

There are a total of 15 LUTs in an HDF4 format. One LUT provides phase function data (needed for the single scattering calculation) and other scattering properties for both phases. There are two LUTs for land retrievals (black albedo surface) – one for each phase – providing the MS reflectances and total reflectance standard derivations corresponding to the effective variance model uncertainty, as well as fluxes/albedos. There are 12 ocean LUTs – 6 for each phase corresponding to 3 MS reflectance and flux/albedo/effective emissivity LUTs and 3 reflectance standard deviation LUTs representing the effective variance and wind direction error sources for the three wind speeds (3.0, 7.0, and 15.0 ms$^{-1}$). Note that the ocean standard devia-

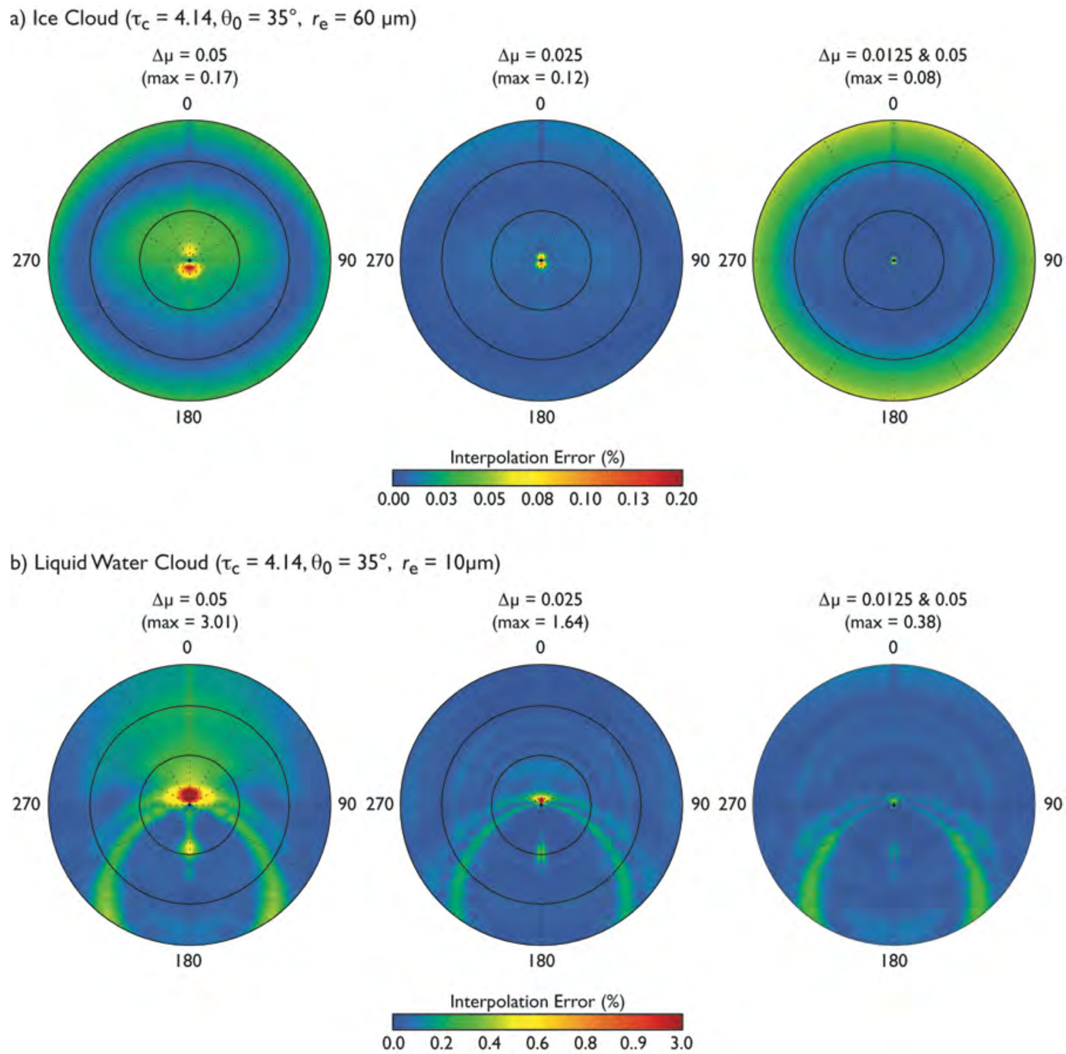


Figure 2.9-3. Maximum interpolation error for COT=4.14, $\theta_0$=35° for the MS part of the reflectance. The top row is for ice clouds with CER=60 μm (severely roughened aggregated columns), and the bottom row is for liquid water clouds with CER=10 μm. The hybrid discretization scheme (right column) has the least error near nadir.

tion LUTs also includes effective surface and cloud emissivity standard deviations associated with wind direction; these are not used in the C6 retrieval uncertainty calculations but were added in anticipation of a future capability. These C6 LUT HDF files will be publicly available in the future.

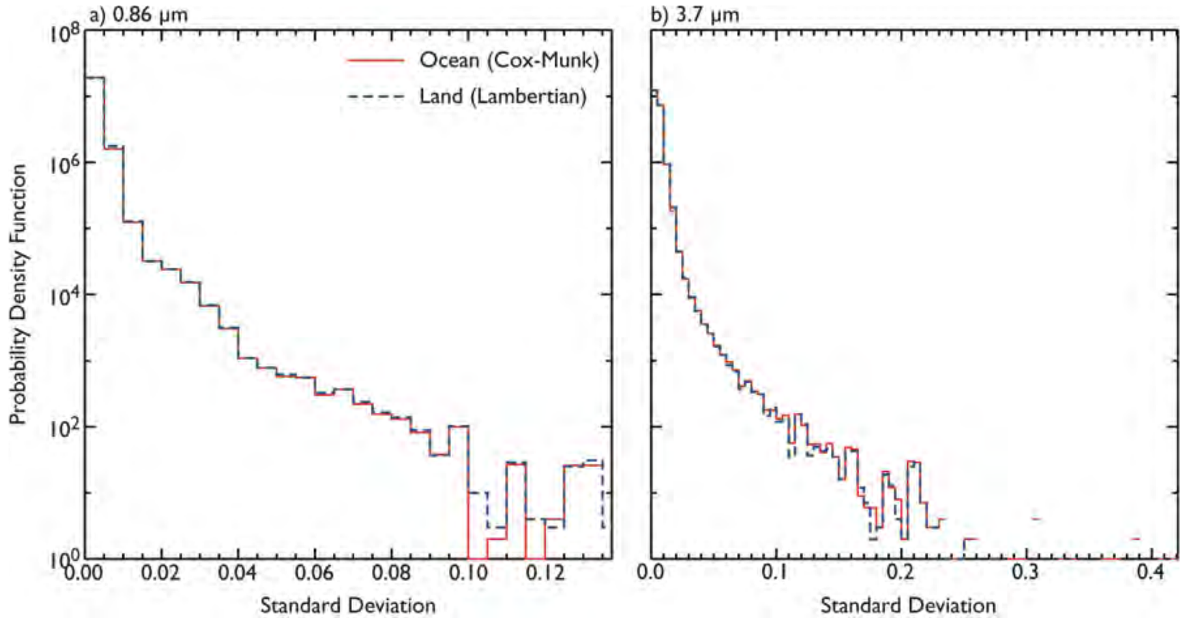


Figure 2.9-4. Histograms of standard deviation calculated for the ocean LUT with $u = 3\,\mathrm{m\,s^{-1}}$ (blue line) and from the land LUT (red line) for MODIS bands 2 and 20. No significant difference can be seen over about 3 orders of magnitude.

## 2.10. Miscellaneous Changes

### *2.10.1. Multilayer cloud detection updates*

The multilayer cloud detection algorithm [*Wind et al.*, 2010] has been updated for C6. An additional multilayer cloud detection method is now applied as outlined in *Pavolonis and Heidinger* [2004]. The Pavolonis and Heidinger (**PH**) algorithm was designed for general-purpose cloud overlap detection, whereas for MOD06 the primary goal is to flag pixels where cloud microphysical retrievals would be adversely affected by cloud overlap. Limited case study analyses have shown the PH results appear to be overly aggressive in flagging multilayer scenes, i.e., producing more detection than necessary. DISORT-based simulations of multilayer clouds run through the PH algorithm also suggest somewhat aggressive multilayer detection by the algorithm. Subsequently a latitude-based 13.6 µm brightness temperature (BT13.6 ) threshold was implemented to help reduce false positives with some success. The PH algorithm is run when BT13.6 is greater than thresholds of 210 K (latitude within ±30°) or 227 K (poleward of ±30° latitude). Regardless, it was decided in later C6 science testing that, while the result of the PH algorithm would be reported in the Byte 6 QA results (discussed later), the test would not be used to determine whether a retrieval is included in the L3 multilayer aggregation SDSs.

**Figure 2.10.1-1** illustrates the issue. Locations where the PH algorithm is the sole contributor to multilayer results, shown in (c), have Cloud_Multi_Layer_Flag SDS values of 3 (light blue color). Whereas it is of course possible that those clouds are indeed multilayered, MOD-06 seeks a specific kind of multilayer situation where cloud layering would have an adverse impact on an assumed single phase cloud effective radius retrieval. The example granule regions where the PH algorithm has made a positive detection do not indicate such a CER sensitivity, thus the algorithm is not entirely optimal for the specified purpose.

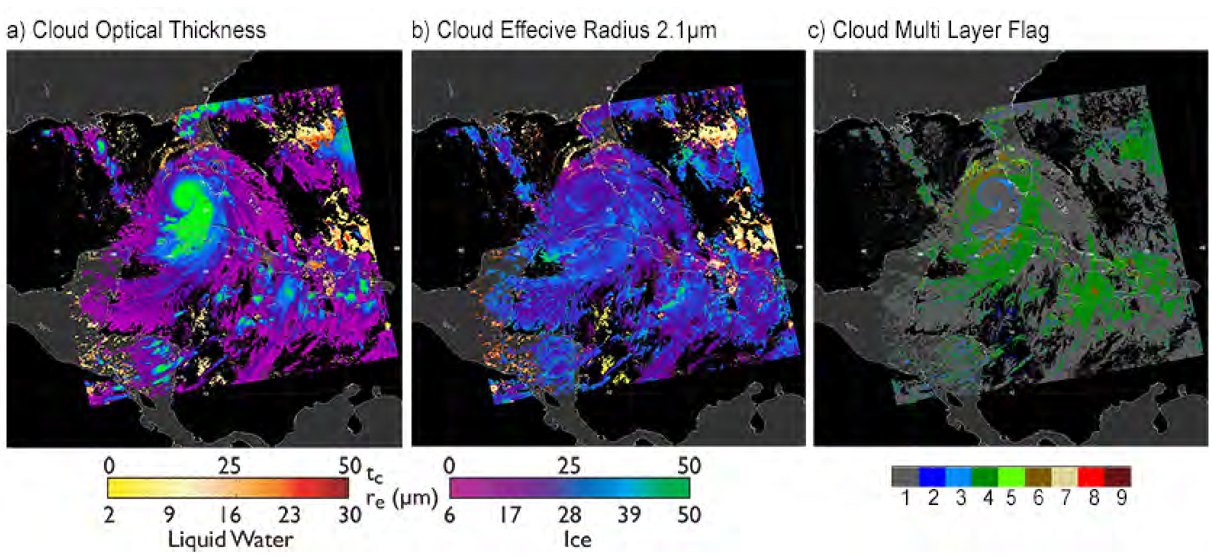


Figure 2.10.1-1. Example VNSWIR-2.1 µm retrievals and multilayer cloud SDS results (Aqua MODIS, day 238, 1840 UTC).

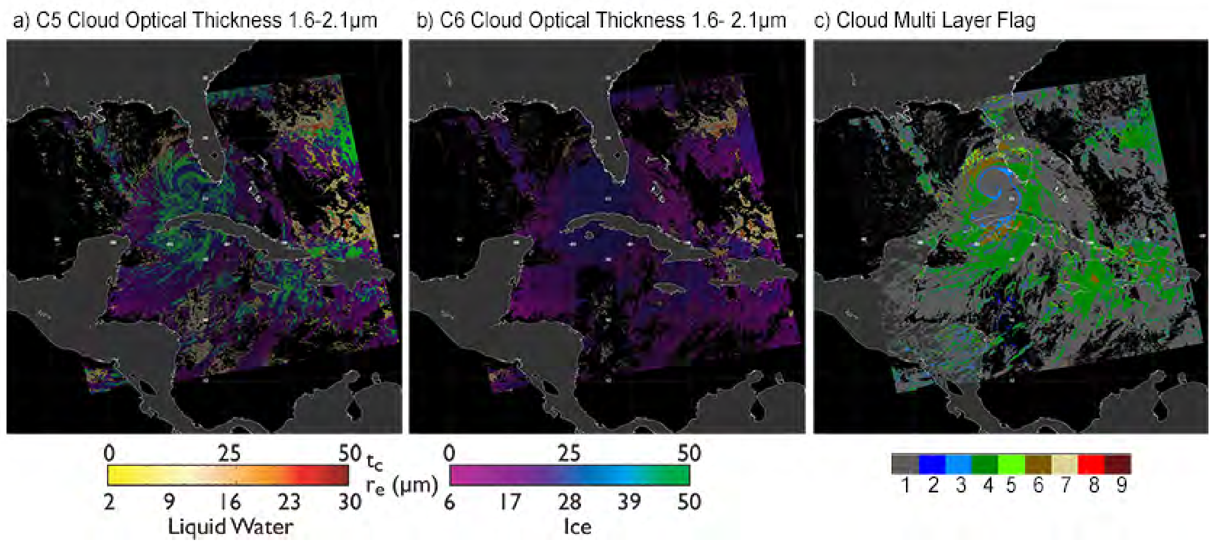


Figure 2.10.1-2. Example 1.6-2.1 μm retrievals and multilayer cloud SDS results (Aqua MODIS, day 238, 1840 UTC).

Additionally, the C6 algorithm includes a new test using COT differences between the standard retrieval (VNSWIR–2.1 μm) and the alternative 1.6–2.1 μm channel pair. It was found in C5 and early C6 testing that a significantly larger 1.6–2.1 μm COT often indicates the presence of multilayer clouds in the scene. In particular this test has some skill in flagging thin cirrus over liquid water clouds, something also confirmed using DISORT multilayer cloud simulations. However, due to a change in the 1.6–2.1 μm retrieval logic, the test is rarely positive anymore. This is because the original C5 solution logic inadvertently allowed 1.6-2.1μm retrievals to be outside the LUT solution space under multilayer cloud conditions while the C6 logic minimizes such a spurious outcome. The solution logic was updated late in the C6 development cycle and so the test remains in C6. **Figure 2.10.1-2** illustrates the change between C5 and C6 COT from the 1.6–2.1 μm retrievals. The C5 retrieval is maximum in areas that are likely multilayered. We will further investigate the source of the multilayer information content that was evident in the C5 retrievals.

A minor modification involves the 0.94 μm-based precipitable water retrieval test. These retrievals have been refined somewhat for C6 by interpolating between the table values of precipitable water instead of using the closest available point.

Finally, output information from the multilayer algorithm has been revised. In C5, integer values in the Cloud_Multi_Layer_Flag SDS indicated which tests were positive for any pixel and it was left to the user to decide the overall confidence level. In C6 each multilayer cloud test is now assigned a pre-defined confidence value, listed in the third column of **Table 2.10.1-1,** and the sum of those values is recorded in the SDS as a pseudo confidence level. As can be inferred from Table 2.10.1-1, the maximum SDS value is 10 when all tests are positive (the default SDS value is 1). The PH test was assigned a high value based on early C6 development and is expected to be reduced in subsequent collections (see previous discussion). In-

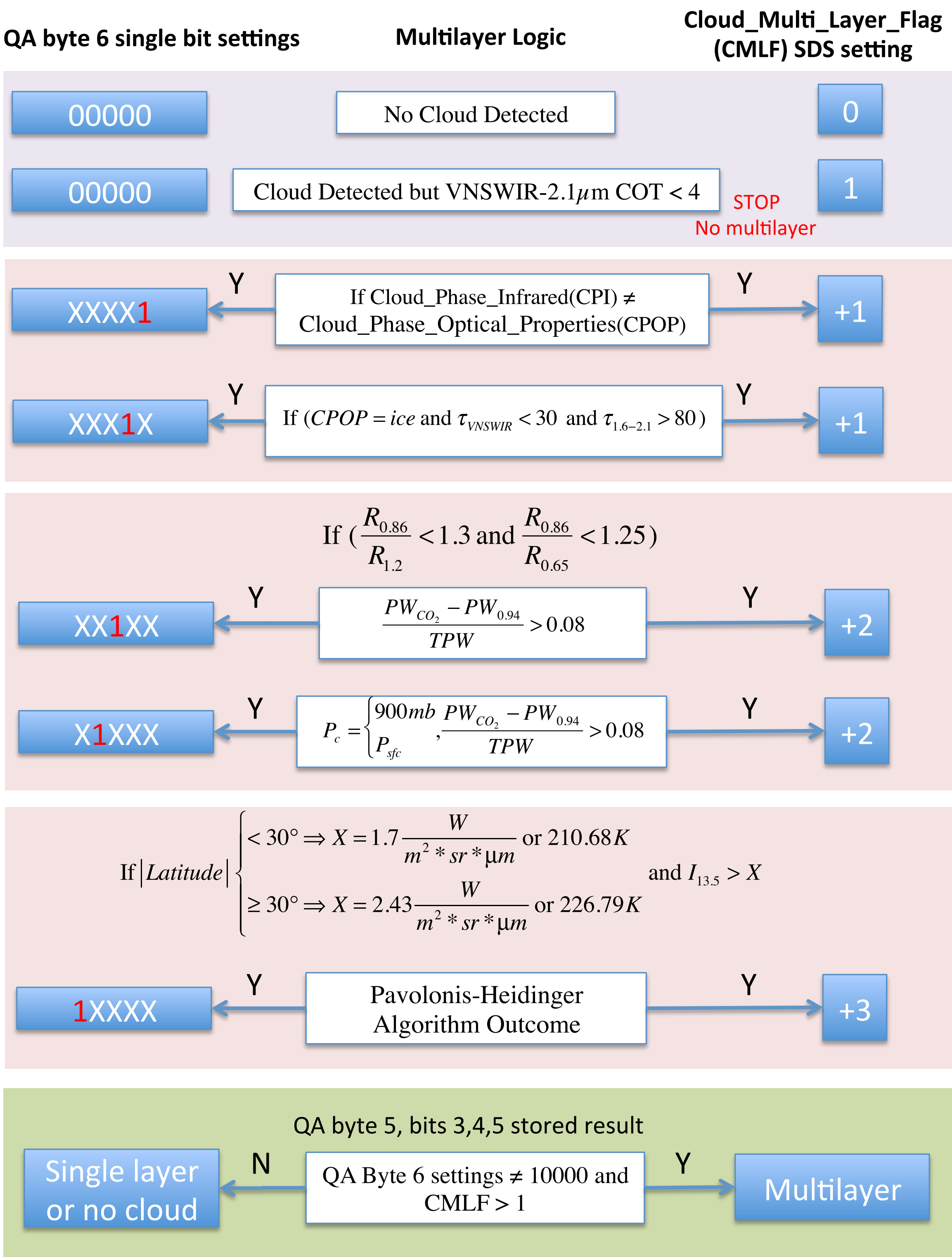


Figure 2.10.1-3. Schematic of multilayer cloud detection logic, and QA and SDS assignments.

dividual results from the five multilayer cloud tests (1 and 0 integer values for positive and negative detection, respectively) are now available in a new Byte 6 of the Quality_Assur-

Table 2.10.1-1. Multilayer cloud detection QA bit assignment in Byte 6.

| Bit position (Big-endian) | Multilayer Test | Detection Confidence Value (added to SDS) |
|---|---|---|
| 0 | IR and SWIR cloud phase difference | +1 |
| 1 | Delta precipitable water | +2 |
| 2 | Delta precipitable water with cloud at 900mb | +2 |
| 3 | VNSWIR-2.1 and 1.6-2.1 μm COT divergence | +1 |
| 4 | Pavolonis-Heidinger | +3 |

ance_1km SDS as described in **Table 2.10.1-1** (also see **Appendix B**). The L3 product aggregates retrievals into multilayer datasets only if one of the tests associated with bit positions 0 through 3 show positive detection. The assignment of multilayer cloud status by phase (QA bits 5, 6, 7 of Byte 5) are the same as in C5. If any multilayer test from Table 2.10.1-1 is positive, including the PH test, then the Byte 5 bits are set to indicate a multilayer cloud. A schematic depiction of the multilayer algorithm logic is shown in **Fig. 2.10.1-3.**

*Recommendation*: Users should look carefully at the Byte 6 results and either (i) use the results as they see fit, or (ii) use the same filtering methodology used by the MOD06 team for L3 multilayer statistical aggregations as described above. Because of the high weighting given to the PH test in early C6 development, users should not use the Cloud_Multi_Layer_Flag SDS to infer overall confidence in the multilayer detection result.

### *2.10.2. Cloud model single scattering properties vs. CER*

The C6 product file now includes arrays of spectral asymmetry parameter ($g_\lambda$), single scattering albedo ($\omega_{0_\lambda}$), and extinction efficiency factor ($Q_{e_\lambda}$) so that users can compare or scale retrievals to their own radiative transfer models should they so desire. These scattering properties are provided for both the ice and liquid water cloud models. This is particularly useful for ice models where variability in assumed ice habit/surface roughness can significantly impact the asymmetry parameter in all solar reflectance bands as well as the single scattering albedo in the SWIR. SDS scattering property names are given in **Table 2.10.2-1**; array formats and values are given in **Appendix D**.

Table 2.10.2-1. Listing of single scattering properties and their respective SDS names. See Appendix D for further details.

| Scattering Property | SDS Name |
|---|---|
| Ice $g_\lambda$ | **Asymmetry_Parameter_Ice** |
| Ice $\omega_{0\lambda}$ | **Single_Scatter_Albedo_Ice** |
| Ice $Q_{e_\lambda}$ | **Extinction_Efficiency_Ice** |
| Liquid water $g_\lambda$ | **Asymmetry_Parameter_Liquid** |
| Liquid water $\omega_{0\lambda}$ | **Single_Scatter_Albedo_Liquid** |
| Liquid water $Q_{e_\lambda}$ | **Extinction_Efficiency_Liquid** |

### *2.10.3. Ancillary data sources*

MOD06 uses several external ancillary data sources, the primary source being NCEP GDAS output [*Derber et al.*, 1991]. The NCEP GDAS files are generated by the spectral Medium Range Forecast model (MRF), which is a version of the NCEP GFS model. The dataset is a 6-hour archive product (also known as Final Run at NCEP) and includes late arriving conventional and satellite data. It is produced every 6 hours, starting at 00:00 UTC each day, and is distributed in GRIB (GRIdded Binary) format on a $1° \times 1°$ grid. **Table 2.10.3-1** lists the 2D and 3D GDAS model data fields utilized by MOD06.

### *2.10.4. Increased vertical resolution of NCEP temperature and moisture profiles*

MOD06 now ingests all 26 levels of atmospheric temperature and moisture from the NCEP GDAS files rather than the lowest 16 levels as in C5. This ancillary information is used in the above cloud atmospheric correction (water vapor attenuation) calculations, as well as for estimating thermal emission in the 3.7 µm channel. In addition, C6 uses the NCEP GDAS analysis of sea surface temperature (SST), which is created by the same algorithm as the weekly Reynolds SST used previously in C5 but is updated every six hours. This SST is necessary for determining the thermal emission from the ocean surface in the 3.7 µm and 11 µm channels.

Table 2.10.3-1. Listing of GDAS model fields used by MOD06.

| Field name | Description |
|---|---|
| TMP:* mb | Level temperature profile at 26 pressure levels between 10 and 1000 mb |
| RH:* mb | Level relative humidity profile at 21 pressure levels between 100 and 1000 mb |
| UGRD/VGRD: 10 m above gnd | *u* and *v* components of wind vector at 10m altitude above ground (not sea level) |
| PRES:sfc | Surface pressure |
| TMP:sfc | Surface Temperature |
| RH: 2m above gnd | Relative humidity at 2m above ground (not sea level) |
| PRMSL | Pressure at mean sea level (MSL) |
| TOZNE: atmos col | Integrated total column ozone amount |

*2.10.5. Spatial interpolation of surface temperature*

Because the TOA radiance at 3.7 µm includes both reflected solar and emitted thermal radiation, and the 3.7 µm cloud optical properties retrieval uses only the reflected solar radiation component, the TOA surface, cloud, and atmospheric emission components must be removed before the retrieval is performed. To characterize the TOA surface component, the GDAS "TMP:sfc" field is used for surface temperature over land; over the ocean we use the GDAS sea surface temperature as discussed in Section 2.10.4. Smoothing of the land surface temperatures is now accomplished via spatial interpolation. Note for ocean surfaces, effective surface and cloud emissivities are contained in the LUTs; for land surfaces these emissivities are calculated from the LUT flux and spherical albedo data.

*2.10.6. Spatially and temporally interpolated column ozone from GDAS*

Spatially and temporally interpolated column ozone data from GDAS are now used as opposed to the TOAST daily column ozone product values (nearest-neighbor lookup) used in C5. This change affects retrievals over land only and primarily impacts the retrieval of cloud optical thickness.

*2.10.7. Adjustment of low cloud top temperature retrievals for non-unity emissivity*

The MOD06 cloud top properties algorithm assumes unity cloud emissivity whenever the 11 µm window channel (MODIS channel 31) is used to infer the temperature of lower tropospheric clouds (see Sect. 1.1.1). To better calculate the 3.7 µm channel effective emission for low clouds, we use the retrieved cloud optical thickness to iteratively adjust the 11 µm cloud emissivity for use in the window cloud-top temperature retrieval. This involves LUTs of 11 µm effective surface and cloud emissivity similar to what is done for the 3.7 µm channel [*Platnick and Valero*, 1994]. A final adjusted cloud top temperature is achieved using a stand-alone version of the University of Wisconsin 11 µm cloud top temperature algorithm coupled with the 3.7 µm COT retrievals, and iterating until convergence is achieved; typically only a couple of iterations are required. This has a modest but predictable effect on the 3.7 µm-derived CER; the non-unity 11 µm cloud emissivity gives rise to warmer cloud top temperatures (for typical surface/cloud temperature contrasts), reducing the 3.7 µm thermal emission which increases the 3.7 µm reflectance component, and ultimately results in a *smaller* 3.7 µm-derived CER.

The iterative procedure is as follows: When the cloud top QA indicates that the $CO_2$ slicing algorithm was run, the 5 km cloud-top temperature (CTT) dataset is used. However, if the QA indicates that the IR window (**IRW**) algorithm was run, then for the 3.7 µm retrievals the CTT is recalculated using a stand-alone 1 km IRW algorithm within the cloud optical properties code. The cloud and surface effective emissivities are a function of COT and CER, and the new CTT is

$$T_c = B^{-1}\left[\frac{B(T_{c,IRW}) - \varepsilon_s(COT,CER)T_s)}{\varepsilon_c(COT,CER)}\right] \cdot \qquad (2.10.1)$$

This new CTT is used in the next 3.7 µm retrieval iteration. The CTT retrieval converges when the difference between the original and new CTT is less than 0.01 K. In practice, the convergence is very rapid and normally occurs within 2-3 iterations. This modified CTT is stored in a new SDS named *IRW_Low_Cloud_Temperature_From_COP*. While this may provide a more realistic CTT for thin low clouds for general users, in the current algorithm it is used solely to improve the 3.7 µm retrievals.

The impact of this change is that CER_37 decreases slightly for optically thin clouds for the typical situation where the surface is warmer than CTT. This is due to the fact that the surface radiance escaping at cloud-top is removed while the net cloud emission is reduced. Since the measured radiance doesn't change, the reflected radiance component is increased and thus the retrieved effective radius decreases.

### *2.10.8. Improved surface albedo at 3.7 µm*

In C6, a land surface emissivity database at 3.7 µm [*Seemann et al.*, 2008] is used to determine the corresponding surface albedo ($A_g = 1 - \varepsilon$). In C5, it was assumed that the surface albedo was one-half of that at 2.1 µm. The emissivity-derived surface albedo is generally *lower* than the previously-used albedo that was extrapolated from the MOD43 dataset (Sect. 2.3). This leads to somewhat *smaller* 3.7 µm CER retrievals.

### *2.10.9. Other 3.7 µm updates: above-cloud emission and solar irradiance*

For C6 we use atmospheric transmittance tables derived from FASCODE instead of MODTRAN, and include the above-cloud atmospheric emission in accounting for the total measured 3.7 µm signal. In addition, the 3.7 µm band-averaged solar irradiance was changed to 10.93 W $m^{-2}$ $\mu m^{-1}$ (vs. 11.74 W $m^{-2}$ $\mu m^{-1}$ in C5), based on *Platnick and Fontenla* [2008].

### *2.10.10. Maximum retrievable cloud optical thickness extended to 150*

The maximum COT value reported in C6 is now 150, rather than the maximum value of 100 used in C5. The choice of 150 was based on analyses of pixel-level uncertainty calculations that often showed the COT uncertainty at COT = 150 to be similar to that for small COTs (~1 or less). **Figure 2.10.10-1** illustrates the relationship between pixel-level COT retrieval uncertainty and retrieved COT for an example granule (Aqua MODIS 6 April 2005, 18:30 UTC). The COT mean uncertainty at COT = 150 for liquid water clouds (red line) is less than that for COT < 0.5, though this relationship is reversed for ice clouds (blue line) in this example granule.

### *2.10.11. Use of new 1 km cloud-top property retrievals*

New 1 km resolution cloud top pressure datasets [*Baum et al.*, 2012] are used in above cloud atmospheric corrections (gaseous absorption and Rayleigh scattering) and the NIR-SWIR cloud thermodynamic phase algorithm instead of the 5 km cloud top pressures used in C5. This leads to more successful retrievals and fewer failed retrievals associated with broken and variable cloud situations, though the 1 km cloud top retrievals are somewhat less spatially consistent when clear sky minus cloudy sky radiance differences are small.

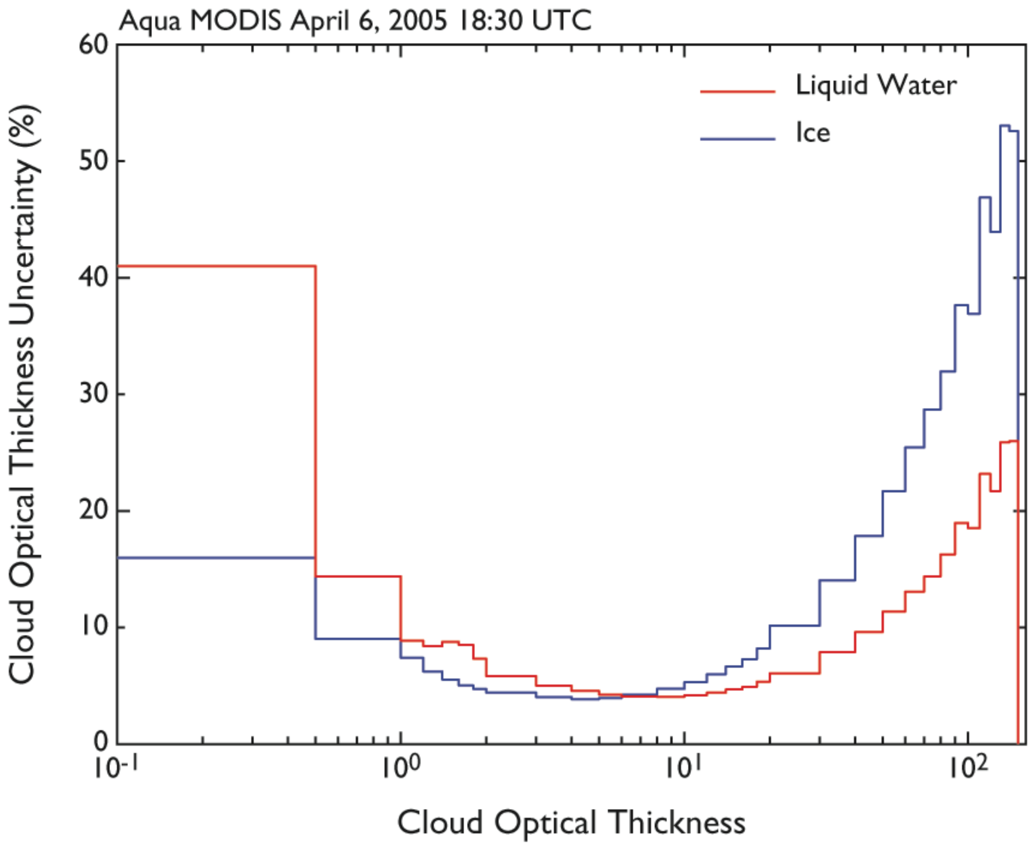


Figure 2.10.10-1: Histogram of cloud optical thickness uncertainty as a function of cloud optical thickness for an example granule.

*2.10.12. Statistics_1km and Statistics_1km_sds*

The C5 MODIS cloud product file template provided for a vector (VData) of various statistics about retrievals within the granule file. However, by omission that vector had never actually been populated (i.e., zeros). A contributing factor was that the file specification defined any 1D dataset as a VData, making it quite difficult to access because a different set of HDF tools must be invoked in order to view the content. Additionally, the attributes of a VData object are invisible unless a special tool from the HDF library is invoked. Thus, even if the values were visible, users would not know what those values meant. In C6 we have correctly populated the VData vector *Statistics_1km* and additionally provided equivalent information in an easy to read 1D SDS named *Statistics_1km_sds*. The SDS provides information for users interested in the set of granule-level statistics shown in **Table 2.10.12-1**.

Table 2.10.12-1. Information continued in Statistics_1km and Statistics_1km_sds.

| Position | Information and units where applicable |
|---|---|
| 1 | Successful retrieval rate (%) |
| 2 | Land cover fraction (%) |
| 3 | Water cover fraction (%) |
| 4 | Snow cover fraction (%) |
| 5 | Cloud cover fraction (%) |
| 6 | LIquid water cloud fraction (%) |
| 7 | Ice cloud fraction (%) |
| 8 | Mean liquid water cloud optical thickness |
| 9 | Mean ice cloud optical thickness |
| 10 | Mean liquid water cloud effective radius (μm) |
| 11 | Mean ice cloud effective radius (μm) |
| 12 | Mean liquid water cloud top pressure (mb) |
| 13 | Mean ice cloud top pressure (mb) |
| 14 | Mean undetermined cloud top pressure (mb) |
| 15 | Mean liquid water cloud top temperature (K) |
| 16 | Mean ice cloud top temperature (K) |
| 17 | Mean undetermined cloud top temperature (K) |

*2.10.13. Cloud_Mask_SPI*

A new Cloud_Mask_SPI SDS has been added that contains the sub-pixel heterogeneity index ($H_{\sigma,\lambda}$), defined as *Liang et al.* [2009] as

$$H_{\sigma,\lambda} = \frac{stdev\left[R\left(\lambda, 250m\right)\right]}{mean\left[R\left(\lambda, 250m\right)\right]} \times 100 \quad , \tag{2.10.2}$$

where $stdev[R(\lambda,250m)]$ and $mean[R(\lambda,250m)]$ are the standard deviation and mean of the measured reflectances, respectively, of the sixteen 250 m resolution sub-pixels within the 1 km MODIS footprint. $H_{\sigma,\lambda}$ is reported for both the 0.66 and 0.87 μm wavelengths (λ). This SDS provides an additional metric for retrieval quality assessment, as large sub-pixel heterogeneity has been shown to be associated with retrieval biases [*Zhang and Platnick*, 2011; *Zhang et al.*, 2012] and increased retrieval failure rates [*Cho et al.*, 2015].

## 3. Level-3 Cloud Optical/Microphysical Dataset Overview

There is a single set of spatially aggregated global L3 files produced by the MODIS Atmosphere Team (including cloud mask and cloud top properties, cloud optical/microphysical properties, aerosol properties, profiles, and water vapor). Temporal aggregations are provided for daily (**MOD08_D3**), eight-day (**MOD08_E3**), and monthly (**MOD08_M3**) periods. A variety of statistical datasets are provided, and include scalars and 1D and 2D histograms. The eight-day (reset at the beginning of each calendar year) and monthly aggregations are derived directly from the daily files. As with previous collections, daily files aggregate all pixels that map into a grid cell for all overpasses during the day, resulting in an aggregation over multiple satellite overpasses for grid cells poleward of about 30° latitude. This section contains a high level description of the L3 datasets relevant to the MOD06 cloud optical properties. For a more detailed description of all available L3 datasets, please refer to the C6 L3 ATBD (modis-atmos.gsfc.nasa.gov/_docs/L3_ATBD_C6.pdf).

All L3 spatial aggregations are on a 1° equal-angle grid. An important property to note when considering L3 gridding occurs due to distortion in the latitude-longitude map projection as one moves poleward. For example, at the equator each 1° grid cell is roughly 12,000 $km^2$ in size, while at the pole each 1° grid cell is less than 100 $km^2$, i.e., over two orders of magnitude difference. It should also be noted that there is a variation of pixel size in the L2 input products due to viewing (scan angle) distortion. For example, the 1 km (nadir) resolution pixel size expands to about 4 km due to view angle distortion when moving from nadir towards the swath edge. These same distortion factors also apply to retrievals produced at 5 and 10 km resolution.

For L2 pixels that fall exactly on a L3 grid boundary, assignment to L3 grid cells is performed using the following convention: L2 pixels that fall exactly on the first whole degree boundary 90°N (+90.0) latitude and 180°W (-180.0) longitude are binned in the L3 grid column and row #1. L2 pixels that fall exactly on the second whole degree boundary 89°N (+89.0) and 179°W (-179.0) are binned in L3 grid column and row #2. The exception to this logic occurs in the last L3 grid row (89°S to 90°S), which contains both whole degree latitude boundary pixels (-89.0 as well as -90.0). There is no exception for the last L3 grid column (179°E to 180°E) since +180.0 and -180.0 represent the same physical location (these L2 pixels are binned in the first L3 grid column).

C6 L3 Changes:

The "definition of the day" for earlier collections coincided with UTC. However, this caused spatial gaps around 0° and 180° longitude that made comparison with other EOS daily L3 products difficult in those regions. For C6, the "definition of the day" has been modified to move the spatial gap (which is impossible to avoid) to the nighttime poles. Specifically, we first subtract/remove early (0000 to 0300 UTC) measurements just to the east of the dateline (daytime observations) and just to the east of the Greenwich meridian (nighttime). Then we add early measurements from the following day to the same longitude zones. This gives orbit-

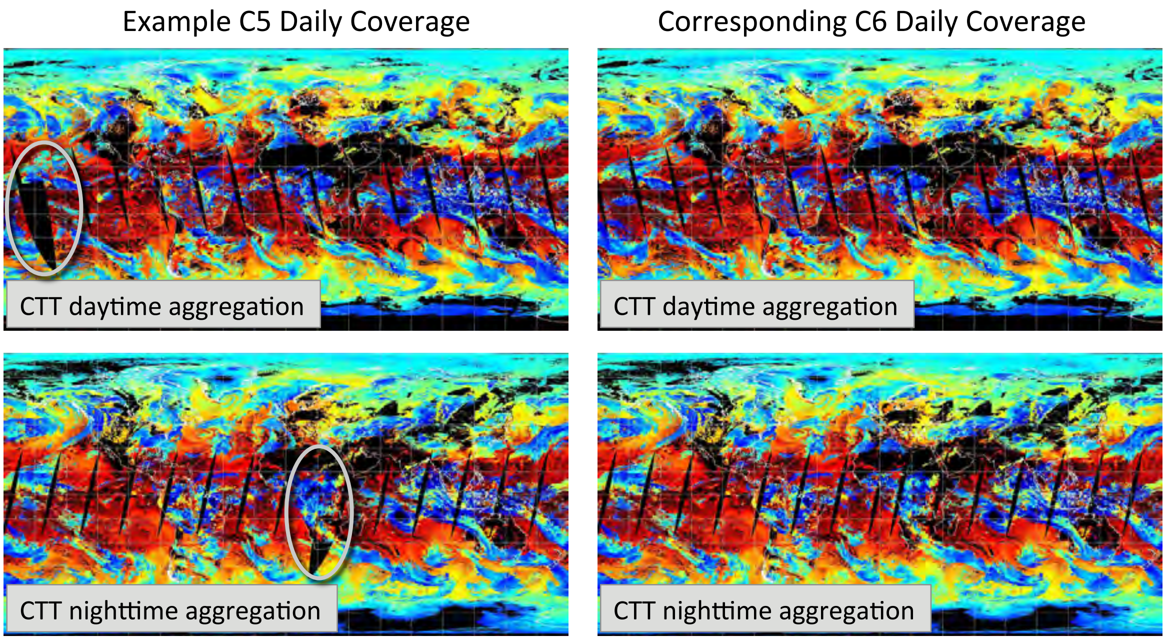


Figure 3-1. Example of daily spatial coverage using "definition of the day" from C5 vs. C6. Cloud top temperature is used for the example since the product has both day and night retrievals. The location of the spatial data gaps caused by using a strict UTC definition for C5 and earlier collections are indicated.

to-orbit continuity except for seams at the Dateline (day) and Greenwich meridian (night). For Terra C6, the exercise is similar with some end-of-day measurements excluded and prior day end-of-day measurements included. All excluded measurements will contribute to the next day. An example is given in **Fig. 3-1**.

Statistics for a number of additional SDSs have been added for C6. For cloud optical properties, the most notable additions are statistics for separate "partly cloudy" retrievals (*_PCL SDS names associated with CSR = 1,3 designations, cf. Sect. 2.8) along with separate aggregations for retrievals from band pairs using the 1.6 µm and 3.7 µm channels (Sect. 2.5). This includes joint COT-CER histograms for the additional spectral retrievals in addition to the usual complement of scalar statistics.

Throughout the C6 L3 file, there have been a number of SDS name changes. For cloud optical properties, one change of note is from the SDS name *Cloud_Fraction_** to *Cloud_Retrieval_Fraction_** (where the asterisk represents Liquid, Ice, Undetermined phase and other spectral retrievals beyond the standard retrieval pair that includes the 2.1 µm channel). This is done to eliminate confusion with the cloud mask fraction (*Cloud_Fraction, Cloud_Fraction_day, Cloud_Fraction_night, etc.*). This name change also better conveys that the fraction represents successful retrievals in a grid cell from the optical retrieval algorithm normalized by the total number of pixels that fall into the grid cell. As with the L2 products, users should always look at the corresponding HDF "long names" that provide details beyond what can be inferred from the SDS "short" names.

A summary of the C6 L3 cloud optical/microphysical statistical parameters is given in **Appendix F**. A complete list of C6 Atmosphere Team L3 statistics is available on the team web site (modis-atmos.gsfc.nasa.gov/products_C006update.html).

Previous L3 versions included QA-weighted cloud optical property statistics. The pixel-level *Retrieval Confidence* QA-weightings were two bit integer values (with 3 being the best quality) used to reduce the impact of retrievals expected to be in a part of the solution space where the uncertainties would be greatest. For C5, reduced confidence QA values were assigned for liquid water clouds only (see modis-atmos.gsfc.nasa.gov/C005_Changes/C005_-CloudOpticalProperties_ver311.pdf). With improved pixel-level COT, CER, and CWP uncertainty estimates in C6, it was decided to drop QA-weightings in the L3 C6 optical property datasets. Instead, users are referred to the uncertainty of the mean SDSs that have been provided in the L3 dataset since C5. For example, for each grid box, the L3 daily SDS *Cloud_Optical_Thickness_Liquid_Mean_Uncertainty* provides an estimate of the uncertainty in the L3 daily mean COT (*Cloud_Optical_Thickness_Liquid_Mean*) based on the L2 uncertainty SDS *Cloud_Optical_Thickness_Uncertainty* for the relevant liquid water pixels (details in modis-atmos.gsfc.nasa.gov/reference_atbd.html). Note that the L3 uncertainty SDSs are in absolute units (e.g, μm for CER) whereas the L2 uncertainty SDSs are in percent.

Due to an HDF4 uncompressed file size limitation of 2 GB, several 2D histograms are only available in the daily MOD08_D3 file (see '*d*' designation in the tables of Appendix F). However, eight-day and monthly aggregations can be computed by calculating pixel-weighted (count-weighted) aggregations directly from the daily files (consult the C6 L3 ATBD for further details: modis-atmos.gsfc.nasa.gov/_docs/L3_ATBD_C6.pdf).

## 4. MODIS-Atmosphere Team Web Site and Browse Imagery

The MODIS Atmosphere Team web site provides L2 and L3 browse imagery for many of the key scalar statistics from the various team data products. L2 imagery is currently displayed on the main browse imagery page (**Fig. 4-1**, modis-atmos.gsfc.nasa.gov/IMAGES) with zoom and rotation functionality; links to L3 browse pages are provided within the left side bar.

For L3 products, users can select specific daily, 8-day, and monthly statistics with separate pages for each major discipline group (see **Figs. 4-2**, **4-3**). Daily and 8-day product browse imagery is only available in the native latitude-longitude rectangular grid. Monthly browse images are also available in an equal-area projection (Hammer-Aitoff), though users should be aware that some mild distortion, and occasionally even loss of data, can be seen while converting from one map projection to another in regions (especially high latitudes) where there are sparse data. The native latitude-longitude projection is the preferred choice for quantitative understanding. A discretized modified-rainbow color bar is applied to each image and the data scale is optimized to maximize image detail. Fill (missing) data are always colored black. Multiple statistics (SDSs) for a single parameter can be viewed by using a built-in "mouse-over" functionality on the web page by rolling the mouse cursor over the statistic "bars" to the right of each image (**Fig. 4-3**).

In addition to browse imagery, there is an assortment of product and reference information that is provided on the team web site including complete file specifications, details on the format and content, modification history, and known problems. Also available are programs and tools that can read and image L3 HDF file SDSs. C6 team documents (including this user guide) are maintained on the following page: modis-atmos.gsfc.nasa.gov/products_C006up-

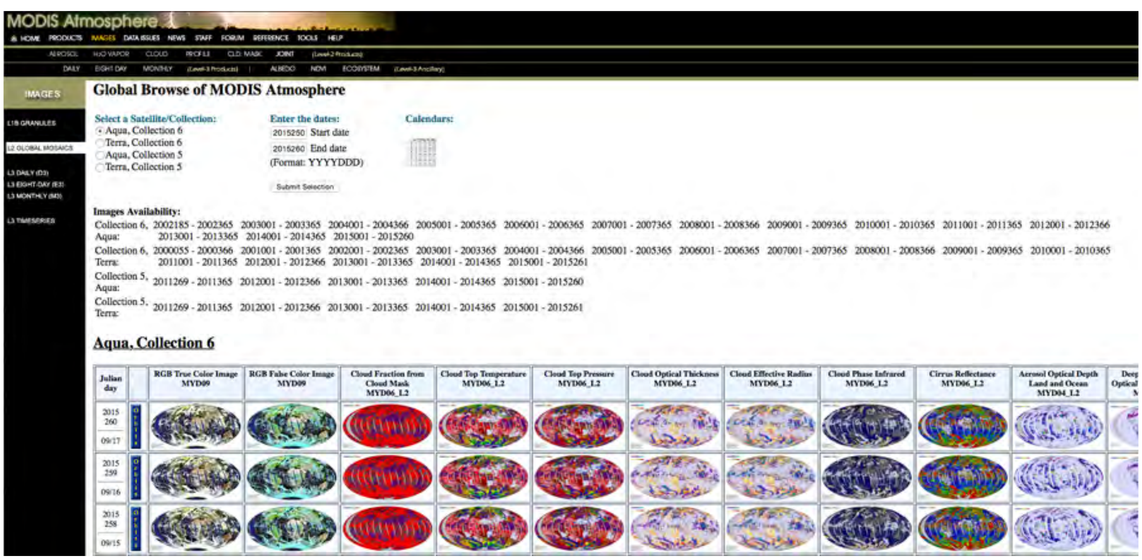


Figure 4-1. Front page of the MODIS Atmosphere Team browse page showing global L2 thumbnail images for a variety of key team SDSs.

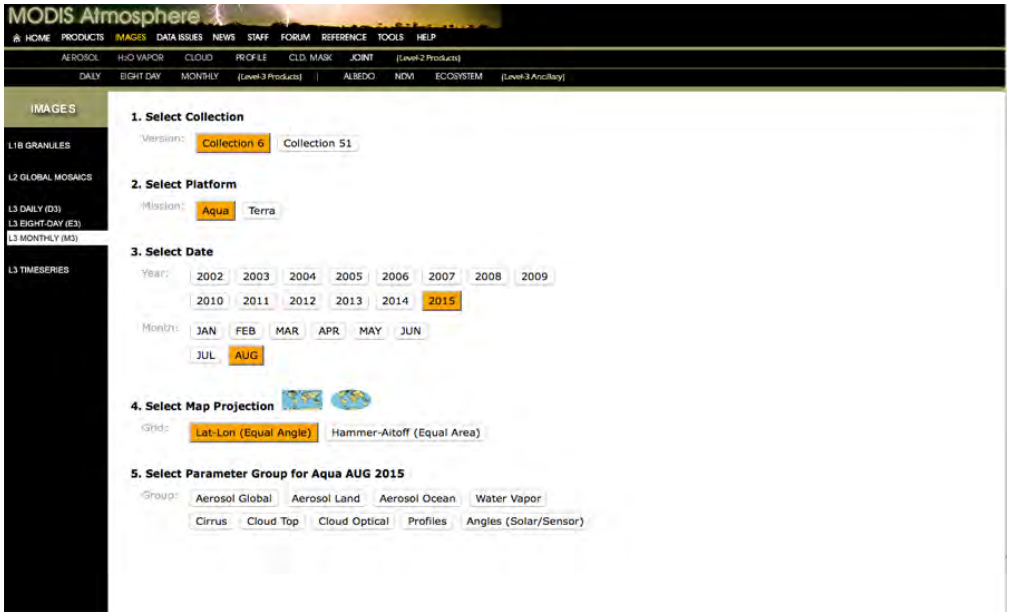


Figure 4-2. The interface that allows viewing of key scalar statistical images in the Atmosphere Team L3 HDF files. A user selects a "derived-from" product group, the time period, and map projection.

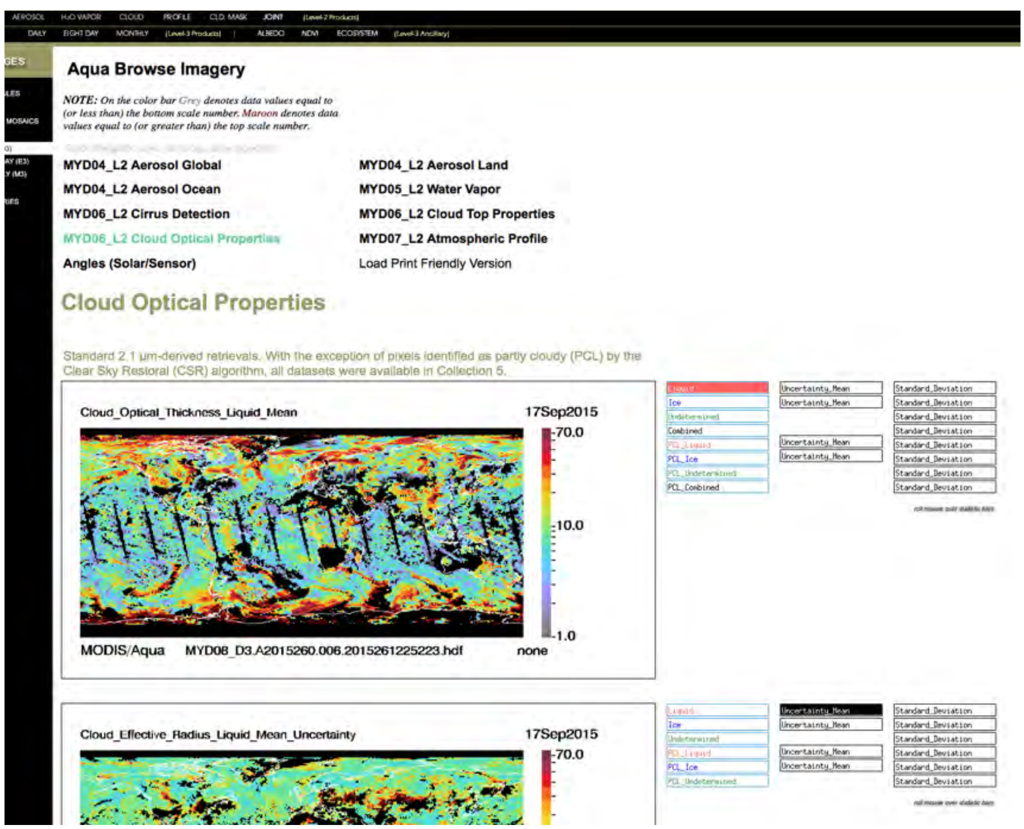


Figure 4-3. Example L3 daily browse images for cloud optical products (URL here). A variety of dataset can be viewed by using a mouse-over function implemented on the mean, uncertainty, and standard deviation bars to the right of each image.

date.html.

## 5. MOD06 Optical Properties Data: Frequently Asked Questions

### Cloud Optical Properties

#### *Q: How do I assess the quality of the optical and microphysical retrievals?*

***A:*** In Collection 5, a Confidence QA bit flag (values from 0 for no confidence to 3 for high confidence) within the *Quality_Assurance_1km* SDS was assigned to each retrieval that, in addition to the pixel-level retrieval uncertainty, provided some measure of retrieval quality. In Collection 6, however, the Confidence QA is set to 3 (i.e., high confidence) for all successful retrievals such that it is no longer useful for quality assessment. Nevertheless, sufficient information is provided in accompanying SDSs for users to infer retrieval quality.

Because large pixel-level retrieval uncertainty implies the observed reflectances lie in a portion of the LUT solution space that is less sensitive to the retrieved quantity, users are advised to determine retrieval quality in part via retrieval uncertainty. Users are also encouraged to look at the new *Cloud_Mask_SPI* SDS that provides the sub-pixel heterogeneity index [*Liang et al.*, 2009] (see **Section 2.10.13** of the MOD06 User Guide). Large sub-pixel heterogeneity has been shown to be associated with retrieval biases [*Zhang and Platnick*, 2011; *Zhang et al.*, 2012] and increased retrieval failure rates [*Cho et al.*, 2015]. Likewise, users can also query the Multi Layer Cloud Flag that is included in the *Quality_Assurance_1km* SDS (see **Section 2.10.1** of the MOD06 User Guide for details and recommended usage), as multi-layer cloud scenes are problematic for retrievals such as MOD06 that assume a single cloud phase.

Finally, in some instances the cloud top retrievals may fail (e.g., due to known saturation issues with the 14 µm $CO_2$-slicing channel), in which case the MOD06 optical and microphysical retrievals default to the surface temperature and pressure for the cloud top assumption and atmospheric corrections, thus yielding suspect retrievals. Users are advised that MOD06 optical and microphysical retrievals that have corresponding 1 km cloud top temperature or pressure retrievals set to fill values should be discarded.

#### *Q: There are three spectral cloud effective radius (CER) retrievals. Which should I use, and how do I interpret their differences?*

***A:*** It depends on your particular application.

While the three spectral channels have been shown to have different penetration depths within a plane-parallel, vertically inhomogeneous cloud [*Platnick*, 2000], users should nevertheless be cautious drawing conclusions from CER retrieval differences, e.g., inferring vertical cloud droplet size distributions. Errors in atmospheric corrections, the 3.7 µm emission correction, etc., may yield artifacts in the spectral CER differences. In addition, 1.6 µm CER retrievals from Aqua MODIS require greater scrutiny due to known non-functioning detectors and potential unknown issues with the remaining functional detectors (see **Section 2.5** of the MOD-06 User Guide).

### Q: Why are there multiple spectral cloud optical thickness (COT) retrievals?

***A:*** To provide the three spectral cloud effective radius (CER) retrievals, the full retrieval process is run for each dual spectral channel combination, and therefore yields three independent COT retrievals. In most cases these three COT retrievals will be nearly identical since each is derived from the same VNSWIR channel reflectance. However, in non-orthogonal regions of the pre-computed look-up table solution space where the SWIR or MWIR reflectance can influence the COT retrieval result, for instance at small COT, the three COT retrievals may differ. Furthermore, because the spectral CER retrievals are known to fail at different rates and under different conditions [e.g., *Cho et al.*, 2015], the cloudy pixel population having successful COT and CER retrievals will be different for each spectral combination. It was therefore decided to report each COT retrieval independently, instead of providing a single combined COT dataset, such that each spectral CER retrieval will have a consistent COT retrieval.

### Q: How do I interpret the PCL (partly cloudy) retrievals?

***A:*** The PCL SDSs contain retrievals for those pixels that are identified as partly cloudy or cloud edge by the Clear Sky Restoral (CSR) algorithm (see **Section 2.8** of the MOD06 User Guide). These pixels are expected to deviate from the retrieval assumptions of an overcast homogenous cloudy FOV and 1-dimensional plane-parallel radiative transfer, conditions that have been shown to be associated with retrieval biases [*Zhang and Platnick*, 2011; *Zhang et al.*, 2012] and increased retrieval failure rates [*Cho et al.*, 2015].

### Q: What is the Retrieval Failure Metric and how is it useful?

***A:*** The *Retrieval_Failure_Metric* (RFM) SDSs represent an attempt to provide additional information about COT and CER retrieval failures, specifically the look-up table (LUT) COT and CER values nearest to the observed reflectances (when applicable) and a Cost Metric that provides a measure of the "degree of failure," i.e., the relative distance of the observed reflectances from the LUT solution space. The RFM COT, CER, and Cost Metric parameters are assigned values such that the user can ascertain how a given spectral retrieval failed. Details of the RFM SDS assignments and interpretation can be found in **Section 2.6** of the MOD06 User Guide.

### Q: What if I would prefer to use my own ice particle habit assumptions instead of those used in producing your ice LUTs?

***A:*** For Collection 6, we are for the first time providing our assumed bulk ice and liquid phase single-scattering properties (i.e., extinction efficiency $Q_e$, asymmetry parameter $g$, and single scatter albedo $\omega_0$) within each MOD06 HDF file (see **Section 2.10.2** of the MOD06 User Guide). These properties can be used to scale the cloud optical retrievals to the radiative model of your choice! For instance, the cloud optical thickness from MOD06 ($\tau$) can be scaled to that of a different ice model ($\tau^*$) using similarity rules [*van de Hulst*, 1974]:

$$\tau^* = \frac{(1-\omega_0 g)}{(1-\omega_0^* g^*)}\tau$$

### *Q: How do I interpret the Cirrus_Reflectance and Cirrus_Reflectance_Flag SDSs?*

***A:*** While very minor updates were made for C6, the algorithm that produces this dataset is no longer being supported by NASA. Please direct queries to product developer Dr. Bo-Cai Gao at gao@nrl.navy.mil.

### *Q: What are the differences between the various cloud phase products?*

***A:*** There are two cloud phase algorithms included in MOD06. The first is an infrared (IR) based algorithm that is run in parallel with the cloud top (CT) property retrievals. It provides cloud phase at 1 km and 5 km spatial resolution for both daytime and nighttime, with results reported in the *Cloud_Phase_Infrared* SDSs. Details of this algorithm can be found in *Baum et al.* [2012].

The second algorithm, run as part of the cloud optical property retrieval algorithm, provides the final phase decision for the COT and CER retrievals and derived cloud water paths (CWP). It employs a variety of shortwave-infrared (SWIR) based tests, in addition to information from the CT and IR phase retrievals, thus yielding phase results for daytime only. Results from this algorithm are reported in the *Cloud_Phase_Optical_Properties* SDS and as a QA bit flag in the *Quality_Assurance_1km* SDS. Details of this algorithm, including changes for C6, can be found in **Section 2.4** of the MOD06 User Guide.

## Cloud Top Properties and IR Phase

### *Q: Why do cloud top retrievals sometimes have anomalous "boxes" or striping?*

***A:*** These features, that usually only appear in the highest altitude cloud top retrievals, are caused by mismatches between the observed infrared (IR) radiances and the 1° resolution NWP model profiles of temperature, moisture, and ozone that are necessary inputs to the $CO_2$-slicing algorithm. Note that no spatial interpolation is performed on the NWP model output, i.e., the profiles are used at their native 1° spatial resolution.

### *Q: Which cloud top property retrievals should I use, 1 km or 5 km?*

***A:*** For C6 a number of updates and improvements were made to the cloud top property products (cloud top pressure, height, temperature and cloud effective emissivity) that are documented extensively in *Menzel et al.* [2008]. In C5 and earlier versions, these parameters were available only at 5 km spatial resolution. In C6, these parameters are now available for the first time at the same 1 km resolution as the cloud optical and microphysical properties. Additional information, including comparisons of C6 cloud top heights to those derived from the CALIOP lidar, are available in *Baum et al.* [2012].

Users should choose between the 1 km and 5 km products based on individual needs. For example, the 1 km product is best if finer spatial resolution is a paramount concern, and the 5 km version is suggested for comparisons with heritage data such as HIRS. The 5 km product generally exhibits higher signal to noise characteristics, i.e., more spatially consistent retrievals when clear-sky minus cloudy-sky radiance differences are very small.

### *Q: Which IR cloud phase retrieval should I use, 1 km or 5 km?*

***A:*** For C6 a number of updates and improvements were made to the IR cloud phase that are documented extensively in Baum et al. [2012], and like the cloud top property retrievals, in C6 it is now available for the first time at the same 1 km resolution as the cloud optical and microphysical properties. Because the older framework for the 5 km IR phase retrieval could not be easily modified without a complete rewrite, among other constraints, algorithm development and evaluation focused instead on the 1 km product. However, instead of replacing the existing 5 km IR phase product with the new 1 km version, the algorithm development team decided to maintain in C6 a version of the 5 km product for continuity with C5. Users should be aware that the processing framework changed significantly for the 1 km IR phase retrieval, and differences between the 1 km and 5 km products should therefore be expected.

The new 1 km IR cloud phase underwent extensive testing and evaluation through comparison with CALIPSO/CALIOP products, and is expected to be of better quality than the heritage 5 km products. Furthermore, it is likely that the 1 km and 5 km products will continue to diverge as further improvements to the 1 km products are made over time. Users are thus advised to use the 1 km IR phase product both now and in the future.

## Miscellaneous

### *Q: What is the definition of a daytime pixel?*

***A:*** The cloud optical and microphysical property retrievals define daytime pixels as those having solar zenith angle less than 81.36°. Note this definition differs from that of the cloud top property and IR phase retrievals, as well as the MOD35 cloud mask; daytime pixels for these products are defined as those pixels having solar zenith angle less than 85°.

***Q: The MOD06 files only include 5 km resolution Latitude and Longitude SDSs. How do I obtain geolocation information for the 1 km cloud products?***

***A:*** In early collections of MOD06, only the 5 km Latitude and Longitude SDSs were included in the files in order to minimize file size. While file size is no longer a concern, the geolocation SDSs in the files remain at 5 km resolution for historical reasons. To obtain the 1 km geolocation data, users can either interpolate/extrapolate the 5 km SDSs to 1 km resolution, or download the MOD03 geolocation file that corresponds to the granule(s) of interest.

***Q: Many retrieval parameters are stored as integers in the HDF file. How do I convert these to something useful?***

***A:*** Nearly all MOD06 retrieval parameters are stored as 16-bit integers to reduce the HDF file size. To convert these back to useful floating point values, one must first read the *scale_factor* and *add_offset* attributes of each SDS. The conversion equation is then:

$$float\_value = scale\_factor * (integer\_value - add\_offset).$$

## 6. MOD08 (Level-3) Product Cloud Datasets: Frequently Asked Questions

### Cloud Fractions

#### *Q: What is the difference between cloud fraction and cloud retrieval fraction?*

***A:*** The simplest answer is that the fractions in the *Cloud_Fraction_<*>* SDSs are the fraction of pixels for a given population (e.g., daytime, nighttime, etc.) within a Level 3 grid box that are determined to be confident or probably cloudy by the MOD35 cloud mask, whereas the fractions in the *Cloud_Retrieval_Fraction_<*>* SDSs are the fraction of the daytime-only pixel population within a Level 3 grid box that have successful MOD06 cloud optical property (COP) retrievals (i.e., both optical thickness and effective particle radius solutions are within the pre-computed look-up table space). Cloud fractions are provided for the daytime, nighttime, and daytime + nighttime pixel populations for aggregations using the entire MODIS swath width as well as only near-nadir pixels (i.e., view zenith angle ≤ 32°). Cloud retrieval fractions are provided for each dual spectral channel pairing (e.g., VNSWIR-2.1 µm, 1.6-2.1 µm, etc.), and are further segregated by cloud thermodynamic phase (liquid, ice, undetermined, combined) and Clear Sky Restoral designation (overcast, PCL); single layer (1L) and multilayer (1L) retrieval fractions are also provided. A complete description of the calculation of all cloud fraction types is provided in the MOD08 Level 3 ATBD (see **Section 7.1**).

#### *Q: Why do I see some grid boxes with retrieval fraction exceeding cloud fraction?*

Users should be aware that the successful cloud optical property retrieval pixel population is a subset of the total daytime cloud mask pixel population, i.e., the various cloud retrieval fractions in most cases will be smaller than the cloud fraction. However, because the solar zenith angle threshold used to define daytime pixels is larger for the MOD35 cloud mask ($\theta_0 \leq 85^\circ$) than for MOD06 ($\theta_0 \leq 81.36^\circ$), the daytime pixel population, i.e., the denominator in the fraction calculation, in Level 3 grid boxes near the terminator will be larger for MOD35 than for MOD06. Thus a combined retrieval fraction, i.e., overcast + PCL for all phases, may in some cases exceed the daytime cloud fraction.

#### *Q: How do I interpret the daily and multi-day (i.e., eight-day and monthly) cloud fractions?*

***A:*** Focusing first on the daily fractions, there is an important distinction between the calculation of the cloud fraction derived from MOD35 (*Cloud_Fraction_<*>*) and the cloud retrieval fraction derived from MOD06 (*Cloud_Retrieval_Fraction_<*>*). Like other daily Level 3 cloud parameters calculated from 1 km Level 2 retrievals, the cloud retrieval fractions are calculated from the 1 km resolution MOD06 product sampled at 5 km resolution; thus the daily cloud retrieval fractions are simply the fraction of the 5 km sampled pixel population within a grid box having successful cloud optical property (COP) retrievals. The cloud fractions from MOD35, on the other hand, are means of the Level 2 5 km cloud fractions that are calculated by the cloud top property retrieval algorithm; thus the daily cloud fractions are properly understood as the fraction of all 1 km pixels within a grid box that are determined to be cloudy by the MOD35 cloud mask. A complete description of the calculation of all daily cloud fraction types is provided in the MOD08 Level 3 ATBD.

For the multi-day products (MOD08_E3 and M3), all cloud mask and cloud retrieval fractions for a given grid box are calculated as the *unweighted mean* of the daily grid box fractions. In other words, each daily grid box fraction is assigned equal weight regardless of the number of L2 pixels that were used in each daily grid box fraction calculation. Therefore the multi-day fractions are not "true" cloud mask or cloud retrieval fractions, but are instead *mean* fractions.

### *Q: How do I obtain "true" multi-day cloud mask or cloud retrieval fractions?*

***A:*** The word "true" requires a bit of clarification. First, it should be noted that there are two primary ways to compute a multi-day average or mean statistic from a sequence of daily statistics.

One can compute a simple arithmetic mean, summing the daily values for a given multi-day time period and dividing by the total number of days. This represents an "unweighted" multi-day mean, where each daily value has the same weight in the computation regardless of the number of observations (i.e., pixels) that were used to compute each daily value. Multi-day cloud fractions computed in this way are thus not considered "true" fractions because they do not represent the actual cloudy fraction of observations in a given grid box for a given multi-day time period.

Alternatively, one can compute a multi-day mean by weighting each daily value by the number of observations used to compute each of those daily values, and dividing by the sum of the weights (i.e., the total number of observations). Using this "pixel count-weighted" approach for multi-day cloud fraction computation yields what can be considered the "true" multi-day fraction because it by definition represents the actual cloudy fraction of observations in a given grid box for a given multi-day time period.

To provide a bit of background on this question and its relevance to the MOD08_E3 (eight day) and MOD08_M3 (monthly) cloud mask and cloud retrieval fractions, it should be noted that during the early stages of the MODIS mission, the (Level 2) Cloud Top Properties retrieval algorithm team requested that their multi-day Level 3 means – for both the standard cloud top retrieval parameters (e.g., Cloud Top Temperature, Cloud Top Pressure) as well as the standard cloud fraction from the MOD35 cloud mask – be computed as unweighted means of the MOD08_D3 daily values. For Cloud Optical Properties, the standard retrieval parameters (e.g., Cloud Optical Thickness, Cloud Effective Radius) are always computed as pixel count-weighted means. However, when it came time to determine how the Cloud Optical Property cloud retrieval fractions should be computed, it was decided that it was preferable to match the scheme used for the cloud mask cloud fraction such that Level 3 multi-day results from those two sources could be directly compared. This unsurprisingly has led to the present confusion.

It is possible to post-process the daily MOD08_D3 cloud fraction and cloud retrieval fraction such that both can be computed as pixel count-weighted, or “true,” multi-day fractions. The critical piece of information needed is the total number of L2 pixels used for both computations in the daily MOD08_D3 product, which can be used to weight each of the daily fractions. This is one source of confusion, in particular when calculating daytime fractions, since the definition of daytime is different between the Cloud Top Properties (solar zenith angle < 85°) and daytime-only Cloud Optical Properties (solar zenith angle < 81.36°). For C6 and previous collections, the total pixel counts used to compute the cloud mask cloud fractions are reported in the *Cloud_Fraction_<*>_Pixel_Counts* SDSs. Thus the multi-day pixel count-weighted cloud fraction for grid box (*i,j*) over *n* days is

$$CF_{i,j} = \frac{\sum_{d=1}^{n} \left[Cloud\_Fraction_{i,j,d} \cdot Cloud\_Fraction\_Pixel\_Counts_{i,j,d}\right]}{\sum_{d=1}^{n} Cloud\_Fraction\_Pixel\_Counts_{i,j,d}}$$

where *Cloud_Fraction* is from the specified MOD08_D3 *Cloud_Fraction_<*>_Mean* SDS (e.g., day, night, etc.), and *Cloud_Fraction_Pixel_Counts* is from the corresponding *Cloud_Fraction_<*>_Pixel_Counts* SDS.

For the Cloud Optical Properties, however, the total pixel counts used to compute the cloud retrieval fractions were not explicitly reported in previous collections (C5 and earlier), but could be “backed out” by dividing the *Cloud_Retrieval_Fraction_<*>_Pixel_Counts* SDSs (i.e., the cloudy pixel counts having successful optical property retrievals) by the respective *Cloud_Retrieval_Fraction_<*>* SDSs. For C6, the total pixel count used to compute the retrieval fractions is now reported, though still not explicitly. The Cloud Optical Properties pixel population is instead reported by cloud phase and Clear Sky Restoral (CSR) designation (see **Section 2.8** for CSR details) in the *COP_Phase_<*>_Histogram_Counts* SDSs, and for size reasons is only reported in the daily MOD08_D3 files. Thus the total pixel counts used to compute the cloud retrieval fractions can be found exactly by summing the COP Phase histograms, such that the total pixel count for grid box (*i,j*) on day *d* is

$$\begin{aligned} COP\_Count_{i,j,d} = \quad & CloudMaskClear_{i,j,d} + RestoredToClear_{i,j,d} \\ & + \sum_{p=1}^{3} \left[Cloudy_{i,j,d,p} + PCL_{i,j,d,p}\right] \end{aligned}$$

where *Cloudy*, *PCL*, and *RestoredToClear* refer to the above COP Phase histogram counts of the cloudy, partly cloudy, and “restored to clear” CSR designations, respectively, and *CloudMaskClear* refers to the histogram count of the MOD35 clear sky pixels; the subscript *p* refers to the three phase bins (i.e., liquid, ice, undetermined) in the *Cloudy* and *PCL* histograms. The multi-day pixel count-weighted cloud retrieval fraction for grid box (*i,j*) over *n* days is then

$$CRF_{i,j} = \frac{\sum_{d=1}^{n} [Retrieval\_Fraction_{i,j,d} \cdot COP\_Count_{i,j,d}]}{\sum_{d=1}^{n} COP\_Count_{i,j,d}}$$

where *Retrieval_Fraction* is from the specified MOD08_D3 phase-dependent *Cloud_Retrieval_Fraction_<*>* SDS (liquid, ice, undetermined, combined). Cloud retrieval fractions can also be computed directly from the retrieval pixel counts, such that

$$CRF_{i,j} = \frac{\sum_{d=1}^{n} Retrieval\_Fraction\_Pixel\_Counts_{i,j,d}}{\sum_{d=1}^{n} COP\_Count_{i,j,d}}$$

where *Retrieval_Fraction_Pixel_Counts* is obtained from the specificed *Cloud_Retrieval_Fraction_<*>_Pixel_Counts* SDS (liquid, ice, undetermined, combined).

### Q: Which daytime cloud fraction should I use?

***A:*** There is no correct answer to this question. It is important to note, however, that the MOD35 cloud mask by design attempts to determine the likelihood of an obstructed field of view and will err on the side of "cloudy" when in doubt. As such, scenes with heavy aerosol loading (e.g., thick smoke or lofted dust), and despite best efforts scenes with exceptionally strong sunglint, can yield "not clear" designations by MOD35 that are otherwise considered "cloudy" in MOD06 and are problematic for cloud optical property retrievals.

Starting in Collection 5, and continuing in Collection 6, a Clear Sky Restoral (CSR) algorithm (see Section 2.8 of the MOD06 User Guide) is implemented within MOD06 to "restore to clear" pixels that are thought to be not cloudy, as well as to identify two categories of pixels that are likely only partly cloudy (PCL) and are expected to be inappropriate for 1-D optical retrievals. Moreover, in Collection 6 the pixel counts of the four discrete CSR categories are for the first time aggregated to Level 3 and reported in the *COP_Phase_<*>_Histogram_Counts* SDSs (see **Section 7.1.2** of the MOD08 Level 3 ATBD), though for file size reasons are only available in the MOD08_D3 daily files. Thus a cloud fraction that excludes pixels determined to be "not clear" for reasons other than cloudiness can be calculated from these histograms. For example, the cloud fraction of grid box (*i,j*) excluding "restored to clear" pixels from the cloudy population can be calculated as

$$CF_{i,j} = \frac{\sum_{p} [Cloudy_{i,j,p} + PCL_{i,j,p}]}{CloudMaskClear_{i,j} + RestoredToClear_{i,j} + \sum_{p} [Cloudy_{i,j,p} + PCL_{i,j,p}]}$$

where *Cloudy*, *PCL*, and *RestoredToClear* refer to the histogram counts of the cloudy, partly cloudy, and "restored to clear" CSR designations, respectively, and *CloudMaskClear* refers to the histogram count of the remaining MOD35 clear pixels after CSR filtering; the subscript *p* refers to the three individual phase bins (i.e., liquid, ice, undetermined) in the *Cloudy* and

*PCL* histograms. *Note this fraction represents the "cloudy" pixel population for which MOD-06 attempts cloud optical property retrievals.*

A final caveat regarding the importance of instrument limitations should be addressed here. At 1 km spatial resolution, MODIS is able to detect most cloud types, optically thin cirrus clouds notwithstanding. Nevertheless, it has been shown that MOD35 performs inconsistently in partially cloudy scenes, such as those with trade wind cumuli that have spatial scales much smaller than the MODIS footprint, and may overestimate grid box cloud fraction [*Zhao and Di Girolamo*, 2006]. While MODIS has a nominal pixel size of 1 km at nadir, geometry (and instrument design) dictates that this size increases towards the edge of scan, potentially exacerbating the sub-pixel cloudiness issue.

### *Q: Why are C6 retrieval fractions smaller than in C5?*

***A***: In C5, those pixels restored to clear by the Clear Sky Restoral algorithm (i.e., those with flag CSR=2) were inadvertently excluded from the denominator in the calculation of fraction. In C6, the retrieval fraction is now correctly defined as the number of successful retrievals divided by the total number of pixels within each grid box. With more pixel counts in the denominator, the impact is a reduction in the retrieval fraction for C6. The global retrieval fraction decrease is about 5% relative.

## Cloud Properties

### *Q: How do I interpret the 2-bit Confidence Flag settings in the C6 Quality_Assurance_1km SDS? Should I use other QA flags?*

***A:*** The Confidence Flag QA is a 2-bit value assigned to various retrievals. In C5 it could have values of 0 [failed retrieval or no retrieval attempted], 1, 2, and 3. The latter three values were used by the Level-3 code to produce weighted aggregation of the statistical datasets. In C6 L3 we no longer have weighted aggregations. Therefore the Confidence Flag is only set to 0 or 3. Further it is shared by both overcast and the new PCL retrievals. The 2-bit flags were kept in the C6 file for historical purposes.

In summary, the Confidence QA bit values are given in **Table 6.1** as follows:

<u>Recommendations</u>: We recommend the user ignore all Confidence Flags in the 06_l2 QA SDS array *Quality_Assurance_1km* as these bits are redundant with other QA settings. Further, for those looking to simply determine if a retrieval was successful, you can now just look at the geophysical SDS; if it has a valid value (not fill) then the retrieval was successful. In terms of weighting the retrievals for aggregated statistics, we suggest all users look at the associated pixel-level uncertainty SDS and decide for themselves what confidence/weighting are appropriate for their specific analysis.

Table 6-1. Confident OA bit value definition.

| Bit Value | Bit Value Definition |
|---|---|
| **0** | No Confidence: both overcast and PCL retrievals are set to fill, a result of a failed retrieval or no retrieval was attempted |
| **1** | Marginal Confidence: not used in C6 |
| **2** | Good Confidence: not used in C6 |
| **3** | Very Good Confidence: default for all non-fill retrievals, can be associated with an overcast or PCL retrieval |

### *Q: There are multiple cloud phase histograms. How are these different?*

***A:*** There are two primary cloud phase products included in MOD06, namely an infrared (IR) algorithm that runs in parallel with the MOD06 cloud top (CT) properties retrieval during both daytime and nighttime [*Baum et al.*, 2012], and a daytime-only algorithm run as part of the MOD06 cloud optical properties retrieval. In L3 the aggregated results of the IR cloud phase algorithm algorithm are reported in SDSs with *Cloud_Phase_Infrared* in the SDS name.

The daytime-only algorithm, that employs a variety of shortwave-infrared (SWIR) based tests in addition to information from the CT and IR phase retrievals (see **Section 2.4** of the MOD06 User Guide), provides the final phase decision for the MOD06 cloud optical properties retrievals. The aggregated results from this algorithm are reported in L3 in SDSs with *Cloud_Phase_Optical_Properties*, or simply *Cloud_Phase*, in the SDS name. In addition, the cloud optical and microphysical retrieval statistics in the L3 daily and multi-day products are phase-dependent, and are aggregated according to the results of the daytime-only phase algorithm (i.e., ice, liquid, undetermined, combined).

Finally, users should note the results of the IR and daytime-only phase algorithms are not expected to agree in all cases.

### *Q: What do the 'undetermined' and 'combined' cloud phases mean?*

***A:*** The undetermined cloud phase means the cloud optical properties retrieval algorithm could not make a determination of the cloud phase (liquid water or ice). This may have been caused by viewing anomalies in the retrieval (sunglint), contamination of the scene by aerosol, or a multi-layer cloud with mixed phases (e.g., thin cirrus overlying liquid water clouds). For these undetermined retrievals the liquid water libraries are used in the cloud optical properties retrievals, but the retrievals are considered to be of lower confidence (and quality) than those that are placed in one of the other primary phase categories. The combined phase is simply a combination of all cloud phase categories: liquid water, ice, and undetermined.

### *Q: Are the cloud top property SDSs (temperature, pressure, height) derived from the 1 km or 5 km L2 data?*

A: All cloud top property SDSs (scalar statistics and histograms) are computed from the MOD06 L2 5 km products. These include the cloud top temperature, pressure, and height parameters, as well as the cloud effective emissivity and IR phase parameters.

### *Q: Why do some cloud optical and microphysical properties have numbers in their names, and what are their differences?*

***A:*** The MOD06 cloud optical and microphysical property retrievals use the well known *Nakajima & King* [1990] bi-spectral approach to retrieve cloud optical thickness (COT) and effective particle radius (CER), pairing a non-absorbing visible, near-, or shortwave-infrared (VNSWIR) channel sensitive to COT (0.66, 0.86, 1.24 µm) with an absorbing shortwave- or mid-wave- infrared (SWIR/MWIR) channel sensitive to CER (1.6, 2.1, 3.7 µm). In addition, an alternate spectral channel combination, namely 1.6-2.1 µm, is also included and is expected to have increased skill for COT-CER retrievals over snow and ice surfaces [*Platnick et al.*, 2001]. The number modifiers attached to the cloud optical and microphysical property SDS names therefore refer to the spectral channel used for retrieving CER, e.g., <*>*_16* uses 1.6 µm and <*>*_37* uses 3.7 µm; the alternate 1.6-2.1 µm retrieval is denoted <*>*_1621*. Optical and microphysical property SDS names without number modifiers refer to the standard, C5 heritage VNSWIR-2.1 µm retrievals.

A number of important differences are expected between the various spectral retrievals. For instance, it has been shown that photon penetration depth within clouds varies with wavelength in the SWIR and MWIR spectral regions [*Platnick*, 2000], thus the spectral CER retrievals may be "sampled" from different portions of the cloud. In addition, though the COT retrievals associated with each spectral CER retrieval will in most cases be nearly identical, since each uses the same VNSWIR channel, COT differences may exist when the reflectance observations lie in a non-orthogonal portion of the retrieval solution space such as at small COT. Moreover, each spectral CER retrieval is known to fail, i.e., have reflectance observations outside of the retrieval solution space, at different rates [*Cho et al.*, 2015], thus the successful retrieval populations, fractions, scalar statistics, and histograms, at L3 for each spectral retrieval will necessarily differ.

### *Q: Do spectral cloud effective particle radius (CER) retrieval differences provide information about cloud vertical size distribution?*

***A:*** While the 1.6, 2.1, and 3.7 µm channels have been shown to have different vertical photon penetration depths within cloud [*Platnick*, 2000], and thus the respective CER retrievals may be "sampled" from different portions of the cloud, users are cautioned from drawing such inferences from the aggregated L3 scalar statistics. Because the spectral COT-CER retrievals are known to fail at different rates and under different circumstances [*Cho et al.*, 2015], the resulting differences in retrieval populations may introduce biases into the aggregated retrievals. Moreover, radiometric issues and/or retrieval errors, i.e., those due to atmospheric correction, emission correction at 3.7 µm, etc., may also play a role.

### *Q: What does "PCL" mean?*

***A:*** The modifier *PCL* stands for "partly cloudy," and refers to the L2 pixel population determined to be either partially cloud-covered or at cloud edge as determined by the MOD06 Clear Sky Restoral (CSR) algorithm (see **Section 2.8** of the MOD06 User Guide). These pixels are expected to deviate from the retrieval assumptions of an overcast homogenous cloudy FOV and 1-dimensional plane-parallel radiative transfer, conditions that have been shown to be associated with retrieval biases [*Zhang and Platnick*, 2011; *Zhang et al.*, 2012] and increased retrieval failure rates [*Cho et al.*, 2015]. Previously in C5, this pixel population was "restored to clear sky" and was excluded from the MOD06 retrievals. In C6, however, optical and microphysical property retrievals are now attempted on these pixels, and successful retrievals are reported in L2 and aggregated to L3, though they are reported separately in the *PCL* SDSs and are segregated from the "overcast" pixel population.

### *Q: How do I compute a "total" retrieval mean that includes the "PCL" pixel population?*

***A:*** While the "overcast" pixel population represents our expected highest-quality MOD06 optical and microphysical property retrievals, users may wish to compare the MODIS daily and multi-day scalar retrieval statistics with products from other sensors that do not perform partly cloudy pixel screening. Users can do so via a pixel-weighted mean of the overcast and *PCL* retrieval means. For instance, the daily "total" mean VNSWIR-2.1 µm liquid phase cloud optical thickness, $\langle COT(i,j)\rangle$, for grid box ($i$,j) can be calculated as

$$\langle COT\,(i,j)\rangle = \frac{N\,(i,j)\cdot COT\,(i,j) + N_{PCL}\,(i,j)\cdot COT_{PCL}\,(i,j)}{N\,(i,j) + N_{PCL}\,(i,j)}$$

where $COT(i,j)$ and $COT_{PCL}(i,j)$ are the daily mean overcast and *PCL* VNSWIR-2.1 µm liquid phase cloud COT, respectively, and $N(i,j)$ and $N_{PCL}(i,j)$ are the overcast and *PCL* liquid phase pixel counts, respectively.

## Miscellaneous

### *Q: Is there a minimum L2 pixel count requirement to compute L3 statistics?*

***A:*** For the L3 daily products, only a single non-fill L2 pixel is needed within any given 1° × 1° grid cell to create L3 daily statistics. This tends to cause an artificial spatial expansion of sparce L2 data when aggregating to L3. For example, a sizable region having only a few scattered L2 retrievals will have solid coverage of the 1° × 1° grid cell statistics. Users, however, can query the *Pixel_Counts* SDSs to monitor the number of L2 pixels that went into L3 statistics for each 1° × 1° grid cell. Likewise for the L3 multi-day products, only a non-fill daily grid cell for a single day is needed to create L3 multi-day statistics.

### *Q: Are statistics within a L3 daily file a single orbit or a multiple orbit average?*

***A:*** All daily L3 SDSs for each grid cell include all daytime only, nighttime only, or combined daytime + nighttime L2 data pixels that fall within that grid cell on that date. Thus even the daytime and nighttime only SDSs may contain observations from multiple Terra or Aqua overpasses (approximately 100 minutes apart), with the exception of grid cells in the tropics, or roughly between 23°N and 23°S latitude, where orbit gaps exist because the MODIS swath is insufficiently wide to overlap with the previous overpass.

### *Q: How can I determine if an SDS contains daytime only, nighttime only, or combined daytime and nighttime data?*

***A:*** To determine if a L3 SDS contains daytime data only, nighttime data only, or combined daytime + nighttime data, one needs to query the local attribute "Included_Nighttime_Data." If this attribute is set to *False*, then it is a daytime only SDS; if this attribute is set to *True*, then it is a combined daytime and nighttime SDS, unless the string *_Night_* appears somewhere in the SDS name, in which case it is a nighttime only SDS. Note the nighttime only case is of low incidence, only occurring in a few cloud top property derived parameters (see L3 ATBD, **Section 7.8**, Table 7).

## 7. References


Ackerman, S. A., R. E. Holz, R. Frey, E. W. Eloranta, B. Maddux, and M. McGill, 2008: Cloud detection with MODIS. Part II: Validation. *J. Atmos. Oceanic Technol.*, **25**, 1073-1086.

Baum, B. A., P. Yang, A. J. Heymsfield, S. Platnick, M. D. King, Y. X. Hu, and S. T. Bedka, 2005: Bulk scattering properties for the remote sensing of ice clouds. 2: Narrowband models. *J. Appl. Meteor.*, **44**, 1896-1911.

Baum, B. A., W. P. Menzel, R. A. Frey, D. Tobin, R. E. Holz, Ackerman, S. A., A. K. Heidinger, and P. Yang, 2012: MODIS cloud top property refinements for Collection 6. *J. Appl. Meteor. Climatol.*, **51**, 1145-1163.

Chahine, M. T., 1974: Remote sounding of cloudy atmospheres. I. The single cloud layer. *J. Atmos. Sci.*, **31**, 232-243.

Cho, H.-M., Z. Zhang, K. Meyer, M. Lebsock, S. Platnick, A. S. Ackerman, L. Di Girolamo, L. C.-Labonnote, C. Cornet, J. Riedi, and R. E. Holz, 2015: Frequency and causes of failed MODIS cloud property retrievals for liquid phase clouds over global oceans. *J. Geophys. Res.*, **120**, 4132-4154.

Cole, C. H., P. Yang, B. A. Baum, J. Riedi, L. C. Labonnote, F. Thieuleux, and S. Platnick, 2013: Comparison of PARASOL observations with polarized reflectances simulated using different ice habit mixtures. *J. Appl. Meteor. Climatol.*, **52**, 186-196.

Cox, C., and W. Munk, 1954: The measurements of the roughness of the sea surface from photographs of the sun's glitter. *J. Opt. Soc. Amer.*, **44**, 838-850.

Curran, R. J. and M. L. C. Wu, 1982: Skylab near-infrared observations of clouds indicating supercooled liquid water droplets. *J. Atmos. Sci.*, **39**, 635-647.

Derber, J. C., D. F. Parrish, and S. J. Lord, 1991,: The new global operational analysis system at the National Meteorological Center. *Weath. Forec.*, **6**, 538-547.

Downing, H. D., and D. Williams, 1975: Optical-constants of water in the infrared. *J. Geophys. Res.*, **80**, 1656-1661.

Gao, B.-C., A. F. H. Goetz, and W. J. Wiscombe, 1993: Cirrus cloud detection from airborne imaging spectrometer data using the 1.38µm water vapor band. *Geophys. Res. Lett.*, **20**, 301-304.

Gassó, S., A. Stein, F. Marino, E. Castellano, R. Udisti, and J. Ceratto, 2010: A combined observational and modeling approach to study modern dust transport from the Patagonia desert to East Antarctica. *Atmos. Chem. Phys.*, **10**, doi:10.5194/acp-10-8287-2010.

Hale, G. M., and M. R. Querry, 1973: Optical constants of water in the 200-nm to 200-µm wavelength region. *Appl. Opt.*, **12**, 555-563.

Han, Q., W. B. Rossow, and A. A. Lacis, 1994: Near-global survey if effective droplet radii in liquid water clouds using ISCCP data, *J. Climate*, **7**, 465-497.

Holz, R. E. S. A. Ackerman, F. W. Nagle, R. Frey, R. E. Kuehn, S. Dutcher, M. A. Vaughan, and B. Baum., 2008: Global MODIS cloud detection and height evaluation using CALIOP. *J. Geophys. Res.*, **113**, D00A19, doi:10.1029/2008JD009837.

Holz, R. E., S. Platnick, S. A. Ackerman, R. Kuehn, D. Winker, M. Vaughan, A. Garnier, and J. Pélon, 2012: Resolving cirrus optical depth biases between active (CALIOP) and passive (MODIS, IIR) using IR retrievals. *International Radiation Symposium*, Berlin, Germany.

Holz, R. E., S. Platnick, K. Meyer, M. Vaughan, G. Wind, S. Dutcher, S. Ackerman, A. Heidinger, N. Amarasinghe, C. Wang, and P. Yang, 2015: Resolving cirrus optical depth biases between CALIOP and MODIS using IR retrievals. *Atmos. Chem. Phys*., submitted Sept. 2015.

Hu, Y. X., B. Wielicki, B. Lin, G. Gibson, S. C. Tsay, K. Stamnes, and T. Wong, 2000: Delta-Fit: A fast and accurate treatment of particle scattering phase functions with weighted singular-value decomposition least-squares fitting. *J. Quant. Spectrosc. Radiat. Trans.*, **65**, 681-690.

Hubanks, P. A., M. D. King, S. A. Platnick, and R. A. Pincus, 2008: MODIS Atmosphere Team Level-3 Algorithm Theoretical Basis Document (ATBD), 100 pp., modis-atmos.gsfc.nasa.gov/MOD08_D3/atbd.html.

Johnson, M. S., N. Meskhidze, V. P. Kiliyanpilakkil, and S. Gassó, 2011: Understanding the transport of Patagonia dust and its influence on marine biological activity in the South Atlantic Ocean. *Atmos. Chem. Phys.*, **11**, doi:10.5194/acp-11-2487-2011.

Joiner, J. A. P. Vasilkov, P. K, Bhartia, G. Wind, S. Platnick, and W. P. Menzel, 2010: Detection of multi-layer and vertically-extended clouds using A-Train sensors. *Atmos. Meas. Tech.*, **3**, 233-247.

Kaufman, Y. J., I. Koren, L. A. Remer, D. Tanré, P. Ginoux, and S. Fan, 2005: Dust transport and deposition observed from the Terra-MODIS spacecraft over the Atlantic Ocean. *J. Geophys. Res.*, **110**, DOI: 10.1029/2003/JC004436.

Koepke, P., 1984: Effective reflectance of oceanic whitecaps," *Appl. Opt.,* 23, 1816-1824.

King, M. D., 1987: Determination of the scaled optical thickness of clouds from reflected solar radiation measurements. *J. Atmos. Sci*., **44**, 1734-1751.

King, M. D., Y. J. Kaufman, W. P. Menzel, and D. Tanré, 1992: Remote sensing of cloud, aerosol, and water vapor properties from the Moderate Resolution Imaging Spectrometer (MODIS). *IEEE Trans. Geosci. Remote Sens*., **30**, 2-27.

King, M. D., S. C. Tsay, S. E. Platnick, M. Wang and K. N. Liou, 1997: *Cloud Retrieval: Al-*

*gorithms for MODIS: Optical Thickness, Effective Particle Radius, and Thermodynamic Phase*. Algorithm Theoretical Basis Document ATBD-MOD-05, 79 pp., modis-atmos.gsfc.nasa.gov/reference_atbd.html.

King, M. D., W. P. Menzel, Y. J. Kaufman, D. Tanré, B.-C. Gao, S. Platnick, S. A. Ackerman, L. A. Remer, R. Pincus, and P. A. Hubanks, 2003: Cloud and aerosol properties, precipitable, water, and profiles of temper- ature and water vapor, *IEEE Trans. Geosci. Remote Sens.*, **41**, 442-458.

King, M. D., S. Platnick, P., G. T. Arnold, M. A. Gray, J. C. Riedi, S. A. Ackerman, and K. N. Liou, 2004: Remote sensing of liquid water and ice cloud optical thickness and effective radius in the arctic: Application of airborne multispectral MAS data. *J. Atmos. Oceanic Technol*., **21**, 857-875.

King, M. D., S. Platnick, G. Wind, G. T. Arnold, and R. T. Dominguez, 2010: Remote sensing of radiative and microphysical properties of clouds during $TC^4$: Results from MAS, MASTER, MODIS, and MISR. *J. Geophys. Res.*, **115**, D00J07, doi: 10.1029/2009JD013277.

King, M. D., S. Platnick, W. P. Menzel, S. A. Ackerman, and P. A. Hubanks, 2013: Spatial and temporal distribution of clouds observed by MODIS onboard the Terra and Aqua satellites. *IEEE Trans. Geosci. Remote Sens.*, **51**, 3826-3852.

Koepke, P., 1984: Effective reflectance of oceanic whitecaps. *Appl. Opt*., **23**, 1816-1824.

Lebsock, M. D., T. S. L'Ecuyer and G. L. Stephens, 2011. Detecting the ratio of rain and cloud water in low-latitude shallow marine clouds. *J. Appl. Meteorol. Clim.*, **50**, 419-432.

Levy, R. C., L. A. Remer, D. Tanré, S. Mattoo, and Y. J. Kaufman, 2009: *Algorithm for remote sensing of tropospheric aerosol over dark targets from MODIS: Collections 005 and 051*, Algorithm Theoretical Basis Document ATBD-MOD-04, 96 pp., modis-atmos.gsfc.nasa.gov/reference_atbd.html.

Liang, L., L. Di Girolamo, and S. Platnick, 2009: View-angle consistency in reflectance, optical depth, and spherical albedo of marine water clouds off the coast of California through MISR-MODIS fusion. *Geophys. Res. Lett.*, **36**, L09811, doi: 10.1029/2008GL037124.

Maddux, B. C., S. A. Ackerman, and S. Platnick, 2010: Viewing geometry dependencies in MODIS cloud products. *J. Atmos. Oceanic Tech.*, **27**, 1519-1528.

Marchant, B., S. Platnick, K. Meyer, G. T. Arnold, and J. Riedi, 2015: MODIS Collection 6 shortwave-derived cloud phase classification algorithm and comparisons with CALIOP. *Atmos. Meas. Tech.*, submitted.

Mayer, B., and A. Kylling, 2005: Technical note: The libRadtran software package for radiative transfer calculations - description and examples of use. *Atmos. Chem. Phys.*, **5**, 1855-1877.

Menzel, W. P., R. A. Frey, H. Zhang, D. P. Wylie, C. C. Moeller, R. E. Holz, B. Maddux, B. A. Baum, K. I. Strabala, and L. E. Gumley, 2008: MODIS global cloud-top pressure and amount estimation: Algorithm description and results. *J. Appl. Meteor. Climatol.*, **47**, 1175-1198.

Minnis, P., P. W. Heck, S. Mayor, and D. F. Young, 1997: A near-global analysis of cloud microphysical properties. *Proc. IRS: Current Probl. Atmos. Radiat.*, W. L. Smith and K. Stamnes, Eds., Hampton, VA, 445-448, Deepak Publ.

Moody, E. G., M. D. King, S., Platnick, C. B. Schaaf, and F. Gao, 2005: Spatially complete global spectral surface albedos: Value-added datasets derived from Terra MODIS land products. *IEEE Trans. Geosci. Remote Sens*., **43**, 144-158.

Moody, E. G., M. D. King, C. B. Schaaf, D. K. Hall, and S. Platnick, 2007: Northern Hemisphere five-year average (2000-2004) spectral albedos of surfaces in the presence of snow: Statistics computed from Terra MODIS land products. *Remote Sens. Environ*., **111**, 337-345.

Moody, E. G., M. D. King, C. B. Schaaf, and S. Platnick, 2008: MODIS-derived spatially complete surface albedo products: Spatial and temporal pixel distribution and zonal averages. *J. Appl. Meteor. Climatol*., **47**, 2879-2894.

Nakajima, T., and M. D. King, 1990: Determination of the optical thickness and effective particle radius of clouds from reflected solar radiation measurements, Part I: Theory. *J. Atmos. Sci.*, **47**, 1878-1893.

Nakajima, T., M. D. King, J. D. Spinhirne, and L. F. Radke, 1991: Determination of the optical thickness and effective particle radius of clouds from reflected solar radiation measurements, Part II: Marine stratocumulus observations. *J. Atmos. Sci.*, **47**, 728-750.

Nakajima, T. Y., K. Suzuki, and G. L. Stephens, 2010: Droplet growth in warm water clouds observed by the A-train. Part I: A multisensor view. *J. Atmos. Sci.*, **67**, 1897-1907.

Palmer, K. F., and D. Williams, 1974: Optical properties of water in the near infrared. *J. Opt. Soc. Amer.*, **64**, 1107-1110.

Pavolonis, M. J., and A. K. Heidinger, 2004: Daytime cloud overlap detection from AVHRR and VIIRS. *J. Appl. Meteor.*, **43**, 762-778.

Pincus, R., S. Platnick, S. A. Ackerman, R. S. Hemler, R. J. P. Hofmann, 2012: Reconciling simulated and observed views of clouds: MODIS, ISCCP, and the limits of instrument simulators. *J. Climate*, **25**, 4699-4720.

Platnick, S., and S. Twomey, 1994: Determining the susceptibility of cloud albedo to changes in droplet concentration with the advanced very high resolution radiometer. *J. Appl. Meteor.*, **33**, 334-347.

Platnick, S., and F. P. J. Valero, 1995: A validation study of a satellite cloud retrieval during ASTEX. *J. Atmo. Sci.*, **52**, 2985-3001.

Platnick, S., 2000: Vertical photon transport in cloud remote sensing problems. *J. Geophys. Res.*, **105**, 22919-22935.

Platnick, S., M. D. King, H. Gerber, P. V. Hobbs. 2001: A solar reflectance technique for cloud retrievals over snow and ice surfaces. *J. Geophys. Res.*, **106**, 15185-15199.

Platnick, S., M. D. King, S. A. Ackerman, W. P. Menzel, B. A. Baum, J. C. Riedl, and R. A. Frey, 2003: The MODIS cloud products: Algorithms and examples from Terra. *IEEE Trans. Geosci. Remote Sens.*, **41**, 459-473.

Platnick, S., R. Pincus, B. Wind, M. D. King, M. Gray, and P. Hubanks, 2004: An initial analysis of the pixel-level uncertainties in global MODIS cloud optical thickness and effective particle size retrievals. P*assive Optical Remote Sensing of the Atmosphere and Clouds IV*, S.-C. Tsay, T. Yokota, and M.-H. Ahn, Eds., *Proc. of SPIE*, **5652**, 30-40.

Platnick, S., and J. M. Fontenla, 2008: Model calculations of solar spectral irradiance in the 3.7-μm band for Earth remote sensing applications. *J. Appl. Meteor. Climatol.*, **47**, 124–134.

Platnick, S., S. A. Ackerman, B. A. Baum, A. K. Heidinger, R. E. Holz, M. D. King, W. P. Menzel, S. Nasiri, El Weisz, and P. Yang, 2013: *Assessment of IDPS VIIRS Cloud Products and Recommendations for EOS-era Cloud Climate Data Record Continuity*, Suomi NPP Science Team report, 19 March.

Yang, P., L. Bi, B. A. Baum, K. N. Liou, G. W. Kattawar, M. I. Mishchenko, and B. Cole, 2013: Spectrally consistent scattering, absorption, and polarization properties of atmospheric ice crystals at wavelengths from 0.2 to 100 μm. *J. Atmos. Sci*., **70**, 330–347.

Rawlins, F., and J. S. Foot, 1990: Remotely sensed measurements of stratocumulus properties during FIRE using the C130 aircraft multichannel radiometer. *J. Atmos. Sci.*, **47**, 2488-2503.

Riedi, J., B. Marchant, S. Platnick, B. Baum, F. Thieuleux, C. Oudard, F. Parol, J-M. Nicolas, and P. Dubuisson, 2010: Cloud thermodynamic phase inferred from merged POLDER and MODIS data. *Atmos. Chem. Phys*., **10**, 11851-11865.

Rodgers, C. D., 2000: *Inverse Methods for Atmospheric Sounding: Theory and Practice*. World Scientific Publishing Co., Inc.: Hackensack, NJ, USA, 238 pp.

Schaaf, C. L. B., J. Liu, F. Gao and A. H. Strahler, 2011: MODIS Albedo and Reflectance Anisotropy Products from Aqua and Terra. *Land Remote Sensing and Global Environmental Change: NASA's Earth Observing System and the Science of ASTER and MODIS.* Remote Sensing and Digital Image Processing Series, Vol. 11, B. Ramachandran, C. Justice, M. Abrams, Eds., Springer- Verlag, 873 pp.

Seemann, S. W., E. E. Borbas, R. O. Knuteson, G. R. Stephenson, and H. L. Huang, 2008: Development of a global infrared land surface emissivity database for application to clear sky sounding retrievals from multispectral satellite radiance measurements. *J. Appl. Meteor. Climatol.*, **47**, 108-123.

Stamnes, K., S. C. Tsay, W. Wiscombe, and K. Jayaweera, 1988: A numerically stable algorithm for discrete-ordinate-method radiative transfer in multiple scattering and emitting layered media. *Appl. Opt.*, **27**, 2502-2509.

Stamnes, K., S. C. Tsay, W. Wiscombe, and I. Laszlo, 2000: DISORT, a General-Purpose Fortran Program for Discrete-Ordinate-Method Radiative Transfer in Scattering and Emitting Layered Media : Documentation of Methodology.

Strow L., S. Hannon, S. Machado, H. Motteler, D. Tobin, 2003: An overview of the AIRS radiative transfer model. *IEEE Trans. Geosci. Remote. Sens.* **41**, 303-313.

Stubenrauch, C. J., W. B. Rossow, S. Kinne, S. Ackerman, G. Cesana, H. Chepfer, B. Getzewich, L. Di Girolamo, A. Guignard, A. Heidinger, B. Maddux, P. Menzel, P. Minnis, C. Pearl, S. Platnick, C. Poulsen, J. Riedi, S. Sun-Mack, A. Walther, D. Winker, S. Zeng, and G. Zhao, 2013: Assessment of global cloud datasets from satellites: Project and database initiated by the GEWEX Radiation Panel. *Bull. Am. Meteor. Soc.*, **94**, 1031-1049.

Sun. J., A. Angal, X. Xiong, H. Chen, X. Geng. A. Wu, T. Choi, and M. Chu, 2012: MODIS reflective solar bands calibration improvements in collection 6. *Proc. of SPIE*, **8528**, doi: 10.1117/12.979733.

Twomey, S., and T. Cocks, 1982: Spectral reflectance of clouds in the near-infrared: Comparison of measurements and calculations. *J. Meteor. Soc. Japan*, **60**, 583-592.

Twomey, S., and T. Cocks, 1989: Remote sensing of cloud parameters from spectral reflectance in the near-infrared. *Beitr. Phys. Atmos.*, **62**, 172-179.

van de Hulst, H. C., 1974: The spherical albedo of a planet covered with a homogeneous cloud layer. *Astron. & Astrophys.*, **35**, 209-214.

Wang, M., and M. D. King, 1997, Correction of Rayleigh scattering effects in cloud optical thickness retrievals, *J. Geophys. Res.*, **102**, 25915-25926.

Wind, G., S. Platnick, M. D. King, P. A. Hubanks, M. J. Pavolonis, A. K. Heidinger, P. Yang, and B. A. Baum, 2010: Multilayer cloud detection with the MODIS near-infrared water vapor absorption band. *J. Appl. Meteor. Climatol.*, **49**, 2315-2333.

Wylie, D. P. and W. P. Menzel, 1999: Eight years of high cloud statistics using HIRS, *J. Climate*, **12**, 170-184.

Yang, P., L. Zhang, G. Hong, S. L. Nasiri, B. A. Baum, H.-L. Huang, M. D. King, and S. Platnick, 2007: Differences between collection 004 and 005 MODIS ice cloud optical/microphysical products and their impact on radiative forcing simulations. *IEEE Trans. Geosci. Remote Sens.*, **45**, 2886-2899.

Yang, P., L. Bi, B. A. Baum, K. N. Liou, G. W. Kattawar, M. Mishchenko, and B. Cole, 2013: Spectrally consistent scattering, absorption, and polarization properties of atmospheric ice crystals at wavelengths from 0.2 to 100 μm. *J. Atmos. Sci*., **70**, 330-347.

Zhang, Z., and S. Platnick, 2011: An assessment of differences between cloud effective particle radius for marine water clouds from three MODIS spectral bands. *J. Geophys. Res.*, **116**, D20215, doi:10.1029/2011JD016216.

Zhang, Z., S. Platnick, P. Yang, A. Heidinger, and J. M. Comstock, 2010: Effect of ice particle size vertical inhomogeneity on the passive remote sensing of ice clouds, *J. Geophys. Res.*, **15**, D17203, doi:10.1029/2010JD013835.

Zhang, Z., A. S. Ackerman, G. Feingold, S. Platnick, R. Pincus, and H. Xue, 2012: Effects of cloud horizontal inhomogeneity and drizzle on remote sensing of cloud droplet effective radius: Case studies based on large-eddy simulations. *J. Geophys. Res.,* **117**, D19208, doi:10.1029/2012JD017655.

Zhao, G., and L. Di Girolamo, 2006: Cloud fraction errors for trade wind cumuli from EOS-Terra instruments. *Geophys. Res. Lett.,* **33**, L20802, doi:10.1029/2006GL027088.

## Appendix A. Scientific Data Sets (SDSs) in the L2 Cloud Product File

For completeness, all SDSs in the MOD/MYD06 file are given in the **Table A.1** below. The highlighted rows in brown indicate just those datasets that are related to the optical and microphysical retrievals discussed in this user guide.

Table A.1. SDSs in the Level 2 MOD06/MYD06 file.

| SDS Name | Long Name | Dataset resolution (if applicable) |
|---|---|---|
| Above_Cloud_Water_Vapor_094 | Above-cloud water vapor amount from 0.94 µm channel, ocean only, tau > 5 | 1 km |
| Asymmetry_Parameter_Ice | Ice Asymmetry Parameter from the phase functions used to generate the forward lookup tables | – |
| Asymmetry_Parameter_Liq | Liquid Water Asymmetry Parameter from the phase functions used to generate the forward lookup tables | – |
| Atm_Corr_Refl | Atmospherically corrected reflectance used during cloud optical and microphysical properties retrieval | 1 km |
| Band_Number | Band_Number | – |
| Brightness_Temperature | Observed Brightness Temperature from Cloudy Averaged Radiances in a 5x5 1-km Pixel Region | 5 km |
| Cirrus_Reflectance | Cirrus Reflectance | 1 km |
| Cirrus_Reflectance_Flag | Cirrus Reflectance Flag | |
| Cloud_Effective_Emissivity | Cloud Effective Emissivity from Cloud Top Pressure Retrieval | 1 km |
| Cloud_Effective_Emissivity_Day | Cloud Effective Emissivity from Cloud Top Pressure Retrieval, Day Only | 5 km |
| Cloud_Effective_Emissivity_Nadir | Cloud Effective Emissivity from Cloud Top Pressure Retrieval for Sensor Zenith (View) Angles ≤ 32° | 5 km |
| Cloud_Effective_Emissivity_Nadir_Day | Cloud Effective Emissivity from Cloud Top Pressure Retrieval for Sensor Zenith (View) Angles ≤ 32°, Day Data Only | 5 km |
| Cloud_Effective_Emissivity_Nadir_Night | Cloud Effective Emissivity from Cloud Top Pressure Retrieval for Sensor Zenith (View) Angles ≤ 32°, Night Data Only | 5 km |
| Cloud_Effective_Emissivity_Night | Cloud Effective Emissivity from Cloud Top Pressure Retrieval, Night Only | 5 km |
| Cloud_Effective_Radius | Cloud Particle Effective Radius two-channel retrieval using band 7(2.1 µm) and either band 1(0.65 µm), 2(0.86um), or 5(1.2 µm) (specified in Quality Assurance 1km)from best points: not failed in any way, not marked for clear sky restoral | 1 km |
| Cloud_Effective_Radius_PCL | Cloud Particle Effective Radius two-channel retrieval using band 7(2.1 µm) and either band 1(0.65 µm), 2(0.86um), or 5(1.2 µm) (specified in Quality Assurance 1km)from points identified as either partly cloudy from 250 m cloud mask test or 1 km cloud edges | 1 km |

| | | |
|---|---|---|
| Cloud_Effective_Radius_16 | Cloud Particle Effective Radius two-channel retrieval using band 6(1.6 μm) and either band 1(0.65 μm), 2(0.86 μm), or 5(1.2 μm) (specified in Quality Assurance 1 km) from best points: not failed in any way, not marked for clear sky restoral | 1 km |
| Cloud_Effective_Radius_16_PCL | Cloud Particle Effective Radius two-channel retrieval using band 6(1.6 μm) and either band 1(0.65 μm), 2(0.86 μm), or 5(1.2um) (specified in Quality Assurance 1 km) from points identified as either partly cloudy from 250 m cloud mask test or 1 km cloud edges | 1 km |
| Cloud_Effective_Radius_1621 | Cloud Particle Effective Radius two-channel retrieval using band 7(2.1 μm) and band 6(1.6 μm) from best points: not failed in any way, not marked for clear sky restoral | 1 km |
| Cloud_Effective_Radius_1621_PCL | Cloud Particle Effective Radius two-channel retrieval using band 7(2.1 μm) and band 6(1.6 μm) from points identified as either partly cloudy from 250 m cloud mask test or 1 km cloud edges | 1 km |
| Cloud_Effective_Radius_37 | Cloud Particle Effective Radius two-channel retrieval using band 20(3.7 μm) and either band 1(0.65 μm), 2(0.86 μm), or 5(1.2 μm) (specified in Quality Assurance 1 km) from best points: not failed in any way, not marked for clear sky restoral | 1 km |
| Cloud_Effective_Radius_37_PCL | Cloud Particle Effective Radius two-channel retrieval using band 20(3.7 μm) and either band 1(0.65 μm), 2(0.86 μm), or 5(1.2 μm) (specified in Quality Assurance 1 km) from points identified as either partly cloudy from 250 m cloud mask test or 1 km cloud edges | 1 km |
| Cloud_Effective_Radius_Uncertainty | Cloud Effective Particle Radius (from band 7(2.1 μm)) Relative Uncertainty (Percent) from both best points and points identified as cloud edge at 1 km resolution or partly cloudy at 250 m | 1 km |
| Cloud_Effective_Radius_Uncertainty_16 | Cloud Effective Particle Radius (from band 6(1.6 μm) Relative Uncertainty (Percent) from both best points and points identified as cloud edge at 1 km resolution or partly cloudy at 250 m | 1 km |
| Cloud_Effective_Radius_Uncertainty_1621 | Cloud Effective Particle Radius Relative Uncertainty (Percent) using band 7(2.1 μm) and band 6(1.6 μm) from both best points and points identified as cloud edge at 1 km resolution or partly cloudy at 250 m | 1 km |
| Cloud_Effective_Radius_Uncertainty_37 | Cloud Effective Particle Radius (from band 20(3.7 μm)) Relative Uncertainty (Percent) from both best points and points identified as cloud edge at 1 km resolution or partly cloudy at 250 m | 1 km |
| cloud_emiss11_1km | 11 μm Cloud Emissivity at 1-km resolution from LEOCAT for All Clouds | 1 km |
| cloud_emiss12_1km | 12 μm Cloud Emissivity at 1-km resolution from LEOCAT for All Clouds | 1 km |
| cloud_emiss13_1km | 13.3 μm Cloud Emissivity at 1-km resolution from LEOCAT for All Clouds | 1 km |
| cloud_emiss85_1km | 8.5 μm Cloud Emissivity at 1-km resolution from LEOCAT for All Clouds | 1 km |

| | | |
|---|---|---|
| cloud_emissivity_1km | Cloud Emissivity at 1-km resolution from LEOCAT Cloud Top Pressure Retrieval | 1 km |
| Cloud_Fraction | Cloud Fraction in Retrieval Region (5×5 1-km Pixels) from 1-km Cloud Mask | 5 km |
| Cloud_Fraction_Day | Cloud Fraction in Retrieval Region (5×5 1-km Pixels) from 1-km Cloud Mask, Day Only | 5 km |
| Cloud_Fraction_Nadir | Cloud Fraction in Retrieval Region (5×5 1-km Pixels) from 1-km Cloud Mask for Sensor Zenith (View) Angles ≤ 32° | 5 km |
| Cloud_Fraction_Nadir_Day | Cloud Fraction in Retrieval Region (5×5 1-km Pixels) from 1-km Cloud Mask for Sensor Zenith (View) Angles ≤ 32°, Day Data Only | 5 km |
| Cloud_Fraction_Nadir_Night | Cloud Fraction in Retrieval Region (5×5 1-km Pixels) from 1-km Cloud Mask for Sensor Zenith (View) Angles ≤ 32°, Night Data Only | 5 km |
| Cloud_Fraction_Night | Cloud Fraction in Retrieval Region (5×5 1-km Pixels) from 1-km Cloud Mask, Night Only | 5 km |
| Cloud_Height_Method | Index Indicating MODIS Bands Used for Cloud Top Pressure Retrieval | 5 km |
| Cloud_Mask_1km | MODIS Cloud Mask, L2 MOD06 QA Plan | 1 km |
| Cloud_Mask_5km | First Byte of MODIS Cloud Mask Plus Additional Stats for L3 (2nd Byte) | 5 km |
| Cloud_Mask_SPI | Dispersion in bands 1 (plane 1) and 2 (plane 2) from 250 m reflectance statistics of cloud mask | 1 km |
| Cloud_Multi_Layer_Flag | Cloud Multi Layer Identification From MODIS Shortwave Observations | 1 km |
| Cloud_Optical_Thickness | Cloud Optical Thickness two-channel retrieval using band 7(2.1 μm) and either band 1(0.65 μm), 2(0.86um), or 5(1.2 μm) (specified in Quality Assurance 1 km) from best points: not failed in any way, not marked for clear sky restoral | 1 km |
| Cloud_Optical_Thickness_PCL | Cloud Optical Thickness two-channel retrieval using band 7(2.1 μm) and either band 1(0.65 μm), 2(0.86um), or 5(1.2 μm) (specified in Quality Assurance 1 km) from points identified as either partly cloudy from 250 m cloud mask test or 1 km cloud edges | 1 km |
| Cloud_Optical_Thickness_16 | Cloud Optical Thickness two-channel retrieval using band 6(1.6 μm) and either band 1(0.65 μm), 2(0.86u μm), or 5(1.2 μm) (specified in Quality Assurance 1 km) from best points: not failed in any way, not marked for clear sky restoral | 1 km |
| Cloud_Optical_Thickness_16_PCL | Cloud Optical Thickness two-channel retrieval using band 6(1.6 μm) and either band 1(0.65u μm), 2(0.86 μm), or 5(1.2u μm) (specified in Quality Assurance 1 km) from points identified as either partly cloudy from 250 m cloud mask test or 1km cloud edges | 1 km |

| | | |
|---|---|---|
| Cloud_Optical_Thickness_1621 | Cloud Optical Thickness two-channel retrieval using band 7(2.1 μm) and band 6(1.6u μm) from best points: not failed in any way, not marked for clear sky restoral | 1 km |
| Cloud_Optical_Thickness_1621_PCL | Cloud Optical Thickness two-channel retrieval using band 7(2.1uμm) and band 6(1.6 μm) from points identified as either partly cloudy from 250m cloud mask test or 1km cloud edges | 1 km |
| Cloud_Optical_Thickness_37 | Cloud Optical Thickness two-channel retrieval using band 20(3.7 μm) and either band 1(0.65 μm), 2(0.86 μm), or 5(1.2 μm) (specified in Quality Assurance 1 km) from best points: not failed in any way, not marked for clear sky restoral | 1 km |
| Cloud_Optical_Thickness_37_PCL | Cloud Optical Thickness two-channel retrieval using band 20(3.7 μm) and either band 1(0.65 μm), 2(0.86 μm), or 5(1.2 μm) (specified in Quality Assurance 1 km) from points identified as either partly cloudy from 250m cloud mask test or 1km cloud edges | 1 km |
| Cloud_Optical_Thickness_Uncertainty | Cloud Optical Thickness Relative Uncertainty (Percent)from both best points and points identified as cloud edge at 1km resolution or partly cloudy at 250 m based on the Cloud Optical Thickness and Cloud Effective Radius results | 1 km |
| Cloud_Optical_Thickness_Uncertainty_16 | Cloud Optical Thickness Relative Uncertainty (Percent)from both best points and points identified as cloud edge at 1 km resolution or partly cloudy at 250m based on the Cloud Optical Thickness 16 and Cloud Effective Radius 16 results | 1 km |
| Cloud_Optical_Thickness_Uncertainty_1621 | Cloud Optical Thickness Relative Uncertainty (Percent) using band 7(2.1 μm) and band 6(1.6 μm) from both best points and points identified as cloud edge at 1km resolution or partly cloudy at 250 m | 1 km |
| Cloud_Optical_Thickness_Uncertainty_37 | Cloud Optical Thickness Relative Uncertainty (Percent)from both best points and points identified as cloud edge at 1 km resolution or partly cloudy at 250 m based on the Cloud Optical Thickness 37 and Cloud Effective Radius 37 results | 1 km |
| Cloud_Phase_Infrared | Cloud Phase from 8.5 and 11 μm Bands | 5 km |
| Cloud_Phase_Infrared_1km | Cloud Phase at 1-km resolution from 8.5- 11 μm BTDs and cloud emissivity ratios (12/11, 8.5/11, and 7.2/11 μm) | 1 km |
| Cloud_Phase_Infrared_Day | Cloud Phase from 8.5 and 11 μm Bands, Day Only | 5 km |
| Cloud_Phase_Infrared_Night | Cloud Phase from 8.5 and 11 uμm Bands, Night Only | 5 km |
| Cloud_Phase_Optical_Properties | Cloud Phase Determination Used in Optical Thickness/Effective Radius Retrieval | 1 km |
| Cloud_Top_Height | Geopotential Height at Retrieved Cloud Top Pressure Level (rounded to nearest 50 m) | 5 km |
| cloud_top_height_1km | Cloud Top Height at 1-km resolution from LEOCAT, Geopotential Height at Retrieved Cloud Top Pressure Level rounded to nearest 50 m | 1 km |

| | | |
|---|---|---|
| Cloud_Top_Height_Nadir | Geopotential Height at Retrieved Cloud Top Pressure Level for Sensor Zenith (View) Angles ≤32° (rounded to nearest 50 m) | 5 km |
| Cloud_Top_Height_Nadir_Day | Geopotential Height at Retrieved Cloud Top Pressure Level for Sensor Zenith (View) Angles ≤32°, Day Data Only (rounded to nearest 50 m) | 5 km |
| Cloud_Top_Height_Nadir_Night | Geopotential Height at Retrieved Cloud Top Pressure Level for Sensor Zenith (View) Angles ≤32°, Night Data Only (rounded to nearest 50 m) | 5 km |
| cloud_top_method_1km | Index Indicating the MODIS Band(s) Used to Produce the Cloud Top Pressure Result | 1 km |
| Cloud_Top_Pressure | Cloud Top Pressure Level (rounded to nearest 5 mb) | 5 km |
| cloud_top_pressure_1km | Cloud Top Pressure at 1-km resolution from LEOCAT, Cloud Top Pressure Level rounded to nearest 5 mb | 1 km |
| Cloud_Top_Pressure_Day | Cloud Top Pressure Level, Day Only (rounded to nearest 5 mb) | 5 km |
| Cloud_Top_Pressure_From_Ratios | Cloud Top Pressure Levels from Ratios of Bands 36/35, 35/34, 35/33, 34/33 from the CO2-slicing Algorithm | 5 km |
| Cloud_Top_Pressure_Infrared | Cloud Top Pressure from IR Window Retrieval | 5 km |
| Cloud_Top_Pressure_Nadir | Cloud Top Pressure Level for Sensor Zenith (View) Angles ≤32° (rounded to nearest 5 mb) | 5 km |
| Cloud_Top_Pressure_Nadir_Day | Cloud Top Pressure Level for Sensor Zenith (View) Angles ≤32° (rounded to nearest 5 mb), Day Data Only | 5 km |
| Cloud_Top_Pressure_Nadir_Night | Cloud Top Pressure Level for Sensor Zenith (View) Angles ≤32° (rounded to nearest 5 mb), Night Data Only | 5 km |
| Cloud_Top_Pressure_Night | Cloud Top Pressure Level, Night Data Only (rounded to nearest 5 mb) | 5 km |
| Cloud_Top_Temperature | Temperature from Ancillary Data at Retrieved Cloud Top Pressure Level | 5 km |
| cloud_top_temperature_1km | Cloud Top Temperature at 1-km resolution from LEOCAT, Temperature from Ancillary Data at Retrieved Cloud Top Pressure Level | 1 km |
| Cloud_Top_Temperature_Day | Temperature from Ancillary Data at Retrieved Cloud Top Pressure Level, Day Only | 5 km |
| Cloud_Top_Temperature_Nadir | Temperature from Ancillary Data at Retrieved Cloud Top Pressure Level for Sensor Zenith (View) Angles ≤32° | 5 km |
| Cloud_Top_Temperature_Nadir_Day | Temperature from Ancillary Data at Retrieved Cloud Top Pressure Level for Sensor Zenith (View) Angles ≤32°, Day Data Only | 5 km |
| Cloud_Top_Temperature_Nadir_Night | Temperature from Ancillary Data at Retrieved Cloud Top Pressure Level for Sensor Zenith (View) Angles ≤32°, Night Data Only | 5 km |
| Cloud_Top_Temperature_Night | Temperature from Ancillary Data at Retrieved Cloud Top Pressure Level, Night Only | 5 km |

| | | |
|---|---|---|
| Cloud_Water_Path | Column Water Path two-channel retrieval using band 7(2.1 μm) and either band 1(0.65 μm), 2(0.86 μm), or 5(1.2 μm) (specified in Quality Assurance 1 km) from best points: not failed in any way, not marked for clear sky restoral | 1 km |
| Cloud_Water_Path_PCL | Column Water Path two-channel retrieval using band 7(2.1 μm) and either band 1(0.65 μm), 2(0.86 μm), or 5(1.2 μm) (specified in Quality Assurance 1 km) from points identified as either partly cloudy from 250 m cloud mask test or 1 km cloud edges | 1 km |
| Cloud_Water_Path_16 | Column Water Path two-channel retrieval using band 6(1.6 μm) and either band 1(0.65 μm), 2(0.86 μm), or 5(1.2 μm) (specified in Quality Assurance 1 km) from best points: not failed in any way, not marked for clear sky restoral | 1 km |
| Cloud_Water_Path_16_PCL | Column Water Path two-channel retrieval using band 6(1.6 μm) and either band 1(0.65 μm), 2(0.86 μm), or 5(1.2 μm) (specified in Quality Assurance 1 km) from points identified as either partly cloudy from 250 m cloud mask test or 1 km cloud edges | 1 km |
| Cloud_Water_Path_1621 | Column Water Path two-channel retrieval using band 7(2.1 μm) and band 6(1.6 μm) from best points: not failed in any way, not marked for clear sky restoral | 1 km |
| Cloud_Water_Path_1621_PCL | Column Water Path two-channel retrieval using band 7(2.1 μm) and band 6(1.6 μm) from points identified as either partly cloudy from 250 m cloud mask test or 1 km cloud edges | 1 km |
| Cloud_Water_Path_37 | Column Water Path two-channel retrieval using band 20(3.7 μm) and either band 1(0.65 μm), 2(0.86 μm), or 5(1.2 μm) (specified in Quality Assurance 1 km) from best points: not failed in any way, not marked for clear sky restoral | 1 km |
| Cloud_Water_Path_37_PCL | Column Water Path two-channel retrieval using band 20(3.7 μm) and either band 1(0.65 μm), 2(0.86 μm), or 5(1.2 μm) (specified in Quality Assurance 1 km) from points identified as either partly cloudy from 250 m cloud mask test or 1 km cloud edges | 1 km |
| Cloud_Water_Path_Uncertainty | Cloud Water Path Relative Uncertainty (Percent) from both best points and points identified as cloud edge at 1km resolution or partly cloudy at 250 m based on the Cloud Water Path result | 1 km |
| Cloud_Water_Path_Uncertainty_16 | Cloud Water Path Relative Uncertainty (Percent) from both best points and points identified as cloud edge at 1km resolution or partly cloudy at 250 m using the VNSWIR-1.6 μm retrieval | 1 km |
| Cloud_Water_Path_Uncertainty_1621 | Cloud Water Path Relative Uncertainty (Percent) using band 7(2.1 μm) and band 6(1.6 μm) from both best points and points identified as cloud edge at 1 km resolution or partly cloudy at 250 m | 1 km |
| Cloud_Water_Path_Uncertainty_37 | Cloud Water Path Relative Uncertainty (Percent) from both best points and points identified as cloud edge at 1 km resolution or partly cloudy at 250 m using the VNSWIR-3.7 μm retrieval | 1 km |
| Extinction_Efficiency_Ice | Ice Extinction Efficiency from the phase functions used to generate the forward lookup tables | 1 km |

| | | |
|---|---|---|
| Extinction_Efficiency_Liq | Liquid Water CE from the phase functions used to generate the forward lookup tables | 1 km |
| IRP_CTH_Consistency_Flag_1km | Indicates Cloud Phase Infrared 1km results changed to ice from water when cloud top method 1km reports valid band 36/35 CO2-slicing result (1=change) | 1 km |
| IRW_Low_Cloud_Temperature_From_COP | Low Cloud Temperature from IR Window retrieval using cloud emissivity based on cloud optical thickness | 1 km |
| os_top_flag_1km | Upper Tropospheric/Lower Stratospheric (UTLS) Cloud Flag at 1-km resolution - valid from -50° to +50° Latitude | 1 km |
| Quality_Assurance_1km | Quality Assurance at 1 × 1 Pixel Resolution | 1 km |
| Quality_Assurance_5km | Quality Assurance at 5 × 5 Pixel Resolution | 5 km |
| Radiance_Variance | Band 31 Radiance Standard Deviation | 5 km |
| Retrieval_Failure_Metric | Retrievals and other information for points that failed to retrievevia standard solution logic for retrieval using band 7 and either band 1, 2, or 5 (specified in Quality Assurance 1km) | 1 km |
| Retrieval_Failure_Metric_16 | Retrievals and other information for points that failed to retrieve via standard solution logic for retrieval using band 6 and either band 1, 2, or 5 (specified in Quality Assurance 1 km) | 1 km |
| Retrieval_Failure_Metric_1621 | Retrievals and other information for points that failed to retrieve via standard solution logic for retrieval using band 6 and band 7 | 1 km |
| Retrieval_Failure_Metric_37 | Retrievals and other information for points that failed to retrieve via standard solution logic for retrieval using band 20 and either band 1, 2, or 5 (specified in Quality Assurance 1 km) | 1 km |
| Scan_Start_Time | TAI time at start of scan replicated across the swath | 5 km |
| Sensor_Azimuth | Sensor Azimuth Angle, Cell to Sensor | 5 km |
| Sensor_Azimuth_Day | Sensor Azimuth Angle, Cell to Sensor, Day Data Only | 5 km |
| Sensor_Azimuth_Night | Sensor Azimuth Angle, Cell to Sensor, Night Data Only | 5 km |
| Sensor_Zenith | Sensor Zenith Angle, Cell to Sensor | 5 km |
| Sensor_Zenith_Day | Sensor Zenith Angle, Cell to Sensor, Day Data Only | 5 km |
| Sensor_Zenith_Night | Sensor Zenith Angle, Cell to Sensor, Night Data Only | 5 km |
| Single_Scatter_Albedo_Ice | Ice single scatter albedo from the phase functions used to generate the forward lookup tables | – |
| Single_Scatter_Albedo_Liq | Liquid Water single scatter albedo from the phase functions used to generate the forward lookup tables | – |
| Solar_Azimuth | Solar Azimuth Angle, Cell to Sun | 5 km |
| Solar_Azimuth_Day | Solar Azimuth Angle, Cell to Sun, Day Data Only | 5 km |
| Solar_Azimuth_Night | Solar Azimuth Angle, Cell to Sun, Night Data Only | 5 km |

| | | |
|---|---|---|
| Solar_Zenith | Solar Zenith Angle, Cell to Sun | 5 km |
| Solar_Zenith_Day | Solar Zenith Angle, Cell to Sun, Day Data Only | 5 km |
| Solar_Zenith_Night | Solar Zenith Angle, Cell to Sun, Night Data Only | 5 km |
| Spectral_Cloud_Forcing | Spectral Cloud Forcing (cloud minus clear | 5 km |
| Statistics_1km | Statistics_1km | – |
| Surface_Pressure | Surface Pressure from Ancillary Data | 5 km |
| Surface_Temperature | Surface Temperature from Ancillary Data | 5 km |
| surface_temperature_1km | Surface Temperature for Each 1-km MODIS Pixel Interplated from Ancillary Data | 5 km |
| surface_temperature_1km | Surface Temperature for Each 1-km MODIS Pixel Interplated from Ancillary Data | 5 km |
| Latitude | Geodetic Latitude | 5 km |
| Longitude | Geodetic Longitude | 5 km |

## Appendix B. Summary SDS and Quality Assurance (QA) Assignments

The mapping of pixel retrieval outcome status to SDS assignments is given in **Table B.1**. **Table B.2** gives a mapping of the QA outcome status to QA assignments, and **Table B.3** provides the retrieval failure outcome assignments, as discussed in Section 2.6.

Table B.1. Mapping of Pixel Retrieval Outcome Status to SDS Assignments.

| SDS or Quality_Assurance_1km Flag | Retrieval Outcome Status | | | | | | | | | | | | | | | | | |
|---|---|---|---|---|---|---|---|---|---|---|---|---|---|---|---|---|---|---|
| | VNSWIR-2.1 µm Retrievals | | | | VNSWIR-1.6 µm CER Retrievals | | | | VNSWIR-3.7 µm Retrievals | | | | 1.6-2.1 µm Retrievals | | | | Cloud Mask 'Not Cloudy' or CSR=2 | No Cloud Mask |
| | Successful COT, CER, WP CSR=0 | | Successful COT, CER, WP CSR=1,3 (PCL) | | Successful 1.6µm CER CSR=0 | | Successful 1.6 µm CER CSR=1,3 (PCL) | | Successful 3.7µm CER CSR=0 | | Successful 3.7µm CER CSR=1,3 (PCL) | | Successful COT, CER, WP CSR=0 | | Successful COT, CER, WP CSR=1,3 (PCL) | | | |
| | Yes | No | Yes | No | Yes | No | Yes | No | Yes | No | Yes | No | Yes | No | Yes | No | | |
| COT, CER, WP | Valid | Fill | Fill | Fill | – | – | – | – | – | – | – | – | – | – | – | – | Fill | Fill |
| COT_PCL, CER_PCL, WP_PCL | Fill | Fill | Valid | Fill | – | – | – | – | – | – | – | – | – | – | – | – | Fill | Fill |
| COT_16, WP_16 | – | – | – | – | Valid | Fill | Fill | Fill | – | – | – | – | – | – | – | – | Fill | Fill |
| CER_16_PCL, WP_16_PCL | – | – | – | – | Fill | Fill | Valid | Fill | – | – | – | – | – | – | – | – | Fill | Fill |
| CER_37, WP_37 | – | – | – | – | – | – | – | – | Valid | Fill | Fill | Fill | – | – | – | – | Fill | Fill |
| CER_37_PCL, WP_37_PCL | – | – | – | – | – | – | – | – | Fill | Fill | Valid | Fill | – | – | – | – | Fill | Fill |
| COT_1621, CER_1621, WP_1621 | – | – | – | – | – | – | – | – | – | – | – | – | Valid | Fill | Fill | Fill | Fill | Fill |
| COT_1621_PCL, CER_1621_PCL, WP_1621_PCL | – | – | – | – | – | – | – | – | – | – | – | – | Fill | Fill | Valid | Fill | Fill | Fill |

Notation: COT = Cloud_Optical_Thickness

CER = Cloud_Effective Radius

WP = Cloud_Water_Path

Table B.2. Mapping of Pixel Retrieval Outcome Status to QA Assignments.

| SDS or Quality_Assurance_1km Flag | Retrieval Outcome Status | | | | | | | | | | | | | | | | | |
|---|---|---|---|---|---|---|---|---|---|---|---|---|---|---|---|---|---|---|
| | **VNSWIR-2.1 µm Retrievals** | | | | **VNSWIR-1.6 µm CER** | | | | **VNSWIR-3.7 µm Retrievals** | | | | **1.6-2.1 µm Retrievals** | | | | Cloud Mask 'Not Cloudy' or CSR=2 | No Cloud Mask |
| | Successful COT, CER, WP CSR=0 | | Successful COT, CER, WP CSR=1,3 (PCL) | | Successful 1.6µm CER CSR=0 | | Successful 1.6 µm CER CSR=1,3 (PCL) | | Successful 3.7µm CER CSR=0 | | Successful 3.7µm CER CSR=1,3 (PCL) | | Successful COT, CER, WP CSR=0 | | Successful COT, CER, WP CSR=1,3 (PCL) | | | |
| | Yes | No | Yes | No | Yes | No | Yes | No | Yes | No | Yes | No | Yes | No | Yes | No | | |
| **Retrieval Phase** (3 bits) | ≥ 2 | ≥2 | ≥2 | ≥2 | ≥ 2 | ≥2 | ≥2 | ≥2 | ≥ 2 | ≥2 | ≥2 | ≥2 | ≥ 2 | ≥2 | ≥2 | ≥2 | 1 | 0 |
| **Multi Layer Cloud Flag** (Byte=4, Bits 3,4,5) | ≥ 2 | ≥2 | ≥2 | ≥2 | ≥ 2 | ≥2 | ≥2 | ≥2 | ≥ 2 | ≥2 | ≥2 | ≥2 | ≥ 2 | ≥2 | ≥2 | ≥2 | 1 | 0 |
| **VNSWIR-2.1 Retrieval Outcome** (Byte=2, Bit 3) *0=Failed/No Attempt* *1=Successful* | 1 | 0 | 0 | 0 | – | – | – | – | – | – | – | – | – | – | – | – | 0 | 0 |
| **VNSWIR-2.1 PCL Retrieval Outcome** (Byte=28, Bit 7) *0=Failed/No Attempt* *1=Successful* | 0 | 0 | 1 | 0 | – | – | – | – | – | – | – | – | – | – | – | – | 0 | 0 |
| **VNSWIR-1.6 Retrieval Outcome** (Byte=6, Bit 3) *0=Failed/No Attempt* *1=Successful* | – | – | – | – | 1 | 0 | 0 | 0 | – | – | – | – | – | – | – | – | 0 | 0 |
| **VNSWIR-1.6 PCL Retrieval Outcome** (Byte=6, Bit 7) *0=Failed/No Attempt* *1=Successful* | – | – | – | – | 0 | 0 | 1 | 0 | – | – | – | – | – | – | – | – | 0 | 0 |
| **VNSWIR-3.7 Retrieval Outcome** (Byte=7, Bit 3) *0=Failed/No Attempt* *1=Successful* | – | – | – | – | – | – | – | – | 1 | 0 | 0 | 0 | – | – | – | – | 0 | 0 |
| **VNSWIR-3.7 PCL Retrieval Outcome** (Byte=7, Bit7) *0=Failed/No Attempt* *1=Successful* | – | – | – | – | – | – | – | – | 0 | 0 | 1 | 0 | – | – | – | – | 0 | 0 |
| **1.6-2.1 Retrieval Outcome** (Byte=1, Bit6) *0=Failed/No Attempt* *1=Successful* | – | – | – | – | – | – | – | – | – | – | – | – | 1 | 0 | 0 | 0 | 0 | 0 |
| **1.6-2.1 PCL Retrieval Outcome** (Byte=8, Bit3) *0=Failed/No Attempt* *1=Successful* | – | – | – | – | – | – | – | – | – | – | – | – | 0 | 0 | 1 | 0 | 0 | 0 |

The *Retrieval Phase* flag contains the processed cloud phase for all cloud optical and microphysical property retrieval SDSs (including the Retrieval Failure Metric SDS. It is repeated (and identical) for each band combination, and always immediately precedes the specific Retrieval Outcome flags

The *Multi Layer Cloud* flag is shared for all retrievals though the multilayer algorithm is only run when VNSWIR-2.1µm retrievals are successful and CSR=0

Table B.3. Mapping of Pixel Retrieval Failure Outcome Status to QA Assignments.

| **Retrieval Band Combinations** | **Retrieval Outcome Status** | **Failure Category[1]** | **Retrieval Failure Metric SDS** | | |
|---|---|---|---|---|---|
| | | | **COT** | **CER** | **Cost Metric (CM)** |
| **VNSWIR-2.1 µm Retrievals** (Primary) | | | **Retrieval Failure Metric** | | |
| | *Successful[2]* | – | *Fill* | *Fill* | *Fill* |
| | *Not Successful[3]* | Cat. 1 | *Valid* | *Max/Min* | ≥ 0 |
| | | Cat. 3 | *Fill* | *Fill* | *Fill* |
| **VNSWIR-1.6 µm CER Retrievals** | | | **Retrieval Failure Metric 16** | | |
| | *Successful* | – | *Fill* | *Fill* | *Fill* |
| | *Not Successful* | Cat. 1 | *Valid* | *Max/Min* | ≥ 0 |
| | | Cat. 3 | *Fill* | *Fill* | *Fill* |
| **VNSWIR-3.7 µm CER Retrievals** | | | **Retrieval Failure Metric 37** | | |
| | *Successful* | – | *Fill* | *Fill* | *Fill* |
| | *Not Successful* | Cat. 1 | *Valid* | *Max/Min* | ≥ 0 |
| | | Cat. 3 | *Fill* | *Fill* | *Fill* |
| **1.6-2.1 µm Retrievals** | | | **Retrieval Failure Metric 1621** | | |
| | *Successful* | – | *Fill* | *Fill* | *Fill* |
| | *Not Successful* | Cat. 1 | *Valid* | *Max/Min* | ≥ 0 |
| | | Cat. 2 | *Fill* | *Valid* | ≥ 0 |
| | | Cat. 3 | *Fill* | *Fill* | *Fill* |
| **All Retrieval Combinations** | *Cloud Mask Not Determined or "Not Cloudy", or CSR=2* | – | *Fill* | *Fill* | *Fill* |

Notes: *Retrieval Failure Metric* SDSs contain diagnostic information regarding optical property retrieval failures for both CSR=0 and CSR=1,3 (PCL) pixels.

Cloud retrieval phase may be obtained from the Retrieval Phase flag in the *Quality_Assurance_1km* SDS.

[1] Failure Categories: Cat. 1: Successful COT with CER set to max/min
Cat. 2: Failed COT for 1.6-2.1 µm pair, successful CER
Cat. 3: Failed COT and CER

[2] Successful COT, CER and WP for CSR=0 or CSR=1,3 (PCL) pixels

[3] Both CSR=0 and CSR=1,3 retrieval SDSs are fill values

The following details on cloud optical property QA bit assignments are taken from the *MODIS Atmosphere Team Quality Assurance Plan*. The document is available for download at: modis-atmos.gsfc.nasa.gov/_docs/QA_Plan_C6_Master_2015_05_05.pdf. Readers should consult this link to ensure they have the most up-to-date documentation.

**Cloud Product: MOD_06_L2 (Terra) & MYD06_L2 (Aqua)**

The MODIS Cloud product consists of a 1 km set of parameters derived from solar reflectance channels (Cloud Optical Properties and Cirrus Reflectance) and a 5 km set of parameters determined from thermal emitted channels (Cloud Top Properties).

**Cloud Optical Properties**

Cloud Optical Property QA flags are stored in 2 separate QA arrays (SDSs). The first SDS, *Cloud_Mask_1km*, contains Cloud Mask QA flags, which are copied from the 35_L2 Cloud Mask product (cf. Table B.4). The second SDS (*Quality_Assurance_1km*) contains product quality, retrieval processing, and scene characteristic flags (cf. Table B.5). Note that the *Qual-*

Table B.4. Cloud _Mask_1km SDS in the Level 2 MOD06/MYD06 file.

***Scientific Data Set (SDS): "Cloud_Mask_1km"***
***Description: Cloud mask QA flags at 1×1 km***
***Length: 2 bytes (16 bits)***

| Flag Name | Number of Bits | Bit Values | Bit Value Definitions |
|---|---|---|---|
| Cloud Mask Status Flag | 1 | 0<br>1 | Undetermined $^{n,f}$<br>Determined |
| Cloud Mask Cloudiness Flag | 2 | 0<br>1<br>2<br>3 | Confident Cloudy (or Fill, if Status Flag = 0)<br>Probably Cloudy<br>Probably Clear<br>Confident Clear |
| Day/Night Flag | 1 | 0<br>1 | Night $^{n,f}$ (or Fill, if Status Flag = 0)<br>Day |
| Sunglint Flag | 1 | 0<br>1 | Yes (or Fill, if Status Flag = 0)<br>No |
| Snow/Ice Flag | 1 | 0<br>1 | Yes (or Fill, if Status Flag = 0)<br>No |
| Surface Type Flag | 2 | 0<br>1<br>2<br>3 | Ocean or Deep Lakes and Rivers (or Fill)<br>Coast or Shallow Lakes and Rivers<br>Desert<br>Land |
| Heavy Aerosol Flag | 1 | 0<br>1 | Yes $^{n,f}$ (or Fill, if Status Flag = 0)<br>No |
| Thin Cirrus Flag *(based on low threshold using 1.38 µm band)* | 1 | 0<br>1 | Yes (or Fill, if Status Flag = 0)<br>No |
| Shadow Flag | 1 | 0<br>1 | Yes $^{n,f}$ (or Fill, if Status Flag = 0)<br>No |
| Spares | 5 | | TBD |

*ity_Assurance_1km* SDS in 06_L2 HDF files was expanded from 5 bytes (in Collection 005/051) to 9 bytes (in Collection 006).

Table B.5. Cloud _Assurance_1km SDS in the Level 2 MOD06/MYD06 file.

***Scientific Data Set (SDS): "Cloud_Assurance_1km***
***Description: Cloud Optical Property product quality and retrieval processing QA flags at 1×1 km***
***Length: 9 bytes (72 bits)***

| Flag Name | Number of Bits | Bit Values | Bit Value Definitions |
|---|---|---|---|
| Primary (VNSWIR - 2.1 µm) Cloud Optical Thickness Usefulness Flag | 1 | 0<br>1 | Not useful<br>Useful |
| Primary (VNSWIR - 2.1 µm) Cloud Optical Thickness Confidence Flag<br><br>*(flag not important in C6)* | 2 | 0<br>1<br>2<br>3 | No Confidence *(used if both Cloudy COT and Partly Cloud (PCL) COT are fill)*<br>Marginal Confidence *(not used in C6)*<br>Good Confidence *(not used in C6)*<br>Very Good Confidence *(default for all non-fill retrievals; however the QA might be associated with either a non-fill Cloudy COT or a non-fill Partly Cloudy (PCL) COT, the other might be fill)* |
| Spares | 2 | | |
| Primary (VNSWIR - 2.1 µm) Cloud Effective Radius Usefulness Flag | 1 | 0<br>1 | Not useful<br>Useful |
| Primary (VNSWIR - 2.1 µm) Cloud Effective Radius Confidence Flag<br><br>*(flag not important in C6)* | 2 | 0<br>1<br>2<br>3 | No Confidence *(used if both Cloudy CER and Partly Cloud (PCL) CER are fill)*<br>Marginal Confidence *(not used in C6)*<br>Good Confidence *(not used in C6)*<br>Very Good Confidence *(default for all non-fill retrievals; however the QA might be associated with either a non-fill Cloudy CER or a non-fill Partly Cloudy (PCL) CER, the other might be fill)* |
| Primary (VNSWIR - 2.1 µm) Cloud Water Path Usefulness Flag | 1 | 0<br>1 | Not Useful<br>No |
| Primary (VNSWIR - 2.1 µm) Cloud Water Path Confidence Flag<br><br>*(flag not important in C6)* | 2 | 0<br>1<br>2<br>3 | No Confidence *(used if both Cloudy CWP and Partly Cloud (PCL) CWP are fill)*<br>Marginal Confidence *(not used in C6)*<br>Good Confidence *(not used in C6)*<br>Very Good Confidence *(default for all non-fill retrievals; however the QA might be associated with either a non-fill Cloudy CWP or a non-fill Partly Cloudy (PCL) CWP, the other might be fill)* |

| | | | |
|---|---|---|---|
| Cloud Retrieval Phase Flag<br>*Cloud Retrieval Phase Flag duplicated from the 3rd byte. For combining with the 1.6 - 2.1 µm Cloud Retrieval Outcome Flag (below). Needed by L3 to properly compute 1621 Cloud Fractions.* | 3 | 0<br>1<br>2<br>3<br>4 | Cloud Mask Undetermined or Non-Snow Land [n,f]<br>Not Processed (typically clear) [f]<br>Liquid Water Cloud<br>Ice Cloud<br>Undetermined Phase Cloud |
| 1.6-2.1 µm<br>Cloud Retrieval Outcome Flag<br>*The Cloud Retrieval Phase Flag and 1621 Outcome Flag are read as a combined flag by L3 to properly compute Primary Cloud Retrieval Fractions.* | 1 | 0<br>1 | Retrieval not attempted or unsuccessful [f]<br>Retrieval successful (over ocean, snow, & ice) |
| Spare | 1 | | TBD |
| Cloud Retrieval Phase Flag<br>*Cloud Retrieval Phase Flag duplicated from the 3rd byte. For combining with the 1.6 - 2.1 µm Cloud Retrieval Outcome Flag (below). Needed by L3 to properly compute 1621 Cloud Fractions.* | 3 | 0<br>1<br>2<br>3<br>4 | Cloud Mask Undetermined or Non-Snow Land [n,f]<br>Not Processed (typically clear) [f]<br>Liquid Water Cloud<br>Ice Cloud<br>Undetermined Phase Cloud |
| Primary (VNSWIR - 2.1 µm)<br>Cloud Retrieval Outcome Flag<br>*Primary Cloud Retrieval Phase Flag and Outcome Flag are read as a combined flag by L3 to properly compute Primary Cloud Retrieval Fractions.* | 1 | 0<br>1 | Retrieval not attempted or unsuccessful [f]<br>Retrieval successful (over ocean, snow, & ice) |
| Rayleigh Correction | 1 | 0<br>1 | No<br>Yes, correction was made |
| Atmosphere Water Vapor Correction | 1 | 0<br>1 | No<br>Yes, correction was made |
| Band Used for Primary Optical Thickness Retrieval | 2 | 0<br>1<br>2<br>3 | Retrieval not attempted<br>0.645 µm (land)<br>0.858 µm (ocean)<br>1.24 µm (snow/ice) |
| 1.6-2.1 µm Cloud Optical Thickness Usefulness Flag | 1 | 0<br>1 | Not useful<br>Useful |
| 1.6-2.1 µm Cloud Optical Thickness Confidence Flag<br><br>*(flag not important in C6)* | 2 | 0<br>1<br>2<br>3 | No Confidence *(used if both Cloudy COT and Partly Cloud (PCL) COT are fill)*<br>Marginal Confidence *(not used in C6)*<br>Good Confidence *(not used in C6)*<br>Very Good Confidence *(default for all non-fill retrievals; however the QA might be associated with either a non-fill Cloudy COT or a non-fill Partly Cloudy (PCL) COT, the other might be fill)* |
| 1.6-2.1 µm Cloud Effective Radius Usefulness Flag | 1 | 0<br>1 | Not useful<br>Useful |

| | | | |
|---|---|---|---|
| 1.6-2.1 µm Cloud Effective Radius Confidence Flag<br><br>*(flag not important in C6)* | 2 | 0<br><br>1<br><br>2<br><br>3 | No Confidence *(used if both Cloudy CER and Partly Cloud (PCL) CER are fill)*<br><br>Marginal Confidence *(not used in C6)*<br><br>Good Confidence *(not used in C6)*<br><br>Very Good Confidence *(default for all non-fill retrievals; however the QA might be associated with either a non-fill Cloudy CER or a non-fill Partly Cloudy (PCL) CER, the other might be fill)* |
| Clear Sky Restoral Flag | 2 | 0<br>1<br><br>2<br>3 | Not Restored<br>Tagged as 'Partly Cloudy' (PCL) via Edge Detection<br>Restored to Clear Sky vis Spatial Variance<br>Tagged as 'Partly Cloudy' (PCL) vis 250 m Tests |
| 1.6-2.1 µm Cloud Water Path Usefulness Flag | 1 | 0<br>1 | Not useful<br>Useful |
| 1.6-2.1 µm Cloud Water Path Confidence Flag<br><br>*(flag not important in C6)* | 2 | 0<br><br>1<br><br>2<br><br>3 | No Confidence *(used if both Cloudy CWP and Partly Cloud (PCL) CWP are fill)*<br><br>Marginal Confidence *(not used in C6)*<br><br>Good Confidence *(not used in C6)*<br><br>Very Good Confidence *(default for all non-fill retrievals; however the QA might be associated with either a non-fill Cloudy CWP or a non-fill Partly Cloudy (PCL) CWP, the other might be fill)* |
| Primary Cloud Retrieval (VNSWIR - 2.1 µm) Multilayer Cloud & Phase Flag | 3 | 0<br>1<br>2<br>3<br>4<br>5<br>6<br>7 | Cloud mask undetermined [n, f]<br>Not Processed (typically clear) [f]<br>Single-Layer Liquid Water Cloud<br>Multi-Layer Liquid Water Cloud<br>Single-Layer Ice Cloud<br>Multi-Layer Ice Cloud<br>Single-Layer Undetermined Phase Cloud<br>Muti-Layer Undetermined Phase Cloud |
| Primary Cloud Retrieval (VNSWIR - 2.1 µm) Outcome Flag<br>*Primary Cloud Retrieval Outcome Flag duplicated from the 3rd byte for combining with the Primary Cloud Retrieval Multi-layer Cloud & Phase Flag (above). Needed by L3 to properly compute 1L and ML Cloud Fractions.* | 1 | 0<br>1 | Retrieval not attempted or unsuccessful [f]<br>Retrieval successful |
| Spare | 1 | | TBD |
| Phase Difference Multilayer Test | 1 | 0<br>1 | No<br>Yes |
| Delta Precipitable Water Multilayer Test | 1 | 0<br>1 | No<br>Yes |
| Delta Precipitable Water at 900 hPa Test | 1 | 0<br>1 | No<br>Yes |

| | | | |
|---|---|---|---|
| Tau Difference VIS-NIR Multilayer Test | 1 | 0<br>1 | No<br>Yes |
| Pavolonis-Heidinger Multilayer Test | 1 | 0<br>1 | No<br>Yes |
| Spares | 3 | | TBD |
| VNSWIR - 1.6 μm<br>Cloud Retrieval Phase & Outcome<br>*The Cloud Retrieval Phase Flag and Outcome Flag can be read as a 'combined' flag as documented here–or read as separate flags–the bit structure is identical.* | 4 | 0<br>1<br>2<br>3<br>4<br>10<br>11<br>12 | Cloud mask undetermined [n, f]<br>Not Processed (typically clear) [f]<br>Failed Liquid Water Cloud Retrieval<br>Failed Ice Cloud Retrieval<br>Failed Undetermined Phase Cloud Retrieval<br>Successful Liquid Water Cloud Retrieval<br>Successful Ice Cloud Retrieval<br>Successful Undetermined Phase Cloud Retrieval |
| VNSWIR - 1.6 μm<br>PCL (Partly Cloudy)<br>Cloud Retrieval Phase & Outcome<br>*The Cloud Retrieval Phase Flag and Outcome Flag can be read as a 'combined' flag as documented here–or read as separate flags–the bit structure is identical.* | 4 | 0<br>1<br>2<br>3<br>4<br>10<br>11<br>12 | Cloud mask undetermined [n, f]<br>Not Processed (typically clear) [f]<br>Failed Liquid Water Cloud Retrieval<br>Failed Ice Cloud Retrieval<br>Failed Undetermined Phase Cloud Retrieval<br>Successful Liquid Water Cloud Retrieval<br>Successful Ice Cloud Retrieval<br>Successful Undetermined Phase Cloud Retrieval |
| VNSWIR - 3.7 μm<br>Cloud Retrieval Phase & Outcome<br>*The Cloud Retrieval Phase Flag and Outcome Flag can be read as a 'combined' flag as documented here–or read as separate flags–the bit structure is identical.* | 4 | 0<br>1<br>2<br>3<br>4<br>10<br>11<br>12 | Cloud mask undetermined [n, f]<br>Not Processed (typically clear) [f]<br>Failed Liquid Water Cloud Retrieval<br>Failed Ice Cloud Retrieval<br>Failed Undetermined Phase Cloud Retrieval<br>Successful Liquid Water Cloud Retrieval<br>Successful Ice Cloud Retrieval<br>Successful Undetermined Phase Cloud Retrieval |
| VNSWIR - 3.7 μm<br>PCL (Partly Cloudy)<br>Cloud Retrieval Phase & Outcome<br>*The Cloud Retrieval Phase Flag and Outcome Flag can be read as a 'combined' flag as documented here–or read as separate flags–the bit structure is identical.* | 4 | 0<br>1<br>2<br>3<br>4<br>10<br>11<br>12 | Cloud mask undetermined [n, f]<br>Not Processed (typically clear) [f]<br>Failed Liquid Water Cloud Retrieval<br>Failed Ice Cloud Retrieval<br>Failed Undetermined Phase Cloud Retrieval<br>Successful Liquid Water Cloud Retrieval<br>Successful Ice Cloud Retrieval<br>Successful Undetermined Phase Cloud Retrieval |
| 1.6-2.1 μm<br>PCL (Partly Cloudy)<br>Cloud Retrieval Phase & Outcome<br>*The Cloud Retrieval Phase Flag and Outcome Flag can be read as a 'combined' flag as documented here–or read as separate flags–the bit structure is identical.* | 4 | 0<br>1<br>2<br>3<br>4<br>10<br>11<br>12 | Cloud mask undetermined [n, f]<br>Not Processed (typically clear) [f]<br>Failed Liquid Water Cloud Retrieval<br>Failed Ice Cloud Retrieval<br>Failed Undetermined Phase Cloud Retrieval<br>Successful Liquid Water Cloud Retrieval<br>Successful Ice Cloud Retrieval<br>Successful Undetermined Phase Cloud Retrieval |

| | | | |
|---|---|---|---|
| VNSWIR - 2.1 µm (Primary)<br>PCL (Partly Cloudy)<br>Cloud Retrieval Phase & Outcome<br>*The Cloud Retrieval Phase Flag and Outcome Flag can be read as a 'combined' flag as documented here–or read as separate flags–the bit structure is identical.* | 4 | 0<br>1<br>2<br>3<br>4<br>10<br>11<br>12 | Cloud mask undetermined [n, f]<br>Not Processed (typically clear) [f]<br>Failed Liquid Water Cloud Retrieval<br>Failed Ice Cloud Retrieval<br>Failed Undetermined Phase Cloud Retrieval<br>Successful Liquid Water Cloud Retrieval<br>Successful Ice Cloud Retrieval<br>Successful Undetermined Phase Cloud Retrieval |

[n] Cloud Optical Property retrieval not attempted

[f] fill values used for Cloud Optical Property retrieval

## Appendix C. Key Acronyms

AOD: Aerosol Optical Depth

C5: Collection 5 MODIS Atmosphere Team processing stream (version), begun in mid-2006

C6: Collection 6 MODIS Atmosphere Team processing stream, began in Dec. 2013 for Aqua L2 products

CALIOP: Cloud-Aerosol Lidar with Orthogonal Polarization, a lidar instrument flow on the NASA CALIPSO mission

CHIMAERA: Cross-platform HIgh resolution Multi-instrument AtmosphEric Retrieval Algorithms. Cloud retrieval team's development environment that simultaneously supports multiple spaceborne and airborne platforms using the same science core.

CFMIP: Cloud Feedback Modeling Intercomparison Project (http://cfmip.metoffice.com)

CER, $r_e$: Cloud Effective particle Radius

COSP: CFMIP Observation Simulator Package (http://cfmip.metoffice.com/COSP.html), includes the MODIS simulator.

COT, $\tau$: Cloud Optical Thickness

CSR: Clear Sky Restoral algorithm

CTH: Cloud-Top Height

CTP: Cloud Top Pressure

CTT: Cloud-Top Temperature

CWP: Cloud Water Path (e.g., $g\,m^{-2}$); LWP: Liquid Water Path; IWP: Ice Water Path

GEWEX: Global Energy and Water Cycle Experiment (under auspices World Climate Research Programme)

GOES-R AWG: NOAA Algorithm Working Group cloud code for the GOES-R ABI imager, similar to PATMOS-x

HDF: Hierarchical Data Format. MODIS data products are in HDF4.

LAADS: Land and Atmospheres Archive and Distribution System used to distribute MODIS Atmosphere Team products

L2: Level-2 products (pixel-level, 1 km resolution at nadir for all optical property products)

L3: Level-3 products (1° aggregated/gridded for all MODIS Atmosphere Team products)

MCST: MODIS Characterization and Support Team

MOD06 /MYD06: MODIS Terra/Aqua cloud-top and optical properties Level-2 product file ID

MOD08/MYD08: MODIS Terra/Aqua Atmosphere Team Level-3 product file ID

MOD35/MYD35: MODIS Terra/Aqua cloud mask Level-2 product file ID

MODATML2/MYDATML2: MODIS Atmosphere Team joint Level-2 product file ID

MODAPS: MODIS Adaptive Processing System—processing system for MODIS atmosphere team products

MODIS: Moderate Resolution Imaging Spectroradiometer

MWIR: Midwave Infrared (e..g., MODIS 3.7 μm channels)

obs4MIPs: Observations for Modeling Intercomparison Studies

PCL: pixels identified as "partly cloudy" by the CSR algorithm (CSR values of 1 and 2)

POLDER: Polarization and Directionality of the Earth's Reflectances

PAF: Phase Agreement Fraction, a metric used to assess thermodynamic phase skill.

QA: Quality Assurance. Often refers to bit assignments used to qualitatively assign pixel-level retrieval accuracy or the accuracy of aggregated statistics. More generically, can refer to any approach for filtering/weighting retrieved pixels.

SDS: Science Data Set. A distinct science data set within an HDF file.

SWIR: Shortwave Infrared (e..g., MODIS 1.2, 1.6, and 2.1 μm MODIS channels)

VNIR: Visible and Near-Infrared (e..g., MODIS 0.66 and 0.87 μm channels, respectively)

VNSWIR: Refers to a retrieval using a Visible or Near-Infrared or SWIR channel as one of the channel pairs (e.g, VIS over land surfaces, NIR over ocean surfaces, 1.2 μm over snow/ice surfaces).

## Appendix D. Cloud Model LUT Scattering Properties

The following six tables give the scattering properties ($g$, $\omega_0$, $Q_e$) for the liquid water and ice cloud models used in Collection 6. Values are shows as a function of the Look-up Table (LUT) effective radii grid points and the MODIS bands directly used in the optical retrieval algorithm. Band numbers correspond to the following nominal central wavelengths (CWL): All table values are available in the MOD06 file. The corresponding Science Data Sets (SDS) for each liquid water and ice parameter is given below.

| MODIS Band No. | 1 | 2 | 5 | 6 | 7 | 20 | 31 |
|---|---|---|---|---|---|---|---|
| CWL (μm) | 0.66 | 0.87 | 1.24 | 1.64 | 2.13 | 3.75 | 11.03 |

Table D.1. Liquid Water Asymmetry Parameter (SDS: *Asymmetry_Parameter_Liq*). Note: For liquid water retrievals, MOD06 only provides successful retrievals for CER ≥ 4 μm.

| Band/ CER (μm) | 1 | 2 | 5 | 6 | 7 | 20 | 31 |
|---|---|---|---|---|---|---|---|
| *2* | *0.805* | *0.785* | *0.767* | *0.808* | *0.850* | *0.800* | *0.423* |
| 4 | 0.838 | 0.827 | 0.804 | 0.783 | 0.790 | 0.793 | 0.753 |
| 5 | 0.845 | 0.836 | 0.820 | 0.802 | 0.789 | 0.768 | 0.817 |
| 6 | 0.850 | 0.843 | 0.830 | 0.817 | 0.802 | 0.755 | 0.856 |
| 7 | 0.854 | 0.848 | 0.836 | 0.827 | 0.815 | 0.758 | 0.882 |
| 8 | 0.857 | 0.852 | 0.841 | 0.834 | 0.827 | 0.771 | 0.901 |
| 9 | 0.860 | 0.854 | 0.845 | 0.839 | 0.835 | 0.785 | 0.914 |
| 10 | 0.862 | 0.857 | 0.849 | 0.844 | 0.842 | 0.799 | 0.924 |
| 12 | 0.865 | 0.861 | 0.854 | 0.850 | 0.851 | 0.821 | 0.938 |
| 14 | 0.867 | 0.864 | 0.858 | 0.855 | 0.858 | 0.835 | 0.947 |
| 16 | 0.869 | 0.866 | 0.861 | 0.859 | 0.863 | 0.846 | 0.953 |
| 18 | 0.871 | 0.868 | 0.863 | 0.862 | 0.867 | 0.854 | 0.958 |
| 20 | 0.872 | 0.869 | 0.865 | 0.864 | 0.870 | 0.861 | 0.961 |
| 22 | 0.873 | 0.871 | 0.867 | 0.867 | 0.873 | 0.867 | 0.964 |
| 24 | 0.874 | 0.872 | 0.868 | 0.869 | 0.876 | 0.873 | 0.966 |
| 26 | 0.875 | 0.873 | 0.870 | 0.870 | 0.878 | 0.878 | 0.968 |
| 28 | 0.875 | 0.873 | 0.871 | 0.872 | 0.881 | 0.882 | 0.969 |
| 30 | 0.876 | 0.874 | 0.872 | 0.873 | 0.883 | 0.886 | 0.970 |

Table D.2. Liquid Water Single Scattering Albedo (SDS: *Single_Scatter_Albedo_Liq*).

| Band/<br>CER (µm) | 1 | 2 | 5 | 6 | 7 | 20 | 31 |
|---|---|---|---|---|---|---|---|
| *2* | *1.000* | *1.000* | *1.000* | *0.999* | *0.996* | *0.979* | *0.152* |
| 4 | 1.000 | 1.000 | 1.000 | 0.998 | 0.991 | 0.967 | 0.295 |
| 5 | 1.000 | 1.000 | 0.999 | 0.997 | 0.988 | 0.954 | 0.345 |
| 6 | 1.000 | 1.000 | 0.999 | 0.996 | 0.986 | 0.941 | 0.384 |
| 7 | 1.000 | 1.000 | 0.999 | 0.996 | 0.983 | 0.928 | 0.415 |
| 8 | 1.000 | 1.000 | 0.999 | 0.995 | 0.981 | 0.918 | 0.439 |
| 9 | 1.000 | 1.000 | 0.999 | 0.994 | 0.979 | 0.909 | 0.458 |
| 10 | 1.000 | 1.000 | 0.999 | 0.994 | 0.976 | 0.900 | 0.473 |
| 12 | 1.000 | 1.000 | 0.999 | 0.993 | 0.972 | 0.885 | 0.494 |
| 14 | 1.000 | 1.000 | 0.998 | 0.992 | 0.968 | 0.871 | 0.506 |
| 16 | 1.000 | 1.000 | 0.998 | 0.991 | 0.964 | 0.857 | 0.513 |
| 18 | 1.000 | 1.000 | 0.998 | 0.990 | 0.960 | 0.845 | 0.516 |
| 20 | 1.000 | 1.000 | 0.998 | 0.989 | 0.956 | 0.833 | 0.516 |
| 22 | 1.000 | 1.000 | 0.998 | 0.988 | 0.953 | 0.821 | 0.515 |
| 24 | 1.000 | 1.000 | 0.998 | 0.987 | 0.949 | 0.810 | 0.513 |
| 26 | 1.000 | 1.000 | 0.997 | 0.986 | 0.945 | 0.799 | 0.511 |
| 28 | 1.000 | 1.000 | 0.997 | 0.985 | 0.941 | 0.789 | 0.508 |
| 30 | 1.000 | 1.000 | 0.997 | 0.983 | 0.938 | 0.780 | 0.506 |

Table D.3. Liquid Water Extinction Efficiency (SDS: *Extinction_Efficiency_Liq*).

| Band/<br>CER (μm) | 1 | 2 | 5 | 6 | 7 | 20 | 31 |
|---|---|---|---|---|---|---|---|
| *2* | *2.291* | *2.403* | *2.531* | *2.977* | *3.252* | *2.587* | *0.375* |
| 4 | 2.187 | 2.225 | 2.302 | 2.359 | 2.521 | 3.163 | 0.770 |
| 5 | 2.160 | 2.194 | 2.257 | 2.310 | 2.374 | 2.825 | 0.966 |
| 6 | 2.142 | 2.172 | 2.225 | 2.275 | 2.324 | 2.575 | 1.150 |
| 7 | 2.128 | 2.155 | 2.202 | 2.246 | 2.296 | 2.449 | 1.319 |
| 8 | 2.116 | 2.141 | 2.184 | 2.224 | 2.271 | 2.392 | 1.471 |
| 9 | 2.107 | 2.131 | 2.169 | 2.205 | 2.250 | 2.361 | 1.607 |
| 10 | 2.100 | 2.121 | 2.157 | 2.191 | 2.231 | 2.338 | 1.725 |
| 12 | 2.089 | 2.107 | 2.138 | 2.168 | 2.203 | 2.301 | 1.916 |
| 14 | 2.080 | 2.096 | 2.125 | 2.150 | 2.181 | 2.270 | 2.052 |
| 16 | 2.073 | 2.088 | 2.114 | 2.137 | 2.165 | 2.245 | 2.145 |
| 18 | 2.067 | 2.081 | 2.105 | 2.126 | 2.152 | 2.225 | 2.205 |
| 20 | 2.063 | 2.076 | 2.098 | 2.118 | 2.141 | 2.209 | 2.240 |
| 22 | 2.059 | 2.071 | 2.092 | 2.110 | 2.132 | 2.195 | 2.259 |
| 24 | 2.056 | 2.067 | 2.086 | 2.104 | 2.124 | 2.184 | 2.266 |
| 26 | 2.053 | 2.064 | 2.082 | 2.098 | 2.118 | 2.174 | 2.266 |
| 28 | 2.050 | 2.061 | 2.078 | 2.093 | 2.112 | 2.165 | 2.261 |
| 30 | 2.048 | 2.058 | 2.074 | 2.089 | 2.107 | 2.158 | 2.254 |

Table D.4. Ice Asymmetry Parameter (SDS: *Asymmetry_Parameter_Ice)*.

| Band/ CER (μm) | 1 | 2 | 5 | 6 | 7 | 20 | 31 |
|---|---|---|---|---|---|---|---|
| 5 | 0.748 | 0.749 | 0.752 | 0.769 | 0.802 | 0.787 | 0.873 |
| 10 | 0.751 | 0.753 | 0.756 | 0.769 | 0.790 | 0.798 | 0.931 |
| 15 | 0.752 | 0.754 | 0.759 | 0.775 | 0.799 | 0.833 | 0.952 |
| 20 | 0.753 | 0.755 | 0.760 | 0.780 | 0.807 | 0.860 | 0.960 |
| 25 | 0.753 | 0.756 | 0.761 | 0.784 | 0.815 | 0.881 | 0.965 |
| 30 | 0.753 | 0.756 | 0.762 | 0.789 | 0.821 | 0.898 | 0.968 |
| 35 | 0.753 | 0.756 | 0.762 | 0.793 | 0.828 | 0.912 | 0.970 |
| 40 | 0.753 | 0.756 | 0.763 | 0.797 | 0.833 | 0.922 | 0.972 |
| 45 | 0.753 | 0.756 | 0.764 | 0.800 | 0.839 | 0.931 | 0.973 |
| 50 | 0.753 | 0.757 | 0.764 | 0.804 | 0.844 | 0.937 | 0.974 |
| 55 | 0.753 | 0.757 | 0.764 | 0.807 | 0.849 | 0.943 | 0.975 |
| 60 | 0.753 | 0.757 | 0.765 | 0.811 | 0.854 | 0.947 | 0.975 |

Table D.5. Ice Single Scattering Albedo (SDS: *Single_Scatter_Albedo_Ice)*.

| Band/ CER (μm) | 1 | 2 | 5 | 6 | 7 | 20 | 31 |
|---|---|---|---|---|---|---|---|
| 5 | 1.000 | 1.000 | 0.999 | 0.991 | 0.981 | 0.887 | 0.317 |
| 10 | 1.000 | 1.000 | 0.999 | 0.981 | 0.962 | 0.804 | 0.424 |
| 15 | 1.000 | 1.000 | 0.998 | 0.972 | 0.946 | 0.755 | 0.466 |
| 20 | 1.000 | 1.000 | 0.998 | 0.964 | 0.930 | 0.717 | 0.485 |
| 25 | 1.000 | 1.000 | 0.997 | 0.955 | 0.915 | 0.686 | 0.497 |
| 30 | 1.000 | 1.000 | 0.996 | 0.946 | 0.900 | 0.662 | 0.504 |
| 35 | 1.000 | 1.000 | 0.996 | 0.938 | 0.886 | 0.642 | 0.509 |
| 40 | 1.000 | 1.000 | 0.995 | 0.930 | 0.873 | 0.626 | 0.513 |
| 45 | 1.000 | 1.000 | 0.994 | 0.922 | 0.861 | 0.613 | 0.515 |
| 50 | 1.000 | 1.000 | 0.994 | 0.915 | 0.849 | 0.602 | 0.518 |
| 55 | 1.000 | 1.000 | 0.993 | 0.907 | 0.838 | 0.593 | 0.520 |
| 60 | 1.000 | 1.000 | 0.992 | 0.900 | 0.827 | 0.586 | 0.521 |

Table D.6. Ice Extinction Efficiency (SDS: *Extinction_Efficiency_Ice*).

| Band/ CER (μm) | 1 | 2 | 5 | 6 | 7 | 20 | 31 |
|---|---|---|---|---|---|---|---|
| 5 | 2.109 | 2.138 | 2.162 | 2.170 | 2.198 | 2.399 | 1.219 |
| 10 | 2.065 | 2.086 | 2.107 | 2.128 | 2.100 | 2.199 | 1.601 |
| 15 | 2.048 | 2.066 | 2.080 | 2.098 | 2.081 | 2.168 | 1.750 |
| 20 | 2.039 | 2.054 | 2.065 | 2.080 | 2.067 | 2.141 | 1.819 |
| 25 | 2.032 | 2.044 | 2.055 | 2.067 | 2.057 | 2.120 | 1.860 |
| 30 | 2.027 | 2.038 | 2.048 | 2.058 | 2.049 | 2.105 | 1.885 |
| 35 | 2.024 | 2.033 | 2.043 | 2.051 | 2.044 | 2.094 | 1.902 |
| 40 | 2.021 | 2.029 | 2.038 | 2.046 | 2.039 | 2.085 | 1.913 |
| 45 | 2.019 | 2.026 | 2.035 | 2.042 | 2.036 | 2.078 | 1.922 |
| 50 | 2.017 | 2.024 | 2.032 | 2.039 | 2.033 | 2.072 | 1.929 |
| 55 | 2.015 | 2.022 | 2.029 | 2.036 | 2.030 | 2.067 | 1.934 |
| 60 | 2.014 | 2.020 | 2.027 | 2.034 | 2.028 | 2.062 | 1.939 |

## Appendix E. Cloud Retrieval Phase Flow chart

Here we summarize the MODIS C6 Cloud Retrieval Thermodynamic Phase discrimination logic flowchart (panels *1 - 3* ) and CER thresholds (panel *4*) corresponding to the logic in panel *2*. The new C6 phase algorithm uses a discrimination logic that includes several tests providing signed integer votes of different weights.

The four main categories of cloud phase test comprise the C6 phase algorithm (*Tri-Spectral IR Tests, Cloud Top Temperature Tests, 1.38 µm Channel Test* and *Cloud Effective Radii Tests*) are shown to the left of each panel.

Panel AE-1

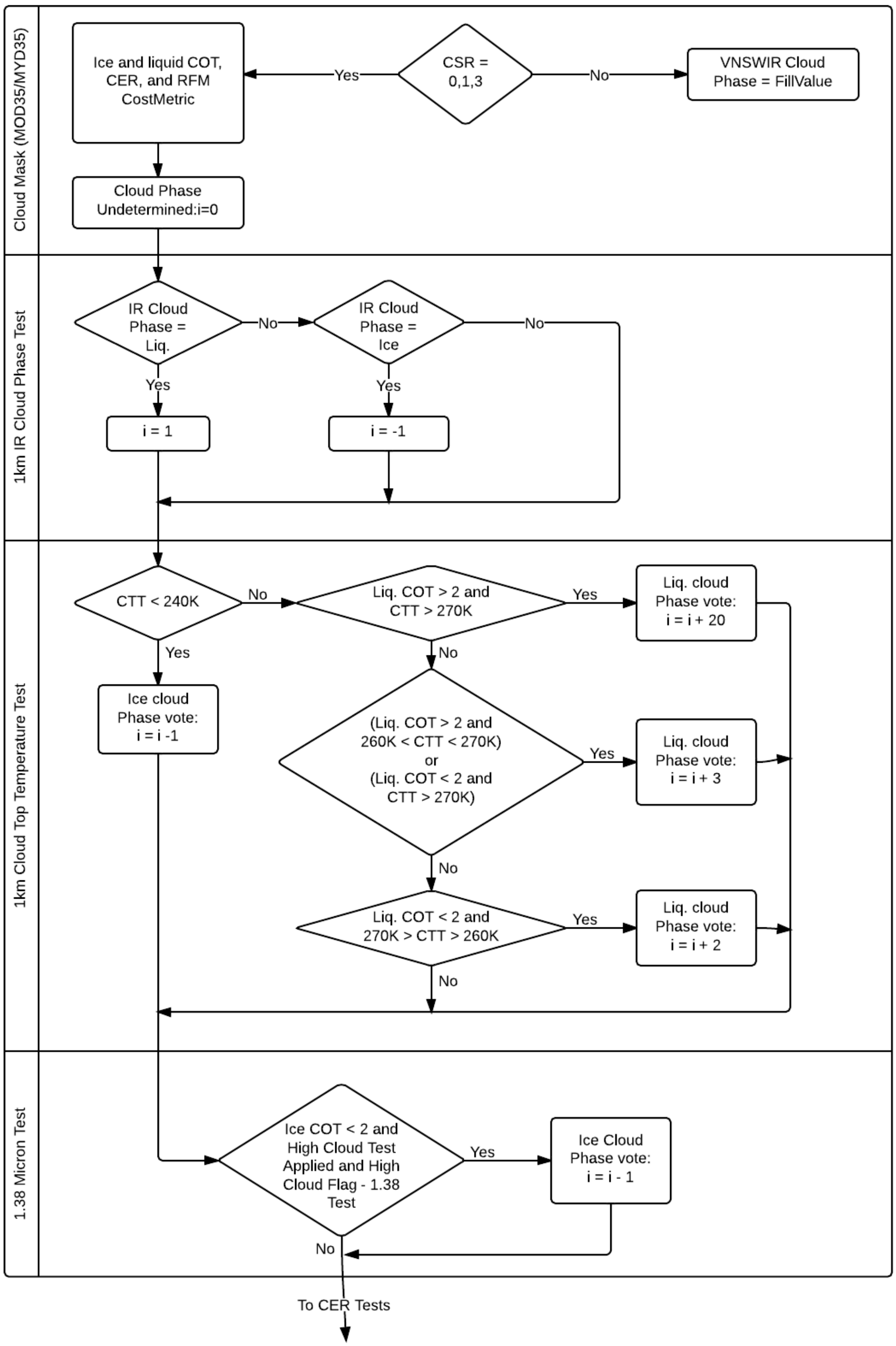
Cloud Mask (MOD35/MYD35)
Ice and liquid COT, CER, and RFM CostMetric
Yes
CSR = 0,1,3
No
VNSWIR Cloud Phase = FillValue
Cloud Phase Undetermined:i=0
1km IR Cloud Phase Test
IR Cloud Phase = Liq.
No
IR Cloud Phase = Ice
No
Yes
Yes
i = 1
i = -1
1km Cloud Top Temperature Test
CTT < 240K
No
Liq. COT > 2 and CTT > 270K
Yes
Liq. cloud Phase vote: i = i + 20
Yes
No
Ice cloud Phase vote: i = i -1
(Liq. COT > 2 and 260K < CTT < 270K) or (Liq. COT < 2 and CTT > 270K)
Yes
Liq. cloud Phase vote: i = i + 3
No
Liq. COT < 2 and 270K > CTT > 260K
Yes
Liq. cloud Phase vote: i = i + 2
No
1.38 Micron Test
Ice COT < 2 and High Cloud Test Applied and High Cloud Flag - 1.38 Test
Yes
Ice Cloud Phase vote: i = i - 1
No
To CER Tests

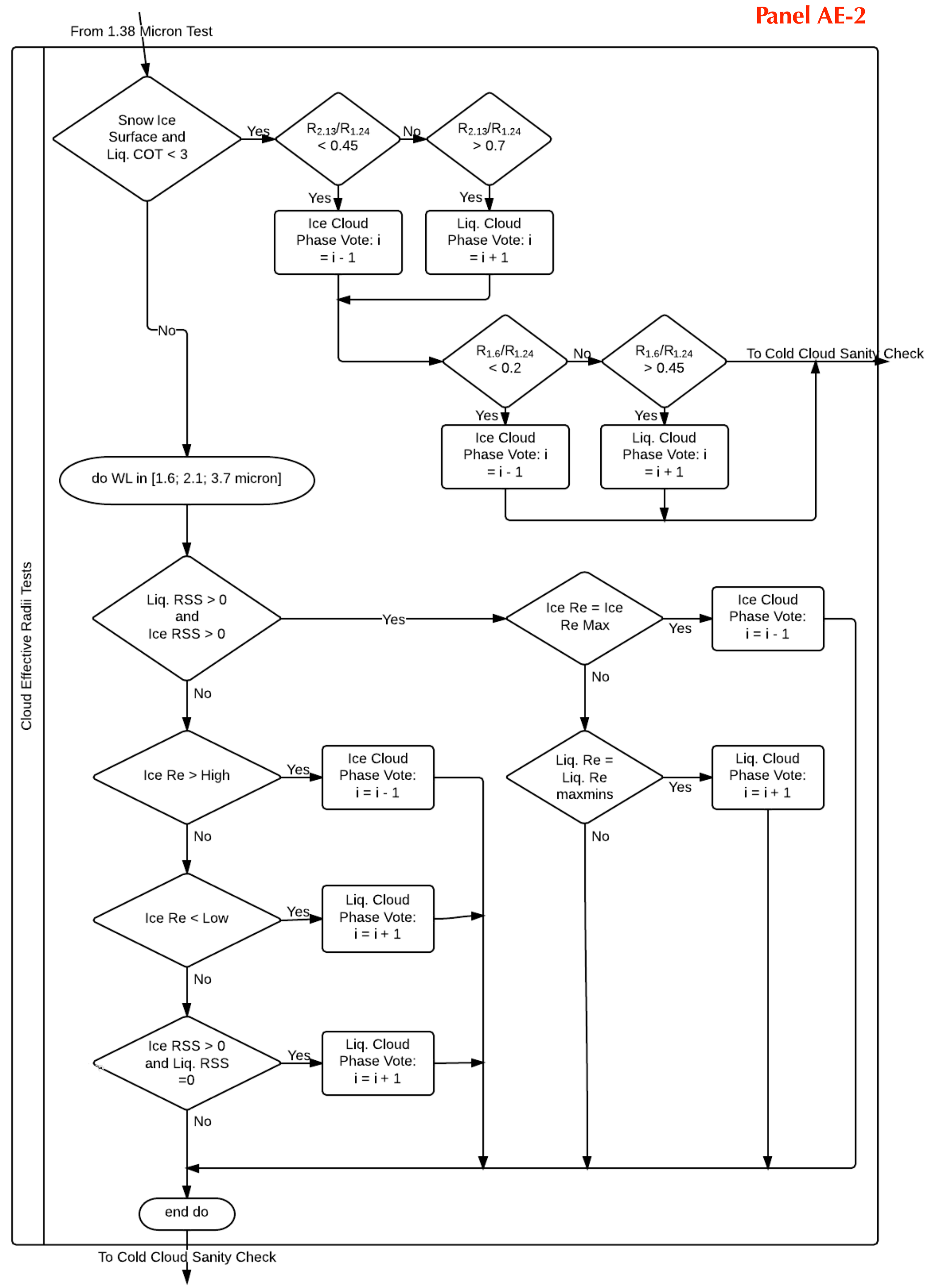
Panel AE-2
From 1.38 Micron Test
Cloud Effective Radii Tests
Snow Ice Surface and Liq. COT < 3
Yes
No
R2.13/R1.24 < 0.45
R2.13/R1.24 > 0.7
Ice Cloud Phase Vote: i = i - 1
Liq. Cloud Phase Vote: i = i + 1
R1.6/R1.24 < 0.2
R1.6/R1.24 > 0.45
To Cold Cloud Sanity Check
do WL in [1.6; 2.1; 3.7 micron]
Liq. RSS > 0 and Ice RSS > 0
Ice Re = Ice Re Max
Liq. Re = Liq. Re maxmins
Ice Re > High
Ice Re < Low
Ice RSS > 0 and Liq. RSS =0
end do
To Cold Cloud Sanity Check

Panel AE-3

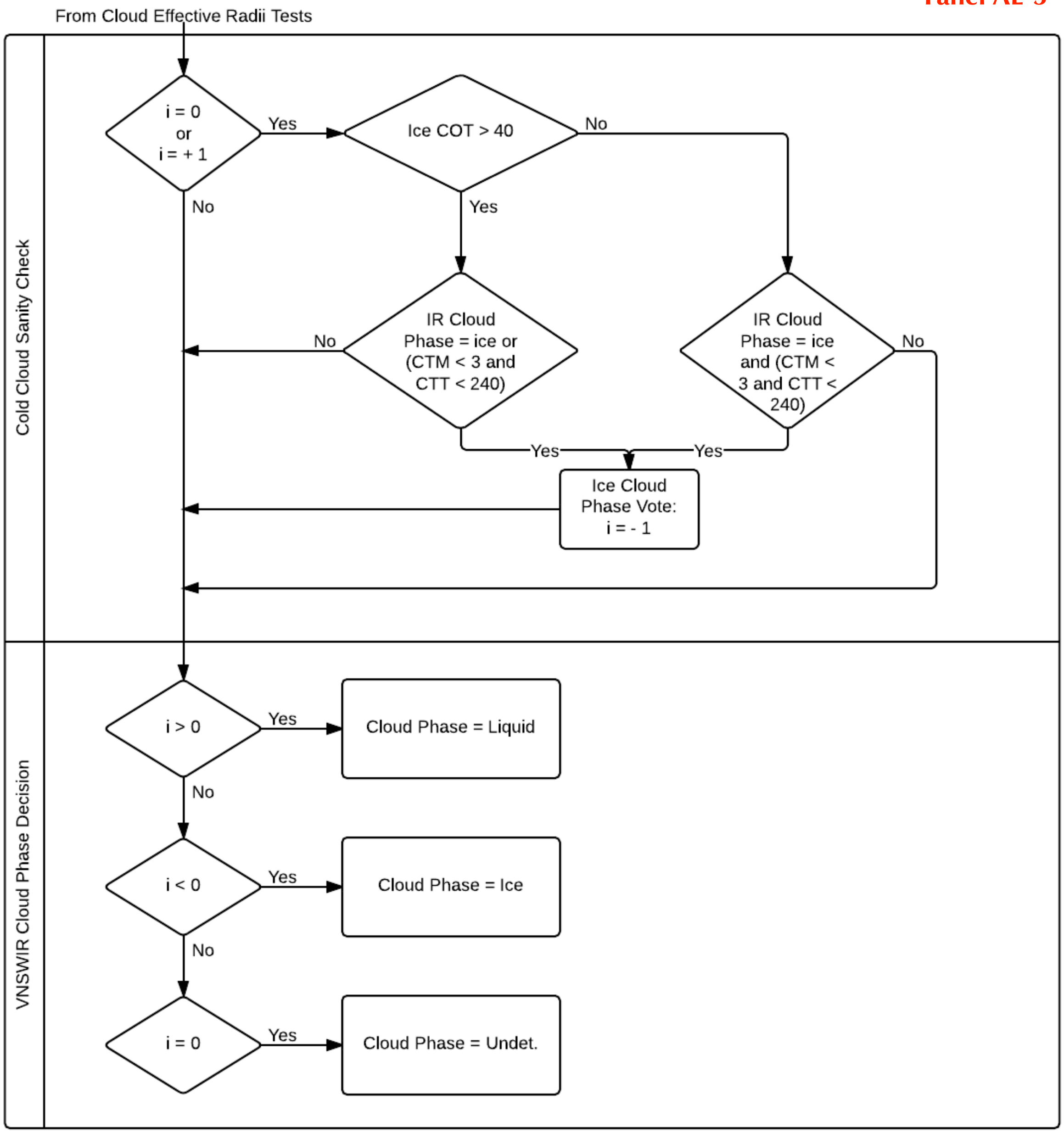
From Cloud Effective Radii Tests
Cold Cloud Sanity Check
i = 0
or
i = + 1
Yes
Ice COT > 40
No
No
Yes
IR Cloud
Phase = ice or
(CTM < 3 and
CTT < 240)
No
IR Cloud
Phase = ice
and (CTM <
3 and CTT <
240)
No
Yes
Yes
Ice Cloud
Phase Vote:
i = - 1
VNSWIR Cloud Phase Decision
i > 0
Yes
Cloud Phase = Liquid
No
i < 0
Yes
Cloud Phase = Ice
No
i = 0
Yes
Cloud Phase = Undet.

Panel AE-4

| MODIS Channel | CER Thresholds | SPI < 30 | SPI ≥ 30 |
|---|---|---|---|
| **6 (1.6 μm)** | Low | 20 μm | 20 μm |
| | High | 30 μm | Max CER for Ice (CER > High ⇒ false???) |
| **7 (2.1 μm)** | Low | 20 μm | 20 μm |
| | High | 30 μm | Max CER for Ice (CER > High ⇒ false???) |
| **20 (3.7 μm)** | Low | 15 μm | 15 μm |
| | High | 25 μm | Max CER for Ice (CER > High ⇒ false???) |

## Appendix F. Cloud Optical/Microphysical Level-3 Statistics

A summary of the C6 L3 parameters cloud optical/microphysical statistical quantities is given here. A complete list of C6 Atmosphere Team L3 statistics is available on the team web site (modis-atmos.gsfc.nasa.gov/products_C006update.html). See Sect. 3 for further details.

# L3 Global Statistics

### Collection 006 Update

= Added = Renamed = Deleted = Modified


**Derived from L2 Cloud (06_L2)**

**Cloud Optical Properties** [PCL:Partly Cloudy Day:SolarZA≤81.3731°]

*(Primary 2.1 Retrieval)* D = SDS in D3 only (not in E3/M3)

| Parameter | Mean | Standard_Deviation | Minimum | Maximum | Histogram_Counts (n) | Fraction | Pixel_Counts | Mean_Uncertainty | Log_Mean_Uncertainty | Log_Mean | Log_Standard_Deviation | JHisto_vs_Eff_Radius (nxn) | JHisto_vs_Eff_Radius_16 (nxn) | JHisto_vs_Eff_Radius_37 (nxn) | JHisto_vs_Temperature (nxn) | JHisto_vs_Emissivity (nxn) | JHisto_vs_Pressure (nxn) |
|---|---|---|---|---|---|---|---|---|---|---|---|---|---|---|---|---|---|
| 01. Cloud_Optical_Thickness_Liquid | • | • | • | • | • | | | • | • | • | • | • | | | • | | • |
| 02. Cloud_Optical_Thickness_Ice | • | • | • | • | • | | | • | • | • | • | • | | | • | D | • |
| 03. Cloud_Optical_Thickness_Undetermined | • | • | • | • | | | | | | • | • | | | | | | |
| 04. Cloud_Optical_Thickness_Combined | • | • | • | • | | | | | | • | • | | | | | | |
| 05. Cloud_Optical_Thickness_PCL_Liquid | • | • | • | • | • | | | • | | | | • | | | | | |
| 06. Cloud_Optical_Thickness_PCL_Ice | • | • | • | • | • | | | • | | | | • | | | | | |
| 07. Cloud_Optical_Thickness_PCL_Undetermined | • | • | • | • | | | | | | | | | | | | | |
| 08. Cloud_Optical_Thickness_PCL_Combined | • | • | • | • | | | | | | | | | | | | | |
| 09. Cloud_Optical_Thickness_ISCCP [8] | | | | | | | | | | | | | | | | | • |
| 10. Cloud_Optical_Thickness_PCL_ISCCP [8] | | | | | | | | | | | | | | | | | • |
| 11. Cloud_Effective_Radius_Liquid | • | • | • | • | • | | | • | | | | | | | • | | D |
| 12. Cloud_Effective_Radius_Ice | • | • | • | • | • | | | • | | | | | | | • | | D |
| 13. Cloud_Effective_Radius_Undetermined | • | • | • | • | | | | | | | | | | | | | |
| 15. Cloud_Effective_Radius_PCL_Liquid | • | • | • | • | | | | • | | | | | | | | | |
| 16. Cloud_Effective_Radius_PCL_Ice | • | • | • | • | | | | • | | | | | | | | | |
| 17. Cloud_Effective_Radius_PCL_Undetermined | • | • | • | • | | | | | | | | | | | | | |
| 18. Cloud_Water_Path_Liquid | • | • | • | • | • | | | • | | | | | | | | | |
| 19. Cloud_Water_Path_Ice | • | • | • | • | • | | | • | | | | | | | | | |
| 20. Cloud_Water_Path_Undetermined | • | • | • | • | | | | | | | | | | | | | |
| 22. Cloud_Water_Path_PCL_Liquid | • | • | • | • | • | | | • | | | | | | | | | |
| 23. Cloud_Water_Path_PCL_Ice | • | • | • | • | • | | | • | | | | | | | | | |


| PARAMETER | Mean | Standard_Deviation | Minimum | Maximum | Histogram_Counts (n) | Fraction | Pixel_Counts | Mean_Uncertainty | Log_Mean_Uncertainty | Log_Mean | Log_Standard_Deviation | JHisto_vs_Eff_Radius (nxn) | JHisto_vs_Eff_Radius_16 (nxn) | JHisto_vs_Eff_Radius_37 (nxn) | JHisto_vs_Temperature (nxn) | JHisto_vs_Emissivity (nxn) | JHisto_vs_Pressure (nxn) |
|---|---|---|---|---|---|---|---|---|---|---|---|---|---|---|---|---|---|
| **24. Cloud_Water_Path_PCL_Undetermined** | • | • | • | • | | | | | | | | | | | | | |
| **25. Cloud_Phase_Optical_Properties** [L, I, U][Cld+PCL][S+F] | | | | | | | | | | | | | | | • | | |
| **26. COP_Phase_Cloudy** [3 cats: Liq, Ice, Undet] CSR=0 [Succ+Fail] | | | | | D | | | | | | | | | | | | |
| **27. COP_Phase_Partly_Cloudy** [Liq, Ice, Undet] CSR=1,3 [S+F] | | | | | D | | | | | | | | | | | | |
| **28. COP_Phase_CloudMaskClear** [Cloud Mask Clear] CSR=0 | | | | | D | | | | | | | | | | | | |
| **29. COP_Phase_RestoredToClear** [Restored To Clear] CSR=2 | | | | | D | | | | | | | | | | | | |
| *(Primary Successful Cloud Retrieval Fraction)* | | | | | | | | | | | | | | | | | |
| **30. Cloud_Retrieval_Fraction_Liquid** [denom. incl. fail in C6] | | | | | | • | • | | | | | | | | | | |
| **31. Cloud_Retrieval_Fraction_Ice** [denom. incl. fail in C6] | | | | | | • | • | | | | | | | | | | |
| **32. Cloud_Retrieval_Fraction_Undetermined** [*] | | | | | | • | • | | | | | | | | | | |
| **33. Cloud_Retrieval_Fraction_Combined** [*] | | | | | | • | • | | | | | | | | | | |
| **34. Cloud_Retrieval_Fraction_PCL_Liquid** [*] | | | | | | • | • | | | | | | | | | | |
| **35. Cloud_Retrieval_Fraction_PCL_Ice** [*] | | | | | | • | • | | | | | | | | | | |
| **36. Cloud_Retrieval_Fraction_PCL_Undetermined** [*] | | | | | | • | • | | | | | | | | | | |
| **37. Cloud_Retrieval_Fraction_PCL_Combined** [*] | | | | | | • | • | | | | | | | | | | |
| *(Primary Retrieval Single-Layer Clouds only)* | | | | | | | | | | | | | | | | | |
| **38. Cloud_Optical_Thickness_1L_Liquid** [4] | • | • | • | • | • | | | • | | | | D | | | | | |
| **39. Cloud_Optical_Thickness_1L_Ice** [5] | • | • | • | • | • | | | • | | | | D | | | | D | |
| **40. Cloud_Effective_Radius_1L_Liquid** | • | • | • | • | • | | | • | | | | | | | | | |
| **41. Cloud_Effective_Radius_1L_Ice** | • | • | • | • | • | | | • | | | | | | | | | |
| **42. Cloud_Water_Path_1L_Liquid** | • | • | • | • | • | | | • | | | | | | | | | |
| **43. Cloud_Water_Path_1L_Ice** | • | • | • | • | • | | | • | | | | | | | | | |
| **44. Cloud_Phase_Optical_Properties1L** | | | | | | | | | | | | | | | D | | |
| *(Single-Layer Cloud Fraction)* | | | | | | | | | | | | | | | | | |
| **45. Cloud_Retrieval_Fraction_1L_Liquid** [denom. incl. fail] | | | | | | • | • | | | | | | | | | | |
| **46. Cloud_Retrieval_Fraction_1L_Ice** [denom. incl. fail] | | | | | | • | • | | | | | | | | | | |
| *(Multi-Layer Cloud Fraction)* | | | | | | | | | | | | | | | | | |
| **47. Cloud_Retrieval_Fraction_ML_Liquid** [denom. incl. fail] | | | | | | • | • | | | | | | | | | | |
| **48. Cloud_Retrieval_Fraction_ML_Ice** [denom. incl. fail] | | | | | | • | • | | | | | | | | | | |


| Parameter | Mean | Standard_Deviation | Minimum | Maximum | Histogram_Counts (n) | Fraction | Pixel_Counts | Mean_Uncertainty | Log_Mean_Uncertainty | Log_Mean | Log_Standard_Deviation | JHisto_vs_Eff_Radius (nxn) | JHisto_vs_Eff_Radius_16 (nxn) | JHisto_vs_Eff_Radius_37 (nxn) | JHisto_vs_Temperature (nxn) | JHisto_vs_Emissivity (nxn) | JHisto_vs_Pressure (nxn) |
|---|---|---|---|---|---|---|---|---|---|---|---|---|---|---|---|---|---|
| **49. Cloud_Retrieval_Fraction_ML_Undetermined** [*] | | | | | | • | • | | | | | | | | | | |
| **50. Cloud_Retrieval_Fraction_ML_Combined** [*] | | | | | | • | • | | | | | | | | | | |
| *(Ratio of Multi-Layer Clouds to All-Layer Clouds by Phase)* | | | | | | | | | | | | | | | | | |
| **51. ML_Ratio_Liquid** [prev. Fraction] | | | | | | • | • | | | | | | | | | | |
| **52. ML_Ratio_Ice** [prev. Fraction] | | | | | | • | • | | | | | | | | | | |
| **53. ML_Ratio_Undetermined** [prev. Fraction] | | | | | | • | • | | | | | | | | | | |
| **54. ML_Ratio_Combind** [prev. Fraction] | | | | | | • | • | | | | | | | | | | |
| *(Supplementary 1.6/2.1 Retrieval)* **vs. Re1621** | | | | | | | | | | | | | | | | | |
| **55. Cloud_Optical_Thickness_1621_Liquid** [6] | • | • | • | • | • | | | • | | | | • | | | | | |
| **56. Cloud_Optical_Thickness_1621_Ice** [7] | • | • | • | • | • | | | • | | | | • | | | | | |
| **57. Cloud_Effective_Radius_1621_Liquid** | • | • | • | • | • | | | • | | | | | | | | | |
| **58. Cloud_Effective_Radius_1621_Ice** | • | • | • | • | • | | | • | | | | | | | | | |
| **59. Cloud_Water_Path_1621_Liquid** | • | • | • | • | • | | | • | | | | | | | | | |
| **60. Cloud_Water_Path_1621_Ice** | • | • | • | • | • | | | • | | | | | | | | | |
| **61. Cloud_Retrieval_Fraction_1621_Liquid** [denom incl. fail] | | | | | | • | • | | | | | | | | | | |
| **62. Cloud_Retrieval_Fraction_1621_Ice** [denom incl. fail] | | | | | | • | • | | | | | | | | | | |
| **63. Cloud_Optical_Thickness_1621_PCL_Liquid** [6] | • | • | • | • | • | | | • | | | | • | | | | | |
| **64. Cloud_Optical_Thickness_1621_PCL_Ice** [7] | • | • | • | • | • | | | • | | | | • | | | | | |
| **65. Cloud_Effective_Radius_1621_PCL_Liquid** | • | • | • | • | • | | | • | | | | | | | | | |
| **66. Cloud_Effective_Radius_1621_PCL_Ice** | • | • | • | • | • | | | • | | | | | | | | | |
| **67. Cloud_Water_Path_1621_PCL_Liquid** | • | • | • | • | • | | | • | | | | | | | | | |
| **68. Cloud_Water_Path_1621_PCL_Ice** | • | • | • | • | • | | | • | | | | | | | | | |
| **69. Cloud_Retrieval_Fraction_1621_PCL_Liquid** | | | | | | • | • | | | | | | | | | | |
| **70. Cloud_Retrieval_Fraction_1621_PCL_Ice** | | | | | | • | • | | | | | | | | | | |
| *(Supplementary 1.6 Retrieval)* | | | | | | | | | | | | | | | | | |
| **71. Cloud_Optical_Thickness_16_Liquid** | • | • | • | • | | | | • | | | | | D | | | | |
| **72. Cloud_Optical_Thickness_16_Ice** | • | • | • | • | | | | • | | | | | D | | | | |
| **73. Cloud_Effective_Radius_16_Liquid** | • | • | • | • | • | | | • | | | | • | | D | D | | |
| **74. Cloud_Effective_Radius_16_Ice** | • | • | • | • | • | | | • | | | | • | | D | D | | |
| **75. Cloud_Water_Path_16_Liquid** | • | • | • | • | • | | | • | | | | | | | | | |


| Parameter | Mean | Standard_Deviation | Minimum | Maximum | Histogram_Counts (n) | Fraction | Pixel_Counts | Mean_Uncertainty | Log_Mean_Uncertainty | Log_Mean | Log_Standard_Deviation | JHisto_vs_Eff_Radius (nxn) | JHisto_vs_Eff_Radius_16 (nxn) | JHisto_vs_Eff_Radius_37 (nxn) | JHisto_vs_Temperature (nxn) | JHisto_vs_Emissivity (nxn) | JHisto_vs_Pressure (nxn) |
|---|---|---|---|---|---|---|---|---|---|---|---|---|---|---|---|---|---|
| 76. Cloud_Water_Path_16_Ice | • | • | • | • | • | | | • | | | | | | | | | |
| 77. Cloud_Retrieval_Fraction_16_Liquid | | | | | | • | • | | | | | | | | | | |
| 78. Cloud_Retrieval_Fraction_16_Ice | | | | | | • | • | | | | | | | | | | |
| 79. Cloud_Optical_Thickness_16_PCL_Liquid | • | • | • | • | | | | • | | | | | D | | | | |
| 80. Cloud_Optical_Thickness_16_PCL_Ice | • | • | • | • | | | | • | | | | | D | | | | |
| 81. Cloud_Effective_Radius_16_PCL_Liquid | • | • | • | • | • | | | • | | | | • | | D | D | | |
| 82. Cloud_Effective_Radius_16_PCL_Ice | • | • | • | • | • | | | • | | | | • | | D | D | | |
| 83. Cloud_Water_Path_16_PCL_Liquid | • | • | • | • | • | | | • | | | | | | | | | |
| 84. Cloud_Water_Path_16_PCL_Ice | • | • | • | • | • | | | • | | | | | | | | | |
| 85. Cloud_Retrieval_Fraction_16_PCL_Liquid | | | | | | • | • | | | | | | | | | | |
| 86. Cloud_Retrieval_Fraction_16_PCL_Ice | | | | | | • | • | | | | | | | | | | |
| *(Supplementary 3.7 Retrieval)* | | | | | | | | | | | | | | | | | |
| 87. Cloud_Optical_Thickness_37_Liquid | • | • | • | • | | | | • | | | | | | D | | | |
| 88. Cloud_Optical_Thickness_37_Ice | • | • | • | • | | | | • | | | | | | D | | | |
| 89. Cloud_Effective_Radius_37_Liquid | • | • | • | • | • | | | • | | | | • | | | D | | |
| 90. Cloud_Effective_Radius_37_Ice | • | • | • | • | • | | | • | | | | • | | | D | | |
| 91. Cloud_Water_Path_37_Liquid | • | • | • | • | • | | | • | | | | | | | | | |
| 92. Cloud_Water_Path_37_Ice | • | • | • | • | • | | | • | | | | | | | | | |
| 93. Cloud_Retrieval_Fraction_37_Liquid | | | | | | • | • | | | | | | | | | | |
| 94. Cloud_Retrieval_Fraction_37_Ice | | | | | | • | • | | | | | | | | | | |
| 95. Cloud_Optical_Thickness_37_PCL_Liquid | • | • | • | • | | | | • | | | | | | D | | | |
| 96. Cloud_Optical_Thickness_37_PCL_Ice | • | • | • | • | | | | • | | | | | | D | | | |
| 97. Cloud_Effective_Radius_37_PCL_Liquid | • | • | • | • | • | | | • | | | | • | | | D | | |
| 98. Cloud_Effective_Radius_37_PCL_Ice | • | • | • | • | • | | | • | | | | • | | | D | | |
| 99. Cloud_Water_Path_37_PCL_Liquid | • | • | • | • | • | | | • | | | | | | | | | |
| 100. Cloud_Water_Path_37_PCL_Ice | • | • | • | • | • | | | • | | | | | | | | | |
| 101. Cloud_Retrieval_Fraction_37_PCL_Liquid | | | | | | • | • | | | | | | | | | | |
| 102. Cloud_Retrieval_Fraction_37_PCL_Ice | | | | | | • | • | | | | | | | | | | |

**D** = SDS in D3 only (not in E3/M3). A total of 19 Joint Histograms were deleted going from D3 to E3/M3 due to 2 GB uncompressed HDF file size limit in HDF4.

## APPENDIX G. SUMMARY OF HIGH-LEVEL MOD06 COLLECTION 6 EFFORTS

The following table provides a summary of the key Collection 6 MOD06 optical/micro-physical algorithm development efforts. The symbol ▵ denotes the main refinement activities that will continue with the proposed support; most of this work is detailed in the main body of the proposal text (see Sect. 3).

| Category | Collection 5 | Collection 6 | Notes |
|---|---|---|---|
| **Radiative Transfer** | | | |
| Cloud Model: all phases | Combined discrete ordinate LUT (small COT) + asymptotic theory parameters (large COT) | Full reflectance, flux, and emissivity LUTs across retrieval space/geometry. LUT entries provided for multiple scattering component only; phase function provided in file for direct calculation of single scattering component. | • Single approach (LUT) => easier retrieval code maintenance.<br>• LUT grid designed to limit median linear interpolation error to << 1%.<br>• Separation of single scattering component => fewer LUT grid points and interpolations during processing.<br>• Required DISORT code mod to improve efficiency for BRF-specified surfaces. |
| △ Ice Cloud Model | Variable habit (smooth) vs. size/empirical distributions. Relatively large asymmetry parameter (*g*) and highly dependent on $r_e$. | Single habit (severely roughened aggregated columns) w/ analytic distribution (gamma, $v_e$=0.10) | • Smaller *g* reduces COT & provides closure with non-opaque IR COT retrievals.<br>• Nearly constant *g* vs. $r_e$.<br>• SWIR/MWIR particle absorption decreases => larger retrieved $r_e$. |
| Surface Ancillary Datasets | Team-designed nominal seasonal gap-filled spectral albedo dataset using Terra C4 product MOD43. | New dynamic gap-filled spectral albedo dataset derived from Aqua+Terra C5 MCD43B3. Emissivity dataset from MOD06 CT product for spectral consistency. | • C6 albedo dataset provides higher temporal resolution than C5 (8 day interval, 16 day average).<br>• Snow and Sea-ice spectral albedo dataset same as for C5. |
| △ Incorporation of Model Error Sources | N/A | LUT includes sensitivity datasets for $v_e$ and Cox-Munk wind vector. | No explicit model error sources used in C5 uncertainty calculations. |
| **Level-1 Analysis/Corrections** | | | |
| △ Band 1,2 trend detection/correction | N/A | COT monthly anomaly trend analysis | Used to justify MCST work with desert site response-vs-scan angle corrections. |
| △ Aqua Band 1,2 250 m⇒1 km aggregation | N/A | Used to improve known Aqua VNIR focal plane misregistration w/SWIR, MWIR, and IR focal planes | Impacts Aqua COT and $r_e$ statistics in heterogeneous low cloud regions. |
| **Algorithm - Retrieval Science** | | | |
| Retrieval channel pairs | $r_e$ differences for VNIR-SWIR/MWIR channel pairs (relative to standard VNIR-2.1 µm). | Full retrievals reported separately for as many as 4 spectral channel pairs. | • Doesn't filter alternate channel pair retrievals by success of standard retrieval.<br>• Allows for separate evaluation/aggregation of all channel pairs. |

| Category | Collection 5 | Collection 6 | Notes |
|---|---|---|---|
| Cloud-Top (CT) Pressure/ Temperature | Used 5 km MOD06 CT product. | Uses new 1km MOD06 CT product. Incorporates non-unity cloud emissivity from optical retrieval into low cloud CT retrievals that use IR window channel. | |
| ᐞ Thermodynamic Phase | Used SWIR/VNIR ratio tests as a proxy for particle size that was then used to indicate phase. | SWIR/VNIR ratio tests replaced w/separate ice and liquid retrievals. Uses new tri-spectral IR phase product. Eliminated use of individual cloud mask tests. Weights applied to various tests in lieu of strict logical approach. | • Algorithm tests/weights validated against CALIOP, POLDER products.<br>• Significant skill improvement seen for most regions (e.g., land, ocean, snow/ ice) though still limited by available spectral bands. |
| ᐞ Misc. | N/A | Numerous science and code infrastructure performance improvements. | • Improved processing efficiency.<br>• Easier code maintenance, porting to other sensors. |
| **Algorithm - Pixel Quality Assessment (QA)/Filtering** | | | |
| ᐞ Updated 'Clear Sky Restoral' (CSR) algorithm | N/A | Improve discrimination between heavy aerosol (smoke/dust) and glint from low uniform cloud population. | Added explicit aerosol model tests. Replaced height/phase discrimination test w/CT 'method' flags. |
| Pixels identified as not-overcast and/or cloudy FOV by CSR algorithm | Do not retrieve CSR-identified pixels | Attempt retrievals on CSR-identified pixels and, if successful, write results to separate dataset (SDS). | Separate SDS allows for analysis of CSR population w/out need to read/interpret QA assignments. |
| Failed Retrieval Metrics ('failure' defined as the simultaneous COT, $r_e$ solution being outside of LUT space) | No failure metrics reported | The following metrics are reported: nearest COT, nearest $r_e$, relative distance from 2D measurement point to nearest LUT solution point. | Allow users to understand failure mode (e.g., large $r_e$, small COT) for cloudy FOVs not meeting 1D fwd. model assumptions. Potentially useful for radiative studies, comparison with other observational datasets, and high resolution LES models. |
| Multilayer cloud detection | *Wind et al.* [2010] | Updated multilayer detection using additional tests from *Pavolonis and Heidinger* (2004). | |
| Retrieval Confidence QA | 2-bit assignment | Not actively assigned. Superseded by pixel-level uncertainty SDS. | QA assignments confusing to users, lack of consistency across products. L3 users directed to "Uncertainty of Mean" SDS derived from pixel-level uncertainties. |

| Category | Collection 5 | Collection 6 | Notes |
|---|---|---|---|
| Sub-pixel Heterogeneity | N/A | Bands 1 & 2 250 m reflectance heterogeneity included in MOD35 and MOD-06 dataset. | Heterogeneity partial predictor for marine liquid water cloud spectral $r_e$ differences. |
| **Algorithm - Pixel Level Uncertainty** | | | |
| Instrument Calibration | Combined with model error sources and fixed at 5% relative | Uses L1B scene-dependent pixel-level spectral uncertainty indices (improved for C6) | Reduces combined uncertainty in many cases. |
| $^{\Delta}$ Model Errors | | See LUT above for details. | |
| $^{\Delta}$ 3.7 µm Emission Error Sources | Not included | Accounts for effective cloud and surface emissivity $T_{sfc}$, and retrieved $T_{cloud}$ including dependence on ancillary water vapor field. | More realistic (larger) 3.7 µm channel $r_e$ and water path uncertainties. |